Novel Antibiotic-Free Scaffold for the Treatment of Infection and Regeneration of Bone

AUTHOR(S)

Emily J. Ryan

CITATION

Ryan, Emily J. (2020): Novel Antibiotic-Free Scaffold for the Treatment of Infection and Regeneration of Bone. Royal College of Surgeons in Ireland. Thesis. https://doi.org/10.25419/rcsi.12776174.v1

DOI

10.25419/rcsi.12776174.v1

RCSI

Novel Antibiotic-Free Scaffold for the Treatment of Infection and Regeneration of Bone

Submitted to the National University of Ireland in fulfilment of the requirements for the degree of

Doctor in Philosophy

Royal College of Surgeons in Ireland

2019

Emily J. Ryan, B Eng

Department of Anatomy, Royal College of Surgeons in Ireland, Dublin.

Supervisors

Prof. Fergal O'Brien & Dr. Cathal Kearney

Declaration

I declare that this thesis, which I submit to RCSI for examination in consideration of the award of a higher degree of Doctor in Philosophy, is my own personal effort. Where any of the content presented is the result of input or data from a related collaborative research programme this is duly acknowledged in the text such that it is possible to ascertain how much of the work is my own. I have not already obtained a degree in RCSI or elsewhere on the basis of this work. Furthermore, I took reasonable care to ensure that the work is original, and, to the best of my knowledge, does not breach copyright law, and has not been taken from other sources except where such work has been cited and acknowledged within the text.

Signed: _____

Student number: _____

Date: _____

Abstract

The bone infection osteomyelitis (typically caused by *Staphylococcus aureus*) usually requires a multistep procedure – long term administration of high-dose systemic antibiotics combined with surgical debridement and bone grafting. However, the disease remains notoriously difficult-to-treat due to the poor penetration of systemic antibiotics into the necrotic bone, antibiotic resistance, and the steep decline in antibiotic discovery. Therefore, osteomyelitis treatment has a dual challenge: ensuring an effective and non-toxic dose of antimicrobial, while ensuring bone regeneration is stimulated. Thus, the overall aim of this thesis was to develop a one-step tissue engineering-based treatment strategy for osteomyelitis that combines local, controlled release of non-antibiotic antibacterials with a regenerative collagen-based scaffold to facilitate bone repair.

In the study presented in Chapter 2 of this thesis, a number of non-antibiotic antibacterial agents (specifically chitosan, copper nanoparticles, silver nanoparticles, zinc nanoparticles, copper chloride salt, silver nitrate salt, and zinc chloride salt) were screened as potential agents for osteomyelitis infection treatment based on their antibacterial effect on three clinically relevant bacterial species (*Staphylococcus aureus*, *Staphylococcus epidermidis*, and *Escherichia coli*) while retaining viable numbers of mammalian cells. The results demonstrate that there is a fine balance between the two, and that in particular chitosan and the metal salts, copper chloride and zinc chloride, may have potential for osteomyelitis infection treatment due to their superior antibacterial activity potential while maintaining mammalian cell viability.

In the study presented in Chapter 3 of this thesis, the optimal antibacterial metal salts identified from the screening process in Chapter 2 were incorporated into 3D collagen/chitosan-based scaffolds via both (i) direct incorporation and (ii) through a chitosan microparticle controlled delivery system, with the aim of minimising toxicity and prolonging bioactivity. The results demonstrated that the two scaffold types were effective in providing different metal salt release quantities and/or profiles which in turn influenced the antibacterial activity of the scaffolds against *S. aureus*. It was also found

that the scaffolds did not elicit a significant toxic effect towards mammalian cells, some scaffolds supported osteogenesis, and all copper-incorporated scaffolds enhanced angiogenesis.

In the study presented in Chapter 4 of this thesis, a range of silver-doped hydroxyapatites were successfully produced and incorporated into collagen scaffolds. The results demonstrate that the composite silver-doped hydroxyapatite /collagen scaffolds demonstrate enhanced microarchitectural and mechanical properties vs. the collagen control, whilst also demonstrating potent antibacterial activity. Although the scaffolds showed toxicity towards mammalian cells *in vitro*, an assessment in an *in vivo* environment may reveal the true cytocompatibility of the scaffolds, as shown previously in the literature for similar scaffolds. Further fine-tuning of the dose of silver-doped hydroxyapatite or its bioactivity through e.g. size or shape changes may also be required to maximise the potential of this nascent system.

In Chapter 5 a second multifunctional material – copper-doped bioactive glass – was tested as an alternative to silver-doped hydroxyapatite due to its potential to enhance both osteogenesis and angiogenesis while retaining antibacterial potency. In addition to promoting osteogenesis and angiogenesis *in vitro*, the scaffolds developed were capable of significant antibacterial activity. Most promisingly, when tested in an *in vivo* chick embryo *ex ovo* model, the copper-doped bioactive glass scaffolds were not only biocompatible, showing no signs of toxicity, but also demonstrated the same pattern of enhanced osteogenesis and angiogenesis as the *in vitro* studies.

Collectively, the research in this thesis presents a number of potential single-stage solutions for osteomyelitis treatment. Such strategies potentially reduce the need for antibiotics and bone grafting, reducing hospital stays and costs. In addition, the platform systems developed in Chapters 3 – 5 might be further modified and used for the controlled delivery of an array of antimicrobial and therapeutic metal ions depending on the intended application, making them attractive candidates for other indication beyond bone including soft tissue applications such as wound healing.

Table of Contents

Acknowledgements

First and foremost, I'd like to thank my supervisors Prof. Fergal O'Brien and Dr. Cathal Kearney for giving me the opportunity to complete this PhD project and for all of your guidance and support over the past few years. I've learned tremendous amount from you! I'd like to express my sincere gratitude for all of the time and effort you have put into me and this project. Thank you for reviewing this document, especially for the last little injection of positivity to get me over the finish line, even if it did involve a football analogy!

Thank you to everyone in the Tissue Engineering Research Group and Kearney Lab, both past and present, for all of your help over the years: Christina, Seona, Joanne, Dave, Rachel, Alice, Amy, Nicola, Rach**a**el, Domhnall, Mark, Rita, Isabel, Rukmani, Tati, Irina, Rosie, Arlyng, Eamon, Caroline, Alan H, Will, Zuzana, Claire, Cian, Laura, Liam, Ronaldo, Catherine, Tauseef, Francesco, and Milicia. Thanks to Paula and Gill (go PEG!) for making working in RCSI in the early years so fun, it was short but sweet!

A special thank you to Sarah, Vinny, and Johnny for the lab support over the years - the place would be a shambles without you! Same goes for you Brenton, your enthusiasm to help other people is wonderful.

Shout out to Caragh, Glenn, Rebecca, and Niall for the breakfasts, lunches, pints, and craic – I'd say it's someone else's turn for the WhatsApp profiler?

To the girls at home, thank you for keeping me sane and realising there's more to life than science! Pam, Niamh, and James - thanks for putting up with my weird working hours, for all the board games and episodes of Jeopardy, and just generally for being great housemates.

To my new Clifden roomies, I can't thank you enough for taking me under your wing this year. I don't think I'll ever be able to repay your kindness. The amazing dinners (Cian), essential oils and sage smoke, and most importantly, a glass of wine or two and a laugh in time(s) of need were massively appreciated.

In particular I'd like to mention my two best friends – Orla and Michaela. Orla – thank you for the PhD rants, for knowing what it's like 'on the inside', and for

everything in between. We're almost there! Thanks for the (few) holidays, for your infectious positivity and get-up-and-go, I couldn't ask for a better travelling partner - here's to some well-funded trips in the future!

Michaela - thank you for having my back, for all of the tea and chats, and most recently for being a fountain of wisdom and support through my career change. You're a wonderful person, friend, and teacher – someone I can only aspire after. Most importantly, thanks for coming back to my house after my mum said she liked your earrings.

A special thanks to my siblings, Lorna and Alan. Lorna – thanks for being the best big sister anyone could ever ask for. Your confidence, selflessness, and general enthusiasm for life are infectious. Thanks for always looking out for me! Alan – thanks for all of your guidance and support and picking me up in times of 'PhD gloom'. You were a fountain of knowledge and advice over the duration of my PhD, whether it was at 12 pm or 12 am, it's safe to say I wouldn't have been able to start or finish this if it wasn't for you.

Tony McHale – having you finish your PhD by my side made it *so* much easier. Thank you for everything – from getting me out of bed at 7am for the lab on Saturday mornings, to making me laugh throughout. Thank you for having confidence in me when I needed it most, and just generally being the best ever. I love you.

Last, but by no means least, a huge thank you to my parents, Una and Cyril. Thank you for constantly supporting me through all my career changes, I swear this is it and I'll finish college soon! Thanks so much for all the love and moral support (and the emergency chocolate supply hidden in the door of the fridge). I hope someday I can repay you.

Dedication

Raising three nerds and birthing two PhD theses - you did something right! I'll be delighted if I become half the parents you are. I dedicate this thesis to you, Mum and Dad.

Prizes, Publications, and Presentations

Journal publications

Nicola Kavanagh*, Emily J. Ryan*, Amro Widaa, Gillian Sexton, Jerome Fennell, Sadhbh O'Rourke, Kevin C. Cahill, Cathal J. Kearney, Fergal J. O'Brien, and Steven W. Kerrigan. *Staphylococcal Osteomyelitis: Disease Progression, Treatment Challenges, and Future Directions.* Clinical Microbiology Reviews, 2018. DOI: 10.1128/CMR.00084-17. * Denotes shared first authorship. (2018 IF = 20.642)
Emily J. Ryan, Alan J. Ryan, Arlyng González-Vázquez, Anahí Philippart, Francesca E. Ciraldo, Christopher Hobbs, Valeria Nicolosi, Aldo R. Boccaccini, Cathal J. Kearney, and Fergal J. O'Brien. *Collagen scaffolds functionalised with copper-eluting bioactive glass reduce infection and enhance osteogenesis and angiogenesis both in vitro and* in vivo*.* Biomaterials, 2019. DOI: 10.1016/j.biomaterials.2019.01.031. (2018 IF = 8.806)
Rukmani Sridharan, Emily J. Ryan, Cathal J. Kearney, Daniel J. Kelly, and Fergal J. O'Brien. *Macrophage polarization in response to collagen scaffold stiffness is dependent on crosslinking agent used to modulate the stiffness.* ACS Biomaterial Science and Engineering, 2018. DOI: 10.1021/acsbiomaterials.8b00910 (2018 IF = 4.432)

Prizes

Travel grant to attend iPromedai week-long training programme focused testing antimicrobial medical devices in Gronigen University and Universiteit van Amsterdam (September 2015).
RCSI Research Day 2016 - Poster presentation prize for best postgraduate poster (February 2016).
RAMI Section of Biomedical Sciences – Donegan Medal winner for best presentation (June 2016).
2017 Robert Langer Student Travel Grant to attend Controlled Release Society conference in Boston (July 2017).

Finalist in Engineers Ireland Biomedical Engineering Research Medal at the Annual Conference of the Bioengineering Section of the Royal Academy of Medicine (January 2018).

Conference abstracts

Conference name:	**Location:**	**Title of presentation or poster:**
BioEngineering in Ireland (Jan 2016)	Galway, Ireland	Presentation: Novel antibiotic-free scaffold for the treatment of infection and regeneration of bone.
RCSI Research Day (Feb 2016)	Dublin, Ireland	Poster: Novel antibiotic-free scaffold for the treatment of infection and regeneration of bone.
RAMI Section of Biomedical Sciences (June 2016)	Cork, Ireland	Presentation: Novel antibiotic-free scaffold for the treatment of infection and regeneration of bone.
Tissue Engineering and Regenerative Medicine Society (June 2016)	Uppsala, Sweden	Poster: Novel antibiotic-free scaffold for the treatment of infection and regeneration of bone.
BioEngineering in Ireland (Jan 2017)	Belfast, Northern Ireland	Presentation: Collagen - copper-doped bioactive glass composite scaffolds for the treatment of infection and regeneration of bone.
RCSI Research Day (Feb 2017)	Dublin, Ireland	Poster: Collagen - copper-doped bioactive glass composite scaffolds for the treatment of infection and regeneration of bone.
Tissue Engineering and Regenerative Medicine	Davos, Switzerland	Presentation: Collagen - copper-doped bioactive glass composite scaffolds for the treatment of infection and regeneration of bone.

Society (June 2017)		
Controlled Release Society (July 2017)	Boston, USA	Presentation: Collagen - copper-doped bioactive glass composite scaffolds for the treatment of infection and regeneration of bone.
Matrix Biology Ireland (Dec 2017)	Dublin, Ireland	Presentation: Collagen scaffolds functionalized with copper-eluting bioactive glass for the treatment of infection and regeneration of vascularised bone.
BioEngineering in Ireland (Jan 2018)	Meath, Ireland	Presentation: Collagen scaffolds functionalised with copper-eluting bioactive glass for the treatment of infection and regeneration of vascularised bone
Orthopaedic Research Society (Mar 2018)	New Orleans, USA	Poster: Collagen scaffolds functionalized with copper-eluting bioactive glass for the treatment of infection and stimulation of osteogenesis and angiogenesis.
European Society for Biomaterials (Sept 2018)	Maastricht, the Netherlands	Poster: Collagen scaffolds functionalised with copper-eluting bioactive glass for the treatment of infection and regeneration of vascularised bone
European Orthopaedic Research Society (Sept 2018)	Galway, Ireland	Presentation: Collagen scaffolds functionalised with copper-eluting bioactive glass for the treatment of infection and regeneration of vascularised bone

List of Figures

List of Tables

Nomenclature

°C	Degrees Celsius
FBC	Full blood count
mecA	Methicillin resistance gene
%DD	Degree of deacetylation
µg	Microgram
µl	Microliter
µM	Micromole
2D	Two – dimensional
3D	Three – dimensional
AAS	Atomic absorption spectroscopy
Ag	Silver
Ag^+	Silver ion
AgHA	Silver-doped hydroxyapatite
$AgNO_3$	Silver nitrate
AgNPs	Silver nanoparticles
agr	Accessory gene regulator
ALP	Alkaline phosphatase
ANOVA	Analysis of variance
atl	Autolysin
ATP	Adenosine triphosphate
BG	Bioactive glass
BHI	Brain heart infusion
BMP	Bone morphogenetic protein
BMP-2	Bone morphogenic protein-2
BSEM	Energy-selective backscatter scanning electron microscopy
BSP	Bone sialoprotein
C57BL/6	C57 black 6 mouse strain
CAM	Chorioallantoic membrane
CAS Number	Chemical Abstracts Service number
CDC	Centre for Disease Control and Prevention
CFU	Colony forming units
CK	Creatine kinase
cm	Centimetre
cm^2	Centimetre squared
CO_2	Carbon dioxide
CO_3^{2-}	Carbonate
ColI	Collagen
Conc	Concentration
CRP	C-reactive protein
CT	Computed tomography
Cu	Copper
Cu^{2+}	Copper ion
CuBG	Copper-doped bioactive glass
CuBG-CS	Copper-doped bioactive glass - collagen scaffold
$CuCl_2$	Copper chloride
Da	Dalton
DA	Deacetylation
dH_20	Distilled water
DHT	Dehydrothermal
DNA	Deoxyribonucleic acid
DPX	Mounting medium - mixture of distyrene, tricresyl phosphate, and xylene
dsDNA	Double-stranded DNA
E. coli	*Escherichia coli*
ECM	Extracellular matrix
EDAC	1-Ethyl-3-(3-dimethylaminopropyl)carbodiimide
ELISA	Enzyme linked immunosorbent assay
ESR	Erythrocyte sedimentation rate
FBS	Fetal bovine serum
FDA	US Food and Drug Administration
FGF-2	Basic fibroblast growth factor
FTIR	Fourier-transform infrared spectroscopy
g	Gram
GI	Gastrointestinal
GRAS	Generally recognised as safe
GTA	Glutaraldehyde
H&E	Haematoxylin and eosin
H_3BO_3	Boric acid
HCL	Hydrochloric acid
HIF-1α	Hypoxia-inducible factor
hMSC	Human mesenchymal stem cell
Hr	Hour
HUVEC	Human umbilical vein endothelial cells
IV	Intravenous
kg	Kilogram
KOH	Potassium hydroxide
kPa	Kilopascal
LL-37	Cathelicidin antimicrobial peptide or CAP-18

LMW	Low molecular weight
M	Molar
MAOI	Monoamine oxidase inhibitor
MBC	Minimum bactericidal concentration
mg	Milligram
MIC	Minimum inhibitory concentration
min	Minute
ml	Millilitre
mM	Millimolar
MMW	Medium molecular weight
mol	Mole
MRI	Magnetic resonance imaging
MRSA	Methicillin resistant *Staphylococcus aureus*
MRSE	Methicillin resistant *Staphylococcus epidermidis*
MSC	Mesenchymal stem cell
MSCRAM	Microbial surface components
MS	recognizing adhesive matrix molecules
MSSA	Methicillin susceptible *Staphylococcus aureus*
MSSE	Methicillin susceptible *Staphylococcus epidermidis*
MW	Molecular weight
N	Newton
N/m	Newton/metre
NaOH	Sodium hydroxide
NHS	N-Hydroxysuccinimide
nm	Nanometre
Ø	Diameter
OCN	Osteocalcin
OD	Optical density
OH^-	Hydroxide
OM	Osteomyelitis
OPAT	Outpatient parenteral antimicrobial therapy
Pa	Pascal
PBS	Phosphate buffered saline
pH	Concentration of the hydrogen ion
PMMA	Polymethylmethacrylate
PO	Per os or to be taken orally
PO_4^{3-}	Phosphate
PTH	Parathyroid hormone
PTHrP	Parathyroid hormone-related protein
q8h	Every 8 hours etc.
r	Pearson product correlation coefficient
rMSCs	Rat mesenchymal stem cells
ROS	Reactive oxygen species
rpm	Revolutions per minute
S. aureus	*Staphylococcus aureus*
S. epidermidis	*Staphylococcus epidermidis*
SCV	Small colony variant
SD	Standard deviation
Sec	Second
SEM	Scanning electron microscopy
SSRI	Selective serotonin reuptake inhibitor
Tabs	Tablets
TRAIL	Tumour necrosis factor related apoptosis inducing ligand
v/v	Volume/volume
VEGF	Vascular endothelial growth factor
w/v	Weight/volume
w/w	Weight/weight
Wt%	Weight percent
XRD	X-ray diffraction
Zn	Zinc
Zn^{2+}	Zinc ion
$ZnCl_2$	Zinc chloride
ZnO	Zinc oxide
α-MEM	Alpha Minimum Essential Medium
λ_{max}	Maximum wavelength
ρ	Density

Chapter 1 Introduction and literature review

The literature review in this chapter has been partially published as Kavanagh N*, Ryan EJ*, Widaa A, Sexton G, Fennell J, O'Rourke S, Cahill KC, Kearney CJ, O'Brien FJ, Kerrigan SW. 2018. *Staphylococcal osteomyelitis: disease progression, treatment challenges, and future directions.* Clin Microbiol Rev. 31:e0008417. (2018 IF = 20.642)

https://doi.org/10.1128/CMR.00084-17.

* Denotes shared first authorship

1.1 Overview

The aim of this thesis was to explore new tissue engineering-based treatment strategies for the notoriously difficult-to-treat bone infection osteomyelitis. Osteomyelitis usually requires aggressive surgical debridement (which may need to be combined with bone grafting) followed by long-term systemic high-dose antibiotics. In addition to the drawback of a multistep procedure, treatment success rates remain low due to the poor penetration of antibiotics into the necrotic bone region and antibiotic resistance. Thus, the aim is to develop a one-step treatment for osteomyelitis that combines local, controlled release of non-antibiotic antibacterials within a regenerative collagen-based scaffold.

The aim of this chapter is to introduce the three main topics that underpin the thesis project – bone, osteomyelitis, and potential new treatment strategies for osteomyelitis. In the first section, Section 1.2, we introduce bone as an organ including the cellular components, bone formation or osteogenesis, and the stages of bone healing. Section 1.3 introduces osteomyelitis and includes information on disease progression, current treatment strategies, and treatment challenges. Following this, Section 1.4 introduces tissue engineering approaches for bone tissue repair and reviews a number of non-antibiotic materials with antimicrobial potential. Finally, in Section 1.5 the overall objectives and specific aims of the thesis are outlined.

1.2 Bone

Bone is highly specialised connective tissue which functions as a support structure, a framework for movement, offers protection, can be a site of blood cell production (or hematopoiesis), and also is a source of inorganic ions which plays a major role in calcium homeostasis in the body [1].

Bone is a tissue composed of organic and inorganic matrices. The stiffness is mainly attributed to the mineralised inorganic matrix, whilst the organic matrix offers a degree of toughness and elasticity. The organic matrix mainly consists of type I collagen (90% or 32% of the volumetric composition) with the remainder composed of proteoglycans (e.g. decorin and biglycan) and non-

collagenous proteins (e.g. osteocalcin, osteonectin, osteopontin, fibronectin, bone sialoprotein, bone morphogenic proteins, and growth factors) [2], [3]. The remaining inorganic matrix is mainly composed of calcium and phosphate crystals in the form of hydroxyapatite ($Ca_{10}(PO_4)_6(OH)_2$). However, other ions such as sodium, potassium, zinc, and strontium are also present in the matrix [1], [3].

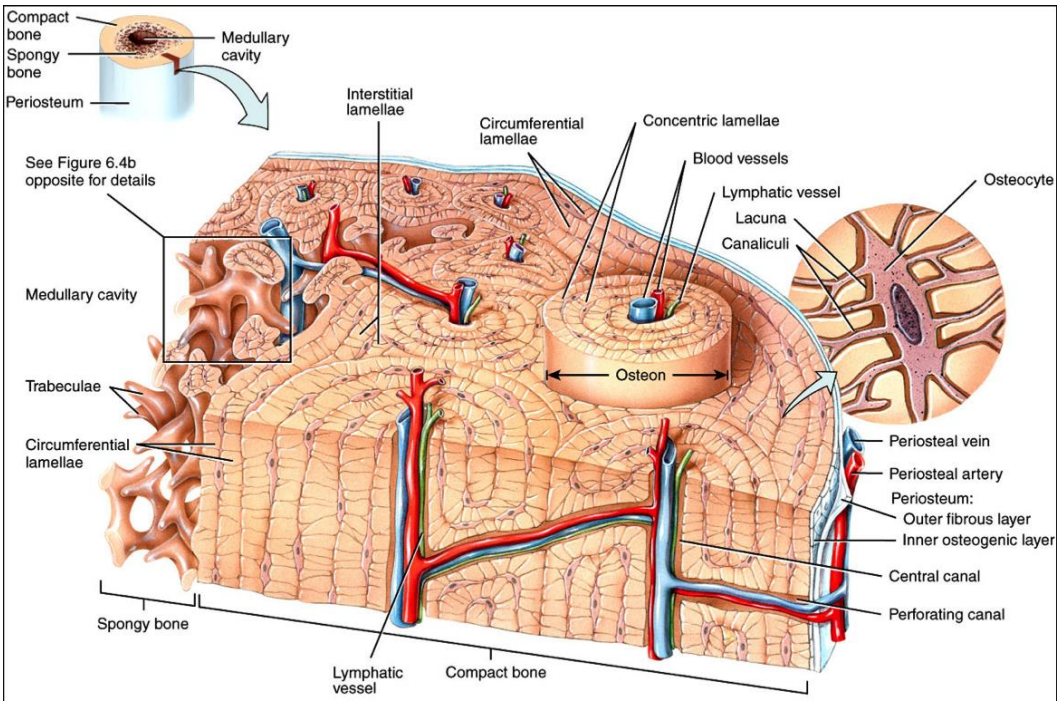

Figure 1.1 Haversian canal
A schematic of bone showing the loosely-arranged cancellous/trabecular bone and densely packed cortical bone. A single harversian system containing an osteocyte trapped within concentric rings of mineralised matrix with blood vessels and lymphatic vessels highlighted [4].

Architecturally and functionally, bone is divided into two different forms: cortical (or compact) and cancellous (or spongy) bone. Cancellous bone is found within the core of the long bones, pelvic bones, ribs, skull, and the vertebrae. Cortical bone surrounds cancellous bone and functions mainly as a mechanical structure of densely packed Haversian systems, or osteons, which consist mainly of osteocytes entrapped within concentric rings of mineralised matrix with blood vessels, lymphatic vessels, and nerves running through the central canal (**Figure 1.1**). Cortical bone is also thought to be the organ's strain-sensing centre which allows for remodelling in areas of increased or decreased loading. On the other hand, cancellous bone has a mainly metabolic function and is a loosely-arranged porous structure.

1.2.1 The cellular components in bone

Bone tissue is lined and penetrated by four different cell types, namely osteoprogenitor cells, osteoblasts, osteocytes, and osteoclasts. Osteoblasts and osteocytes originate from osteoprogenitor cells – progenitor cells derived from mesenchymal stem cells (MSCs) produced in the bone marrow which are committed to the bone cell lineage. Inactive osteoprogenitor cells become flattened and are found on the inner layer of the periosteum, a thin fibrous membrane that envelopes all bones (except at joints) [1].

Osteoblasts make up approximately 5% of the bone cell population, are cuboidal in morphology, and are found along the surface of the bone. The main function of osteoblasts is the formation of new bone. To do so, the osteoblasts first produce an unmineralised matrix, called osteoid, which is rich in collagen type I (90%) and non-collagenous proteins such as osteocalcin and alkaline phosphatase (ALP) [5]. Calcium ions and phosphatase ions released from the ALP become immobilised on the proteoglycans where they join to the calcium ions and form hydroxyapatite crystals. Osteoblasts which are not producing bone can become quiescent flattened osteoblasts, termed bone lining cells. Osteoblasts that get trapped within the mineralised matrix can further differentiate into osteocytes.

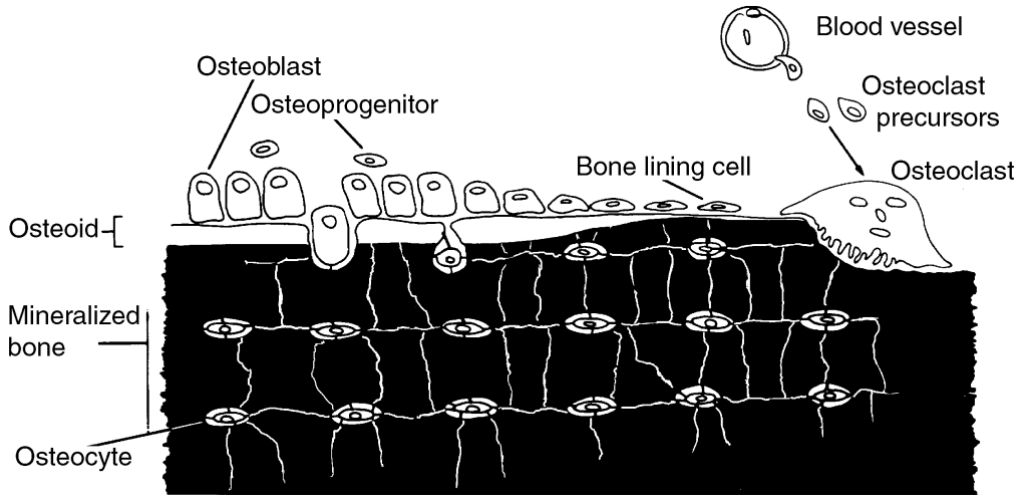

Figure 1.2 Location of bone cells within matrix
Topographical relationship between the different cell types in bone namely osteoprogenitor cells, osteoblasts, bone lining cells, osteocytes, and osteoclasts [6].

Osteocytes are dendritic cells that compromise ~95% of the bone cell population. The cell bodies are located inside the lacuna with numerous cytoplasmic projections extending out of the bony matrix through small tunnels called canaliculi [6]. The projections allow osteocytes to receive oxygen and nutrients and interact with other osteocytes and osteoblasts. Osteocytes also have a mechanosensory function which allows the bone to remodel and adapt to areas of increased or decreased loading by regulation of both osteoblast and osteoclast activity [3].

Osteoclasts are large multinucleated cells which are derived from mononuclear cells of the haematopoietic stem cell lineage and function to destruct bone tissue [3], [7]. To do this, osteoclasts release hydrogen ions which create an acidic environment to degrade the hydroxyapatite crystals and enzymes to break down the remainder of the organic bone matrix. During bone remodelling, osteoclasts have also been shown to produce factors that control osteoblast function, termed coupling of bone formation [8].

1.2.2 Osteogenesis

There are two mechanisms of bone formation – direct intramembranous ossification and indirect endochondral ossification [1]. Intramembranous ossification occurs during embryonic development in flat bones such as those of the skull and some facial bones and occurs due to the direct differentiation of MSCs into osteoblasts [9]. Endochondral ossification, on the other hand, which is responsible for the formation of the majority of bones, first involves the differentiation of MSCs into cartilage-forming chondrocytes, the production of cartilage, and subsequent replacement of cartilage tissue by bone (**Figure 1.3**).

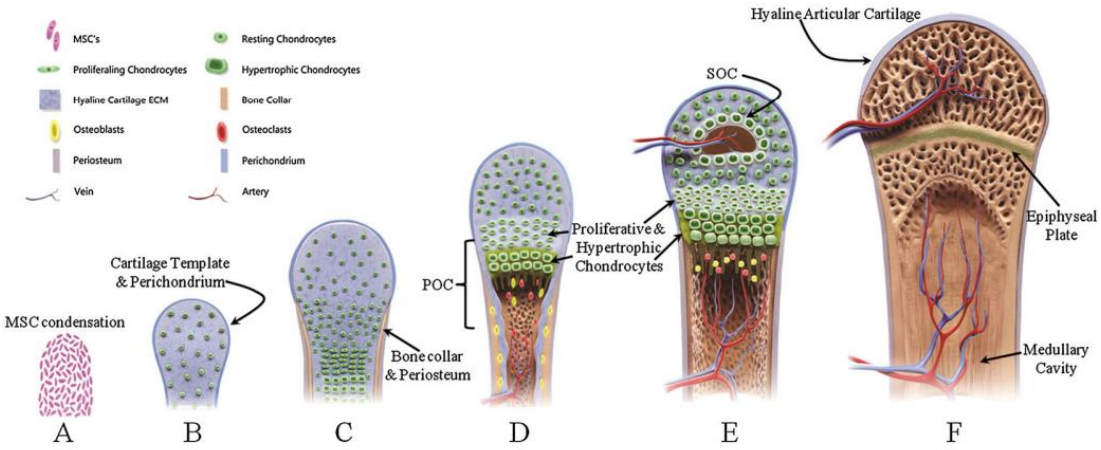

Figure 1.3 Endochondral ossification
Stages of endochondral ossification adapted from [10]*. (A) Condensation of MSCs. (B) Rapid proliferation of chondrocytes forming a dense avascular cartilage matrix. (C) Formation of hypertrophic cartilage at the centre. (D) Infiltration of blood vessels to hypertrophic region and differentiation into osteoblasts. (E) Lengthening of bone by continued proliferation of chondrocytes and osteoblasts. (F) Growth plates develop, secondary ossification occurs, and bone marrow forms.*

The chondrocytes proliferate rapidly and produce a dense cartilage matrix. Next, the chondrocytes in the centre stop dividing and become very enlarged, known as hypertrophic chondrocytes, and produce other extracellular matrix (ECM) proteins such as collagen type X and fibronectin, and primary ossification ensues. This area of cartilage then becomes vascularised and the hypertrophic chondrocytes undergo apoptosis leaving behind a core which will become the bone marrow. The cells which line the core differentiate into osteoblasts, eventually replacing the cartilage by bone. In long bones, the area of primary ossification extends in both directions from the centre of the diaphysis towards the epiphysis, producing calcified bone and pushing the hypertrophic cartilage towards the ends of the bone. This produces a zone termed the epiphyseal growth plate which can continue to allow the growth and lengthening of bones until the end of puberty at around 18 years of age, known as secondary ossification.

1.2.3 Bone healing

The repair of bone can be by intramembranous (direct) and/or endochondral ossification (by callus formation). After an injury or trauma there is usually an initial tearing of the periosteum and bleeding [9]. A blood clot, or haematoma, then forms and initiates an inflammatory response which attracts immune cells

such as platelets, macrophages, lymphocytes, and monocytes which control infection and secrete cytokines and growth factors (e.g. bone morphogenetic proteins - BMPs and vascular endothelial growth factor - VEGF) which attract more inflammatory cells and mesenchymal stem cells from the periosteum, bone marrow, and surrounding tissues (**Figure 1.4**) [11].

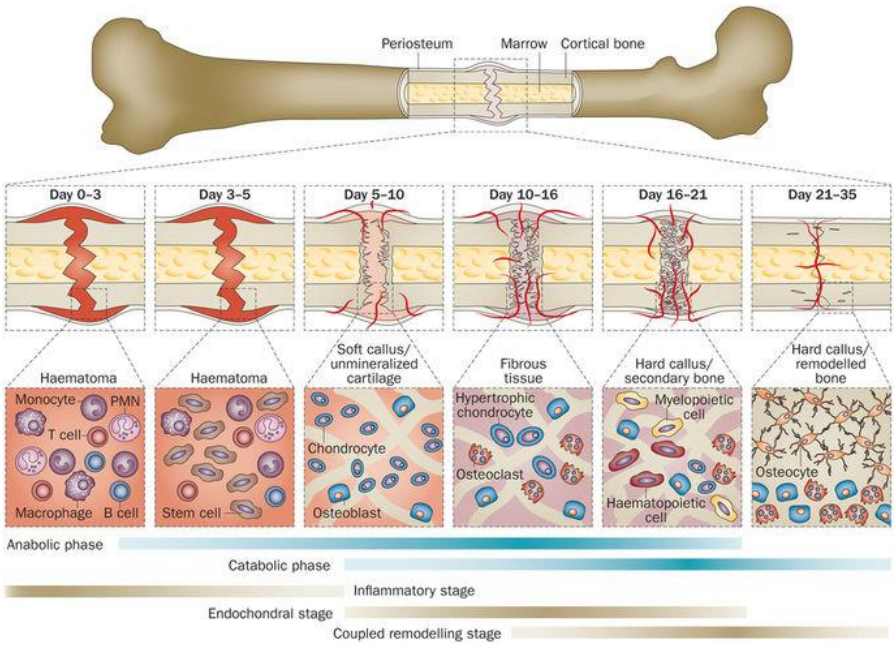

Figure 1.4 Fracture repair of bone
Stages of bone fracture repair from haematoma formation and callus and fibrous tissue formation to remodelled bone, adapted from [12].

Following the inflammatory response there is primary bone formation where an initial deposition of avascular matrix (callus formation) in a randomly orientated pattern, known as woven bone, is used as a scaffold for deposition and remodelling into a more organised lamellar bone structure (secondary bone formation). Structurally, woven bone consists of randomly orientated collagen fibrils which renders the area mechanically weak [9]. Replacement with lamellar bone is achieved through osteoblast/osteoclast remodelling [11].

1.3 Osteomyelitis

Osteomyelitis is an infection localised to the skeletal system. Translated literally from Greek it means inflammation of the bone marrow (‘Osteo’ – bone, ‘Myelos’ – marrow, and ‘Itis’ – inflammation). The infection can be restricted to a single portion of the bone or can involve several regions, such as the marrow,

cortex, and periosteum (**Figure 1.5**) [13]. Although it can be caused by a variety of pathogens, osteomyelitis is most commonly caused by the opportunistic gram positive bacteria *Staphylococcus aureus* (*S. aureus*) and *Staphylococcus epidermidis* (*S. epidermidis*) (approx. 75% of cases) [14].

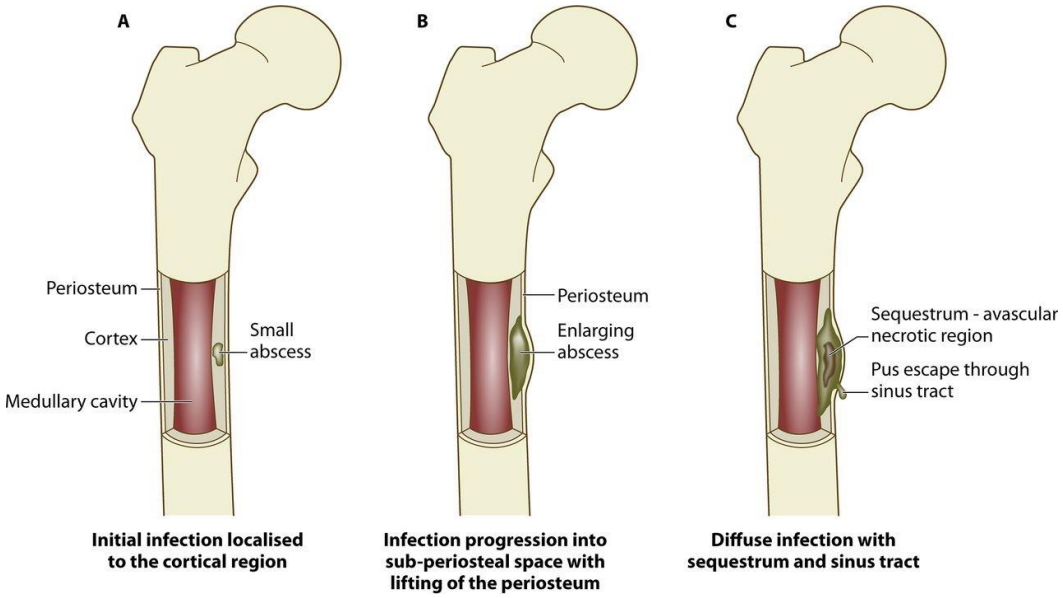

Figure 1.5 Progression of osteomyelitis
An abscess develops from localized infection that constricts the blood flow to the area (A), resulting in avascular region of necrotic bone tissue called the sequestrum (B), followed by development of new bone surrounding the sequestrum, termed the involucrum, which may also have a sinus tract through which purulence can escape (C) [15]

The pathology of osteomyelitis is characterized by severe inflammation, impairment of vasculature, and localized bone loss and destruction. In an attempt to overcome the infective microorganisms, leukocytes produce inflammatory cytokines and enzymes that breakdown the infected and surrounding tissue [16]. Purulence consisting of dead leukocytes and host/bacterial cells can fill intercellular spaces around the infection and form an abscess. In chronic infection, abscesses can impair blood flow and strip the periosteum creating an area of vascularized, necrotic bone called a sequestrum [17]. Vascular impairment makes the foci of chronic infection impervious to the immune system and systemic antibiotics. The sequestrum is indicative of a chronic infection and compromises the bone's integrity. Often the formation of new bone – involucrum – occurs, which forms from remaining intact fragments of the periosteum and functions to provide axial support to weight bearing bones and prevent pathological fracture [18], [19]. Exudate or

purulence from the infection may escape through an opening in the bone called a sinus tract (**Figure 1.5**).

1.3.1 Modes of bone infection

There are many contributing factors that predispose a patient to developing osteomyelitis including age, diabetes, peripheral vascular disease, intravenous drug use, surgical implants, and those with immunodeficiencies due to disease or immunosuppressant drugs [18]. The causative organisms in osteomyelitis can originate from either a haematogenous or contiguously spread source, often referred to as endogenous or exogenous sources, respectively [20].

Haematogenous osteomyelitis is usually mono-microbial [21]. It most commonly occurs in patients lacking any prior risk factors or infection; however, it can also be caused by the seeding of circulating pathogens in the blood, which can arise from an existing infection. Haematogenous osteomyelitis represents just 20% of all osteomyelitis infections; however, the majority of osteomyelitis cases in children are haematogenous (85% of cases for patients under 17 years old) [20].

In contrast to haematogeneous osteomyelitis, contiguous spread of infection is most often poly-microbial and most commonly affects adults [22]–[24]. Contiguous spread osteomyelitis can originate from trauma, direct inoculation during operative procedures, or can spread from surrounding infected soft tissues. It is estimated that half of osteomyelitis cases in adults are due to trauma [25]. Trauma can result in either open or closed fractures (presence or absence of exposed bone). Damaged connective tissues, including skin, muscle, and bone, expose proteins such as collagen and fibronectin which bacteria readily bind to, increasing the chance of inoculation [26]. In a clinical study carried out by Merritt *et al.*, up to 1 in 5 patients who acquired open fractures were reported to have developed infections [27]. People with soft tissue infections who develop underlying infection of the bone are most commonly over the age of 40 and have diabetes mellitus [28]. Osteomyelitis spreading from diabetic ulcers due to neuropathy and vascular insufficiency most commonly occurs in the bones of the feet; the toes, metatarsal heads,

and calcaneum [29]. According to Malhotra *et al.,* and Lavery *et al.,* 12-20% of those with diabetic foot ulcers develop an infection of the underlying bone [30], [31] and in severe cases of foot ulcers this prevalence can be higher than 66% [32].

1.3.2 Clinical presentation and diagnosis

Diagnosing osteomyelitis is often a difficult challenge as there is a vast variation in clinical presentation. Early diagnosis is the key to the successful treatment of osteomyelitis. Schmidt *et al*. developed a diagnostic tool for osteomyelitis using a scoring system based on clinical, laboratory, and technical information [33]. The scoring system is based on: 1) Clinical history and risk factors; 2) clinical examination and laboratory test results: leukocyte counts and inflammatory markers such as erythrocyte sedimentation rate (ESR) and C-reactive protein (CRP); 3) Diagnostic imaging such as ultrasound, radiology, CT, or MRI; 4) microbiology analysis and 5) histopathology. Unfortunately, many of these individual diagnostic methods lack specificity and sensitivity and are associated with many issues, as Tiemann *et al*. outlines [34]. Lab test results involving leucocyte counts and inflammatory markers are often not reliable. For example, in a review by Scott *et al*., 41% of patients who presented with acute haematogenous osteomyelitis presented with a leucocyte count of less than 10,500, which is within the normal range of ~4,500 - 11,000 [35]. In up to 40% of osteomyelitis cases, microbiological tests produce false-negative results. This may be due to the difficulty in culturing the causative organism secondary to location, inability to undergo surgical intervention, or the fact that the patient may have been started on antibiotics prior to the collection of specimens for culture, thus altering the results of laboratory testing. In addition, diagnosing osteomyelitis through imaging methods is often delayed as bone necrosis is difficult to detect using plain radiograph until week 3 of infection, with a reported positive diagnosis rate of only 20% after 2 weeks [26].

1.3.3 Traditional treatment strategies

Osteomyelitis therapy requires an interdisciplinary approach involving a combination of patient evaluation, antibiotic therapy, and surgical intervention [36]–[38]. Treatment can be difficult and is largely based on expert opinion as there is varying advice for the duration and route of treatment, and confusion exists regarding the superiority of intravenous/parenteral treatment to oral. Dedicated treatment guidelines for acute osteomyelitis are still awaited, however the treatment strategies described below are generally applied.

1.3.3.1 Systemic antibiotic treatments

Ideally, in non-life-threatening osteomyelitis cases, antibiotic therapy should be withheld until the causative organism and susceptibility have been identified. The gold standard for diagnosis is bone biopsy [39]. Having found an organism to treat, the results of susceptibility testing can then inform the optimal agent, penetrance of the chosen agent into bone, and the route and duration of treatment. The most important susceptibility distinction is the oxacillin/methicillin susceptibility result, which defines whether methicillin susceptible or resistant *S. aureus* or *S. epidermidis* (MSSA/MSSE or MRSA/MRSE) is involved. Antibiotics are often administered intravenously for 2-4 weeks, followed by oral therapy that can last an additional 8-10 weeks. However, due to the avascular nature of the bone, penetration of the antibiotics to the infected site can be poor. As such, high doses of antibiotics over long time periods are required, which can result in systemic toxicity.

An indication of the success of the selected treatment method may be given by a reduction in the Erythrocyte Sedimentation Rate (ESR) and C-Reactive Protein (CRP) levels. The main treatment choices for both methicillin susceptible and resistant *S. aureus* and *S. epidermidis* all achieve therapeutic levels of bone penetration and are shown in **Table 1.1** below [40], [41]. Rifamcin or fusidic acid may also be added in combination with the chosen antibiotic for the initial 2 weeks as they have been shown to be effective against slow growing bacteria present in biofilms and the antibiotic combinations have been shown to improve cure rates [42], [43].

Table 1.1 *Therapeutic options for the treatment of S. aureus and S. epidermidis osteomyelitis* [15], [40], [41], [44]–[47]

Recommended intravenous agents for the treatment of *S. aureus* and *S. epidermidis* osteomyelitis					
Agent (Class)	**Dose**	**MSSA/ MRSA**	**Interactions**	**Side Effects**	**Comments**
Flucloxacillin (penicillin)	2 g q6h	MSSA/MSSE	Nil significant	Rash, nausea, vomiting, diarrhea, cholestatic hepatitis	First line treatment for MSSA/MSSE
Nafcillin (penicillin)	2 g q4h	MSSA/MSSE	Tetracyclines, warfarin	Phlebitis, rash, neutropenia, interstitial nephritis	First line treatment for MSSA/MSSE
Oxacillin (penicillin)	2 g q4h	MSSA/MSSE	Tetracyclines	Phlebitis, rash, hepatitis	First line treatment for MSSA/MSSE
Cefazolin (cephalosporin)	2 g q8h	MSSA/MSSE	Probenecid – increase in cephalosporin serum concentration, warfarin	Phlebitis, rash, fever, eosinophilia	Convenient for OPAT
Ceftriaxone (cephalosporin)	2 g q24h	MSSA/MSSE	Calcium containing solutions, probenecid (as above), warfarin, lansoprazole	Pseudo-cholelithiasis, phlebitis, rash, fever	Convenient for OPAT
Vancomycin (glycopeptide)	15 mg/kg q12h	MRSA/MRSE	Non-depolarizing muscle relaxants, nephrotoxic agents	Nephrotoxicity, ototoxicity, thrombocytopenia, red man syndrome	Target trough 15-20 mg/L, consider combination therapy, may be less effective against strains with MICs of 1-2 mcg/ml
Teicoplanin (glycopeptide)	12 mg/kg q24h	MRSA/MRSE	Nephrotoxic agents, ototoxic agents	Thrombophlebitis, rash, neutropenia, eosinophilia, ototoxicity	Target trough >20 mcg/mL
Daptomycin (cyclic lipopeptide)	6 mg/kg q24h	MRSA/MRSE	Statins	CK elevation, eosinophilic pneumonia	Monitor CK Convenient for OPAT

Oral treatment options for either MSSA/MSSE or MRSA/MRSE osteomyelitis (when susceptible)

Levofloxacin (flouroquinolone)	750 mg q24h	MSSA/MSSE MRSA/MRSE	QTc prolonging agents, warfarin	Diarrhea, phototoxicity, QTc prolongation, tendon rupture, seizures	Use combination therapy
Trimethoprim-sulfamethoxazole (anti-folate)	DS 2 tabs q12h	MSSA/MSSE MRSA/MRSE	ACE inhibitors, azathioprine, cyclosporine, folinic acid, para-aminobenzoic acid, phenytoin, sulfonylureas, oral contraceptives, warfarin	Nausea, vomiting, rash, hyperkalemia, bone marrow suppression	Consider combination therapy
Doxycycline (tetracycline)	100 mg q12h	MSSA/MSSE MRSA/MRSE	Acitretin, barbiturates, bismuth salts, carbamazepine, digoxin, oral contraceptives, penicillins, warfarin	GI intolerance, photosensitivity, dental deposition	
Minocycline (tetracycline)	100 mg q12h	MSSA/MSSE MRSA/MRSE	Acitretin, barbiturates, bismuth salts, carbamazepine, digoxin, oral contraceptives, penicillins, warfarin	Vertigo, ataxia, hypersensitivity pneumonitis, rash, GI intolerance, photosensitivity, dental deposition	Consider combination therapy
Linezolid (oxazolidinone)	600 mg q12h	MSSA/MSSE MRSA/MRSE	SSRIs, MAOIs, tricyclic antidepressants, adrenergic agents, rifampicin	Thrombocytopenia, anemia, optic neuropathy, peripheral neuropathy	Reserve for use when alternatives not available. Monitor FBC.
Clindamycin (lincosamide)	600 mg q6h (IV) 450 mg q6h (PO)	MSSA/MSSE MRSA/MRSE	Erythromycin, kaolin-pectin, loperamide, non-depolarizing muscle relaxants	Diarrhea, nausea, vomiting, anorexia, rash	Check for inducible clindamycin resistance if erythromycin resistant

Rifampicin (rifamycin)	300-450 mg q12h or 600 mg q24h	MSSA/MSSE MRSA/MRSE	Numerous – check interactions when prescribing	Orange discoloration of urine, tears, sweat, hepatitis, GI intolerance, flu-like syndrome	Use in combination therapy only as *S. aureus* resistance develops quickly to monotherapy. Particularly effective in treatment of biofilms and infected prosthetic material.
Fusidic acid (fusidane)	500 mg q6h	MSSA/MSSE MRSA/MRSE	Statins, ritonavir	Phlebitis, nausea, vomiting, diarrhea, elevated bilirubin	Use in combination therapy only as *S. aureus* resistance develops quickly to monotherapy

Abbreviations: CK, creatine kinase; FBC, full blood count; GI, gastrointestinal; IV, intravenous; MAOI, monoamine oxidase inhibitor; MIC, minimum inhibitory concentration; MRSA, methicillin resistant *Staphylococcus aureus;* MRSE, methicillin resistant *Staphylococcus epidermidis;* MSSA, methicillin susceptible *Staphylococcus aureus*; MSSE, methicillin susceptible *Staphylococcus epidermidis*; OPAT, outpatient parenteral antimicrobial therapy; PO, per os; SSRI, selective serotonin reuptake inhibitor.

1.3.3.2 Surgical intervention

Whilst antibiotics can be successful at treating acute osteomyelitis, chronic infection also requires surgical intervention. Debridement of the bone aims to remove necrotic tissue and also reduce the bioburden of the infection in the area. It involves multiple debridement in a staged fashion and excision should obtain margins in normal healthy bleeding tissue [37], [48]. However, despite extensive tissue debridement, the vast dispersion of bacterial colonization throughout the bone and surrounding tissue makes it difficult to ensure the complete elimination of infection, and local and systemic antimicrobial treatment is also essential. Despite surgical debridement and antibiotic therapy, chronic osteomyelitis has a high rate of reoccurrence in adults (30% at 12 months) due to the poor penetration of antibiotics into necrotic bone and antibiotic resistance [36].

1.3.3.3 Dead space management

Following debridement of the infected site, the void remaining is referred to as dead space. Dead space management typically involves harvesting autologous or autogenous bone grafts, most often from the pelvic iliac crest followed by implantation into the defect site. Autologous bone grafts remain the gold standard for promoting healing, with an estimated 2.2 million procedures per annum [49], [50]. Grafts of this kind have optimal biological performance in terms of osteogenicity, osteoinductivity and osteoconductivity [51]. However, the use of autologous bone grafts is limited by considerable donor site morbidity, postoperative pain and risk of infection, and the lack of available tissue. Allogenic bone grafts can also be employed, most commonly by transplantation of sterilised cadaveric bone; however; this is also restricted due to viral transmission and immune rejection issues [20], [52].

1.3.3.4 Local antibiotic delivery strategies

The systemic administration of a sufficiently high dose of antibiotics to reach the necrotic region and clear the infection often results in toxicity. Therefore, a number of products have emerged in recent years that are focused on the local delivery of antibiotics to the site of infection whilst simultaneously regenerating

bone [53]. There are a range of products currently on the market (**Table 1.2**) which are typically classified according to the degree of biodegradability of the carrier and which vary with regard to material type, antibiotic type and the delivery method. Each technique ultimately aims to reduce the dependence on systemic antibiotics, decrease hospitalisation costs and, importantly, prevent late relapse, which is common in chronic osteomyelitis.

Table 1.2 *Commercially available antimicrobial products for use in the treatment of osteomyelitis* [15]

Collagen-based sponges			
Product	**Company**	**Description**	**Indications**
Collatamp® G/EG	EUSA Pharma	Resorbable collagen implant impregnated with gentamicin	Prevent and treat surgical site infections through local antibiotic delivery
GENTA-COLL®	RESORBA	Hemostyptic collagen sponge containing gentamicin	Hemostasis in wounds when there is high risk of infection (including in OM)
Septocoll E	Biomet UK Ltd.	Resorbable Equine collagen fleece containing 2 forms of gentamicin (Gentamicin sulfate; Rapid release and Gentamicin crobefate; Protracted release)	Potentially/contaminated wounds. Revision operations in septic surgery
Bone cement/beads			
Product	**Company**	**Description**	**Indications**
Septopal	Biomet UK Ltd.	PMMA chains loaded with gentamicin sulfate	Local drug delivery after surgical debridement
STIMULAN®	Biocomposites®	Calcium Sulfate (Can mix with Gentamicin, Vancomycin and Tobramycin)	Complements dead space and infection management strategies (e.g. Infected non-unions, OM and periprosthetic joint infection)
PALACOS®	Heraeus Medical	Bone cement – available with Gentamicin	Orthopaedic replacement procedures

Non-biodegradable antibiotic delivery systems are based on the acrylic material polymethylmethacrylate (PMMA), either in the form of cement (PALACOS®) or beads (Septopal®). These can be combined with a number

of antibiotics and have been extensively used in surgery to locally deliver antibiotics in the treatment of various musculoskeletal infections. Notably, this treatment is limited due to toxicity and the requirement for a thermally stable antibiotic [54]. Additionally, these antibiotic-loaded cements tend to release a bolus of antibiotic within the first 24 hrs followed by minimal or no release thereafter. Research has shown that as little as 0.9% - 2.1% of the antibiotic incorporated into cement spacers is released over a 6-week period [55]. Thus, surgeons must be cautious in order to avoid reoccurrence of infection due to low antibiotic doses or even causing antibiotic resistance. Furthermore, PMMA products require removal, giving rise to the risk of re-infection. This drawback can be overcome by the use of biodegradable antimicrobial products.

Biodegradable delivery systems using calcium sulphate beads and collagen sponges loaded with antibiotics have been in use for the past decade. These biodegradable delivery systems allow for the local delivery of antibiotics to the site of infection, whilst providing a scaffold for the repair and regeneration of bone. Such products include STIMULAN® beads, which can be combined with a number of antibiotics, Collatamp® G/EG (EUSA Pharma) and GENTA-COLL® (RESORBA). Although more large-scale randomised controlled studies are needed to fully elucidate the results, the literature reports good clinical success rates for gentamicin-loaded collagen fleeces [56]. In terms of orthopaedic wound healing, gentamicin-loaded collagen fleeces have shown more complete wound healing, shorter healing time, improved clinical outcome, and reduced convalescence time compared to empty defects [57]–[59]. In terms of osteomyelitis treatment, gentamicin-loaded collagen fleeces have demonstrated a range of treatment success rates, from 74-94% [56], [60]–[62], and when compared to PMMA beads loaded with gentamicin they had significantly lower rate of re-operation [56], [63].

1.3.4 Complications in osteomyelitis treatment

1.3.4.1 Staphylococcal biofilm development

The ability of bacteria to form biofilms is a natural mechanism. The stages of biofilm development are: attachment, accumulation, and dispersal (**Figure 1.6**). A number of factors mediate attachment, including autolysin (atl), teichoic acids, and microbial surface components recognizing adhesive matrix molecules (MSCRAMMS) [64], which allow positioning of the premature biofilm. The presence of human serum proteins alone enhances the expression of MSCRAMMs that promote biofilm formation [65]. Once attached, the bacterial cells within the matrix multiply and accumulate, shaping the matrix surrounding them to include complexities such as water channels for nutrient and waste diffusion. It is thought that through quorum sensing governed by the accessory gene regulator (agr) system, bacteria are able to sense their environment and can disperse from the mature biofilm matrix and spread to other areas [66], [67].

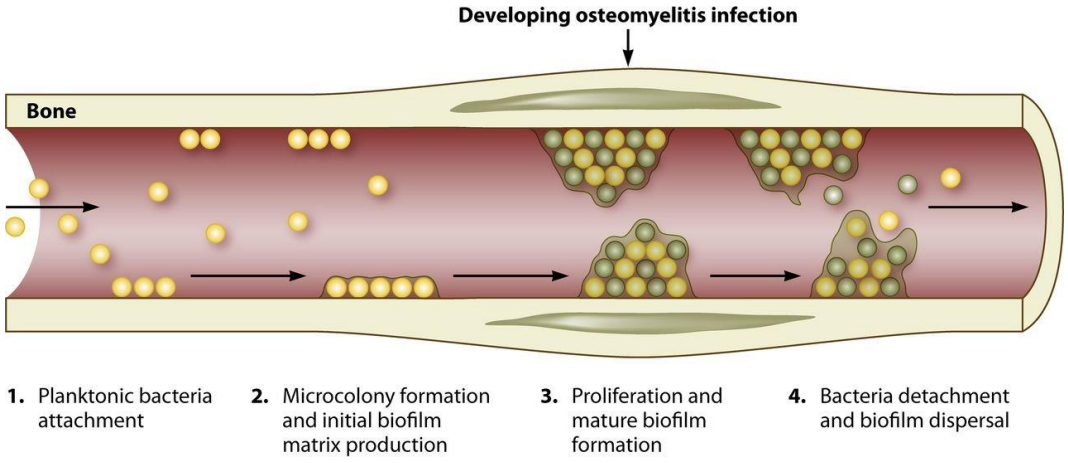

Figure 1.6 Stages of biofilm development
The first stage of biofilm formation in bone is attachment. Once attached, the bacteria begin to accumulate and produce a sticky matrix, which is the initial biofilm. This accumulation results in the formation of biofilm microcolonies, and development of mature biofilm. The biofilm may then finally break down and release the bacteria from within, causing dissemination throughout the host [15]

In chronic osteomyelitis, the ability of staphylococci to persist and re-infect is partially attributed to the development of these biofilms. The presence of biofilms has been suggested as the main cause of clinical quiescence of

chronic osteomyelitis. Biofilms can provide protection from antibiotic arsenal, the host immune response, and shear stresses. The biofilms further enhance the survival of the staphylococci residing within them by functioning to seize and concentrate important environmental nutrients [23], [68].

As with most cases of chronic osteomyelitis, surgical intervention is usually required for removal of the sequestrum. The sequestrum has a decreased vascularity and oxygen tension, providing optimum conditions for bacterial attachment and biofilm formation. Debridement of the infected area would also include the removal of the sequestra as antibiotic therapy alone is unable to sufficiently penetrate the biofilm matrix and eradicate the infection within. Surgical revisions can result in infection relapse in up to 40% of cases, however if the sequestra remains present in the bone, it will facilitate spreading of the infection throughout the bone. Spreading of the infection will result eventually in radical debridement and possible limb amputation [69], [70].

1.3.4.2 Persistent small colony variant (SCV) staphylococci

In conjunction with the biofilm matrix, which provides protection for the bacteria within it, alterations of the bacterial metabolic activity are also observed, which confers resistance to antibiotics. Persister cells and small colony variants (SCVs) are found within biofilms and have been investigated extensively in the staphylococcal species [71], [72]. SCVs have been described in osteomyelitis cases and have been deemed responsible for the recurrent infection associated with the disease due to their ability to survive intracellularly in a dormant state for many years, to then remerge as the parent strain and cause reinfection [73]. Invasion and persistence of *S. aureus* in naturally non-phagocytic cells has been described in a range of cell types including endothelial cells and keratinocytes [74], [75]. This internalization has two possible outcomes: either the *S. aureus* invader activates production of the tumor necrosis factor related apoptosis inducing ligand (TRAIL), which in turn causes osteoblast apoptosis, or it can persist intracellularly as a SCV and cause recurrent infection months or years later [76], [77].

1.3.4.3 Antibiotic resistance

Antibiotic resistance is a global health threat that affects both developed and developing countries. It has quickly become a serious risk to public health with more than 70% of hospital acquired bacterial infections being resistant to one or more of the antibiotics that are generally used to eradicate them [78]. The World Health Organization (WHO) and the Centre for Disease: Control and Prevention (CDC) estimate that in both the EU and the USA, more than 23,000 people die annually as a result of antimicrobial resistance, with *S. aureus* responsible for nearly 50% of those deaths. In addition, there has been a steep decline in antibiotic approval over the last 30 years, with only two antibiotics approved by the US Food and Drug Administration (FDA) between 2008 and 2012 (**Figure 1.7**). Thus, research has been driven to investigate non-antibiotic alternatives.

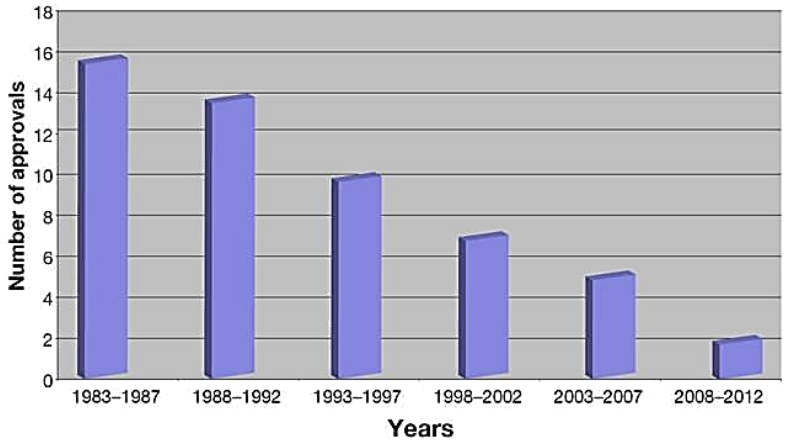

Figure 1.7 Decline in antibiotic approvals by the FDA
The steep decline in antibiotic approvals by the US Food and Drug Administration (FDA) from 1983 to 2012 [79].

Approximately 1% of bacteria are innately resistant to more than one class of antimicrobial agents [80], while the rest acquire resistance by a variety of mechanisms and adaptations (**Figure 1.8**):

1) The bacteria can produce new enzymes that can destroy the antibiotic before it even enters the cell through acquired genes, such as β-lactamases or penicillinase.
2) If a specific binding site on the cell wall is the site of action for the antimicrobial, bacteria also have the ability to modify their cell wall –

upon acquiring specific genes – so that the antimicrobial no longer binds/enters the cell, e.g. methicillin resistance gene, mecA.

3) If the antibacterial agent does enter the cell, bacteria that have developed efflux pumps can eliminate the antibacterial agent before it reaches its site of action within the cell [80]–[82].

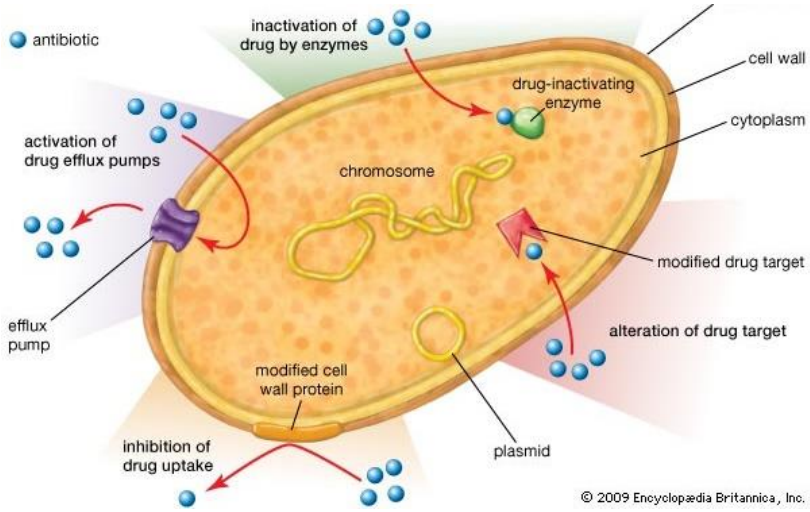

Figure 1.8 Mechanisms of bacterial antibiotic resistance
There are multiple mechanisms by which bacteria can incur antibiotic resistance including enzymatic degradation, modification of drug targets, and the activation of efflux pumps [83].

Through these mechanisms, the bacteria's susceptibility to an antibiotic can be reduced or become completely resistant. Minimal new antibiotic discoveries combined with an alarming number of emerging cases of microbial resistance to 'last resort' antibiotics has forced research to focus on discovering and developing non-antibiotic antimicrobials.

1.4 Potential new treatment strategies for osteomyelitis

In summary, there are numerous treatment challenges associated with osteomyelitis including dead space management, lack of local antibiotic penetration to the necrotic region, and the development of antibiotic resistance. Thus, in this thesis potential new treatment strategies for osteomyelitis are examined which combine a number of non-antibiotic antibacterials that might evade antimicrobial resistance, with tissue engineered scaffolds to act both as a local delivery vehicle for the antibacterials whilst potentially enhancing tissue regeneration.

1.4.1 Tissue engineering and scaffolds for orthopaedic applications

Tissue engineering involves the combination of scaffolds, cells, and signals to repair and regenerate both the structure and function of biological tissues, often referred to as the 'tissue engineering triad' (**Figure 1.9**) [84]. In this thesis we mainly focus on the biomaterial scaffold aspect of the tissue engineering triad. Biomaterial scaffolds provide structural support for cells in a 3D environment and mimic the natural extracellular matrix. There are a number of requirements for tissue engineered scaffolds that are often application specific [2] including biocompatibility, biodegradability, scaffold architecture, and scaffold mechanical properties.

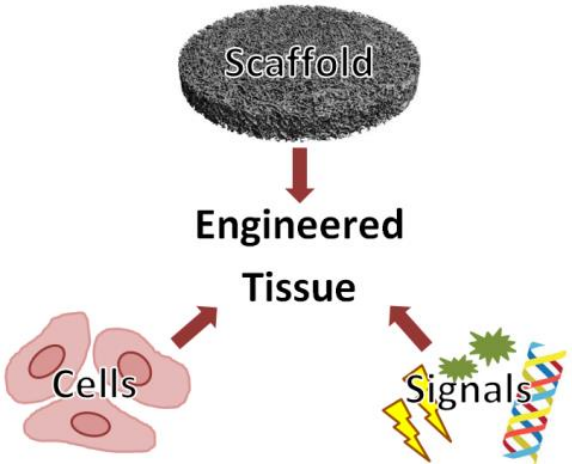

Figure 1.9 Tissue engineering triad
The tissue engineering triad – a combination of scaffolds, cells, and growth factors or signals for the growth and repair of functional tissue

In terms of biocompatibility, the tissue engineered construct must allow for cell infiltration, attachment, proliferation, new matrix production, and tissue remodelling. In addition, to negate the risk of implant rejection, the scaffold, including any of its degradation products, must not elicit an adverse immune response.

The overall purpose of the scaffolds is to allow the body's own cells (or donor cells) to replace it with healthy tissue. Thus, scaffold biodegradability is crucial. Ideally, the rate of tissue repair should match the rate of scaffold degradation and this can often be fine-tuned using crosslinking techniques, depending on material composition.

The architecture of the implanted scaffold is also vital in successful tissue regeneration. An interconnected pore structure and high degrees of porosity are advantageous for cell infiltration and adequate transport of nutrients and waste products throughout the construct. Pore size is also important; an ideal pore size must be large enough to allow cell migration but small enough to allow a large area of surface attachment for cells. Porosity, interconnectivity, and pore size all play a role in avoiding core necrosis of implanted scaffolds due to lack of nutrient/waste transport and vascularisation, an issue faced by the majority of tissue engineered implants.

The mechanical properties of the scaffold should be appropriate for the tissue type to be targeted for regeneration. Traditionally, it was thought that the mechanical properties of the scaffold should be appropriate for the site of implantation and must be able to withstand the natural biological loading of the area. However, it is now generally accepted that it is not the bulk stiffness of the scaffold that is of most importance. In fact, it is the local scaffold stiffness that plays a major role in tissue regeneration, providing cues for cellular attachment, proliferation, and differentiation [85], [86]. That being said, bulk mechanical robustness from the perspective of surgical handling is also essential.

The Tissue Engineering Research Group (TERG) in RCSI have developed a series of highly porous collagen-based scaffolds for the regeneration of a variety of tissues including bone, cartilage, ocular, nerve, cardiovascular, and

respiratory tissues [87]–[91]. Collagen is an ideal scaffolding material as it is a natural, biodegradable material that facilitates cell attachment and migration, and, despite the fact that it is xenographic (bovine origin), it does not elicit a negative host immune response [2]. In bone, it makes up 89 % of the organic matrix and 32 % of the volumetric composition [2].

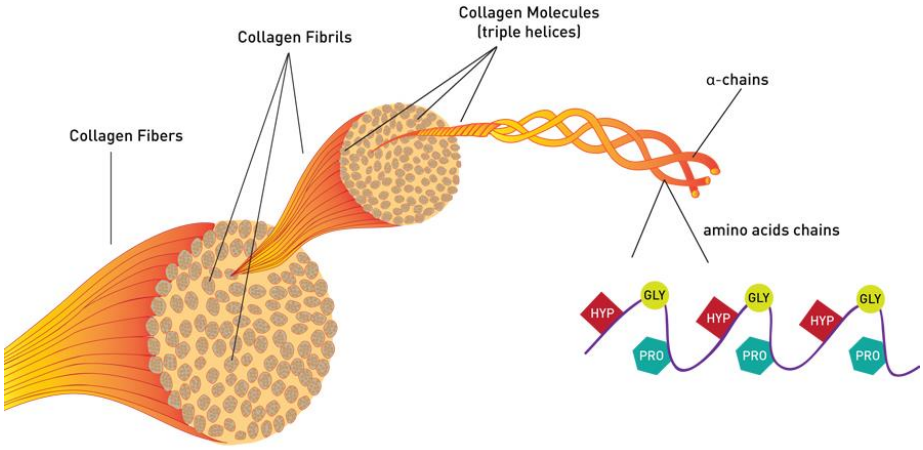

Figure 1.10 Structure of collagen
A triple helical molecule made up of chains of three amino acids, glycine, proline, and hydroxyproline [92]

However, collagen has poor compressive strength in comparison to native bone. Therefore, in scaffolds for bone tissue engineering, collagen is often combined with other materials for structural integrity, such as hydroxyapatite or bioactive glass. The mechanical properties of collagen-based scaffolds can otherwise be enhanced through either physical or chemical crosslinking of the construct.

1.4.1.1 Improving the mechanical properties of scaffolds for orthopaedic applications through crosslinking

Collagen scaffolds lack mechanical strength. Thus, to control both the stiffness and stability or degradation of the scaffolds we propose the use of several methods of both physical and chemical crosslinking in this thesis. Crosslinks are formed between the amino acids of collagen molecules and increase the stiffness of the overall construct by preventing the motion between fibrils within the collagen fibres (**Figure 1.10**) [93].

Dehydrothermal crosslinking

Dehydrothermal (DHT) treatment is a physical crosslinking method which involves heating the scaffolds to a high temperature (105°C) for 24 hrs under a vacuum (0.05 bar). This process forms intermolecular crosslinks between the collagen molecules through a condensation reaction which removes the water from the collagen molecules by either conversion of carboxylic acids to esters (esterification) or by replacing the hydroxyl group in carboxylic acid by an amine (amide formation) (**Figure 1.11**). This method is advantageous for two reasons; it does not involve toxic chemical crosslinkers and it also functions to sterilise the scaffolds before use in cell culture [94], [95]. However, physical crosslinkers cannot achieve as high a yield of crosslinking as chemical crosslinkers [96].

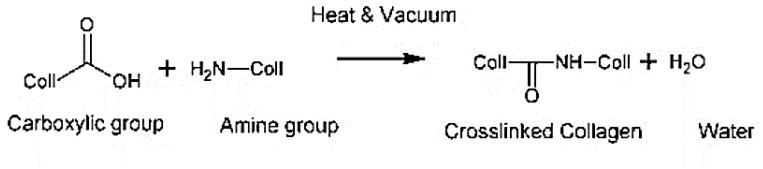

Figure 1.11 Dehydrothermal (DHT) crosslinking reaction
DHT crosslinking treatment produces a condensation reaction between a carboxylic acid group and an amine group in collagen to form a crosslink. Figure modified from [97].

EDAC/NHS crosslinking

The chemical crosslinking method using EDAC/NHS or 1-Ethyl-3-(3-dimethylaminopropyl)carbodiimide (EDAC) and N-Hydroxysuccinimide (NHS) is a commonly used method to crosslink collagen-based scaffolds. EDAC crosslinking forms 'zero length' crosslinks which are chemically the same as those formed during dehydrothermal crosslinking [97] (**Figure 1.12**). Favourably, EDAC does not add any potentially toxic long polymer chains into the collagen structure; however, this means it can only form crosslinks between collagen molecules that are adjacent to one another at a maximum distance of 1 nm apart. The EDAC/NHS reaction produces urea as a bi-product of the reaction, which needs to be removed from the scaffold using several washing steps before use in cell culture or *in vivo* conditions.

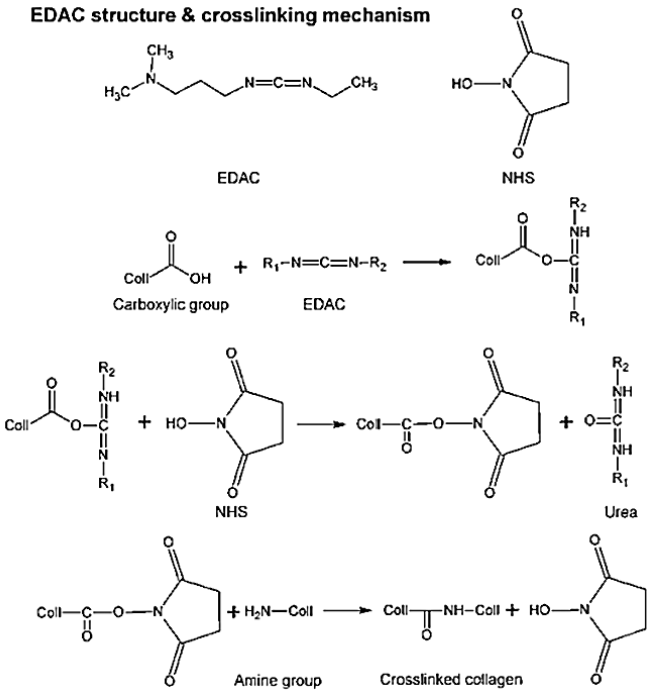

Figure 1.12 EDAC crosslinking reaction
EDAC and NHS crosslinking reaction – first a reaction between a carboxylic acid group and an NHS molecule occurs, followed by a reaction with a free amine group to produce a crosslink. Figure modified from [97].

Later in this thesis, chitosan (a naturally found polysaccharide) is also introduced into the collagen scaffold as both a scaffolding material combined with collagen and for its antimicrobial activities. However, although the chitosan molecule contains amino acid groups, it lacks carboxylic acid groups which make it unsuitable for both DHT and EDAC/NHS crosslinking methods which are commonly used in our lab [98]. Thus, we sought to investigate another crosslinking method which might be suitable for chitosan-chitosan, chitosan-collagen, or collagen-collagen crosslinking: glutaraldehyde crosslinking.

Glutaraldehyde crosslinking

Glutaraldehyde (GTA) is one of the most common crosslinking agents for biomedical materials. It can form covalent polymer crosslinks (relatively long chains) between the aldehyde groups on the glutaraldehyde and the amine groups present on collagen and/or chitosan [97] (**Figure 1.13**). There have been some reports in literature with regards to potential toxicity and calcification of glutaraldehyde crosslinked constructs; however, there are

conflicting views on this [97], [99], [100]. Glutaraldehyde is a versatile crosslinker that can also be used in vapour form to crosslink collagen and/or chitosan. This is advantageous for several reasons including reduced toxicity vs. immersion in liquid glutaraldehyde. This also negates leaching of bioactive ions or molecules loaded into the scaffold construct during crosslinking in liquid solvents [100], [101].

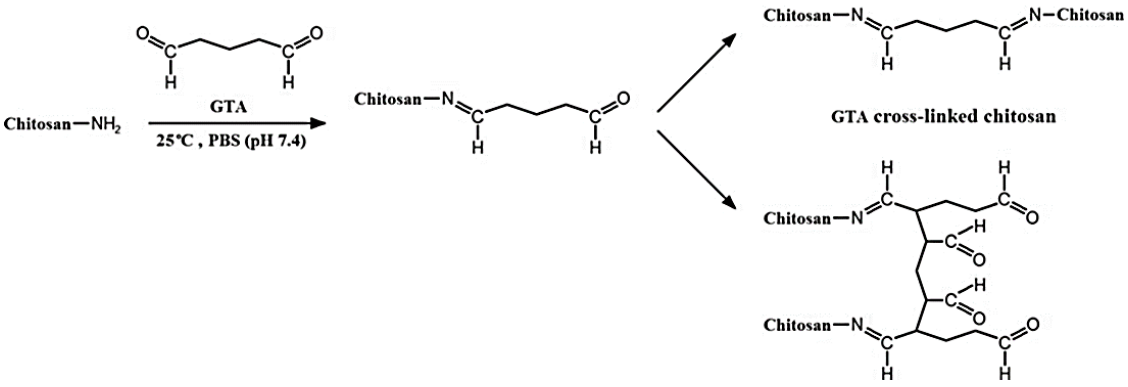

Figure 1.13 Glutaraldehyde crosslinking reaction with chitosan
The aldehyde group on glutaraldehyde reacts with an amine group on either collagen or chitosan to form a crosslink. Figure modified from [98]*.*

Thus, through a range of different crosslinking methods, we have the ability to modify the compressive strength and degradation characteristics of the collagen-based tissue engineered scaffolds developed in our lab. These scaffolds have shown immense tissue regenerative potential and are tuneable to be applied in a host of different areas, e.g. by adding hydroxyapatite for bone repair, elastin for vascular regeneration, or graphene for cardiac repair [88], [102], [103]. We next want to functionalise these scaffolds with non-antibiotic antimicrobials for the treatment of infection, as an alternative to local antibiotic delivery strategies (described in Section 1.4.2). To do so, a range of non-antibiotic antibacterial materials were investigated, namely chitosan, copper, silver, and zinc. The potential of silver-doped hydroxyapatite and copper-doped bioactive glass were also investigated as bi-functional osteogenic and antibacterial agents.

1.4.2 Non-antibiotic antimicrobials

There are a vast number of non-antibiotic materials that demonstrate antimicrobial activity. Some classifications include: peptides (e.g. LL-37 released by the human innate immune system), natural extracts and essential oils (e.g. curcumin derived from turmeric or peppermint oil), polymeric materials (e.g. chitosan), and metals (e.g. copper, silver, and zinc). This thesis focuses on four material categories: chitosan (Section 1.4.2.1), metals (Section 1.4.2.2), and hydroxyapatite and bioactive glass doped with antimicrobial metal ions (Sections 1.4.2.3 and 1.4.2.4, respectively)

1.4.2.1 Chitosan

Chitosan is a natural positively charged linear polysaccharide which is similar in structure to cellulose and is biodegradable, biocompatible, non-toxic, generally recognised as safe (GRAS) by the US Food and Administration (FDA) in some applications. Most importantly from the perspective of this thesis, it displays antimicrobial activity [104]. Chitosan is derived from chitin, most often extracted from the exoskeletons of crab and shrimp (15-40% wt), but can also be derived from the mycelia of fungi [105]. Chitin is the second most abundant natural polysaccharide, after cellulose, and it is estimated that organisms produce up to 100 billion tonnes of chitin annually [106], [107]. Chitin is extremely cost effective as it is harvested from the shells of crab and shrimp which are considered a waste product from the fishing industry. It is a white, hard, inelastic and hydrophobic polysaccharide that is insoluble in water and many organic solvents. Thus, chitin is processed further into chitosan. First, both the calcium carbonate and proteins must be removed to produce pure chitin using usually hydrochloric acid (HCL) followed by sodium hydroxide (NaOH) at an elevated temperature. Demineralisation and deproteinisation can also be carried out using microorganisms and enzymes to digest the mineral and proteins [108].

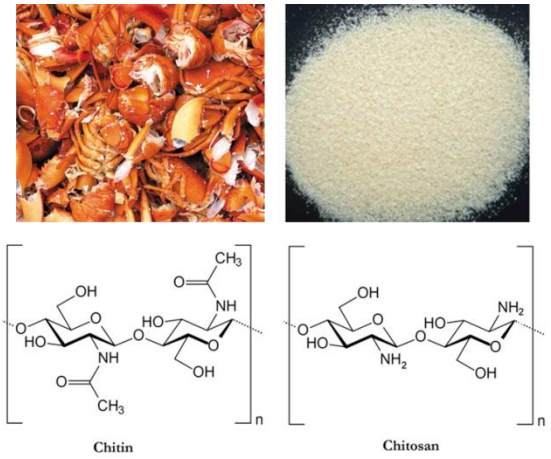

Figure 1.14 Chitosan
Example source (crustacean shells), appearance of chitosan powder, and chemical structure of chitin and chitosan adapted from [107], [109].

Next, the purified chitin is deacetylated (DA) to varying degrees into chitosan using either chemical (alkali deacetylation using NaOH) or enzymatic processes (chitin deacetylase), which can also alter the molecular weight (MW) of chitosan [108]. Chitosan at a DA% lower than 50% mol. becomes soluble in dilute acids such as acetic acid, lactic acid, and HCL. Finally, chitosan can be further processed for tissue engineering purposes and cast into films, freeze-dried into scaffolds, electrospun, and also sprayed into microparticles to regenerate a variety of biological tissues [110]–[113].

In addition to being biodegradable, biocompatible, non-toxic, widely abundant, and cost effective, chitosan also displays broad-spectrum antimicrobial activity against a variety of bacteria and fungi [114]–[116]. There are two main factors that are suggested to increase the antimicrobial activity of chitosan: increasing degree of deacetylation (%DD) due to the increase in positive charge density [116] and reduction in molecular weight [115]. The mechanism of action is debated, but it is attributed to the fact that chitosan is a positive charged and highly viscous molecule that can alter cell wall permeability and nutrient transport or even essentially suffocate the cell by encapsulation [114]–[116]. Chitosan also has excellent metal binding properties as it is a chelating agent and it is often combined with metal ions to increase its antimicrobial activity [117], [118].

In this thesis, chitosan is screened for its antimicrobial activity and effect of mammalian cells (Chapter 2) and it is incorporated into 3D collagen-based scaffolds in Chapter 3.

1.4.2.2 Metals as antimicrobials

A number of metals have been shown to possess antimicrobial properties including copper (Cu), silver (Ag), and zinc (Zn). In contrast to antibiotics, metals are cost effective, do not pose the risk of decomposition, and they can usually be processed at high temperatures and pressures [119]. Metals have even been shown to be potential antimicrobial agents against drug resistant bacteria including methicillin-resistant *S. aureus* (MRSA) and methicillin-resistant *S. epidermidis* (MRSE) [120]. The specific mechanism by which each of these metals destroy microbes is only partially known. Most share several common mechanisms, including ions penetrating the cells and inactivating essential microbial enzymes, while other effects induced by metals include production of reactive oxygen species (ROS), inhibition of the transport of essential ions, prevention of protein synthesis, or causing damage to the cell membrane function [121]. Nanoparticles of these metals possess stronger antimicrobial activity than larger particles due to an increased surface area (and thus increased ion release from the surface) and also demonstrate increased biocompatibility [122]. It is believed that the ions released from metals are mainly responsible for the antimicrobial ability, and not the nanoparticles themselves [123]. In addition to their nanoparticle form, metals are also available as salts. Metal salts are ionic compounds made up of a negatively charged anion and a positively charged cation that dissociate in solution. Therefore, the salt forms of the metals should provide potent antimicrobial activity as they quickly release their ions upon dissolution in water [123]. In this thesis, copper, silver, and zinc are screened for their antimicrobial activity and effect of mammalian cells (Chapter 2) and they are incorporated into 3D collagen-based scaffolds in Chapter 3.

Copper

Copper is a well-known antimicrobial metal that shows activity against gram-positive and gram-negative bacteria and fungi [124]. It is effective in both its bulk and salt forms, with copper chloride being one of the most popular copper salts used in antimicrobial applications [125], [126] (**Figure 1.15**). In terms of the mechanism of action of copper against bacterial cells, it is thought to confer antibacterial activity through three main mechanisms: (1) Accumulation of ions on the bacterial inner membrane that disrupt membrane permeability; (2) generation of reactive oxygen species (ROS) which cause damage to cellular structures; and (3) disruption of deoxyribonucleic acid (DNA) replication [127], [128].

Figure 1.15 Copper element, bulk appearance, copper chloride chemical structure

Copper as an antibacterial agent is most widely used in agriculture as a pesticide in the wine making industry and in organic crop cultivation [129], [130]. Copper has also been investigated as a surfacing material in healthcare settings in place of stainless steel, where the bacterial load on surfaces such as copper bed rails can have a reduced microbial burden by 99% [131], [132] (**Figure 1.16**).

Figure 1.16 Commercial products on the market containing copper for antimicrobial activity
Copper-containing hospital bed handles to reduce bacterial bioburden, copper sulphate as a pesticide in the wine making industry, and copper-containing socks for diabetic feet [133]–[135].

As copper is an essential ion in humans and crucial in many bodily functions including immunity and collagen and bone formation [136], many researchers are examining the beneficial effects of copper on mammalian cells. Research has shown that copper, in addition to showing antimicrobial activity, can stimulate both angiogenesis and vasculogenisis, two essential processes in tissue repair and regeneration [137], [138].

Silver

Silver is the most-widely explored metal in controlling bacterial growth, both in research and application. Silver has been shown to be an effective antimicrobial in both its bulk and salt forms [139], with silver nitrate being one of the most popular silver salts used in antimicrobial applications. Silver, in its various forms, has been shown to be effective against gram-positive and gram-negative bacteria and fungi [122]. It has also been shown to be effective against some drug-resistant bacteria alone [140], [141], and it has shown a synergistic effect when used in combination with antibiotics [142]–[144]. The mechanism of action of silver has been mainly attributed to: (1) the destabilisation of the bacterial cell inner membrane, which results in a loss of potassium ions and a decrease in adenosine triphosphate (ATP) levels due to bonding with phospholipids; (2) interaction with molecules, nucleic acids and enzymes within the cell to disrupt normal metabolism and function and (3) the production of reactive oxygen species (ROS) [145]–[147].

Figure 1.17 Silver element, bulk appearance, and silver nitrate chemical structure

Clinically, silver is currently being used in products including topical creams, wound dressings, and urinary catheters [148]–[150] (**Figure 1.18**). For example, Silvadene Cream® or Flamazine® (Silver sulfadiazine) is widely available on the market, included in the 'WHO Model List of Essential Medicines (EML)', and indicated to prevent sepsis on 2nd-3rd degree burns

[151]. However, a 2013 Cochraine review reported toxic side effects such as sloughing of the wound surface and poor wound healing, in comparison to hydrogel or silver-impregnated dressings such as Acticoat® [152]. Acticoat® is a woven wound dressing which contains nanocrystaline silver used as a barrier for microbial infection [148]. Acticoat® is an attractive option as it has been shown to be effective in reducing wound bioburden and also has a reduced frequency of dressing changes [153]. Additionally, the use of silver ions in urinary catheters has also yielded promising results – a number of large studies and reviews report a significant decline in urinary tract infection occurrence and cost saving as a result [154]–[156].

Figure 1.18 Commercial products on the market containing silver for antimicrobial activity
Antibacterial silver-containing wound dressing Acticaot®, Flamazine® or silver sulfadiazine cream for topical application, and Bardex® silver-containing infection control urinary catheter [150], [157], [158].

Beyond its antibacterial activity, there is little reported in the literature with regards to silver's affect(s) on osteogenesis or angiogenesis. One recent study reports that AgNPs do not impair the ability of hMSCs to be differentiated down an osteogenic lineage when cultured with osteogenic supplements [159], and a second recent study reports that silver nanoparticle based coatings direct hMSCs down an adipogenic lineage [160].

Zinc

Zinc is another commonly used non-antibiotic antimicrobial metal used daily in both bulk nanoparticle form and in salt form (zinc chloride most common) [161]. Zinc shows broad-spectrum antimicrobial activity and is effective against gram-positive and gram-negative bacteria and fungi [162]. In terms of antibacterial activity, zinc behaves similarly to silver: it disrupts the inner cell

membrane function of bacteria, reacts with nucleic acids and enzymes, and also produces reactive oxygen species (ROS) [161], [162].

Figure 1.19 Zinc element, bulk appearance, and zinc chloride chemical structure

Zinc oxide is on the US Food and Drug Administration's (FDA) Generally Recognised as Safe (GRAS) list (21CFR182.8991) for food supplementation [163]. It is widely known that zinc deficiency can impair wound healing [164], [165]. To combat this, researchers have found that the topical application of zinc oxide can improve wound healing; however, zinc sulphate topical application or oral zinc supplementation has been unable to show the same [166]. Zinc oxide is commonly used in topical creams and cosmetics such as Sudocrem®, toothpaste, and suncream [167]–[169] (**Figure 1.20**).

Figure 1.20 Commercial products on the market containing zinc for antimicrobial activity and wound healing
Zinc-containing topical creams Neosporin® and Sudocrem® for antimicrobial activity [170], [171] *and zinc-containing toothpaste and topical cream for sun protection* [172], [173].

In addition to showing antimicrobial activity, zinc plays a central role in a multitude of cellular processes and is essential in immunity and DNA synthesis [174]. In terms of osteogenesis, zinc has been shown to promote osteoblast proliferation and differentiation and to enhance bone formation [175]–[177].

1.4.2.3 Doped-hydroxyapatite

The inorganic matrix of bone is mainly made up of hydroxyapatite crystals (calcium phosphate, $Ca_{10}(PO_4)_6(OH)_2$) – 60-70% of the weight or 40% of the total bone volume [178], [179]. Hydroxyapatite is widely used in bone tissue engineering as it is an osteoconductive material that shows good biocompatibility and biodegradability [2], [180], [181]. The favourable biocompatibility is attributed to the fact that each of the ions which compose these calcium phosphate-based ceramics are commonly found in physiological fluid [182].

Clinically, hydroxyapatite is used either on its own in powdered form added directly into the bone defect as a paste, or as a coating on medical devices to enhance osseous ingrowth and prevent loosening [183]–[187] (**Figure 1.21**). However, bioactive glass and calcium phosphate-based cements such as hydroxyapatite are in fact much stiffer and more brittle than normal bone. Thus, similar to the composition of native bone, they are often combined with polymers (e.g., collagen) for added elasticity and toughness in scaffolds for bone tissue engineering. The addition of hydroxyapatite to tissue engineered scaffolds for bone regeneration has also been shown to increase the stiffness of the constructs, which not only provides greater ease in surgical handling, but also has been shown to increase osteogenic potential and healing capacity [86], [102], [188].

Figure 1.21 Commercially available hydroxyapatite-containing products for enhanced osteogenesis
Corail® hydroxyapatite-coated hip implant for osteointegration, Bio-Oss® bone graft substitute (bovine xenogeneic hydroxyapatite), and Pro Osteon bone graft substitute (hydroxyapatite and calcium carbonate) [184], [185], [187].

The crystals of hydroxyapatite can also be doped with metal ions for desirable effects such as osteogenesis (e.g. strontium) [189], angiogenesis (e.g. cobalt) [190], and antibacterial activity (e.g. silver or zinc) [191], [192], although these remain in research phase. In this thesis, silver-doped hydroxyapatite is investigated as a potential bi-functional antimicrobial and osteogenic material incorporated into collagen scaffolds (Chapter 4).

1.4.2.4 Doped-bioactive glass

Bioglass is an osteoinductive, biocompatible, biodegradable, and FDA approved material that was first developed by Hench et. al. in 1969 [193]. Bioactive glass is usually fabricated from a combination of calcium, phosphorous, silica, and sodium in different ratios. The term Bioglass® was trademarked by the University of Florida and only refers to a specific composition, namely '45S5' (45% Silica and a 5:1 molar ratio between calcium and phosphorus) [194]. Upon implantation in the body, bioactive glass reacts with body fluid and a layer of hydroxyapatite forms on the surface, which can form firm bonds with bone and soft tissue (**Figure 1.22**) [138], [193]. Growth factors, blood proteins, and collagen are thought to readily bind to the apatite layer and cellular attachment follows [195]. Osteoprogenitor cells are then differentiated into osteoblastic cells due to the hydroxyapatite stimulus and bone formation occurs.

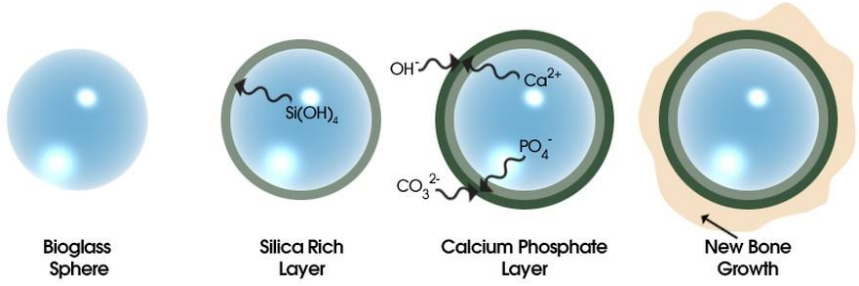

Figure 1.22 Bioactive glass reaction with body fluid
Formation of calcium phosphate (hydroxyapatite) layer on the surface of bioactive glass in body fluid [196]

Bioactive glass is commonly used clinically to heal bone defects in facial reconstruction, dentistry, in benign bone tumour treatment, and osteomyelitis treatment. Bioactive glass can be used in the form of plates and granules in a

range of sizes and shapes, all with favourable postoperative bone defect healing results [197] (**Figure 1.23**).

Figure 1.23 Commercially available bioactive glass products for enhanced osteogenesis
NanoFUSE bioactive matrix (demineralised bone combined with 45S5 Bioglass®) and BonAlive granules (S53P4 bioactive glass) and putty (S53P4 bioactive glass, PEG, and glycerol) for enhanced osteogenesis [198], [199].

Like hydroxyapatite, elements can be substituted into the silica network for enhanced bioactivity including stimulation of angiogenesis [190], bone formation [200], and – most importantly in this application – antimicrobial activity [137], [138], [201], although these remain in research phase also. In this thesis, copper-doped bioactive glass is investigated as a potential multi-functional antimicrobial, angiogenic, and osteogenic material incorporated into collagen scaffolds (Chapter 5).

1.5 Thesis Objectives/Aims

The primary goal of the research presented in this thesis was to develop a series of collagen-based non-antibiotic antimicrobial scaffolds for the treatment of osteomyelitis. To achieve this, we sought to screen a number of reported non-antibiotic antimicrobial materials and incorporate them into collagen-based scaffolds and analyse their effect on antibacterial activity and osteogenesis. To accomplish this, the specific objectives of the thesis were as follows:

1) To screen a set of non-antibiotic antibacterial materials (chitosan, copper, silver, and zinc) and examine their antibacterial activity, while minimising mammalian cell toxicity (Chapter 2)

2) To incorporate the antimicrobials selected from the screening process in Chapter 2 into 3D collagen-based scaffold platforms at bioactive concentrations. The antimicrobials were incorporated via both direct incorporation and through a microparticle delivery system and the *in vitro* ability of the scaffold to support cell viability, osteogenesis, and angiogenesis (Chapter 3)

3) To fabricate antimicrobial silver-doped hydroxyapatite and incorporate it into 3D collagen-based scaffolds, examine its effect on scaffold structural/mechanical properties, and assess the scaffold's antibacterial activity and the *in vitro* ability of the scaffold to support cell viability and osteogenesis (Chapter 4)

4) To fabricate 3D antimicrobial collagen- copper-doped bioactive glass scaffolds, examine the effect of bioactive glass incorporation on scaffold structural and mechanical properties, and assess the scaffold's antibacterial activity, and the *in vitro* ability of the scaffold to support cell viability and osteogenesis. In addition, the most favourable scaffolds were assessed for their effect on angiogenesis and osteogenesis in a chick embryo *in vivo* model new to our laboratory (Chapter 5)

Chapter 2 Effect of non-antibiotic antimicrobial materials on bacterial and mammalian cells in a 2D environment

2.1 Introduction

Minimal new antibiotic discoveries combined with an alarming number of emerging cases of microbial resistance to 'last resort' antibiotics is threatening our ability to treat infections such as osteomyelitis and has driven research to focus on discovering and developing non-antibiotic antimicrobials.

There are a vast number of non-antibiotic materials that demonstrate antimicrobial activity including peptides (e.g. LL-37 released by the human innate immune system), natural extracts and essential oils (e.g. curcumin derived from turmeric or peppermint oil), polymeric materials (e.g. chitosan), and metals (e.g. copper, silver, and zinc). Chitosan is a natural polysaccharide that is widely-abundant, cost-effective, biodegradable, biocompatible, and shows antimicrobial activity. Chitosan's antimicrobial activity is suggested to be affected by the degree of deacetylation (%DD) and the molecular weight [115], [116].

Metals have been widely-used throughout history as antimicrobial materials. The most popular metals examined are copper (Cu), silver (Ag), and zinc (Zn) in either their bulk-form or in salt form. For bulk metals, reducing particle size generally increases antimicrobial activity due to an increased surface area [122] as metals owe the majority of their antimicrobial ability to the ions released from their surface [123]. As metal salts are ionic compounds that dissociate in solution, they may provide potent antimicrobial activity as they quickly release their ions upon dissolution in water [123]. In this chapter, the aim is to compare and contrast metals in their bulk nanoparticle and salt forms in terms of antibacterial activity and their effect on the viability of mammalian cells. In terms of the mechanism of action of metals against bacterial cells, copper, silver, and zinc are all thought to confer antibacterial activity through three main mechanisms: 1) Accumulation of ions on the bacterial inner membrane, disrupting membrane permeability and decreasing ATP levels due to phospholipid binding; 2) production of reactive oxygen species (ROS) which cause damage to internal cellular structures including nucleic acids and enzymes; and 3) disruption in DNA replication [26], [127], [128], [145]–[147], [162]. There has been a rapid increase in the use of silver as an antibacterial

agent recently. It is being utilised in topical creams, medical device coatings and bandages, and antibacterial textiles and glass [149], [157], [202], [203]. However, beyond its antibacterial activity, there is little reported in the literature with regards to silver's affect(s) on osteogenesis or angiogenesis. On the other hand, copper and zinc are both essential ions of the human body, regulating immunity, DNA synthesis, collagen, and bone formation [136], [174]. Additionally, copper has been shown to stimulate angiogenesis and vasculogenesis and both copper and zinc can stimulate osteogenesis [137], [138], [175]–[177].

In order to assess the antibacterial potential of new materials, a screening process must be employed which is simple, reproducible, both time and cost effective, and that allows for high throughput screening of a number of antibacterial materials at a range of concentrations [204]. For antibacterial agent screening, the most commonly utilised *in vitro* methods for such are agar diffusion and broth dilution methods. Agar diffusion methods are semi-quantitative at best, but give a good initial idea as to whether a material displays antibacterial activity, or not. Broth dilution methods are fully quantitative methods whose outputs can allow us to determine the minimum inhibitory concentration (MIC) of the antibacterial substance. The MIC of compounds being examined may be reported in the existing literature, however there is no standardised methodology used across publications and there is often much variety in terms of bacterial strains, inoculum preparation and size, growth media choice, and incubation conditions, thus, a screening process is necessary [204]. The use of 2D screening is also advantageous to allow for quick and cost-effective screening for mammalian cell viability. This is because of the disadvantage with the majority of antibacterial materials, including antibiotics, is that there is a trade-off between bacteria-killing ability and toxic effects in the body, so the dosage level is critical [205]–[209].

The overall aim of the study presented in this chapter was to identify the optimal dosage concentration of chitosan, copper, silver, and zinc that will effectively kill bacteria, while maintaining acceptable mammalian cell viability in a 2D environment. This will inform the studies in Chapter 3 where the

materials will be incorporated into a 3D scaffold at biologically relevant concentrations. Thus, the specific objectives of this chapter were to:

1) Characterise the bacterial strains to be used throughout the thesis
2) Investigate chitosan as a potential treatment agent for osteomyelitis by identifying the optimal molecular weight and concentration of chitosan to maximise antibacterial activity and mammalian cell viability
3) Investigate a series of metals as potential treatment agents for osteomyelitis by identifying the optimal concentrations of the metal nanoparticles (copper, silver, and zinc oxide) and metal salts (copper chloride, silver nitrate, and zinc chloride) to maximise antibacterial activity and mammalian cell viability *in vitro*
4) Investigate and compare the ion release from the metal nanoparticles and their metal salts
5) Select the most effective antibacterial materials to incorporate into 3D scaffolds in biologically relevant concentrations in Chapter 3

2.2 Materials and methods

Staphylococcus aureus (*S. aureus*), *Staphylococcus epidermidis* (*S. epidermidis*), and *Escherichia coli* (*E. coli*) were the bacteria species chosen in this chapter. It was decided to include the gram-negative bacteria *E. coli* in the study as – although it is only responsible for a small proportion of osteomyelitis infections – if a material is deemed to be effective against both gram-positive and gram-negative bacteria it would demonstrate the potential for use in a wide range of other infection applications. The specific strains of bacteria used were *S. aureus* Newman, *S. epidermidis* HB, and *E. coli* CFT073, all of which are clinical isolates from osteomyelitis infections or bacteraemia received from Prof. Timothy Foster and Dr. Stephen Smith, Trinity College Dublin.

An antibacterial agent is deemed either bacteriostatic, if it prevents the growth of bacteria, or bactericidal, if it kills bacteria. The minimum inhibitory concentration (MIC) of an antibacterial agent is the concentration required to stop the growth of bacteria. The minimum bactericidal concentration (MBC) is the concentration required to kill bacteria. Low MIC and MBC concentrations are desirable as there is typically a trade-off between bacteria killing and mammalian cell toxicity. A bacteria concentration of $5x10^5$ colony forming units per ml (CFU/ml) is used throughout the thesis as an initial inoculation number for assays as specified by the Clinical and Laboratory Standards Institute (CLSI) [210].

MC3T3-E1 cells are a well-studied pre-osteoblast cell line, originally derived from mouse (C57BL/6) calvaria , that have the ability to differentiate into both osteoblasts and osteocytes [211]–[213]. Only MC3T3-E1 subclones 4 and 14 have been shown to mineralise the collagenous extracellular matrix [214]. MC3T3-E1 subclone 4 cells have been used in this thesis as they have been shown previously to have the highest osteogenic potential, showing upregulated bone markers such as osteocalcin (OCN), bone sialoprotein (BSP), alkaline phosphatase (ALP), and parathyroid hormone (PTH)/parathyroid hormone-related protein (PTHrP) [214]–[216]. Although MC3T3-E1 cells are an immortalised cell line, as with many cell lines, there

are limitations to the number of passages the cells can undergo before irreversible changes in cell behaviour and morphology. One study has reported that passaging MC3T3-E1 cells >65 times in comparison to those which are <20 changes the cell morphology, reduces osteoblast function, and reduces osteoblast differentiation [217]. Another study which looked at the same cells but at a number of different passages found that the mineralisation capacity of MC3T3-E1s diminishes at passages >34 [215]. Thus, throughout this thesis, the MC3T3-E1 cells used have not been passaged further than passage 30 (P30).

2.2.1 Characterisation of the bacteria strains to be used throughout the thesis

The relationship between the optical density (OD) of a bacterial suspension and the number of colony forming units per ml (CFU/ml) was evaluated in order to relate the opacity of the bacterial sample to the number of colony forming units. This was then used throughout the rest of the thesis to rapidly convert from OD to CFU/ml [218], [219]. A 1 ml vial of either *S. aureus*, *S. epidermidis*, or *E. coli* was added to a conical flask with 50 ml Brain Heart Infusion (BHI) broth (Sigma Aldrich Ireland, product #53286). The flask was incubated at 37°C in a shaking incubator at 225 rpm. At regular time intervals, a sample was removed from the flask and the optical density was measured using a spectrophotometer (Victor3 1420-012, Perkin Elmer, USA). The number of CFU/ml in the sample was then determined by using the using the Miles and Misra method [220]. Briefly, the sample was serially diluted (1:10 dilutions) until an estimated solution of 1 CFU/ml was obtained (approx. 8 dilutions). 10 µl of the dilutions were plated on BHI agar plates (Sigma Aldrich Ireland, product #70138) divided into sections and the plates were inverted and incubated for 18-24 hrs (**Figure 2.1**). The sections with the highest countable number of colonies between 2-20 were counted (considered statistically robust). The number of colony forming units per ml can then be calculated by multiplication. This was repeated in triplicate for the three bacteria species.

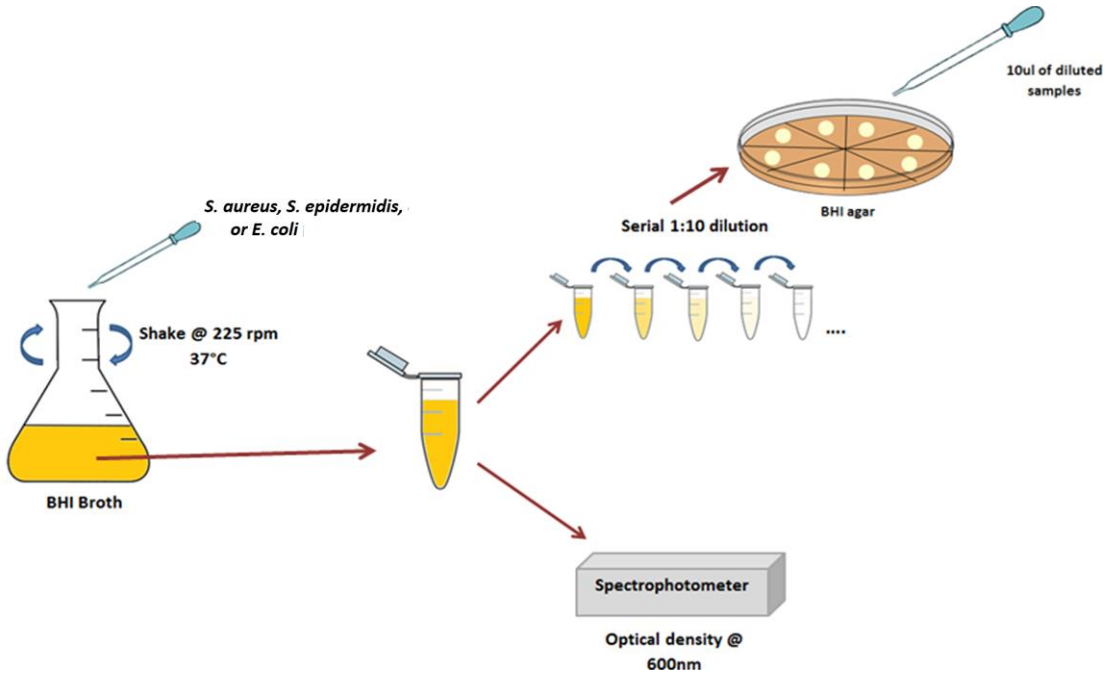

Figure 2.1 Schematic of protocol to characterise* S. aureus*, S. epidermidis, and* E. coli*.
A small volume of bacterial culture suspension was removed at regular time intervals and the optical density was measured using a spectrophotometer. Bacterial colonies were counted after incubation for 24 hrs at 37°C.

2.2.2 Identification of the optimal concentration of chitosan to maximise antibacterial activity and osteoblast viability

In order to identify the optimum concentration of chitosan required to maximise the ratio between mammalian viability/bacteria killing, the effect of a range of concentrations of chitosan on the viability of osteoblasts and the bacteria *S. aureus*, *S. epidermidis*, and *E. coli* were examined. The effect of changing the molecular weight of chitosan was also examined, as it has been suggested in the literature to affect its antibacterial activity [115]. Note: Chitosan was dissolved in 1% (v/v) acetic acid (Sigma Aldrich Ireland, CAS #64-19-7) throughout the thesis.

2.2.2.1 Antibacterial activity of chitosan

First, it was investigated whether low molecular weight chitosan (50,000-190,000 Da) (Sigma Aldrich Ireland, product #448869) or medium molecular weight chitosan (190,000-310,000 Da) (Sigma Aldrich Ireland, product #448877) would have higher antibacterial activity. Briefly, melted BHI agar was

mixed with either low or medium molecular weight chitosan and poured into Petri-dishes and allowed to set at room temperature to produce composite chitosan/BHI agar. Next, $5x10^5$ CFU/ml of *S. aureus* Newman was spread on the surface of the agar and the plate was incubated, inverted, at 37°C for 18-24 hrs [221]. The number of colony forming units on the low and medium molecular weight chitosan/BHI agar plates were compared (**Figure 2.2**). From this, low molecular weight chitosan was selected for all further experiments.

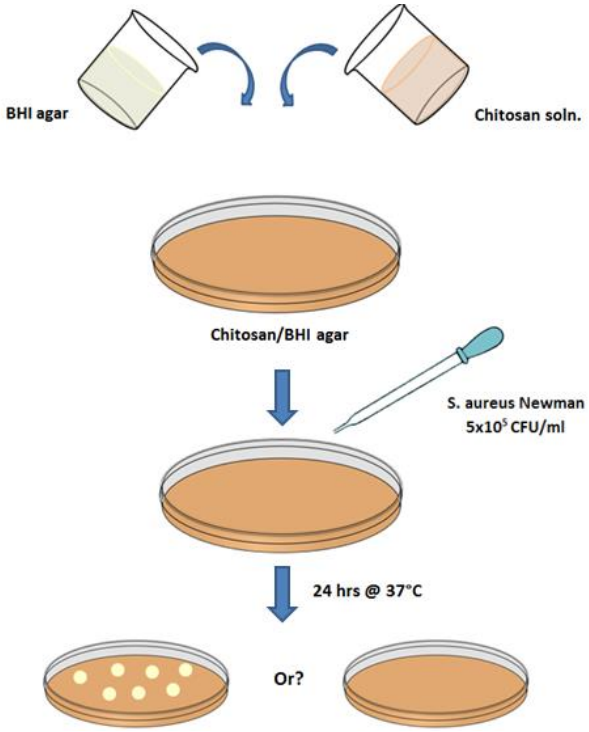

***Figure 2.2 Schematic of protocol to compare toxicity of low vs. medium molecular weight chitosan against* S. aureus**
Either low or medium molecular weight chitosan (at a number of different concentrations) was combined with liquid agar and allowed to set. The plates were lawned with S. aureus *and inspected for bacterial growth after an overnight incubation.*

Secondly, the minimum inhibitory concentration (MIC) of low molecular weight chitosan and whether it was bacteriostatic (prevents the growth of bacteria) or bactericidal (kills bacteria) at these concentrations was investigated. To determine the MIC of low molecular weight chitosan, a solution of chitosan was serially diluted (1:2) from 7.5 mg/ml to 0.23 mg/ml and 0.5 ml of the solutions were mixed with 0.5 ml of BHI broth and added to 15 ml falcon tubes. The solutions were inoculated with $5x10^5$ CFU of *S. aureus*, *S. epidermidis*, or *E. coli* and incubated at 37°C for 18-24 hrs (**Figure 2.3**). This was repeated in

triplicate for the three bacteria species. To determine whether chitosan demonstrates bacteriostatic or bactericidal activity, swabs from the solutions without visual bacteria growth were streaked on fresh BHI agar plates and tested for bacterial growth.

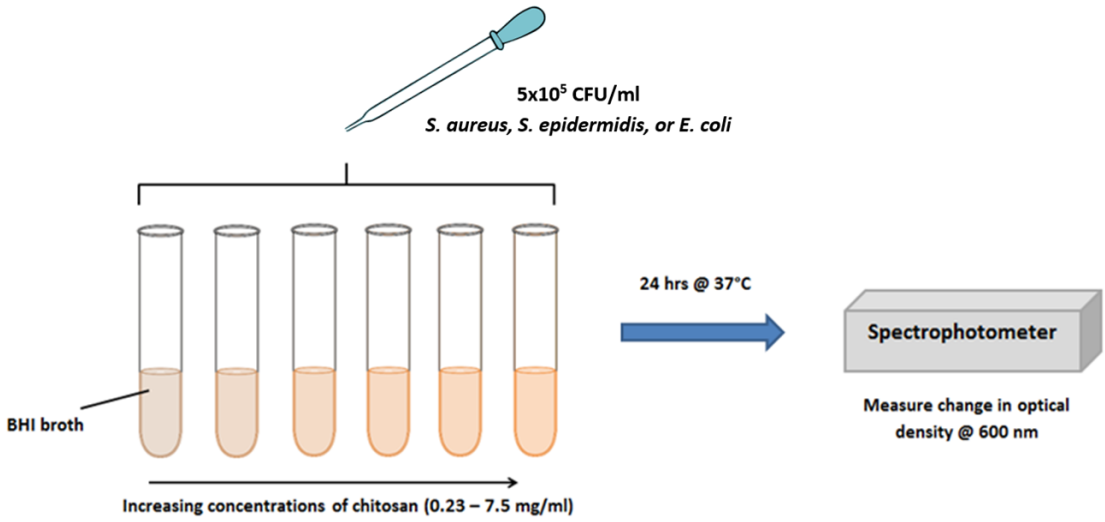

***Figure 2.3 Schematic of protocol to measure the minimum inhibitory concentration (MIC) of chitosan against* S. aureus, S. epidermidis, *and* E.coli**
Solutions of increasing concentrations of chitosan in BHI broth were inoculated with S. aureus, S. epidermidis*, or* E. coli*. After a 24 hr incubation period, the bacterial growth was quantified by monitoring the change in optical density of the solutions using a spectrophotometer.*

2.2.2.2 Effect of chitosan on osteoblast viability

Having determined the effect of chitosan on bacterial cells, we next sought to determine its effect on mammalian cells. Chitosan in the form of films were used here as an appropriate 2D surface to culture cells. Films were fabricated by casting 5 ml solutions of 2% chitosan in 1% acetic acid into wells of a 6-well plate and allowing to dry at room temperature under laminar flow for 72 hrs. Films were then washed in 100% ethanol and followed by phosphate buffered saline (PBS). The films were seeded with $3.2x10^4$ osteoblasts (MC3T3-E1, European Collection of Authenticated Cell Cultures, Product #99072810) cells/cm^2 and incubated under regular mammalian cell culture conditions (37°C, 5% CO_2, humidified atmosphere) for 24 hrs. Uncoated wells were used as a positive control. The effect of chitosan films on osteoblast viability was then examined using a PicoGreen® assay as per the

manufacturer's instructions (Quanti-iT™ PicoGreen dsDNA, Molecular Probes, OR, USA) (**Figure 2.4**).

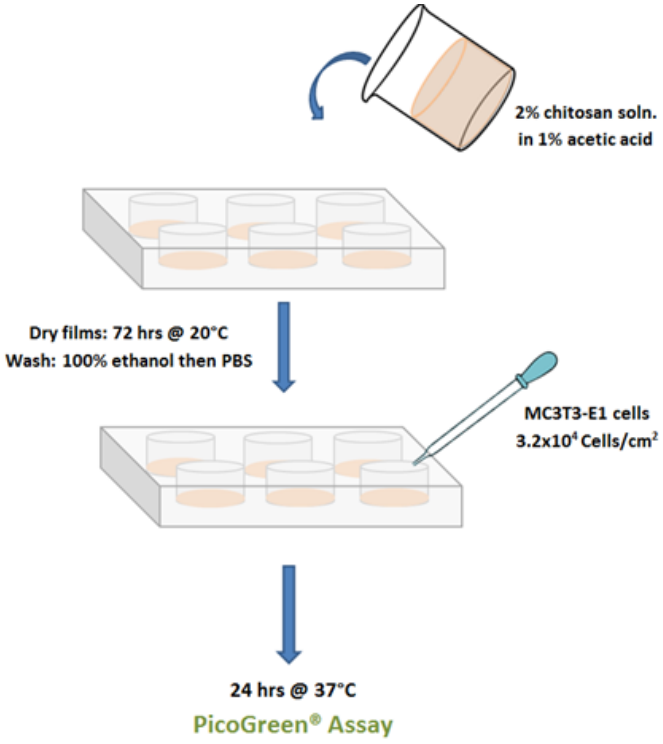

Figure 2.4 Schematic of protocol to assess the effect of chitosan on mammalian cell viability
Chitosan films were formed by solvent evaporation at room temperature for 72 hrs. After sterilising and washing, the films were seeded with MC3T3-E1 osteoblasts. The cells were cultured on the films for 24 hrs before a PicoGreen assay was performed.

2.2.3 Identification of the optimal concentrations of the metal nanoparticles and metal salts to maximise antibacterial activity and osteoblast viability

In order to identify the optimum concentration of the metal nanoparticles to maximise the ratio between mammalian viability/bacteria killing, the effect of a range of concentrations of the metal nanoparticles copper, silver, and zinc oxide or metal salts copper chloride, silver nitrate, and zinc chloride on the viability of osteoblasts and the bacteria S. aureus, S. epidermidis, and E. coli were examined. The metal nanoparticles were utilised as similar as possible in size in order to solely assess the effect of the different metal types on antibacterial activity, eliminating the size variable, which is known to affect antibacterial activity. The properties of the metal nanoparticles are summarised in **Table 2.1**.

Table 2.1 *Properties of metal nanoparticles examined*

	Copper (Cu)	Silver (Ag)	Zinc Oxide (ZnO)
Size	60 – 80 nm	<100 nm	<100 nm
Density	8.92 g/cm^3	10.49 g/cm^3	5.61 g/cm^3
Capping agent	-	polyvinylpyrrolidone (water soluble)	-

2.2.3.1 Antibacterial activity of metal nanoparticles and metal salts

The MIC of the metal nanoparticles and metal salts against the three bacterial strains was investigated. Briefly, suspensions of metal nanoparticles or solution of metal salts were created in 1 ml BHI broth in 15 ml falcon tubes at a range of different concentrations (**Figure 2.5**). The solutions were inoculated with 5x10^5 CFU of *S. aureus*, *S. epidermidis*, or *E. coli* and incubated at 37°C for 18-24 hrs. The MIC values reported were those that were visually clear from microbial growth. This was repeated in triplicate.

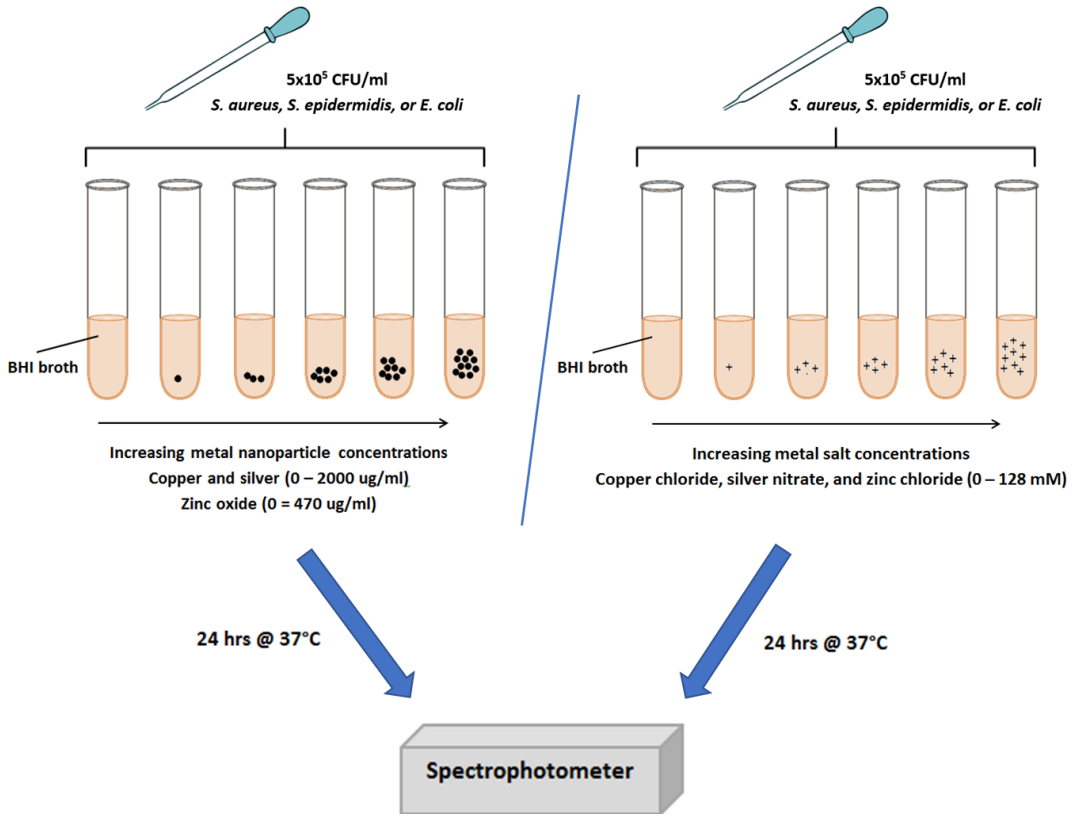

***Figure 2.5 Schematic of protocol to examine the toxicity of metal nanoparticles and metal salts against* S. aureus, S. epidermidis*, and* E. coli**
Solutions of increasing concentrations of either the metal nanoparticles or metal salts in BHI broth were inoculated with S. aureus, S. epidermidis, *or* E. coli*. After a 24 hr incubation period, the bacterial growth was quantified by monitoring the change in optical density of the solutions using a spectrophotometer.*

Additionally, as the metal salts proved to be the most effective antibacterial agents, the MBC of the metal salts was investigated: 10 µl of the solutions from the remaining visually clear wells were added to BHI agar plates, allowed to air dry for 15 minutes, and incubated for 18-24 hrs at 37°C. The lowest concentration on the solutions that did not show any growth was termed the MBC of the salt. This was repeated in triplicate for the three bacteria species.

2.2.3.2 Effect of metal nanoparticles and metal salts on osteoblast viability

The effect of the metal nanoparticles and metal salts on mammalian cell viability was examined using a PicoGreen® assay. Briefly, MC3T3-E1 cells were seeded in a 96 well plate at a density of $3.2x10^4$ cells/cm^2 and incubated for 24 hrs at 37°C. The media was removed from the cells and 100 µl of media containing metal nanoparticles or metal salts in various concentrations (**Table 2.2**) were added.

Table 2.2 *Concentrations of metal nanoparticles and salts used for mammalian cell viability assay*

Metal nanoparticle	**Concentration**
Copper (Cu)	0, 10, 100, 500, 1000, 2000 µg/ml
Silver (Ag)	0, 10, 100, 500, 1000, 2000 µg/ml
Zinc oxide (ZnO)	0, 30, 160, 230, 310, 470 µg/ml
Metal salt	**Concentration**
Copper chloride ($CuCl_2$)	0, 1, 8, 16, 32, and 64 mM
Silver nitrate ($AgNO_3$)	0, 1, 8, 16, 32, and 64 mM
Zinc chloride ($ZnCl_2$)	0, 1, 8, 16, 32, and 64 mM

The cells were incubated for a further 24 hrs at 37°C. The solutions were then removed from the cells and they were washed 2 times in PBS. Cells were lysed using carbonate buffer (100 µl of 0.2 M sodium carbonate with 1% Triton) (Sigma Aldrich Ireland, CAS Number: 497-19-8 and 9002-93-1, respectively) and three freeze-thaw cycles and then a PicoGreen® assay was performed

with appropriate controls as per the manufacturer's instructions (Quanti-iT™ PicoGreen dsDNA, Molecular Probes, OR, USA).

2.2.4 Investigation and comparison of the ion release from the metal nanoparticles and their metal salts

Having determined the effect of the metal nanoparticles and metal salts on the viability of bacterial and mammalian cells (<24 hrs), we sought to investigate the temporal ion release profiles from metal nanoparticles and their metal salts. Metal ions in solution can be quantified using atomic absorption spectroscopy (AAS) (Dublin Institute of Technology, Dublin, Ireland). In short, atoms of different elements emit different wavelengths of light. AAS atomises the sample to be analysed using a flame, the absorbed wavelengths are measured, and the amount of light absorbed is proportional to the amount of the element in the sample. Briefly, equal masses of either metal nanoparticles or metal salts (20 mg) were added to deionised water and incubated in a water bath at 37°C. At days 1, 2, 3, and 7 the solutions were centrifuged, and the supernatant was analysed for metal ion content using AAS (**Figure 2.6**). This was repeated in triplicate.

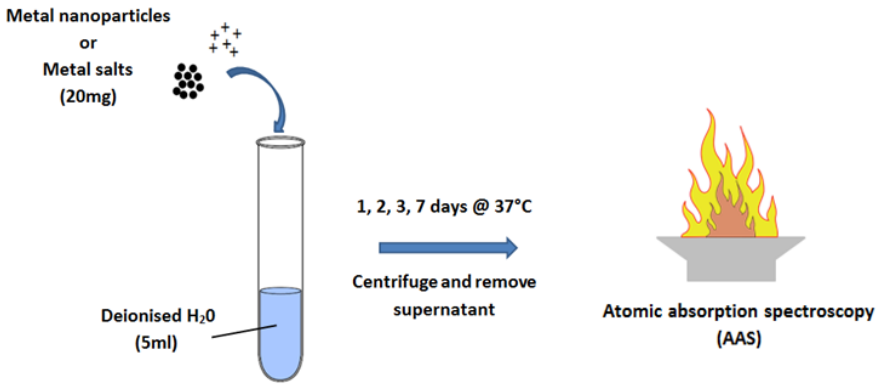

Figure 2.6 Schematic of protocol to compare ion release from metal nanoparticles and metal salts
The ions released from solutions of either metal salts or metal nanoparticles were quantified over 1-7 days using atomic absorption spectroscopy.

2.2.5 Statistical analysis

Data are presented as mean ± standard deviation. Statistical analysis was performed using GraphPad Prism software. Two-tailed unpaired t-tests or one-way or two-way ANOVAs were conducted where appropriate followed by a

Bonferroni post-hoc test for multiple pairwise comparisons between groups. A p-value of 0.05 or less was considered statistically significant ($p \leq 0.05$). The Pearson product correlation coefficient (r) was used to determine the strength and direction of a linear relationship. An r value of 0.7-1 was considered a strong positive correlation. Three biological and three technical repeats were performed for all experiments and assays.

2.3 Results

2.3.1 Bacterial strains growth curves

When examining the activity of antibacterial agents in solution, a rapid method to determine activity is to measure the optical density (OD), or turbidity, of the solution spectrophotometrically using a plate reader. However, the relationship between a range of optical densities of each bacteria species being examined and the corresponding number of colony forming units per ml (CFU/ml) must first be established. Thus, this relationship along with the growth curves for each of the species was examined. The relationship between optical density and colony forming units per ml are approximately linear up to OD=1 for all of the bacteria strains (**Figure 2.7**). After this, as optical density increases, the number of colony forming units only slowly increases. The information obtained from these experiments were then used throughout the rest of the thesis to efficiently convert from optical density readings to colony forming units per ml.

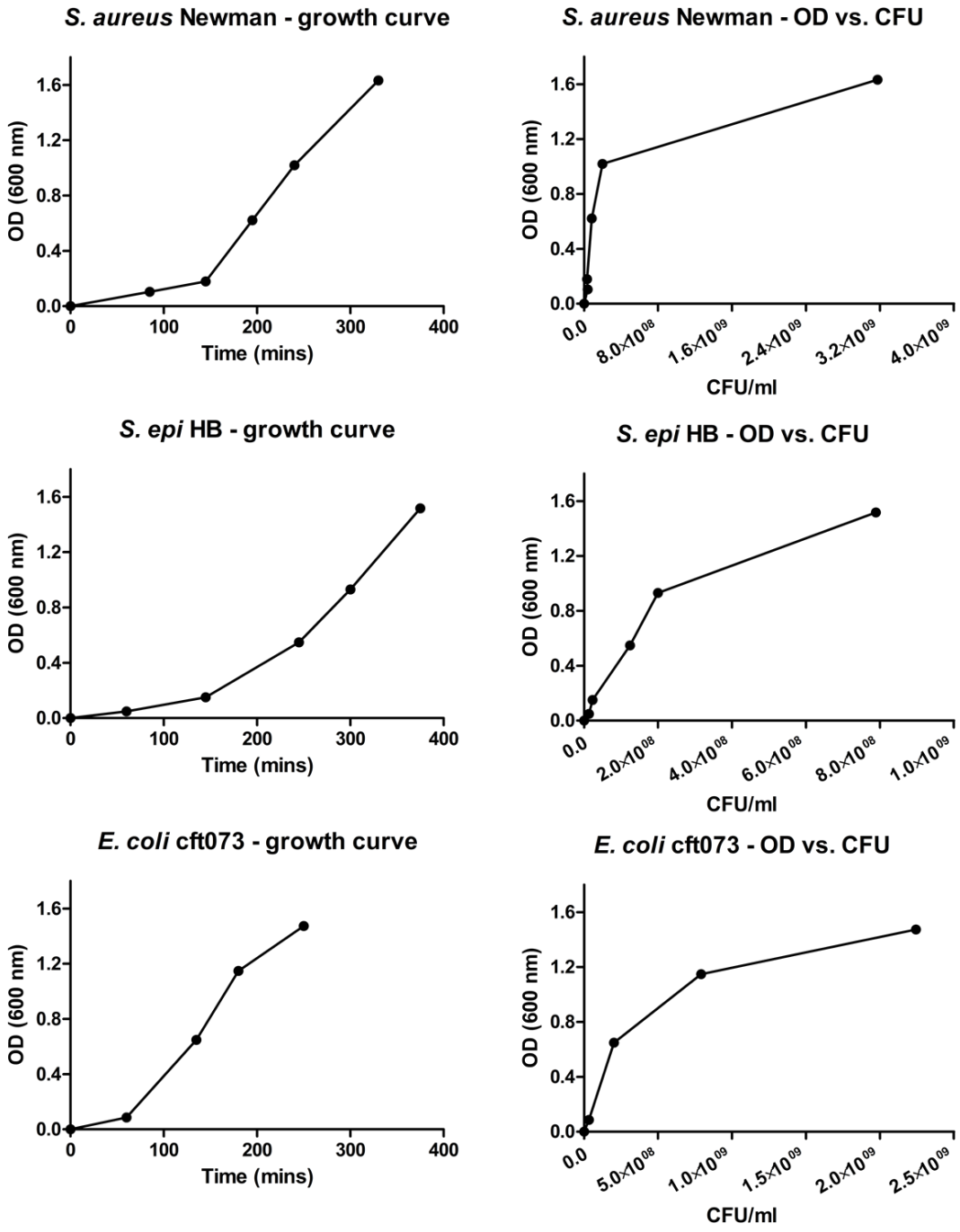

***Figure 2.7 Growth curve for* S. aureus, S. epidermidis*, and* E. coli**
Growth curve (left) and the relationship between optical density (OD) and colony forming units per ml (CFU/ml) (right) for S. aureus, S. epidermidis, *and* E. coli*. Note the approximately linear relationship between OD and CFU/ml up to OD=1. Representative curves from n=3 repeats shown.*

2.3.2 Identification of the optimal concentration of chitosan to maximise antibacterial activity and osteoblast viability

2.3.2.1 Chitosan shows bacteriostatic antibacterial activity against *S. aureus, S. epidermidis,* and *E. coli*

First, we examined whether the molecular weight of chitosan had an effect on antibacterial activity by comparing low molecular weight (LMW) or medium molecular weight (MMW) chitosan incorporated into agar plates against *S. aureus*. The results demonstrate that low molecular weight chitosan shows superior toxicity against *S. aureus* in comparison to medium molecular weight, as shown by the absence of bacterial growth on both the 7.5 mg/ml and 10 mg/ml LMW plates vs only the 10 mg/ml MMW plates (**Figure 2.8**). Low molecular weight chitosan was selected to be used throughout the remainder of the thesis due to its increased antibacterial activity.

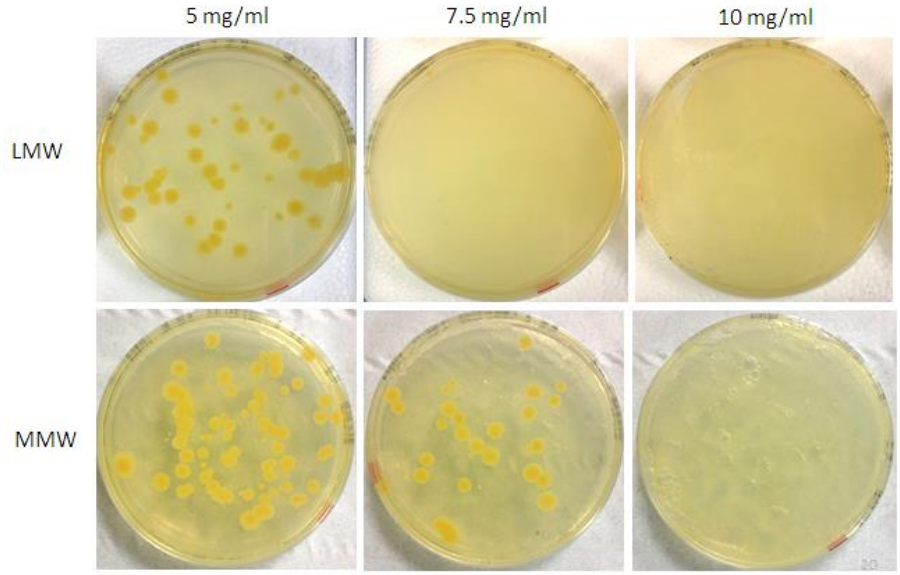

Figure 2.8 Low vs medium molecular weight chitosan
Agar incorporated with low molecular weight (LMW) (top) and medium molecular weight (MMW) (bottom) chitosan at a range of concentrations (5, 7.5, and 10 mg/ml) after 7 days of culture. Note the absence of S. aureus *colonies on the 7.5 and 10 mg/ml LMW agar and 10 mg/ml MMW agar.*

Next, the minimum inhibitory concentration (MIC) of low molecular weight chitosan solutions against *S. aureus, S. epidermidis*, and *E. coli* were investigated. For all three bacteria species, increasing the concentration of chitosan increased antibacterial activity and the MIC was found to be 1.88 mg/ml for all (**Figure 2.9** A-C). To determine whether this antibacterial action

was bacteriostatic (prevented the growth of bacteria) or bactericidal (killed the bacteria), swabs from the solutions that were visually clear of microbial growth were streaked on agar plates and incubated for a further 24 hrs. The results demonstrate the bacteriostatic action of chitosan at these concentrations, due to the growth of bacteria from the solutions ≥MIC concentrations (**Figure 2.9** D).

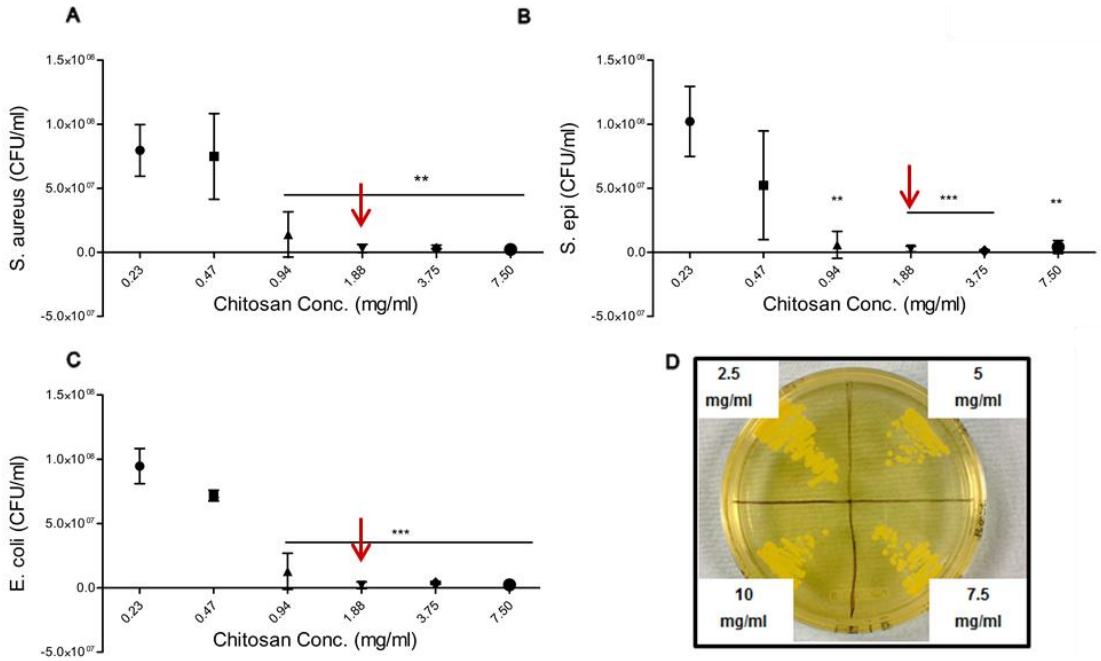

Figure 2.9 Antibacterial activity of chitosan
Antibacterial activity of chitosan against (A) Staphylococcus aureus (S. aureus), *(B)* Escherichia coli (E. coli), *and (C)* Staphylococcus epidermidis (S. epidermidis), *and (D) swabs from chitosan solutions visually clear of bacteria growth showing the bacteriostatic action of chitosan. Note: red arrows indicate the MIC value identified by visually inspecting the assay (All = 1.88 mg/ml). Data presented as mean ± SD, n=3, p-values are calculated using one-way ANOVA with Bonferroni post-hoc test. All statistical significance shown in comparison to lowest chitosan conc. unless otherwise stated, *p < 0.05, **p < 0.01, ***p < 0.001.*

2.3.2.2 Osteoblast viability is decreased on 2D chitosan films

To determine the effect of chitosan on the viability of osteoblasts, MC3T3-E1 cells were cultured on chitosan films for 24 hrs and the number of viable cells was measured with a PicoGreen® assay. Cells cultured on chitosan films saw a decrease in cellular viability, however, the films maintained 47% of the cells when compared to the positive tissue culture plastic control (*p < 0.05) (**Figure 2.10**).

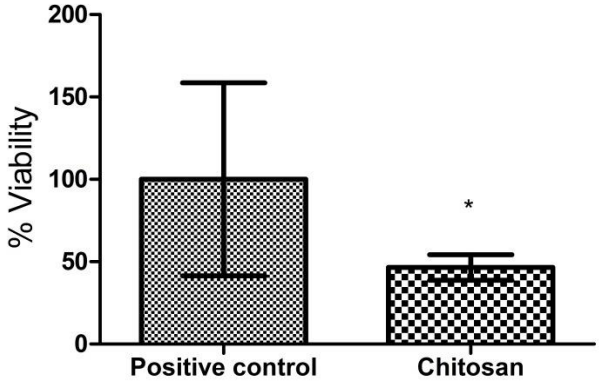

Figure 2.10 Effect of chitosan on mammalian cell viability
*Percentage viability of MC3T3-E1 cells cultured on chitosan film normalised to positive control using a PicoGreen® assay. Data presented as mean ± SD, n=3, p-values are calculated using two-tailed t-test, *p < 0.05, **p < 0.01, ***p < 0.001.*

2.3.3 Identification of the optimal concentrations of the metal nanoparticles and metal salts to maximise antibacterial activity and osteoblast viability

2.3.3.1 Metal salts show superior antibacterial activity in comparison to the metal nanoparticles vs *S. aureus, S. epidermidis,* and *E. coli*

The antibacterial activity of the metal nanoparticles (copper, silver, and zinc oxide) and the metal salts (copper chloride, silver nitrate, and zinc chloride) against *S. aureus, S. epidermidis*, and *E. coli* was next investigated (**Figure 2.11**). To summarise the results from this grid of graphs: copper nanoparticles reduced the growth of all three bacteria species with increasing concentration, although it did not completely inhibit them (**Figure 2.11** A, D, G). Silver did not inhibit the growth of *S. aureus* or *S. epidermidis*, however it was the only metal nanoparticle to inhibit the growth of *E. coli* (MIC = 1000 µg/ml). Surprisingly, at 1000 µg/ml, silver nanoparticles increased the growth of *S. aureus* and *S. epidermidis* (**Figure 2.11** B, E, H), although this not uncommon for sub-inhibitory concentrations of silver nanoparticles [222], [223] and may be due to oxidation or an increased surface area. Finally, Zinc oxide was the only nanoparticle which inhibited the growth of *S. aureus* and *S. epidermidis* (both MIC = 230 µg/ml) at the concentrations tested. Zinc oxide decreased the

growth of *E. coli*; however, it did not inhibit its growth fully (**Figure 2.11** C, F, I).

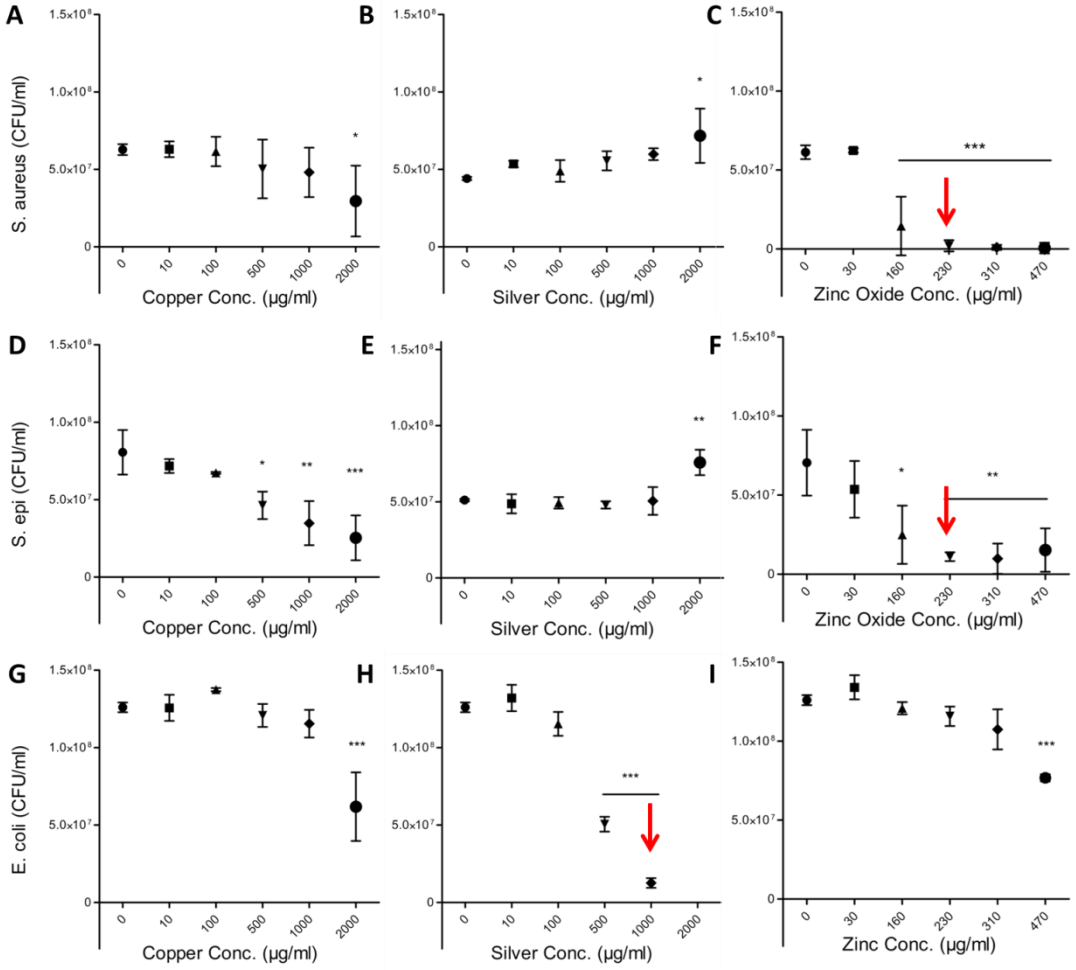

Figure 2.11 Effect of metal nanoparticles on bacterial viability
Bacterial toxicity of metal nanoparticles copper, silver, and zinc oxide against Staphylococcus aureus (S. aureus), Staphylococcus epidermidis (S. epidermidis), *and* Escherichia coli (E. coli). *Note: red arrows indicate the MIC value identified by visually inspecting the assay (C = 230 µg/ml, F = 230 µg/ml, H = 1000 µg/ml). Data presented as mean ± SD, n=3, p-values are calculated using one-way ANOVA with Bonferroni post-hoc test. All statistical significance shown in comparison to 0 µg/ml positive control unless otherwise stated, *p < 0.05, **p < 0.01, ***p < 0.001.*

Having determined the antibacterial activity of the metals in nanoparticle form, we next sought to determine and compare the effect of the metals in salt form against *S. aureus, S. epidermidis*, and *E.coli* (**Figure 2.12**). The most important result to note immediately is that all three of the metal salts, copper chloride, silver nitrate, and zinc chloride, achieved complete inhibition of the growth of all three of the bacteria species within the concentration ranges tested. To summarise the results from this grid of graphs: copper chloride had

the highest MIC of 16 mM against *S. aureus, S. epidermidis,* and *E.coli* (**Figure 2.12** A, D, G), silver nitrate had the lowest MIC values for all three bacteria strains (MIC = 1, 1, ≤ 0.25 mM, respectively) (**Figure 2.12** B, E, H), and zinc chloride had MIC values of 4, 4, and 8 mM against *S. aureus, S. epidermidis,* and *E.coli,* respectively (**Figure 2.12** C, F, I).

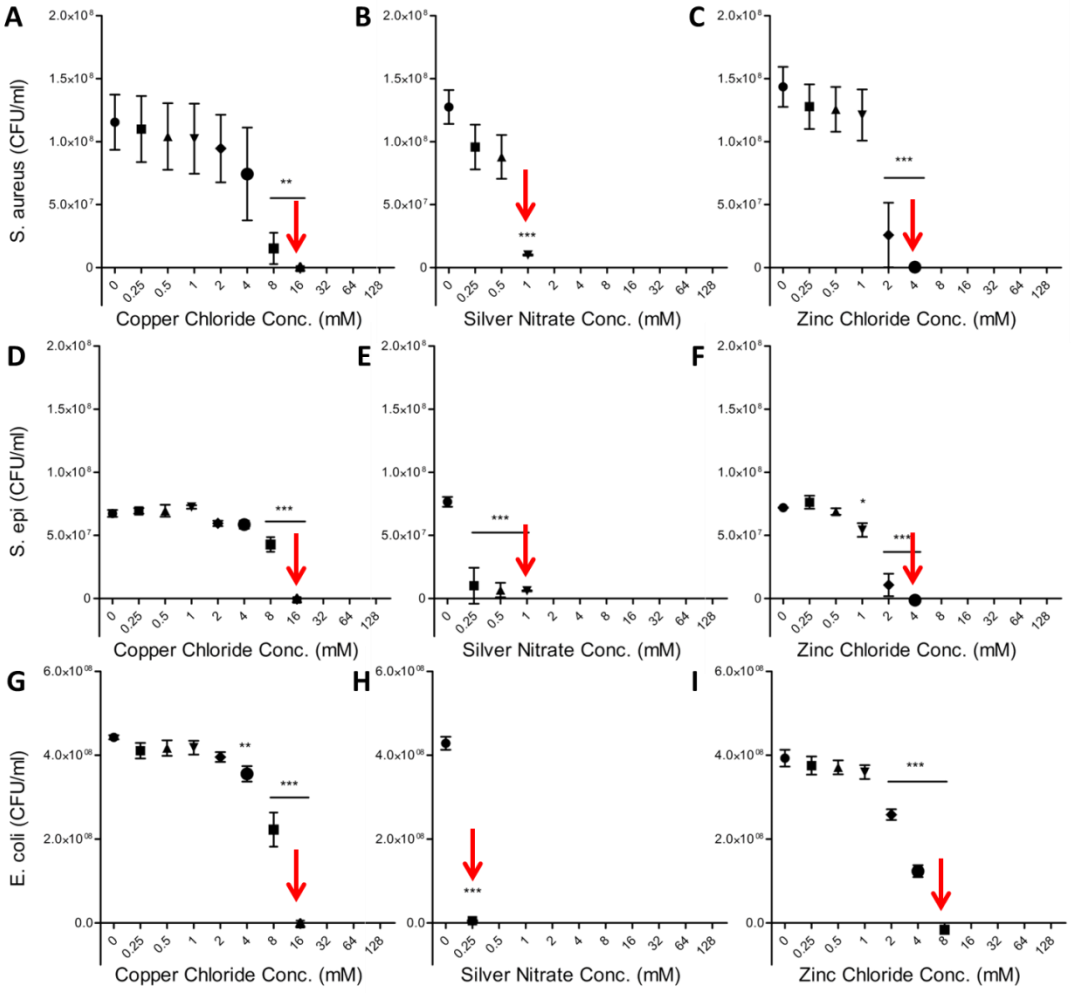

Figure 2.12 Effect of metal salts on bacterial viability
Bacterial toxicity of metal salts copper chloride, silver nitrate, and zinc chloride against Staphylococcus aureus (S. aureus), Staphylococcus epidermidis (S. epidermidis), *and* Escherichia coli (E. coli)*. Note: red arrows indicate the MIC value identified by visually inspecting the assay (A = 16 mM, B = 1 mM, C = 4 mM, D = 16 mM, E = 1 mM, F = 4 mM, G = 16 mM, H = ≤0.25 mM, I = 8 mM). Data presented as mean ± SD, n=3, p-values are calculated using one-way ANOVA with Bonferroni post-hoc test. All statistical significance shown in comparison to 0 µg/ml positive control unless otherwise stated, *p < 0.05, **p < 0.01, ***p < 0.001.*

Next, we wanted to determine whether the metal salts, which we showed are capable of fully inhibiting the growth of all three bacteria species, solely prevented the growth of bacteria (bacteriostatic) or whether they could kill

bacteria (bactericidal) at, or above the MIC concentration. The MBC values for the metal salts are shown in **Table 2.3** below. To summarise, silver nitrate has the lowest range of MBC values across all bacteria species (0.5 – 4 mM). Copper chloride and zinc chloride had the same range of MBC values (8 – 32 mM).

Table 2.3 *Minimum bactericidal concentration of metal salts*
Minimum Bactericidal Concentration (MBC) ranges of copper chloride, silver nitrate, and zinc chloride against three bacteria types: S. aureus, S. epidermidis, *and* E. coli.

	S. aureus	***S. epi***	***E. coli***	**Range across bacteria species**
Copper chloride (mM)	8	8-32	8-16	8-32
Silver nitrate (mM)	1-2	2-4	0.5-2	0.5-4
Zinc chloride (mM)	16	8-32	16-32	8-32

Although low MIC and MBC values may seem desirable for an antibacterial agent for the treatment of osteomyelitis, this is only true when the toxicity towards mammalian cells is also low. Hence, we next sought to determine the effect of both the metal nanoparticles and metal salts on mammalian osteoblast cells.

2.3.3.2 Osteoblast viability decreases with increasing metal nanoparticle or metal salt concentrations

The effect of the metal nanoparticles on the viability of osteoblast cells was next investigated. The results show that increasing metal nanoparticle concentration decreases cellular viability (**Figure 2.13**). To relate these mammalian cell viability results back to the concentrations required to reduce bacterial growth identified in the previous section (Section 2.3.3.1) (although full bacterial inhibition was largely not achieved), copper, silver, and zinc oxide nanoparticles reduce mammalian viability to 25%, 13%, and 24%, respectively at these concentrations.

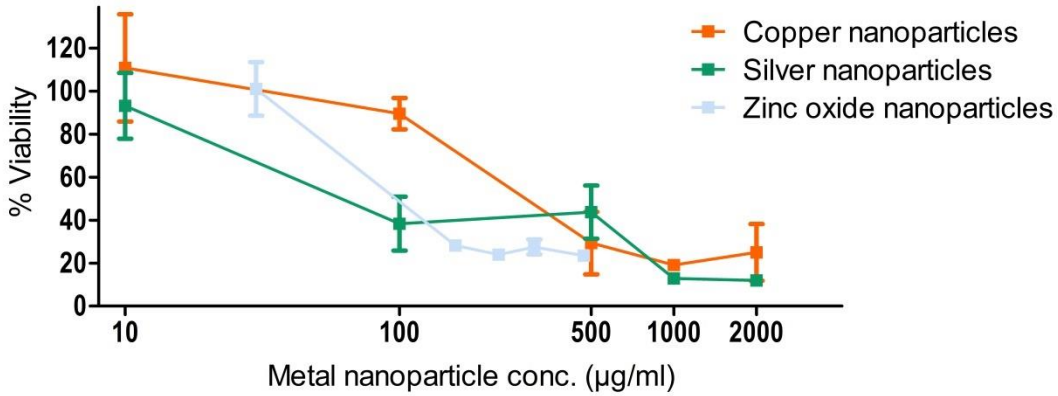

Figure 2.13 Effect of metal nanoparticles on mammalian cell viability
Effect of a range of concentrations of copper, silver, and zinc oxide nanoparticles on the viability of MC3T3-E1 cells using PicoGreen® assay. Note the reduction in cell viability with increasing metal nanoparticle concentration. X-axis values are displayed on a Log base 2 scale.

Next, the effect of the metal salts on the viability of osteoblast cells was investigated. The results show a similar trend to the metal nanoparticles, in that increasing metal salt concentration decreases cellular viability (**Figure 2.14**). At the concentrations required to prevent bacterial growth or kill bacteria (MIC and MBC concentrations), copper chloride, silver nitrate, and zinc chloride salts show similar toxicity towards mammalian cells (26-39%, 26-37%, and 16-24% viability, respectively), however they are generally improved in comparison to the respective metal nanoparticles.

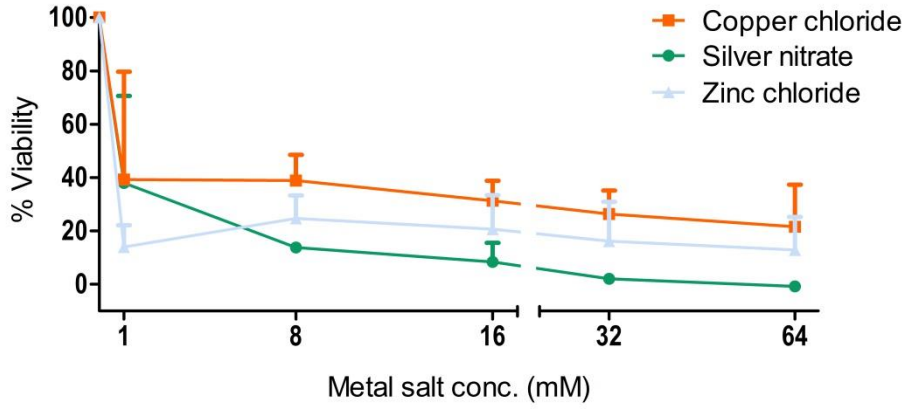

Figure 2.14 Effect of metal salts on mammalian cell viability
Effect of a range of concentrations (1, 4, 8, 32, 64 mM) of copper chloride, silver nitrate, and zinc chloride on the viability of MC3T3-E1 cells using PicoGreen® assay. Note the reduction in cell viability with increasing metal ion concentration.

2.3.4 Metal nanoparticles slowly release ions over time vs immediately dissociated metal salts

Having determined the effect of a range of concentrations of metal nanoparticles and salts on antibacterial activity and mammalian cell viability, we next wanted to investigate the ion release profiles achieved in order to further elucidate the possible mechanisms behind the results achieved, as the antibacterial activity of metals is suggested to be mainly attributed to ion release [123]. The metal salts copper chloride, silver nitrate, and zinc chloride immediately dissociate on day 1 in comparison to the nanoparticles, silver, copper, and zinc oxide, which release their ions more slowly over the 7 day time period (**Figure 2.15**). Note that all materials are normalised by mass (20 mg of each substance).

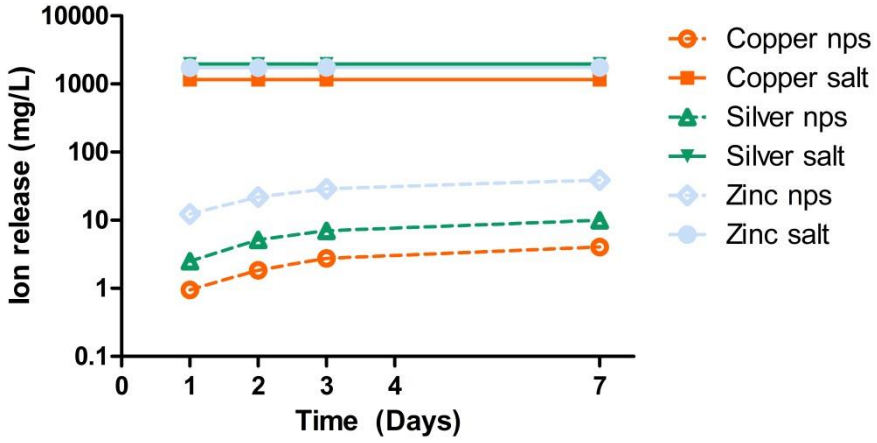

Figure 2.15 Ion release profiles from metal nanoparticles and metal salts
Cumulative ion release profiles from 20 mg of metal nanoparticles and metal salts over 7 days. Y-axis values are displayed on a Log base 10 scale. Note the reduced ion release of all metal nanoparticles when compared to the corresponding metal salts.

2.4 Discussion

The overall aim of this study was to screen a number of non-antibiotic antimicrobials (chitosan, copper, silver, and zinc) as potential agents for osteomyelitis infection treatment based on their effect on mammalian cells and clinically relevant bacterial species. The results demonstrate that the majority of the non-antibiotic antimicrobial materials tested have a dose-dependent effect on both bacterial and mammalian cell viability and, as predicted, a trade-off between antibacterial activity and mammalian viability was identified. More specifically, chitosan performed well in terms of antibacterial activity, inhibiting the growth of all three bacteria species, *S. aureus*, *S. epidermidis*, and *E. coli*, whilst maintaining reasonable mammalian cell viability. The metal salts (copper chloride, silver nitrate, and zinc chloride) out-performed their respective bulk nano-sized particles (copper, silver, and zinc oxide) both in terms of antibacterial activity and mammalian cell viability as the metal nanoparticles failed to release a dose of ions to produce adequate antibacterial activity. Taken together, the results demonstrate that chitosan and the metal salts show promise as potential agents for osteomyelitis infection treatment and were selected to progress to Chapter 3.

In this study, chitosan was first examined as a potential treatment agent for osteomyelitis infection. In terms of antibacterial activity, chitosan demonstrated broad-spectrum effects, inhibiting the growth of all three bacteria species tested (included both gram positive and gram-negative bacteria) in a concentration-dependent manner. Additionally, it inhibited all of the bacteria species at the same concentration, MIC = 1.88 mg/ml, suggesting that chitosan's mechanism of action might be multifunctional (e.g. via alteration of cell wall permeability and nutrient transport) and may not be species specific. The broad-spectrum antibacterial activity that chitosan displays is advantageous as – although osteomyelitis is predominately caused by *S. aureus* – the causative organism may be of any bacterial species, or the infection could be polymicrobial. In addition to osteomyelitis treatment, owing to its broad-spectrum effects, chitosan-based scaffolds could also be applied in a host of different infections applications. Further experimentation revealed

chitosan's bacteriostatic rather than bactericidal action at the concentrations tested, i.e., it prevented the growth of the bacteria rather than killing them, which is also the general consensus in the literature [115]. Although it may seem preferable for an antibacterial agent to kill the bacteria, rather than prevent its growth, in a clinical scenario there is little reported in the literature to support this [224]. Additionally, with the rise in antimicrobial resistance, intuitive attitudes towards bacteriostatic treatment strategies must be reassessed and based on proper scientific research. In terms of mammalian viability, when cultured on chitosan films, osteoblasts displayed reduced viability; however, they maintained 47% of the cells when compared to the positive tissue culture plastic control. This could be due to cell death due to toxicity or a reduction in the ability to proliferate as the films displayed unavoidable significant swelling after hydration with media. Thus, the cytocompatibility of chitosan-incorporated 3D scaffolds was instead examined in Chapter 3 as freeze-dried scaffolds not only negate these swelling issues, but also more closely mimic the natural extracellular matrix.

The metal nanoparticles, copper, silver, and zinc oxide were next examined for antibacterial activity (results summarised in **Table 2.4**). Although all metal nanoparticles had a detectable antibacterial effect on some or all bacteria species, none achieved full inhibition across all three bacteria species.

Table 2.4 *Summary of nanoparticles vs bacteria results*

	Detectable effect?			Full inhibition?		
	S. aureus	S. epi	E. coli	S. aureus	S. epi	E. coli
Copper nanoparticles	✓	✓	✓	✗	✗	✗
Silver nanoparticles	✗	✗	✓	✗	✗	✓
Zinc oxide nanoparticles	✓	✓	✓	✓	✓	✗

Silver nanoparticles were the only metal nanoparticle to achieve full inhibitory action against gram-negative *E. coli* and only zinc oxide nanoparticles achieved full inhibition against gram-positive *S. aureus* and *S. epidermidis.* Interestingly, Kim et. al. present similar results – out of the metal ions silver, copper, and zinc, silver was the only ion to be effective against *E.coli* [121]. Another study which compared the effect of zinc oxide nanoparticles on the growth of *S. aureus* and *E. coli* found the zinc oxide to be more effective

against *S. aureus*, similar to results in our study [225]. Thus, in contrast to chitosan, the metal nanoparticles show select toxicity towards the bacterial species examined, and, if to be used clinically for the treatment of osteomyelitis infection, might require a combinatory approach or prior knowledge of the causative organism.

The toxicity of the metal nanoparticles against mammalian cells was next examined. Generally, mammalian cell viability was low after culture with all three metal nanoparticle types. Copper nanoparticles did not reach a bacterial MIC concentration up to the maximum concentration tested, and even at this sub-inhibitory concentration, mammalian cell viability was 25%. Mammalian cell viability with silver nanoparticles was 13% at the MIC for *E. coli* and at the MIC for *S. aureus* and *S. epidermidis*, zinc oxide nanoparticles resulted in a mammalian viability of 24%. It has been shown that mammalian cells can endocytose particles less than 100 nanometres in size [226]. Therefore, the metal nanoparticles might be endocytosed by mammalian cells causing a toxic effect additional to the toxicity of the metal ions released from them. However, when it comes to bacteria, the metal nanoparticles are likely too big to be endocytosed, with only ion release responsible for antibacterial activity. Overall, the nanoparticles only show select toxicity towards bacteria species and cause a substantial reduction in mammalian cell viability at these concentrations.

In contrast to the metal nanoparticles, all of the metals in their salt form achieved complete inhibition of bacterial growth against *S. aureus, S. epidermidis*, and *E. coli* in the concentration ranges tested. Further experimentation revealed that all of the metal salts achieved bactericidal activity at either the MIC concentration, or higher. The effect of the metal salts on the viability of mammalian cells was next examined and the toxicity of copper chloride, silver nitrate, and zinc nitrate towards mammalian cells at the MIC concentrations were found to be similar, at approximately 39%, 37%, and 24% viability, respectively. It must be noted that at these concentrations, full bacterial clearance is achieved. When compared to the bacterial toxicity/mammalian viability ratio results of the metals in nanoparticle form, the metal salts demonstrated the most favourable results.

Finally, in order to further elucidate the possible mechanisms behind the results achieved, the ion release profile from the metal nanoparticles was compared to that of the metal salts. The slow release of ions from the metal nanoparticles was confirmed. Of the total ions that were released from the nanoparticles, 18-32% was released at day 1, in contrast to all of the ions from the metal salts. It was therefore decided to bring the metal salts forward for further studies for a number of reasons. The metal salts displayed a superior bacterial toxicity/mammalian cell viability relationship than the nanoparticles tested. A vast quantity of nanoparticles would be required in order to reach a therapeutic antibacterial dose of ions from the nanoparticles, a concentration that would without doubt result in excess mammalian cell toxicity. Metal nanoparticles are currently being effectively utilized in a variety of topical wound applications where they are removed after the desired effect [157], [227]–[229]. However, since metal nanoparticles would take an extensive time to dissolve, if at all, in the patient's lifetime, implanting them into the body would be undesirable as they could have unpredictable effects in the long term. By contrast, the activity of metal salts is much more predictable and controllable.

The aim of this thesis as a whole is to examine the suitability of these non-antimicrobials for the treatment of osteomyelitis. There is literature to suggest that the metal ions copper and zinc can enhance both angiogenesis and osteogenesis [137], [138], [175]–[177], however the same cannot be said for the silver ion (unless, perhaps, if combined with an osteogenic carrier). Thus, it was chosen to bring forward the metal salts copper chloride and zinc chloride only. Additionally, although it was insightful to see the effect of the non-antibiotic antimicrobials against three different bacteria species, to facilitate more in-depth analysis of antibacterial activity, it was chosen to bring forward *S. aureus* (the primary causative agent in osteomyelitis [18]) as the bacteria strain to study the effect of the treatment platforms developed in the following thesis chapters.

2.5 Conclusion

In this study, a number of non-antibiotic antimicrobials were successfully screened as potential agents for osteomyelitis infection treatment based on

their effect on mammalian cells and clinically relevant bacterial species. The concentrations of the antimicrobial materials that show antibacterial activity and the corresponding effect on mammalian cell viability were identified, demonstrating that there is a fine balance between the two. The results demonstrated that chitosan and the metal salts were the most effective due to their superior bacterial toxicity/mammalian cell viability ratio. In summary, chitosan, copper chloride, and zinc chloride were identified to show promise as potential agents for osteomyelitis infection treatment and selected to move forward to Chapter 3 for incorporation into 3D scaffolds at biologically relevant concentrations.

Chapter 3 Development of a 3D antimicrobial delivery platform to modulate antimicrobial ion release while retaining bioactivity

3.1 Introduction

Successful osteomyelitis treatment relies heavily on the ability of the antibacterial agent to reach the site of infection at sufficient and controlled concentrations [224]. One way to achieve this is to deliver the antibacterial agents locally, in a 3D scaffold that controls the release of such agents. While this will help treat the infection, this approach offers the additional advantage that the 3D scaffold functions to repair and regenerate the bone tissue.

Chitosan displays broad-spectrum antimicrobial activity against a variety of bacteria and fungi [114]–[116]. In addition, chitosan has excellent metal binding properties as it is a chelating agent and it is often combined with metal ions to increase its antimicrobial activity [117], [118]. In addition to its antimicrobial activity, chitosan has also been used as a scaffolding material, either alone or in combination with other materials, such as collagen. Furthermore, chitosan, both directly and in the form of microparticles, can be used as a delivery vehicle for drugs and small molecules due to its charge interactions [230], [231].

Collagen is an ideal scaffolding material as it is a natural, biodegradable material that facilitates cell attachment, migration, and proliferation. Chitosan addition to collagen scaffolds has been shown previously to mechanically reinforce the collagen scaffold, improve cellular attachment and proliferation, and enhance both chondrogenesis (increased sulphated GAG levels) and osteogenesis (higher calcium deposition) [110], [232].

In Chapter 2, copper chloride and zinc chloride were identified as potential agents for osteomyelitis infection treatment due to their superior bacterial toxicity/mammalian cell viability ratio. In addition to their potent antimicrobial activities, copper and zinc are essential ions for normal body function, regulating immunity, DNA synthesis, collagen, and bone formation [136], [174]. Additionally, copper has been shown to stimulate angiogenesis and vasculogenesis and both copper and zinc can stimulate osteogenesis [137], [138], [175]–[177].

In this chapter, antimicrobial materials (chitosan, copper chloride, zinc chloride) were incorporated in collagen scaffolds as a treatment strategy for osteomyelitis. In addition to its direct antimicrobial role, we proposed the use of chitosan as a delivery vehicle (in scaffold or microparticle form) for the metal salts as well as mechanism to mechanically reinforce the scaffold. Two different scaffold systems were developed herein: a 'directly-loaded' scaffold group and a 'microparticle-loaded' scaffold group. By developing two different scaffold systems, the aim was to achieve two distinctive metal ion release profiles, which were compared to assess their ability to maximise antibacterial activity and minimise mammalian cell toxicity.

Thus, the specific objectives were to:

1) Develop and assess a crosslinking method suitable to crosslink the collagen/chitosan-based directly-loaded scaffold and collagen-based microparticle-loaded scaffold systems
2) Develop a method for producing the directly-loaded metal salt collagen/chitosan scaffold system. Additionally, to develop a method to produce chitosan microparticles with metal salts encapsulated within, followed by the incorporation of the microparticles into collagen scaffolds
3) Measure the metal ion release profiles from both scaffold types and determine their antibacterial activity
4) Analyse the mechanical and microarchitectural properties of the directly-loaded and microparticle-loaded scaffolds
5) Investigate the ability of the directly-loaded and microparticle-loaded scaffolds to support mammalian cells and to and to assess their osteogenic potential *in vitro*
6) Investigate the ability of the directly-loaded and microparticle-loaded scaffolds to support angiogenesis *in vitro*

3.2 Materials and methods

3.2.1 Development and assessment of a crosslinking method for scaffold systems

3.2.1.1 Glutaraldehyde vapour crosslinking

Prior to the fabrication of the directly-loaded and microparticle-loaded scaffolds, the development of a method to crosslink the scaffolds was necessary. The collagen-based scaffold chemical crosslinking methods that are typically used in our laboratory involve immersing the scaffolds in a solution containing the crosslinking agent (e.g. EDAC/NHS, genipin, or Riboflavin/ultraviolet (UV) crosslinking) for >3 hrs followed by multiple washing steps. To limit leaching of the metal ions from the scaffolds, a solution-less method suitable to crosslink both the collagen/chitosan-based directly-loaded scaffold and collagen-based microparticle-loaded scaffolds was explored, namely, glutaraldehyde vapour crosslinking. Glutaraldehyde vapour crosslinking was performed inside a vacuum desiccator chamber (Nalgene, Thermo Scientific) (**Figure 3.1**).

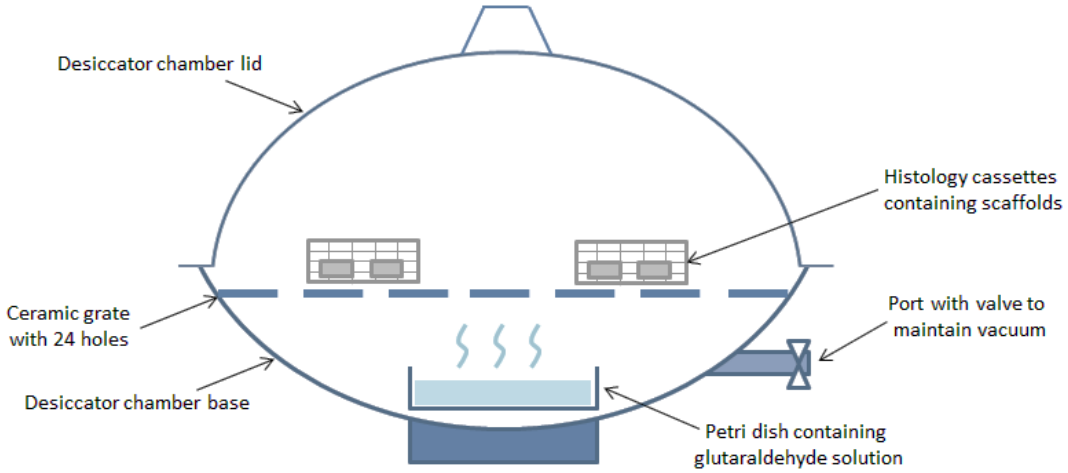

Figure 3.1 Schematic of glutaraldehyde vapour crosslinking method
Glutaraldehyde vapour crosslinking setup. The scaffolds contained within histology cassettes were crosslinked over a petri dish of glutaraldehyde solution inside a desiccator chamber under vacuum for 4 or 24 hrs.

Scaffolds were placed within large pore histology cassettes on a ceramic grate over a petri dish containing 25 ml of 25% glutaraldehyde (wt.%) in H_20. Scaffolds were crosslinked under vacuum for 4 or 24 hrs. After glutaraldehyde

vapour treatment, the scaffolds were removed from the desiccator and exposed to clean air flow in a fume hood for 12 hrs to remove residual glutaraldehyde vapour. In order to confirm crosslinking was induced, the effect of the duration of glutaraldehyde vapour treatment (4 or 24 hrs) on the structural and mechanical properties of a collagen/chitosan scaffold was first investigated.

3.2.1.2 Effect of glutaraldehyde vapour crosslinking on the mechanical properties of collagen/chitosan scaffolds

In order to investigate the effect of glutaraldehyde vapour crosslinking on scaffold compressive modulus, unconfined, wet compression testing of the scaffolds was performed using a uniaxial tensile testing machine (Z050, Zwick/Roell, Germany) fitted with a 5 N load cell [94]. Scaffolds were pre-hydrated in PBS and tested at a rate of 10% strain/minute up to a maximum strain of 10%. The compressive modulus of the scaffolds was calculated in the 2-5% strain range (n=3 scaffolds, 3 repeats per scaffold) [94] (**Figure 3.2**).

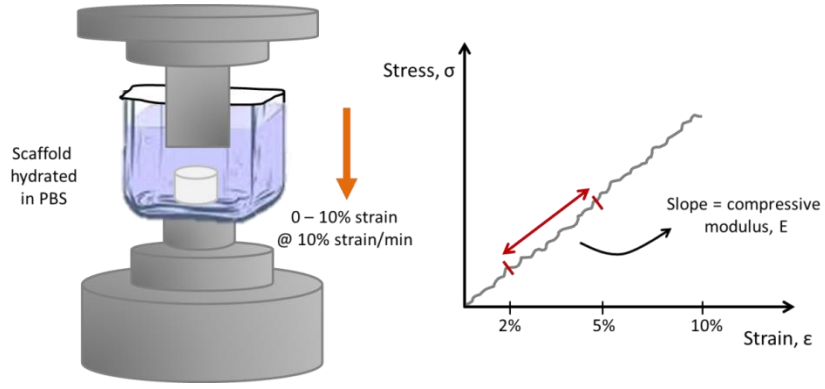

Figure 3.2 Schematic of method for compressive modulus analysis of collagen/chitosan scaffolds
The compressive modulus of collagen/chitosan scaffolds was investigated using unconfined wet compression testing. The compressive modulus was calculated between 2-5% strain.

An optimum crosslinking duration was selected from these investigations (as both scaffolds showed similar levels of mechanical enhancement, 4 hrs was selected over the 24 hr treatment duration in terms of reduced processing time) and the effect of the collagen/chitosan scaffolds crosslinked for 4 hrs on mammalian cell viability was examined.

3.2.1.3 Effect of glutaraldehyde vapour crosslinking on mammalian cell cytocompatibility

The cytocompatibility of the glutaraldehyde vapour-crosslinked scaffolds was investigated to examine potential cytotoxic effects. Three scaffold groups were compared (**Table 3.1**); including scaffolds washed in glycine as it has been shown that washing with glycine can deactivate non-crosslinked glutaraldehyde residues [101], [233].

Table 3.1 *Scaffold groups used to test mammalian cell cytocompatibility on glutaraldehyde vapour treated scaffolds*

	Collagen-chitosan (no crosslinking)	**Collagen-chitosan (glut)**	**Collagen-chitosan (glut + glycine wash)**
Glut vapour crosslinked?	None	4 hrs	4 hrs
Wash 1 (30 mins)	dH_20	dH_20	dH_20
Wash 2 (3 x 20 mins)	PBS	PBS	0.1 M glycine

$5x10^5$ osteoblast cells (MC3T3-E1 cell line) were seeded on scaffolds in growth medium consisting of Alpha Minimum Essential Medium (α-MEM) (Sigma Aldrich, Ireland) supplemented with 10% Fetal Bovine Serum (FBS) (Labtech, UK), 2% penicillin/streptomycin, and 1% L-Glutamine (Sigma Aldrich, Ireland) cultured under standard culture conditions (37°C, 5% C02, and 95% relative humidity). After 24 hrs, cell metabolism was investigated via alamarBlue® Cell Viability Reagent (Invitrogen™, USA) (total incubation time – 4 hrs) and DNA, as an indicator of cell number and survival, was quantified on the same samples using a Quant-iT™ PicoGreen™ dsDNA Assay Kit (Molecular Probes, USA), as per the manufacturer's instructions (n=3 scaffolds per group). The background reading obtained from cell-free control scaffolds cultured under identical conditions to the test samples was subtracted from cell-seeded sample readings.

3.2.2 Fabrication of directly-loaded scaffolds

To achieve the bioactive metal salt concentrations identified in Chapter 2, a range of different concentrations of the metal salts were incorporated into the scaffolds (0 mM, 16 mM, 24 mM, and 32 mM of copper chloride or zinc

chloride). The scaffolds were fabricated by freeze-drying a co-suspension of collagen, chitosan, and/or metal salts - similar to methods previously developed within our group to fabricate collagen-chitosan scaffolds (**Figure 3.3**) [110].

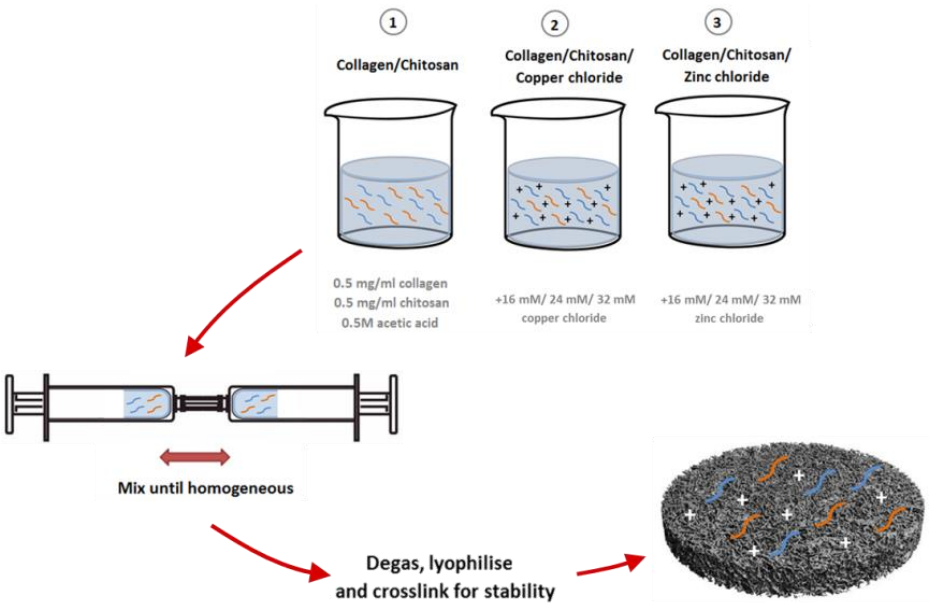

Figure 3.3 Directly-loaded 3D scaffold fabrication
Fabrication method of directly-loaded 3D scaffold groups containing collagen/chitosan ± copper chloride or zinc chloride at 16, 24, or 32 mM. The metal salts were added to a collagen/chitosan slurry, mixed until homogeneous, degassed, and lyophilised into porous scaffolds.

Briefly, a collagen slurry was produced by mixing type I collagen (10 mg/ml) isolated from bovine tendon (Integra Life Sciences, Plainsboro, NJ) in aqueous 0.5 M acetic acid solution (Fisher Scientific, UK). A chitosan slurry (10 mg/ml) was also produced by mixing low molecular weight chitosan derived from the exoskeleton of crustaceans (Sigma Aldrich, Ireland) first in water to aid in dissolution followed by glacial acetic acid to a final concentration of 0.5 M. Equal volumes of the collagen and chitosan slurries were then mixed until homogeneous to produce collagen/chitosan solution (collagen = 5 mg/ml; chitosan = 5 mg/ml). The metal salts were added to the slurry and mixed between two syringes connected with a luer lock until a homogeneous suspension was obtained. The slurry suspension was then degassed using a vacuum chamber and freeze-dried in a custom built mould (10 mm ⌀ x 5mm discs) until a final temperature of -40°C, based on a previously published freeze-drying profile [234]. Scaffolds were sterilised and physically crosslinked using dehydrothermal (DHT) treatment at 105°C for 24 hrs at 0.05 bar [94].

Scaffolds were then further chemically crosslinked using the glutaraldehyde vapour crosslinking method outlined in Section 3.

3.2.3 Fabrication of chitosan/metal salt containing microparticles and microparticle-loaded scaffolds

3.2.3.1 Microparticle fabrication, crosslinking, size analysis, and morphology characterisation

With the aim of further controlling the release of metal ions from the scaffold to minimise toxicity to prolong bioactivity, chitosan microparticles with and without metal salts were fabricated as follows: 1% w/v LMW chitosan was dissolved in 1% (v/v) acetic acid. Copper chloride or zinc chloride salts were added to the chitosan solution to a final concentration of 16 mM. The chitosan solutions were spray-dried (Buchi Mini Spray Dryer B-290) using the machine parameters in **Table 3.2**. Metal salt-free chitosan-only microparticles were used as controls (referred to as 'blank-microparticles').

Table 3.2 *Spray dryer machine parameters used to produce chitosan/metal salt microparticles*

Parameter	Setting
Inlet (°C)	160
Outlet (°C)	89
Aspirator (%)	100
Pump (%)	15 (4.65 ml/min)
Nozzle cleaner	4

The percentage microparticle yield was calculated using Equation 3.1.

$$\%\, Yield = \frac{Actual\ yield}{Theoretical\ yield}\ x\ 100$$

Equation 3.1

Covalent crosslinking of the microparticles with glutaraldehyde solution was completed as follows: 150 mg of chitosan/metal salt microparticles were suspended in 3 ml of 100% ethanol and vortexed briefly. The microparticle/ethanol solution was added to 50 ml 0.1% solution of glutaraldehyde in phosphate buffered saline (PBS) under stirring. After 2 hrs of stirring, the microparticle solution was centrifuged, the supernatant was removed, and the particles were washed 3 times in dH_20. The size of the

microparticles both before and after crosslinking was investigated using a Mastersizer (Malvern Mastersizer 2000). Briefly, 5 mg of the microparticles were suspended in 5 ml of 100% ethanol and this was added dropwise to the dispersant chamber. The dispersant chamber contained ethanol stirring at 1260 rpm. The suspension was added until the laser obscuration value was >10%. Particle sizing was measured (n = 3). The refractive index for ethanol and the chitosan microparticles were approximated as 1.36 and 1.468, respectively. Additionally, the chitosan microparticles morphology was investigated using light microscopy.

3.2.3.2 Microparticle-loaded scaffold fabrication & crosslinking

Having successfully produced chitosan microparticles loaded with metal salts of a suitable size (2-80 µm), the microparticles were incorporated into the scaffolds at a maximum achievable concentration of 300% w/w microparticles to collagen (**Figure 3.4**).

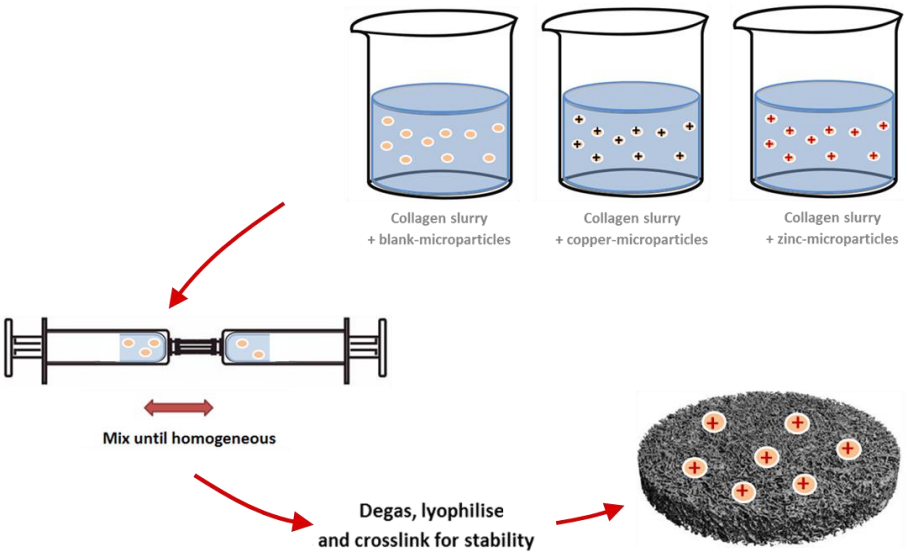

Figure 3.4 Microparticle-loaded 3D scaffold fabrication
Fabrication method of microparticle-loaded 3D scaffold groups containing chitosan microparticles loaded with/without copper chloride or zinc chloride. The microparticles were added to a collagen slurry, mixed until homogeneous, degassed, and lyophilised into porous scaffolds.

Briefly, a collagen slurry was produced by mixing type I collagen (5 mg/ml) in aqueous 0.5 M acetic acid solution. The crosslinked, washed, and centrifuged chitosan/metal salt microparticles were added to the collagen slurry (final microparticle concentration = 15 mg/ml, or 3:1 wt:wt microparticle:collagen)

and mixed between two syringes connected with a luer lock until a homogeneous suspension was obtained. The slurry suspension was then degassed, freeze-dried, sterilised using DHT, and crosslinked using glutaraldehyde vapour as outlined in Section 3.2.2.

3.2.4 Metal ion release studies for directly loaded and microparticle loaded scaffolds

Zincon (2-Carboxy-2′-hydroxy-5′-sulfoformazyl-benzene monosodium salt) (Fisher Scientific, Ireland) acts as an excellent chromophore for the quantification of both zinc and copper ions in solution [235]. Zincon assay method: A 1.6 mM stock solution of Zincon was prepared by dissolving 43.5 mg salt (85% dye content) in 1 ml of 1 M NaOH and made up to 50 ml with dH_20. A stock solution of boric acid (52.63 mM) containing urea was prepared by dissolving 325 mg of H_3BO_3 in 90 ml dH_20. The pH was adjusted to 9.0 using either 5 M NaOH or 6 M HCL and the final volume was made up to 100 ml with dH_20. For the assay, 950 µl borate buffer, 25 µl of the diluted sample/standard, and 25 µl of the Zincon stock solution was added to the wells of a 48 well plate. Standard curves were constructed using a concentration range of 0 – 40 µM of either copper chloride or zinc chloride solutions. The absorbance of copper and zinc ions in solution were measured photometrically using λ_{max} 600 nm and 620 nm, respectively [235].

3.2.4.1 Metal ion release from directly-loaded scaffolds

Metal ion release was analysed from the directly-loaded scaffolds described in Section 3.2.3 containing either 0, 16, 24, or 32 mM concentrations of copper chloride or zinc chloride over 28 days (**Figure 3.5**).

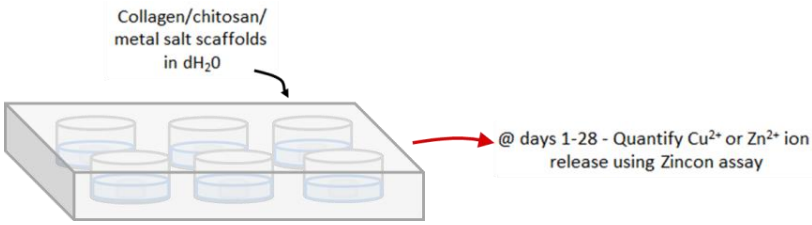

Figure 3.5 Schematic of protocol to analyse copper or zinc ion release from directly-loaded scaffolds
Eluate from directly-loaded scaffolds was collected at various time points over 28 days. Copper or zinc ion concentration was measured using a Zincon assay.

Scaffolds were added to 1 ml deionised water in 24 well plates and the eluate was collected at days 1, 2, 3, 4, 7, 14, and 28. The Zincon assay was used to measure copper or zinc ions at each time point (n = 3)

3.2.4.2 Metal ion release profile from chitosan/metal salt microparticles

Prior to incorporation into collagen scaffolds, metal ion release was analysed from the chitosan/metal salt microparticles over 28 days (**Figure 3.6**).

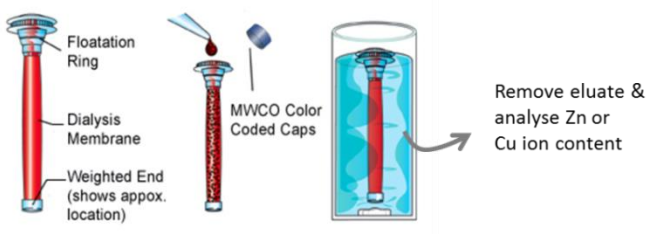

Figure 3.6 Schematic of protocol to analyse copper or zinc ion release from chitosan/metal salt microparticles
Microparticle solutions were added to Float-a-lyzer dialysis tubing and the eluate was collected at various time points over 28 days. Copper or zinc ion concentration was measured using a Zincon assay (image modified from [236]*).*

To do so, 37.5 mg of the glutaraldehyde crosslinked microparticles were added to 1 ml of deionised water. The 1 ml solutions were added to the inside of a Float-a-Lyzer® (MWCO 3.5-5 kDa; n=3 per group), which was suspended in 3 ml of deionised water. At days 1, 2, 3, 4, 7, 14, and 28 the 3 ml eluate surrounding the dialysis membrane was collected, replaced with 3 ml of fresh deionised water. The Zincon assay was used to measure copper or zinc ion content at each time point (n=3).

3.2.4.3 Metal ion release profile from microparticle-loaded scaffolds

The copper and zinc ion release profiles from the collagen scaffolds loaded with chitosan/metal salt microparticles over 28 days was analysed using the same method as the directly-loaded scaffolds in Section 3.2.4.1 above.

3.2.5 Antibacterial characterisation of metal salt incorporated scaffolds

Having determined the metal ion release profiles from both the directly-loaded and microparticle-loaded scaffolds, they were next examined for antibacterial

activity using two different methods: A and B. First, the scaffolds were assessed via an agar diffusion assay (**Figure 3.7** A). Brain heart infusion (BHI) agar plates were lawned with 100 µl of 1x10^8 CFU/ml *S. aureus* Newman and allowed to air dry for 15 mins before the scaffolds were placed in sectioned quadrants of the agar plates. After a further 15 mins, the plates were inverted and incubated for 18-24 hrs before being examined for antibacterial activity in the form of zones of inhibition. The scaffolds were also assessed for antibacterial activity via a time-kill assay in BHI broth over a 24 hr time-period (**Figure 3.7** B). Scaffolds were added to 1ml of BHI broth in 24 well-plates and inoculated with *S. aureus* Newman to a final concentration of 5x10^5 CFU/ml. The plates were incubated in an orbital shaker (MaxQ 4000, Thermo Fisher Scientific, USA) (150 rpm, 37°C) and the bacterial growth was quantified via optical density measurements (with scaffolds temporarily removed) using a plate reader (1420 Victor V3, Perkin Elmer, Dublin, Ireland) at a series of time points over 24 hrs.

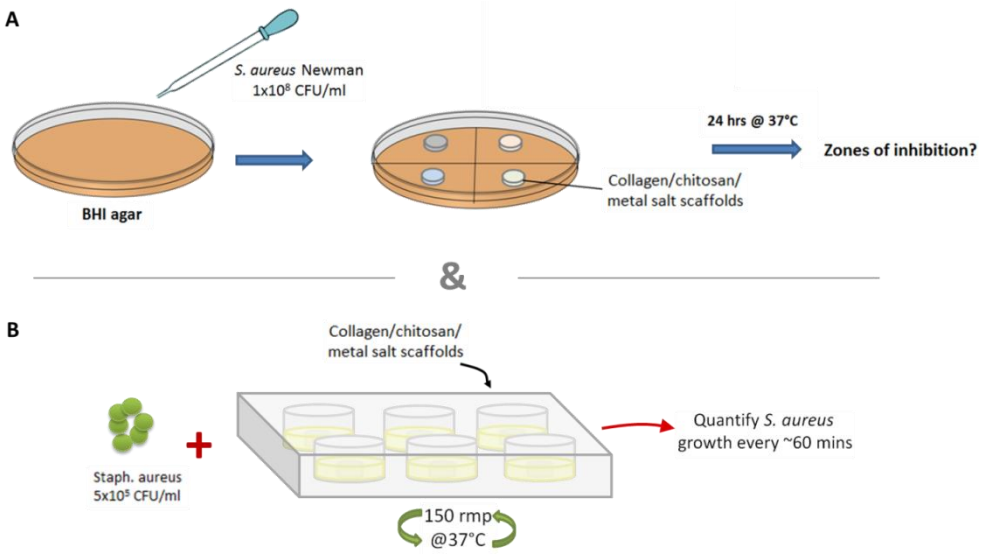

***Figure 3.7 Schematic of protocol to investigate the effect of directly-loaded and microparticle-loaded scaffolds against* S. aureus**
The effect of directly-loaded and microparticle-loaded scaffolds on the growth of S. aureus *over 24 hrs was analysed by (A) agar diffusion assay on BHI agar and (B) a time-kill assay. In the time-kill assay, scaffolds were inoculated with* S. aureus *in BHI broth, incubated in an orbital shaker, and bacterial growth was quantified at regular time intervals.*

3.2.6 Effect of metal salt incorporation on scaffold porosity, pore size, and mechanical properties

In order to minimise toxicity towards mammalian cells, the lowest concentration of the directly-loaded scaffolds which displayed antibacterial activity (16 mM) and the 16 mM microparticle-loaded scaffolds were brought forward for all further analysis. Scanning electron microscopy (SEM) was used to characterize the scaffold morphology and pore size (Carl Zeiss Ultra SEM (Carl Zeiss, Germany). The porosity of the scaffolds was calculated by measuring the density of the scaffold in relation to the density of the individual scaffold components as per Equation 3.2 (directly-loaded scaffolds) and Equation 3.3 (microparticle-loaded scaffolds) below.

$$\text{Scaffold porosity } (\%) = \left(1 - \frac{\rho_{\text{scaffold}}}{(\rho_{\text{collagen}})(\%\text{ wt collagen}) + (\rho_{\text{chitosan}})(\%\text{ wt chitosan}) + (\rho_{\text{metal salt}})(\%\text{ wt metal salt})}\right) x100$$

Equation 3.2

$$\text{Scaffold porosity } (\%) = \left(1 - \frac{\rho_{\text{scaffold}}}{(\rho_{\text{collagen}})(\%\text{ wt collagen}) + (\rho_{\text{microparticles}})(\%\text{ wt microparticles})}\right) x100$$

Equation 3.3

The scaffold density was calculated by dividing the measured weight (Digital scale, Mettler Toledo MX5; Mason Technology, Accuracy 0.01 mg) by the volume, using an average of two diameter and height measurements per scaffold (Vernier callipers, Krunstoffwerke; Radionics, Ireland). The density of collagen, chitosan, copper chloride, and zinc chloride used were 1.3, 0.23, 2.53, and 2.93 g/cm^3, respectively, as per supplier datasheet and theoretical density [237]. For scaffold pore size analysis, scaffolds were sectioned longitudinally, and SEM images of all scaffolds were captured at 150X. The mean pore diameter was analysed using Image J. For each pore selected at random, the maximum diameter and the diameter perpendicular to the maximum were averaged and the mean pore diameter calculated from these values (n=30 pores per scaffold) (**Figure 3.8**) [238], [239].

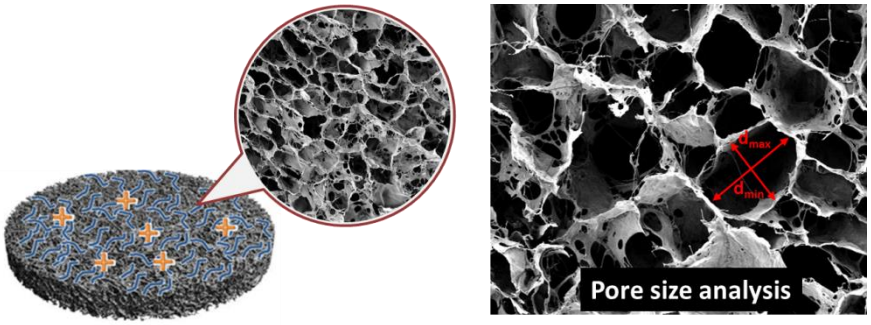

Figure 3.8 Schematic of method for pore size analysis of scaffolds
SEM images of the directly-loaded and microparticle-loaded scaffolds were analysed for pore size using ImageJ software

3.2.7 Biological characterisation of metal salt incorporated scaffolds – analysis of osteogenesis

3.2.7.1 Osteoblast culture and seeding

To assess the ability of the directly-loaded and microparticle-loaded scaffolds to support osteogenesis, MC3T3-E1 cells were cultured in growth medium consisting of Alpha Minimum Essential Medium (α-MEM) (Sigma Aldrich, Ireland) supplemented with 10% Fetal Bovine Serum (FBS) (Labtech, UK), 2% penicillin/streptomycin, and 1% L-Glutamine (Sigma Aldrich, Ireland). All scaffolds were seeded with 500,000 cells and were cultured in growth medium for the first two days prior to supplementation with osteogenic medium. For MC3T3-E1 osteogenic medium, the following supplements were added to the above-described growth medium: 50 μM ascorbic acid 2-P, 100 nM dexamethasone, and 10 mM β-glycerophosphate (Sigma Aldrich, Ireland). All cells were cultured under standard culture conditions (37°C, 5% C02, and 95% relative humidity).

3.2.7.2 DNA quantification

DNA – as an indicator of cell number and survival – was quantified using a Quant-iT™ PicoGreen™ dsDNA Assay Kit (Molecular Probes, USA). Three scaffolds per group on day 0 (12 hrs post-seeding as an indication of initial attachment and proliferation), 7 and 28, were washed twice in PBS and added to 1 ml lysis buffer (0.2 M carbonate buffer with 1% Triton). The scaffold solutions were subjected to three freeze-thaw cycles at -80°C to assist in cell

lysis. The resulting lysate was analysed for DNA content as per the manufacturer's instructions. The background reading obtained from cell-free control scaffolds cultured under identical conditions to the test samples was subtracted from cell-seeded sample readings.

3.2.7.3 Alkaline phosphatase activity and cell-mediated mineralisation

Alkaline phosphatase (ALP) activity was quantified as an early marker for osteoblast differentiation using the cell-lysis eluate from the PicoGreen™ assay at day 7. Additionally, cell-mediated calcium production was quantified using a Calcium (CPC) LiquiColor™ test (Stanbio, Ireland). Three scaffolds per group (n=3) at day 28 were added to 1 ml of 0.5 M hydrochloric acid. Samples were left shaking overnight (18-24 hrs) at 4°C before performing the assay as per the manufacturer's instructions.

3.2.8 Biological characterisation of metal salt incorporated scaffolds – analysis of angiogenesis

3.2.8.1 Cell culture and seeding

Human Umbilical Vein Endothelial Cells (HUVECs) were cultured in EndoGRO complete culture medium (SCME002, Merck Millipore) under standard culture conditions (37°C, 5% CO_2, and 95% relative humidity).

3.2.8.2 Matrigel assay

The ability of the eluate from both scaffold systems to support tubule formation was assessed using a Matrigel® assay. Matrigel® basement membrane matrix (Corning, USA) was added to 24-well plates (120 µl/well) and the plates were incubated for 30 mins at 37°C. HUVECs were seeded at 30,000 cells/well. Seperately, cell-free scaffolds (n=3) were placed in 1 ml of endothelial medium and incubated at 37°C under standard cell culture conditions for 24 hrs and the 1 ml of eluate was added to the seeded HUVECs. At 4, 12, and 24 hrs the Matrigel cultures were imaged using a digital microscope (Lecia DMIL, Lecia Microsystems). Three images per well were

captured and analysed for total tubule length using ImageJ software and an in-house developed plug-in.

3.2.9 Statistical analysis

Data are presented as mean ± standard deviation. Statistical analysis was performed using GraphPad Prism software. Two-tailed unpaired t-tests or one-way or two-way ANOVAs were conducted where appropriate followed by a Bonferroni post-hoc test for multiple pairwise comparisons between groups. A p-value of 0.05 or less was considered statistically significant ($p \leq 0.05$). The Pearson product correlation coefficient (r) was used to determine the strength and direction of a linear relationship. An r value of 0.7-1 was considered a strong positive correlation. Three biological and three technical repeats were performed for all experiments and assays.

3.3 Results

3.3.1 Glutaraldehyde vapour crosslinking improves scaffold mechanical properties and supports mammalian cell viability

Exposing the scaffolds to glutaraldehyde vapour for 4 or 12 hrs resulted in a significant increase in scaffold compressive modulus vs. the non-crosslinked collagen/chitosan control ($p < 0.001$), greater than 2.5- or 2-fold, respectively (**Figure 3.9** A). In addition, the crosslinked scaffolds maintained their height upon hydration; the non-crosslinked collagen/chitosan control showed a significant height reduction when hydrated ($p < 0.01$) (**Figure 3.9** B&C).

Figure 3.9 Effect of glutaraldehyde vapour crosslinking on scaffold compressive modulus and hydrated height
*(A) Compressive modulus of collagen/chitosan scaffolds crosslinked with glutaraldehyde vapour for 0, 4, or 24 hrs (non-x-linked, 4 hrs glut, and 24 hrs glut, respectively) (B) Glutaraldehyde vapour crosslinked scaffolds maintain their height upon hydration when compared to the non-crosslinked control. (C) Visual appearance of non-crosslinked scaffolds and 4 hrs glut crosslinked scaffolds upon hydration. Data presented as mean ± SD, n=3, p-values are calculated using one-way ANOVA with Bonferroni post-hoc test. All statistical significance shown in comparison to non-crosslinked collagen/chitosan control unless otherwise stated, *p < 0.05, **p < 0.01, ***p < 0.001.*

Based on these results, 4 hrs was selected over the 24 hr treatment duration to reduce processing times and minimise the potential for toxicity.

A glycine wash step post-glutaraldehyde vapour treatment was included in cytocompatibility testing as it has been shown that washing with glycine can deactivate non-crosslinked glutaraldehyde residues [101], [233]. When cytocompatibility was assessed at 24 hrs post seeding, all 4 hrs glut treated scaffolds reduced the metabolic activity of the cells (alamarBlue® assay, $p < 0.001$) (**Figure 3.10** A). However, levels of DNA (or cell number) on glutaraldehyde treated scaffolds were maintained in comparison to the non-crosslinked collagen/chitosan control scaffold (**Figure 3.10** B). In addition, when the metabolic activity per cell is analysed, the 4 hrs glut scaffold with the addition of a glycine wash step post-treatment show improved cytocompatibility ($p < 0.01$) (**Figure 3.10** C).

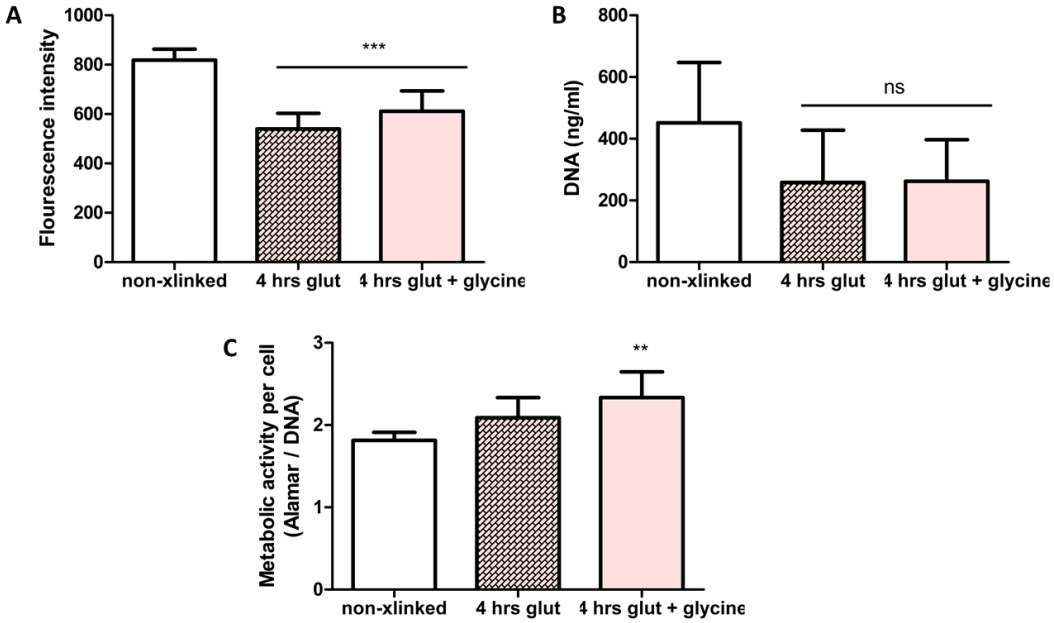

Figure 3.10 Effect of glutaraldehyde vapour crosslinking on mammalian cell cytocompatibility

(A) *Cell metabolism was measured using alamarBlue® assay; (B) DNA as a measure of cell number measured using PicoGreen™ assay, and (C) Metabolic activity per cell or alamarBlue® normalised to DNA on cell-seeded scaffolds which were either non-crosslinked collagen/chitosan scaffolds (non-x-linked), scaffolds crosslinked using glutaraldehyde vapour for 4 hrs (4 hrs glut), or scaffolds crosslinked using glutaraldehyde vapour for 4 hrs plus a glycine wash post-crosslinking (4 hrs glut + glycine). Data presented as mean ± SD, n=3, p-values are calculated using one-way ANOVA with Bonferroni post-hoc test. All statistical significance shown in comparison to non-crosslinked collagen/chitosan control unless otherwise stated, *p < 0.05, **p < 0.01, ***p < 0.001.*

To summarise, glutaraldehyde vapour treatment successfully crosslinked collagen/chitosan control scaffolds as demonstrated by increased compressive modulus. In addition, glutaraldehyde treated scaffolds with the addition of a glycine wash step post-treatment showed improved cytocompatibility. Thus, moving forward, all scaffolds undergoing glutaraldehyde vapour crosslinking were crosslinked for 4 hrs, followed by a glycine wash step.

3.3.3 Chitosan microparticle encapsulation resulted in a high particle yield and suitable size

Chitosan microparticles with and without metal salts were fabricated via a spray-drying process which resulted in the successful production of particles at a high average yield of approximately 75% (**Table 3.3**).

Table 3.3 *Percentage yield of chitosan/metal salt microparticles*

Chitosan microparticle yield	
Blank-microparticles	74.5 %
Copper-microparticles	73.6 %
Zinc-microparticles	78.24 %

The microparticles were confirmed to be within the 0.1-20 µm range upon Mastersizing analysis, with a bimodal size distribution, which is common in these particle types [240] (**Figure 3.11**). Immersing the particles within aqueous glutaraldehyde solution for crosslinking resulted in a change in particle colour (referred to as glutaraldehyde *tanning* [241]) and particle swelling that resulted in a subsequent shift in particle size to 2-80 µm, as confirmed by light microscopy (**Figure 3.11** A-F). The final particle size achieved is known to be suitable to withstand endocytosis by mammalian cells [226].

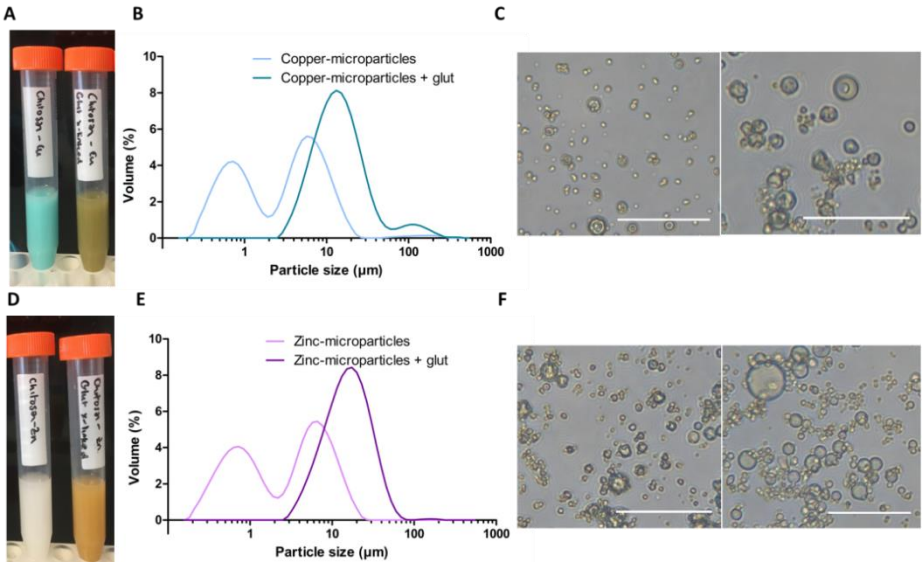

Figure 3.11 Size and morphology of chitosan metal salt encapsulated microparticles

(A) *Macroscopic appearance of copper-microparticles before crosslinking (left) and after glutaraldehyde crosslinking (right). (B) Size range of copper-microparticles before and after crosslinking. (C) Microscopic appearance of microparticles before crosslinking (left) and after glutaraldehyde crosslinking (right). (D-F) Same as top figures, but for chitosan zinc-microparticles. Note swelling of particles post-crosslinking in aqueous glutaraldehyde to 2-80 µm. Scale bars 200 µm.*

3.3.4 Directly-loaded and microparticle-loaded scaffolds offer two distinct copper and zinc ion release profiles

3.3.4.1 Metal ions undergo burst release from directly-loaded scaffolds

A range of concentrations of metal salts were directly incorporated into the collagen/chitosan scaffolds (0, 16, 24, and 32 mM of copper chloride or zinc chloride) and ion release over a 28-day time period was analysed. For all copper chloride and zinc chloride loaded scaffolds, increasing the initial loading concentration (0 – 32 mM) increased the total released concentration (0 – 18.9 mM). Additionally, glutaraldehyde vapour crosslinking increased the total percentage of metal ions released from the scaffolds over the 28 days (**Figure 3.12** A-H). In terms of crosslinked scaffolds, the initial concentration of metal ions incorporated into the scaffold did not affect the total percent of released ions on day 28 (normalised to loaded ions): 56-59% for copper and 50-63% for zinc. However, in terms of the rate of initial ion release (up to 24 hrs), copper chloride scaffolds released ions more gradually than zinc chloride scaffolds, with 33-40% and 40-49% of the ions being released, respectively.

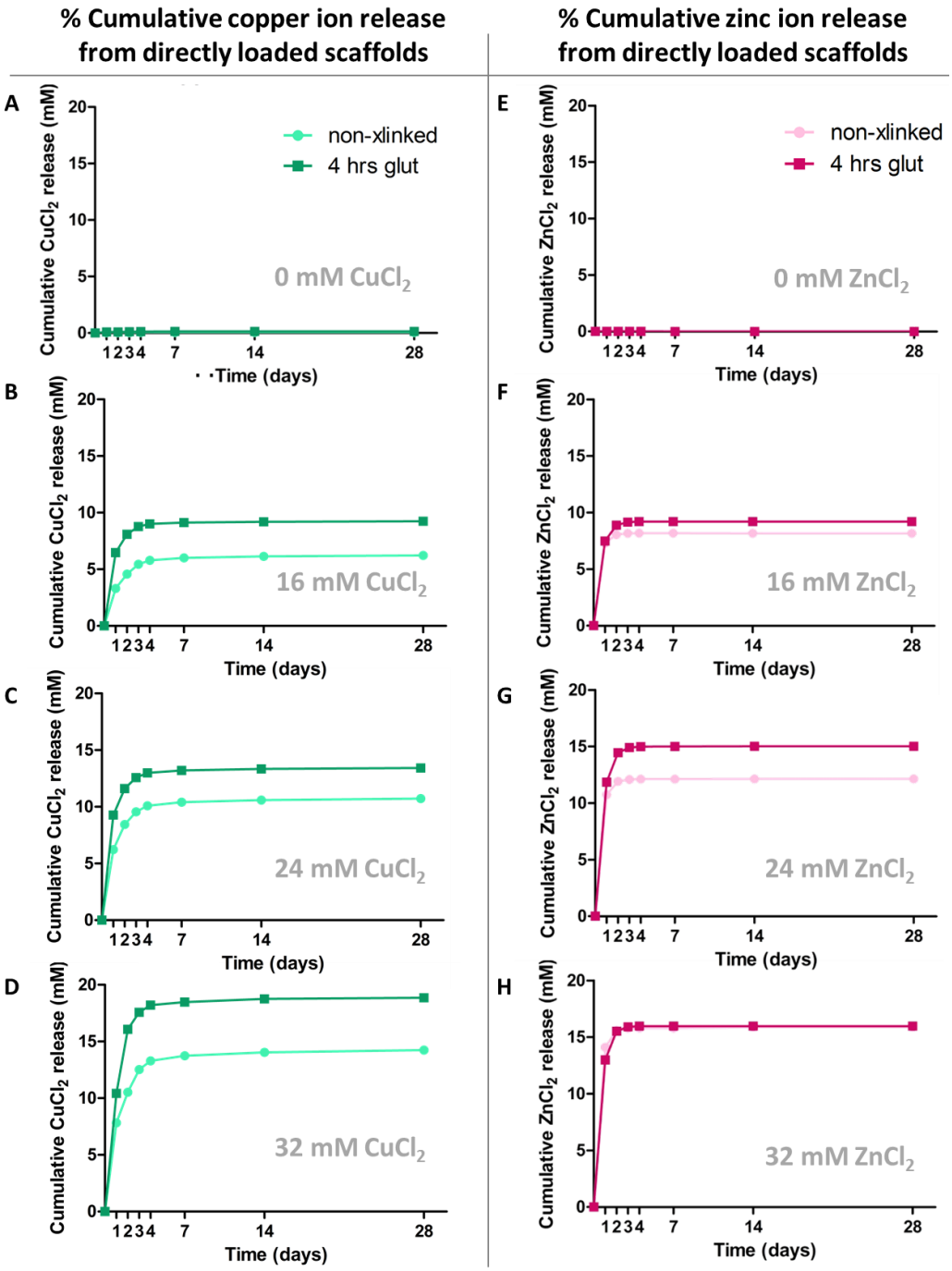

Figure 3.12 Cumulative release of copper and zinc ions from directly-loaded scaffolds

(A-D) Cumulative copper and (E-F) zinc ion release from directly-loaded 0, 16, 24, and 32 mM copper chloride and zinc chloride scaffolds over 28 days for both non-crosslinked (non-x-linked) and 4 hrs glut scaffolds. Note burst release of ions and the increased ion release from all glutaraldehyde crosslinked scaffolds vs non-crosslinked.

3.3.4.2 Microparticles and microparticle-loaded scaffolds prolong the release of metal ions

The microparticles successfully controlled the release of metal salts over the 28 day time period, with close to zero order release kinetics (released at a constant rate) from both copper- and zinc-microparticles (R^2 = 0.9801 and 0.9744, respectively) (**Figure 3.13** A&C – figure represents ion release from 15 mg of particles equivalent to 3:1 loaded into scaffolds). When copper-microparticles are incorporated into collagen scaffolds, the release profile is modulated: there is a controlled, rapid release phase up to day 5, followed by a more gradual release that was continuous to day 28 (80% released by day 5) (**Figure 3.13** B). For zinc-microparticles, the release kinetics appear more similar to the directly-loaded scaffolds, with a burst release up to day 3 and no evidence of release thereafter. However, the total amount of zinc released is lower than the microparticles alone (total released ions – 1.49 vs. 0.59 mM, respectively) (**Figure 3.13** D).

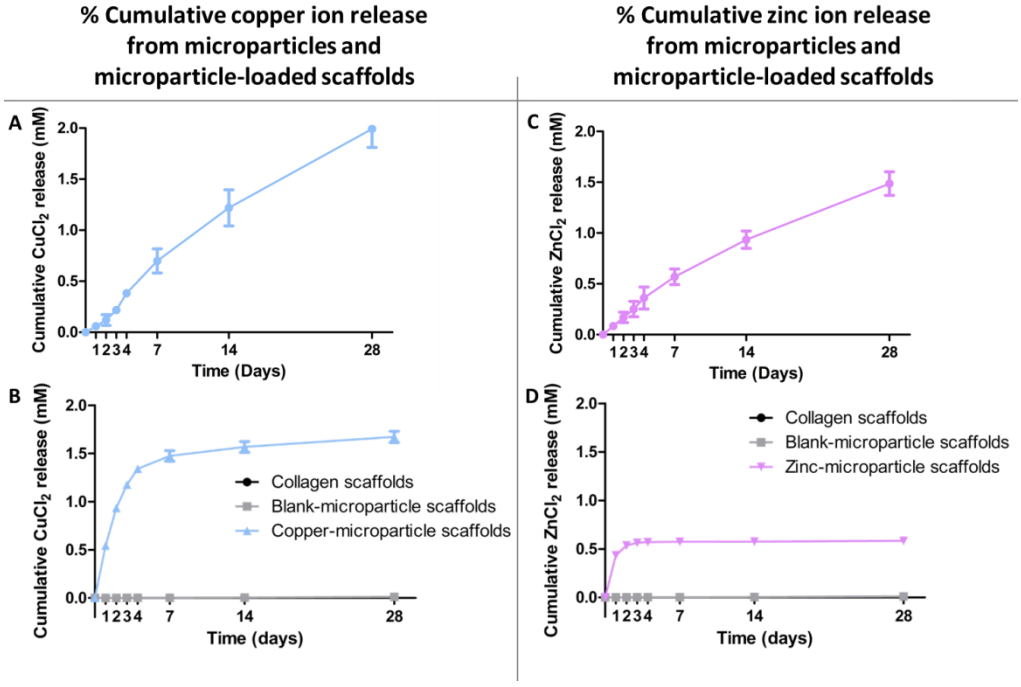

Figure 3.13 Cumulative release of copper and zinc ions from microparticles and microparticle-loaded scaffolds
(A) *Cumulative copper ions released from copper-microparticles and (B) cumulative copper ions released from copper-microparticle scaffolds over 28 days. (C) Cumulative zinc ions released from zinc-microparticles and (D) cumulative zinc ions released from zinc-microparticle scaffolds over 28 days. Note controlled ion release rate from both microparticles. A&C represent ion release from 15 mg of particles equivalent to the 300% loaded into scaffolds.*

3.3.5 Directly-loaded and microparticle-loaded scaffolds demonstrate antibacterial activity against *Staphylococcus aureus*

All copper chloride and zinc chloride directly-loaded scaffolds show significant antibacterial activity against *S. aureus* on agar plates as assessed by both macroscopic inspection (**Figure 3.14** A&D) and by quantification of the zones of inhibition (**Figure 3.14** B&E). Notably, increasing the concentration of metal salt within the scaffold increases the zone of inhibition (24 mM & 32 mM $CuCl_2$ & 32 mM $ZnCl_2$). In the time-kill assay, all scaffolds showed significant antibacterial activity against *S. aureus* in comparison to the collagen control (**Figure 3.14** C&F). Interestingly, although they did not show visible antibacterial activity on agar, 0 mM collagen/chitosan control scaffolds show almost complete inhibition in both time-kill assays.

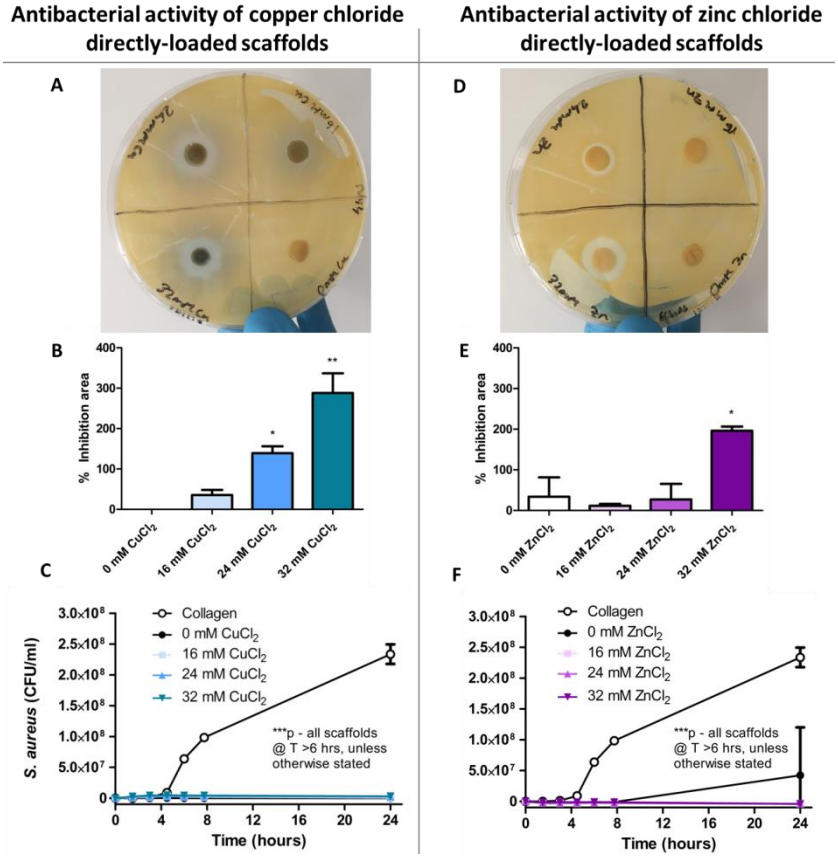

Figure 3.14 Antibacterial activity of directly-loaded scaffolds
Results for directly-loaded (A-C) copper chloride and (D-F) zinc chloride scaffolds. (A&D) Antibacterial activity against S. aureus *lawned agar plates via zones of inhibition. (B&E) Quantified zones of inhibition. (C&F) Time-kill assay in broth over 24 hr time period. Note: 0 mM scaffolds are collagen/chitosan only. Data presented as mean ± SD, n=3, p-values are calculated using one and two-way ANOVA with Bonferroni post-hoc test. All statistical significance shown in B&E is in comparison to 0 mM control and C&F is in comparison to collagen control, unless otherwise stated, *p < 0.05, **p < 0.01, ***p < 0.001.*

The copper-microparticle and zinc-microparticle loaded scaffolds have small increases in their zones of inhibition vs. *S. aureus* when compared to collagen only and blank-microparticle loaded collagen scaffolds (**Figure 3.15** A). This was confirmed by quantification (>6 – 7% increase in zone of inhibition, $p < 0.01$) (**Figure 3.15** B). In the time-kill assay, copper-microparticle loaded scaffolds induce a small but significant delay the growth of *S. aureus* between 6 and 24 hrs in comparison to the collagen control ($p < 0.001$) (**Figure 3.15** C). Zinc-microparticle loaded scaffolds also showed a marginal yet significant reduction in growth at 6 hrs and at 24 hrs ($p < 0.05$ and $p < 0.001$, respectively) (**Figure 3.15** D).

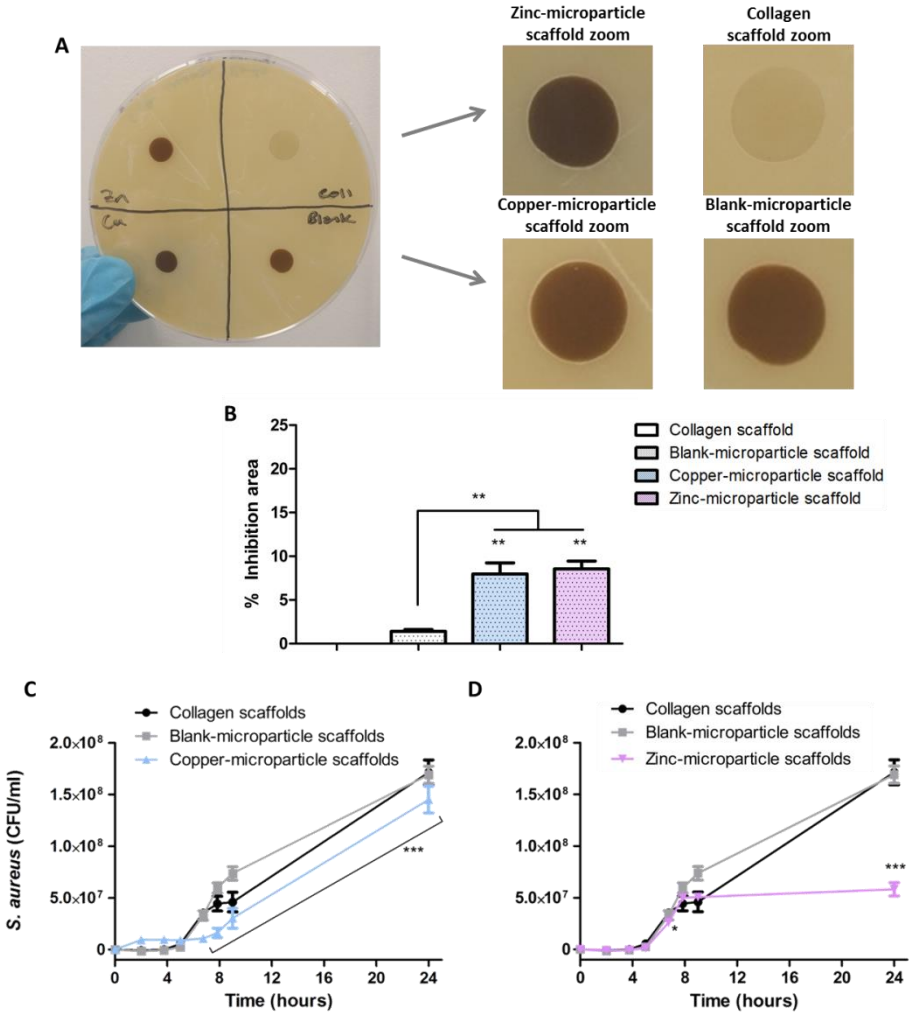

Figure 3.15 Antibacterial activity of microparticle loaded scaffolds
(A) Antibacterial activity of copper- and zinc-microparticle loaded scaffolds against S. aureus *lawned agar plates via zones of inhibition. (B) Quantified zones of inhibition. (C&D) Time-kill assay in broth over 24 hr time period. Data presented as mean ± SD, n=3, p-values are calculated using one and two-way ANOVA with Bonferroni post-hoc test. All statistical significance shown in comparison to collagen control unless otherwise stated, *p < 0.05, **p < 0.01, ***p < 0.001.*

In general, although both scaffold types successfully showed antibacterial activity, the microparticle-loaded scaffolds did not have as profound an effect as the directly-loaded scaffolds against *S. aureus.* This was true both in terms of zone of inhibition size on agar and in the time-kill assay and was attributed to reduced metal salt release (approx. 7 mM vs. 1 mM for copper and zinc directly-loaded and microparticle-loaded scaffolds at day 1, respectively). Thus, in order to minimise toxicity towards mammalian cells (data from Chapter 2), the lowest concentration of the directly-loaded scaffolds that display antibacterial activity (16 mM) and 0 mM control were brought forward for all further analysis. The microparticle-loaded scaffolds and controls (collagen and blank-microparticle scaffolds) were also brought forward for all further analysis (**Table 3.4**).

Table 3.4 *Scaffold groups brought forward for all further assessment including* in vitro *cytocompatibility, osteogenic, and angiogenic potential assessment* in vitro

	Directly-loaded collagen/chitosan scaffolds	**Chitosan microparticle-loaded scaffolds**
Controls	0 mM (collagen/chitosan scaffold)	Collagen scaffold
	-	Blank-microparticle scaffold
Copper	16 mM $CuCl_2$ scaffold	Copper-microparticle scaffold
Zinc	16 mM $ZnCl_2$ scaffold	Zinc-microparticle scaffold

3.3.6 Microarchitectural & mechanical properties of directly-loaded and microparticle-loaded scaffolds are suitable for bone tissue engineering

Having shown the antibacterial potential of the scaffolds, the microarchitectural and mechanical properties of the scaffolds were next investigated. In terms of porosity, all directly-loaded scaffolds are extremely porous at more than 98% and there was a significant, albeit marginal, increase in scaffold porosity upon copper and zinc addition in comparison to the collagen/chitosan control scaffold ($p < 0.001$) (**Figure 3.16** A). In contrast, but

not surprisingly, there was a decrease in the porosity of scaffolds upon microparticle addition ($p < 0.001$) and there was a significant increase in porosity upon copper and zinc incorporation within the microparticles ($p < 0.001$) (**Figure 3.16** D). However, all microparticle-loaded scaffolds remain highly porous at >94%, which is greater than the reported suitable porosity required for tissue engineering applications (90%) [242].

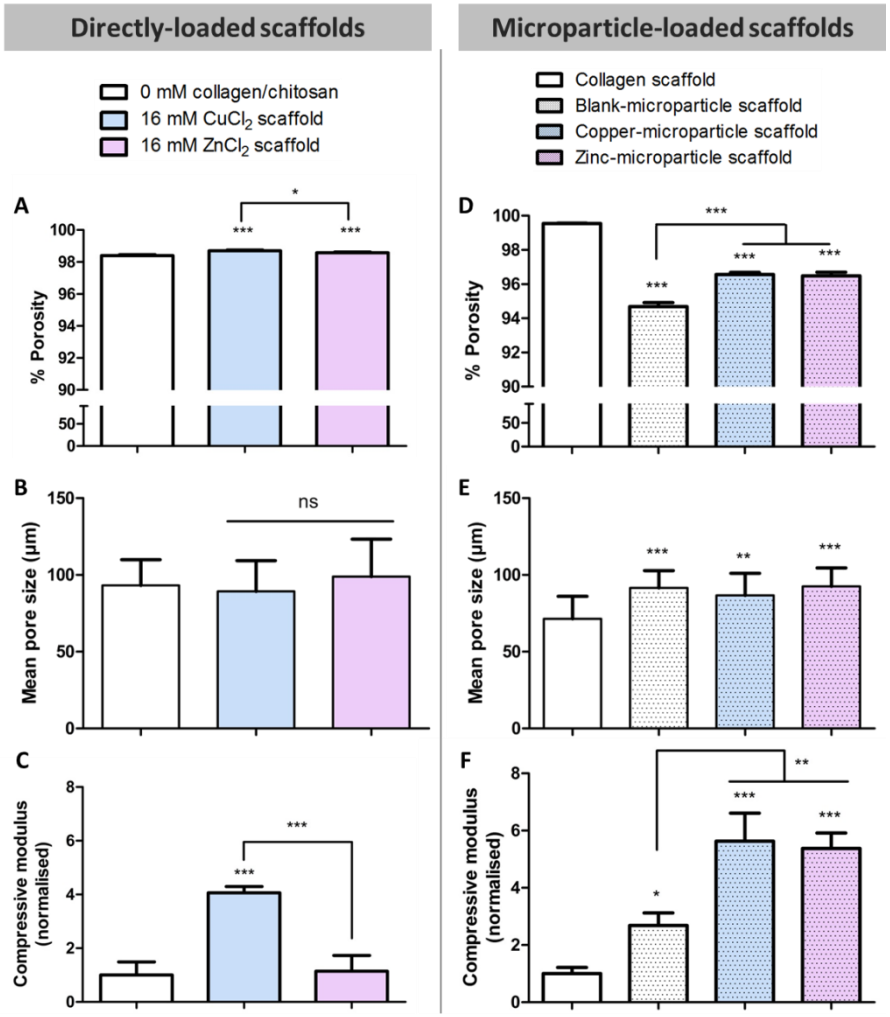

Figure 3.16 Microarchitectural and mechanical properties of directly-loaded and microparticle-loaded scaffolds
*Results for directly-loaded (A-C) and microparticle-loaded (D-F) scaffolds showing (A&D) scaffold porosity, (B&E) pore size, and (C&F) compressive modulus normalised to control (0mM or collagen). Data presented as mean ± SD, n=3, p-values are calculated using one-way ANOVA with Bonferroni post-hoc test. All statistical significance shown in comparison to collagen/chitosan or collagen control unless otherwise stated, *p < 0.05, **p < 0.01, ***p < 0.001.*

For directly-loaded scaffolds, the addition of copper chloride or zinc chloride did not significantly affect scaffold pore size, with all scaffolds achieving a mean pore size ranging from 89-99 µm (**Figure 3.16** B). The addition of

microparticles resulted in a significant increase in scaffold mean pore size (from 71 to 87-93 μm) (**Figure 3.16** E).

The addition of copper chloride to directly-loaded scaffolds significantly increased the compressive modulus of the collagen/chitosan control ($p < 0.001$) (**Figure 3.16** C). However, zinc chloride directly-loaded scaffolds did not have the same increase in compressive modulus. Notably, the addition of microparticles to the collagen scaffold significantly increased its compressive modulus (2.7-fold, $p < 0.001$), with metal salt-loaded microparticles further enhancing this effect (>5-fold increase vs. control, $p < 0.01$) (**Figure 3.16** F).

3.3.7 Directly-loaded and microparticle-loaded scaffolds support mammalian cell growth and osteogenesis *in vitro*

Having demonstrated the antibacterial potential of the directly-loaded and microparticle-loaded scaffolds, the scaffold's ability to maintain mammalian cells and support osteogenesis *in vitro* was tested next. This is crucial given the fine balance between antibacterial activity and mammalian cell toxicity as identified in Chapter 2. In terms of cell survival, the results show that the directly-loaded scaffolds (specifically copper chloride loaded scaffolds) experienced reduced cell number at each time point in comparison to the 0 mM control (**Figure 3.17** A). However, although cell numbers generally drop-off slightly at day 7 on the directly-loaded scaffolds, they then increase over time at 28 days. On the other hand, when the release is minimised within a microparticle-loaded scaffold (**Figure 3.17** E), the scaffolds maintain cell numbers in comparison to controls at each time point. The cell numbers are generally maintained for the microparticle-loaded scaffolds, with a minimal reduction over time. Zinc-microparticle scaffolds do not show toxicity issues – likely due to reduced ion release, but interestingly, the directly-loaded zinc scaffolds also do not show toxicity issues.

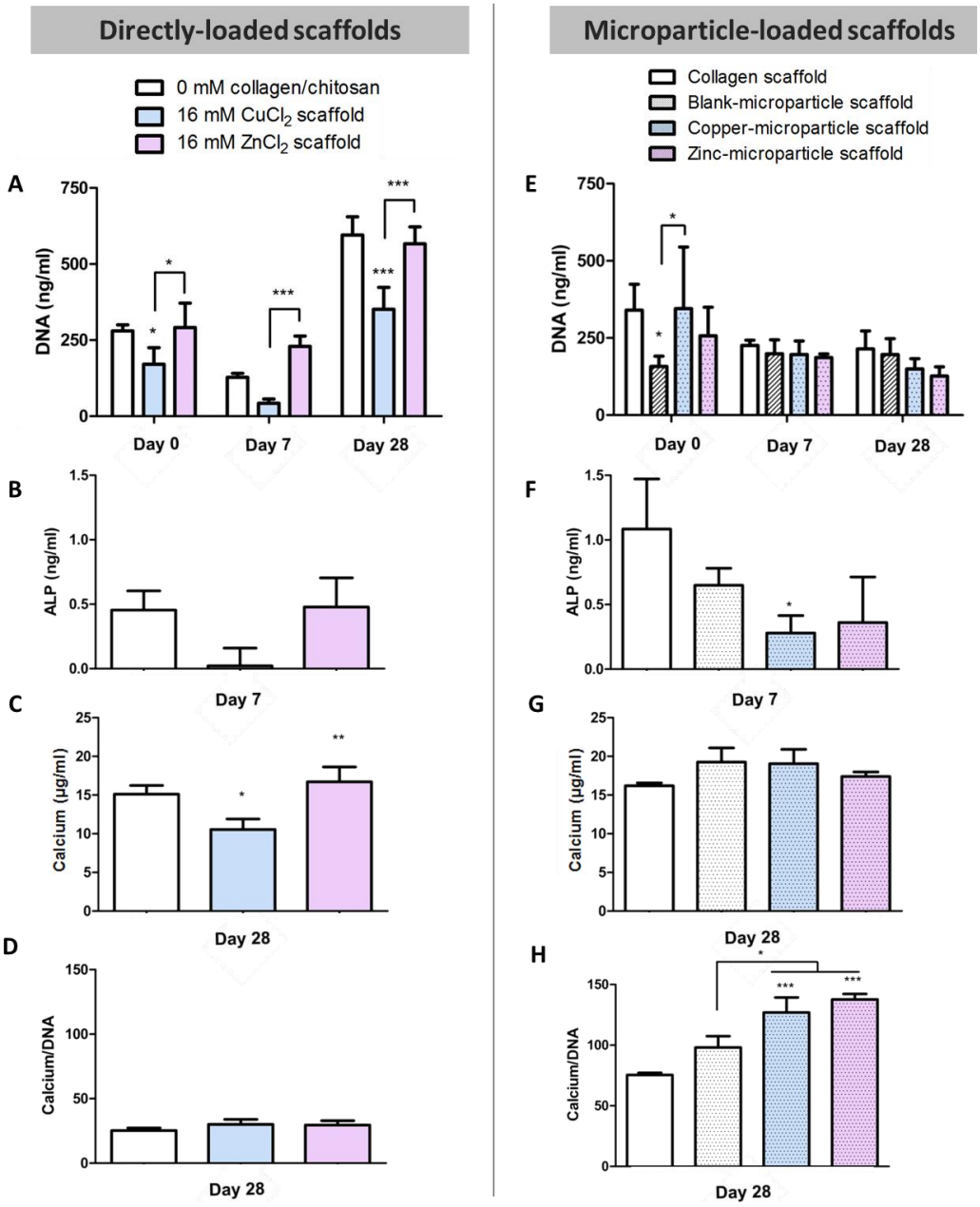

Figure 3.17 Effect of directly-loaded and microparticle-loaded scaffolds on osteogenesis

*Results for directly-loaded (A-D) and microparticle-loaded (D-H) scaffolds showing (A&E) PicoGreen™ assay on scaffolds at days 0, 7, and 28 days after supplementation with osteogenic medium. (B&F) Alkaline phosphatase (ALP) activity on scaffolds at day 7. (C&G) Total raw calcium values from scaffolds at day 28. (D&H) Calcium values normalised to DNA at day 28. Data presented as mean ± SD, n=3, p-values are calculated using one-way or two-way ANOVA with Bonferroni post-hoc test. All statistical significance shown in comparison to collagen/chitosan or collagen control unless otherwise stated, *p < 0.05, **p < 0.01, ***p < 0.001.*

In terms of osteogenic response, the alkaline phosphatase (ALP) activity is not increased on any scaffold at day 7 in comparison to the controls (**Figure 3.17** B&F). In fact, all copper containing scaffolds show significantly reduced ALP

activity. When calcium levels were quantified, the directly-loaded copper chloride scaffolds show decreased calcium levels in comparison to the control ($p < 0.05$), whereas directly-loaded zinc chloride scaffolds show significantly increased calcium levels in comparison to the control ($p < 0.01$) (**Figure 3.17** C). However, when normalised to cell number, this effect is lost (**Figure 3.17** D). The opposite is seen, however, for the microparticle-loaded scaffolds – little difference is seen between raw calcium values (**Figure 3.17** G), but, when normalised to cell number, the calcium levels in metal salt microparticle-loaded scaffolds are significantly higher than the collagen control ($p < 0.001$), with zinc-microparticles producing the highest result (**Figure 3.17** H).

3.3.8 Metal ions released from directly-loaded and microparticle-loaded scaffolds can enhance angiogenesis *in vitro*

The results above show that, with the exception of the copper chloride directly-loaded scaffolds, the majority of scaffolds supported cell viability and did not inhibit osteogenesis. Thus, the ability of the scaffolds to support angiogenesis was next investigated, as copper has previously been suggested to be pro-angiogenic by upregulating VEGF production [137]. To do so, eluate was collected from scaffolds incubated in media for 24 hrs and added to the Matrigel® assay. Tubule formation was analysed at 4, 12, and 24 hrs after eluate addition. The eluate from copper chloride directly-loaded scaffolds was shown to significantly increase total tubule length in the Matrigel® assay at 12 hrs in comparison to all other scaffolds ($p < 0.001$) (**Figure 3.18** A). However, this effect was lost at 24 hrs. Similar to the directly-loaded scaffolds, copper-microparticle-loaded scaffolds showed increased total tubule length vs. the collagen and control, however, this increased tubule length was maintained from 4-24 hrs ($p < 0.01$) (**Figure 3.18** B). Interestingly, for the microparticle-loaded scaffolds, zinc-microparticle scaffolds showed significantly increased total tubule length at 12 and 24 hrs ($p < 0.001$). Taken together, the data demonstrates the pro-angiogenic ability of copper in both systems, however, in comparison to the directly-loaded scaffolds, the smaller dose released from the microparticle-loaded scaffolds had the ability to prolong the angiogenic response over the three time points analysed.

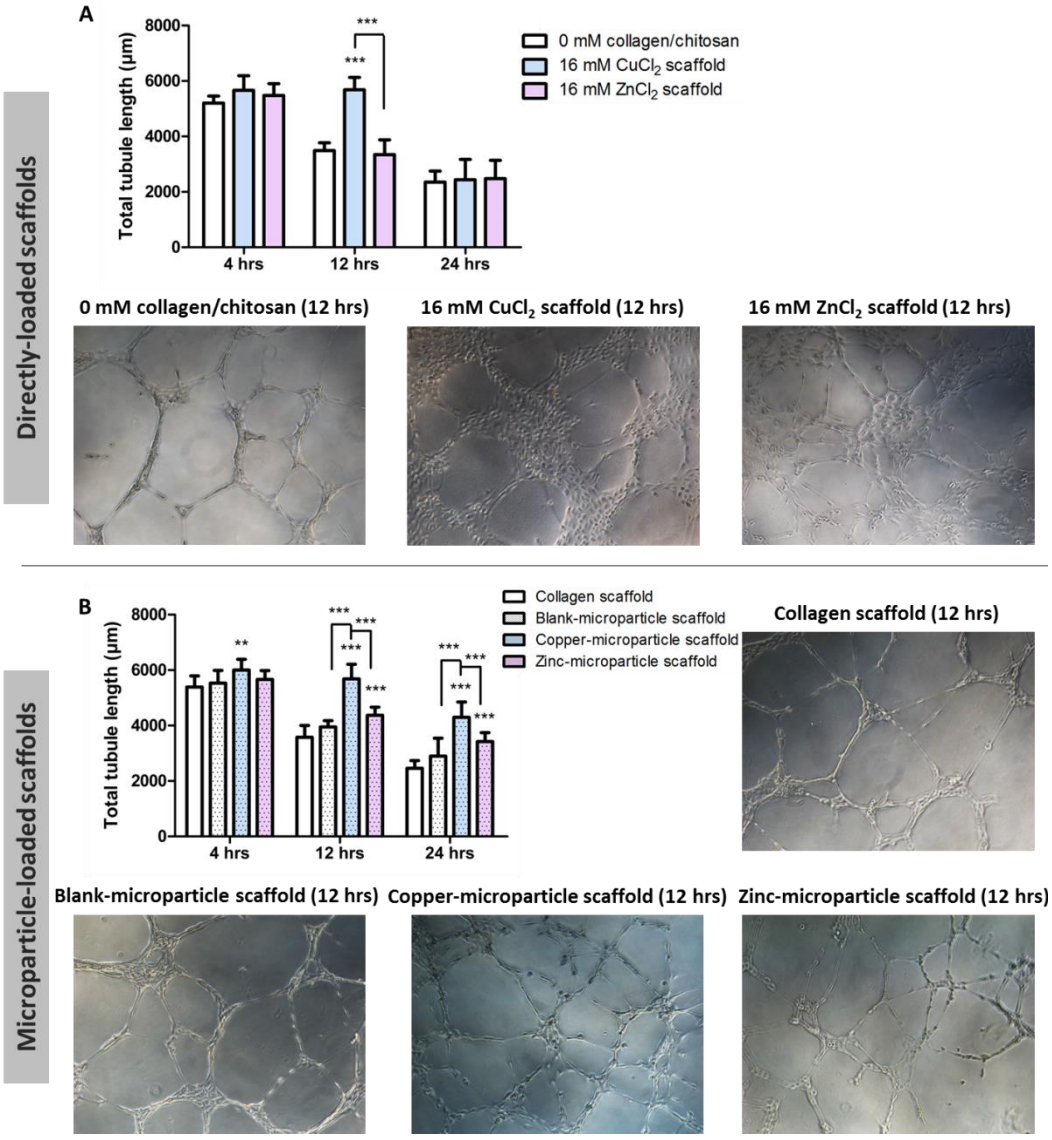

Figure 3.18 Effect of directly-loaded and microparticle-loaded scaffolds on angiogenesis

*Total tubule length (µm) quantification from Matrigel® assay at 4, 12, and 24 hrs with brightfield images of tubule formation in assay at 12 hrs post-seeding of human endothelial vascular endothelial (HUVEC) cells cultured with conditioned medium from (A) directly-loaded scaffolds and (B) microparticle-loaded scaffolds. Data presented as mean ± SD, n=3, p-values are calculated using two-way ANOVA with Bonferroni post-hoc test. All statistical significance shown in comparison to collagen/chitosan or collagen control unless otherwise stated, *p < 0.05, **p < 0.01, ***p < 0.001.*

3.4 Discussion

The objective of this study was to develop a 3D scaffold that releases copper of zinc ions at a release rate that provides antibacterial activity, with minimal mammalian cell toxicity. The aim of these scaffolds is thus to have a dual function: treat osteomyelitis infection, while facilitating or enhancing bone tissue formation. We successfully developed fabrication strategies for two different ion release systems: a directly-loaded scaffold group and a microparticle-loaded scaffold group. The results demonstrate that, for copper loaded microparticles specifically, the microparticles controlled the metal salt release from the scaffolds over a 28-day time period, in comparison to the directly-loaded scaffolds. Both the directly-loaded and microparticle-loaded scaffolds display antibacterial activity to varying degrees, with directly-loaded scaffolds showing the most potent activity against *S. aureus*. In terms of microarchitectural and mechanical properties, both scaffold formulations were highly porous and had suitable pore size for bone tissue engineering. The directly-loaded microparticle-loaded scaffolds at least maintained the compressive modulus, but in most cases enhanced the scaffold compressive modulus. Most importantly, all directly-loaded and microparticle-loaded scaffolds supported mammalian cell survival. In addition, zinc incorporated directly-loaded and microparticle-loaded scaffolds performed well in terms in terms of osteogenic effect by supporting calcium production. Finally, the copper-containing directly-loaded and microparticle-loaded scaffolds both enhanced angiogenesis at the majority of time points tested.

Initially in this chapter, the effect of glutaraldehyde vapour treatment on collagen/chitosan scaffolds was assessed in terms of mechanical properties and cytocompatibility. The results demonstrate that the treatment successfully crosslinked the scaffolds whilst having a minimal effect on cell compatibility. This new crosslinking technique has now been introduced to our lab and was particularly useful here to negate the premature loss of metal ions from the scaffolds. Furthermore, this crosslinking technique could be (and has been) applied to a host of different scaffolds developed which incorporate precious cargo such as growth factors or genetic material, without leaching.

When the release kinetics from both of the scaffold systems was investigated, it was found that the directly-loaded scaffolds released their metal ions in a typical manner, with a quick burst release of 33-49% of incorporated ions within 24 hrs. Interestingly, the scaffolds that underwent glutaraldehyde vapour crosslinking showed an increase in the total released metal salt from all directly-loaded scaffolds in comparison to non-crosslinked scaffolds. This may be attributed to the glutaraldehyde crosslinking allowing a more robust scaffold with an open, porous structure which does not collapse upon hydration (as shown in **Figure 3.9** C) and thus, allows a higher percentage of metal ion release. The metal salt-loaded chitosan microparticles produced achieved near zero-order release kinetics (released at a constant rate) over the 28 days. When these were incorporated into the scaffold and glutaraldehyde crosslinked, specifically for copper-microparticle scaffolds, some controlled release kinetics were retained; controlled rapid release rate up to day 5 and continued release up to day 28. However, for zinc-microparticle scaffolds there was a burst release until day 3 with no further release thereafter. This may be affected by the microparticles being immersed in the acidic scaffold slurry during fabrication, as chitosan microparticles have been shown previously to be pH-responsive, with increased swelling at lower pH and thus increased drug release via increased permeation [243], [244]. However, the copper-microparticles maintain some of their controlled release properties with continued salt release occurring up until day 28, in comparison to directly-loaded scaffolds where approximately all of the released salts occur by day 4. It must be noted that in general, the microparticle-loaded scaffolds release a significantly lower level of ions than the directly-loaded scaffolds (approx. 1 mM vs 7 mM). In a clinical scenario, a burst release of antibacterial salts above the MIC may assist in infection clearance; however, this would possibly be required over a number of days, until the infection is cleared. Therefore, a combinatory burst and controlled-release system, such as in the form of chitosan microparticles produced here, would be advantageous.

It was found that all scaffolds containing copper chloride or zinc chloride incorporated via direct-loading or microparticle-loading proved to be effective against *S. aureus* and produced a zone of inhibition on agar pates,

microparticle-loaded scaffolds albeit marginal. Notably, increasing the concentration of metal salt within the directly-loaded scaffold increased the zone of inhibition while the microparticle-loaded scaffolds showed smaller zones of inhibition due to reduced metal salt release. These results are supported by the broth time-kill assays, where all directly-loaded scaffolds (including collagen/chitosan control) show significant antibacterial activity against *S. aureus* in comparison to the collagen secondary control. Not surprisingly, as their function is to modulate metal ion release, the microparticle-loaded scaffolds did not have as profound an effect as directly-loaded scaffolds; however, they did achieve significantly delayed *S. aureus* growth at various time points vs. the collagen control. Perhaps, in future work, increasing the concentration of metal salts within the microparticles or using a combinatory approach of directly-loaded collagen/chitosan scaffolds loaded with microparticles (as suggested previously), might be advantageous.

It was found that following addition of directly-loaded copper chloride and zinc chloride, all scaffolds remained highly porous, at >98%. While a decrease in scaffold porosity was observed upon microparticle addition, an effect previously observed within our lab upon polymeric microparticle addition to collagen scaffolds [245], all microparticle-loaded scaffolds remained almost as porous at >94%. A decrease in scaffold porosity was For all scaffolds containing copper and zinc (16 mM $CuCl_2$ scaffold, 16 mM $ZnCl_2$ scaffold, copper-microparticle scaffold, and zinc-microparticle scaffold), there was a significant increase in scaffold porosity in comparison to the control scaffolds (0 mM and blank-microparticle scaffold), which might be attributed to a production of a gaseous vapour between the acetic acid solvent and the copper chloride and zinc chloride salts which would increase the number of nucleation points during freeze drying, and hence the number of pores. All scaffolds fabricated achieved porosities >90% - a porosity level that is generally recommended to achieve good cell infiltration and nutrient/waste transport throughout the construct; all scaffolds fabricated are in this range [246], [247]. Additionally, the pore sizes for the directly-loaded and microparticle-loaded scaffolds (89-99 μm and 71-92 μm, respectively) are within the ideal range for bone tissue engineering applications [248]–[250].

Mechanical robustness is advantageous for tissue engineered scaffolds, not only from a surgical handling perspective, but also for cell infiltration and as an additional osteogenic stimulus, as increased scaffold stiffness has previously been shown to influence the differentiation of mesenchymal stem cells (MSC) down an osteogenic lineage [86]. The directly loaded copper chloride scaffolds had a significantly increased compressive modulus vs. the collagen/chitosan control; however, directly loaded zinc chloride scaffolds did not show the same mechanical enhancement. This was surprising, as upon handling the scaffolds in their pre-hydrated state, there was a noticeable increase in apparent mechanical strength of zinc-loaded scaffolds vs. the control that was not reflected in the mechanical testing results. This is possibly attributable to a more rapid release of zinc from the scaffolds during the hydrated mechanical testing (see discussion on zinc release). Notably, the addition of microparticles to the collagen scaffold significantly increased its compressive modulus. A similar result was also previously observed within our lab upon polymeric microparticle addition to collagen scaffolds [245].

Having demonstrated the antibacterial activity and favourable mechanical and microarchitectural properties of the scaffolds, the ability of the scaffolds to support mammalian cells was next examined - crucial given the fine balance between antibacterial activity and mammalian cell toxicity as identified in Chapter 2. Overall, both scaffold systems support mammalian cell survival over the 28 days, with microparticle-incorporated scaffolds inducing less toxic effects in comparison to directly-loaded scaffolds at each time point, presumably due to the controlled/reduced metal salt release from the scaffolds, as discussed previously. Interestingly, cell numbers generally increased over the 28-day time period on the directly-loaded scaffolds – an effect not seen on the microparticle-loaded scaffolds. This may be explained by looking at the osteogenic response to the scaffolds – calcium levels are generally raised on microparticle-loaded scaffolds, in comparison to directly-loaded scaffolds, which may indicate terminal differentiation of osteoblasts, and thus may explain the maintenance, rather than rise in cell number over the 28-day period. Of note, and in contrast to copper directly-loaded scaffolds, zinc directly-loaded scaffolds performed well in terms in terms of osteogenic

effect by supporting calcium production. This is in agreement with the literature which suggests that zinc can promote osteogenesis through osteoblast proliferation and differentiation [175]–[177]. Both copper and zinc-microparticle scaffolds supported calcium production, presumably due to reduced ion release.

Finally, all copper-containing scaffolds enhanced angiogenesis at select time points as measured by increased total tubule length in a Matrigel® assay; however, the microparticle-loaded scaffolds out-performed the directly-loaded scaffolds. This is due to the reduced metal ion release from the scaffolds, which might be either less toxic towards the HUVEC cells or at the appropriate concentration to enhance angiogenesis. It is well-known that copper, in addition to showing antimicrobial activity, can stimulate angiogenesis and vasculogenisis, two essential processes in tissue repair and regeneration [138], [139]. In fact, a similar concentration of copper sulphate (0.5 mM) to the copper chloride ions released from the copper-microparticle scaffolds has been shown previously to enhance endothelial cell proliferation 2-fold [251]. Discovering the pro-angiogenic response to zinc-microparticle-loaded scaffolds here, on the other hand, was interesting as zinc has mixed reports in literature, being reported as both anti-angiogenic and pro-angiogenic metal [252]–[254].

In summary, and in terms of choosing a scaffold system, or parts of, for osteomyelitis treatment based on the results from this study, perhaps an ideal combination would be a base collagen/chitosan scaffold with zinc chloride salt directly-incorporated for a burst release of ions to clear the infection, followed by controlled release of copper ions the from microparticle system to stimulate angiogenesis. Once the ions have been depleted, the base collagen/chitosan scaffold might prevent infection reoccurrence whilst tissue regeneration is underway.

3.5 Conclusion

In this study, two different scaffold-based metal salt delivery systems were successfully developed; a directly-loaded scaffold group and a controlled-

release microparticle-loaded scaffold group. The results demonstrate that both scaffold types provided distinct metal salt release quantities and/or profiles which in turn influenced the antibacterial activity of the scaffolds against *S. aureus*. It was also found that the scaffolds did not elicit a significant toxic effect towards mammalian cells, some scaffolds supported osteogenesis, and all copper-incorporated scaffolds enhanced angiogenesis. In Chapters 4 and 5, the potential of two alternative materials are examined, hydroxyapatite and bioactive glass doped with antimicrobial metal ions, which we hypothesised might reduce infection whilst also enhancing osteogenesis.

Chapter 4 Development of a silver-doped hydroxyapatite scaffold for the release of antimicrobial ions and enhanced osteogenesis

4.1 Introduction

Hydroxyapatite, the main inorganic constituent of bone matrix, is widely used in bone tissue engineering as it is an osteoconductive material that shows good biocompatibility and biodegradability [2], [180], [181]. Clinically, hydroxyapatite is typically used either in powdered form where it is added directly into the bone defect as a paste, or as a coating on medical devices to enhance osseous ingrowth and prevent loosening [183]–[187].

For effective osteomyelitis treatment a combinatorial approach might be effective i.e. materials capable of osteogenic stimulation combined with materials capable of antimicrobial activity. One way to achieve a combinatorial approach is to merge both materials. For example, hydroxyapatite crystals can be doped with metal ions in order to enhance desirable effects such as osteogenesis (e.g. strontium) [189], angiogenesis (e.g. cobalt) [190], and antibacterial activity (e.g. silver or zinc) [191], [192]. Thus, in this chapter we wanted to investigate whether incorporating silver into an osteogenic carrier, such as hydroxyapatite, would render it more desirable for use in osteomyelitis treatment.

Silver is the most widely explored metal in controlling microbial growth, both in research and application, demonstrating effective antimicrobial activity against gram-positive and gram-negative bacteria as well as fungi [122]. However, beyond its potent antibacterial activity, there is nothing reported in the literature with regards to potential beneficial effects of silver on osteogenesis or angiogenesis – key processes in bone regeneration. In fact, there are a number of publications which report cytotoxicity issues with silver use, so controlling the dosage is crucial [255]–[258].

The overall aim of the study presented in this chapter was to investigate the potential bi-functional antibacterial and osteogenic capacity of collagen scaffolds functionalised with silver-doped hydroxyapatite (AgHA). We proposed that doping the silver into the hydroxyapatite would control its release from the scaffold which might limit potential cytotoxicity.

The specific objectives were to:

1) Fabricate and characterise various concentrations of silver-doped hydroxyapatite (0, 2, and 5% mol Ag)
2) Develop a method for incorporating the silver-doped hydroxyapatite at various concentrations into the collagen scaffold (based on antibacterial efficacy study results from Chapter 2), and investigate the effect of silver-doped hydroxyapatite addition on scaffold mechanical and microarchitectural properties
3) Examine the effect of both silver-doping percentage within the hydroxyapatite (0, 2, and 5% Ag) and the weight percentage of silver-doped hydroxyapatite (vs. collagen weight) in scaffolds on the antibacterial activity of the scaffolds
4) Assess the ability of silver-doped hydroxyapatite scaffolds to support osteoblast viability and to assess their osteogenic potential *in vitro*

4.2 Materials and methods

4.2.1 Effect of silver ions on bacterial toxicity and mammalian cell viability in 2D culture

To identify an appropriate concentration range of silver-doped hydroxyapatite to incorporate into the collagen scaffold, the data collected from 2D studies in Chapter 2 was utilised. To summarise, the effect of silver ions on *S. aureus*, *S. epidermidis*, *E. coli*, and mammalian cells in 2D culture was assessed by adding a range of silver nitrate concentrations (0 – 16 mM $AgNO_3$, equivalent to 0 – 1.02 mg Ag^+/ml) to either bacterial cells in bacterial brain heart infusion (BHI) broth or to mammalian pre-osteoblast cells (MC3T3-E1) in cell culture media. The number of viable cells in both experiments were analysed as a measure of cell viability/toxicity (**Figure 4.1**).

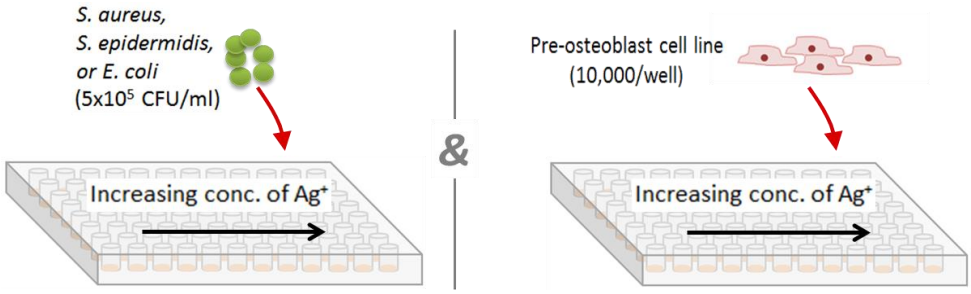

Figure 4.1 Schematic of protocol to examine the effect of silver ions on bacterial toxicity and mammalian cell viability in 2D culture
Silver ions were added to cultures of either S. aureus, S. epidermidis, E. coli, or mammalian pre-osteoblast cells at a range of concentrations. Toxicity was assessed after 24 hrs.

4.2.2 Silver-doped hydroxyapatite (AgHA) synthesis and characterisation

4.2.2.1 AgHA synthesis

Silver-doped hydroxyapatite was synthesised in our laboratory using methods described by our collaborators, Prof. Paul Hatton's group at School of Clinical Dentistry at the University of Sheffield [191], [259]. Briefly, 3.71 g of calcium hydroxide with either 0, 0.17, or 0.42 g of silver nitrate (corresponding to 0%, 2%, or 5% mol Ag) was added to 500 ml of deionised water in a beaker stirring at 400 rpm for 1 hr at 90°C. A solution of phosphorus (3.459 g of 85% phosphoric acid in 250 ml deionised water) was stirred quickly into the calcium

hydroxide/silver solution and stirred for a further hr. Silver-doped particles were then formed from the ability of silver ions to substitute into the HA lattice in place of calcium ions in solution [260]–[262]. The suspension of particles was left to settle overnight. The supernatant was removed, and the particle suspensions were washed three times by adding 500ml of fresh deionised water, stirring at 400 rpm for 2 mins, settling again for 2 hrs, and repeating. Finally, the particle suspensions were allowed to dry in an oven at 80°C. The dried powders were then ground using a glass mortar and pestle until fine and then sieved using a 100 μm test sieve (**Figure 4.2**). The particles were characterised using mastersizing for size, Fourier-transform infrared spectroscopy (FTIR), and X-ray powder diffraction (XRD) analysis.

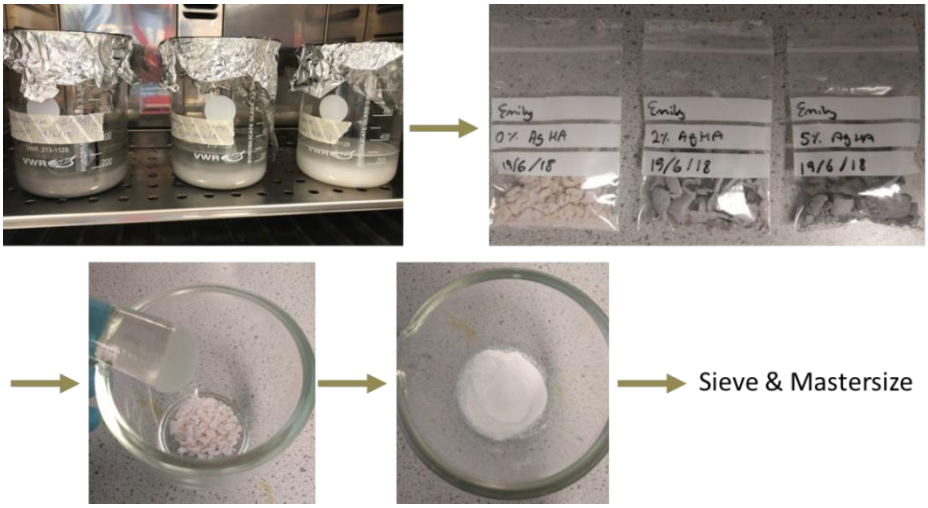

Figure 4.2 Hydroxyapatite particle fabrication method
The suspensions of hydroxyapatite (0, 2, or 5% mol silver-doped) were dried in an oven at 80°C, ground to a fine powder using a mortar and pestle, and sieved.

4.2.2.2 AgHA characterisation - size analysis, X-ray powder diffraction (XRD), and Fourier-transform infrared spectroscopy (FTIR)

Particle size was measured by dynamic light scattering using a Mastersizer 2000 (Malvern Instruments, UK) as described in Chapter 3, Section 3.2.4.1. The refractive index of ethanol and hydroxyapatite were taken to be 1.36 and 1.64, respectively [263], [264]. X-ray powder diffraction and Fourier-transform infrared spectroscopy were utilised to detect the characteristic hydroxyl and phosphate bands of hydroxyapatite. Briefly, XRD was performed with settings of 40 kV and 35 mA, Cu Kα radiation, and a 2θ range of 10-70° (Siemens D500

X-ray Diffractometer, Trinity College Dublin) and for FTIR, approximately 100 mg of each powder was analysed with a scan range of 400 – 4000 cm^{-1} and resolution of 0.48 cm^{-1} (Nicolet iS10 FT-IR Spectrometer, Thermo Scientific).

4.2.3 Collagen – AgHA composite scaffold fabrication

Having identified the optimal concentration range of silver required to kill bacteria and minimise mammalian cell toxicity, the appropriate concentration range of 2% (mol Ag) and 5% (mol Ag) silver-doped hydroxyapatite to incorporate into the collagen scaffolds was estimated (e.g. 2% Ag–2:1HA scaffolds or 5% Ag–2:1HA scaffolds = 1.468 mM or 3.536 mM $AgNO_3$/ml slurry – abbreviations explained below). The scaffolds were fabricated by freeze-drying a co-suspension of collagen and silver-doped hydroxyapatite particles (± silver doping) at a range of different concentrations with groups and nomenclature shown in **Table 4.1** below, similar to methods previously developed within our group incorporate ceramics into collagen scaffolds (**Figure 4.3**) [188], [190], [265].

Table 4.1 *Scaffold groups, including a collagen only control scaffold, fabricated and assessed throughout the chapter for various properties*

		Silver: Hydroxyapatite within incorporated particles (mol %)		
		0% Ag	**2% Ag**	**5% Ag**
Hydroxyapatite: Collagen in scaffold (wt:wt, 5 mg collagen/ml)	**0.2:1**	-	2% Ag–0.2:1HA	5% Ag–0.2:1HA
	1:1	0% Ag–1:1HA	2% Ag–1:1HA	5% Ag–1:1HA
	2:1	0% Ag–2:1HA	2% Ag–2:1HA	5% Ag–2:1HA
	3:1	0% Ag–3:1HA	2% Ag–3:1HA	5% Ag–3:1HA

Briefly, a collagen slurry was produced by mixing type I collagen (5 mg/ml) isolated from bovine tendon (Integra Life Sciences, Plainsboro, NJ) in aqueous 0.5 M acetic acid solution (Fisher Scientific, UK). The hydroxyapatite was

added to the collagen slurry and was mixed between two syringes connected with a luer lock until a homogeneous suspension was obtained. The slurry suspension was then degassed using a vacuum chamber and freeze-dried in a custom built mould (10 mm ⌀ x 5mm discs) until a final temperature of -40°C using a previously published freeze-drying profile [234]. Scaffolds were sterilised and physically crosslinked using dehydrothermal (DHT) treatment at 105°C for 24 hrs at 0.05 bar [94]. Scaffolds were then further chemically crosslinked using EDAC [1-ethyl-3-(3-dimethyl aminopropyl) carbodiimide] (6 mM) and NHS (N-hydroxysuccinimide) (2.4 mM), as previously described [97].

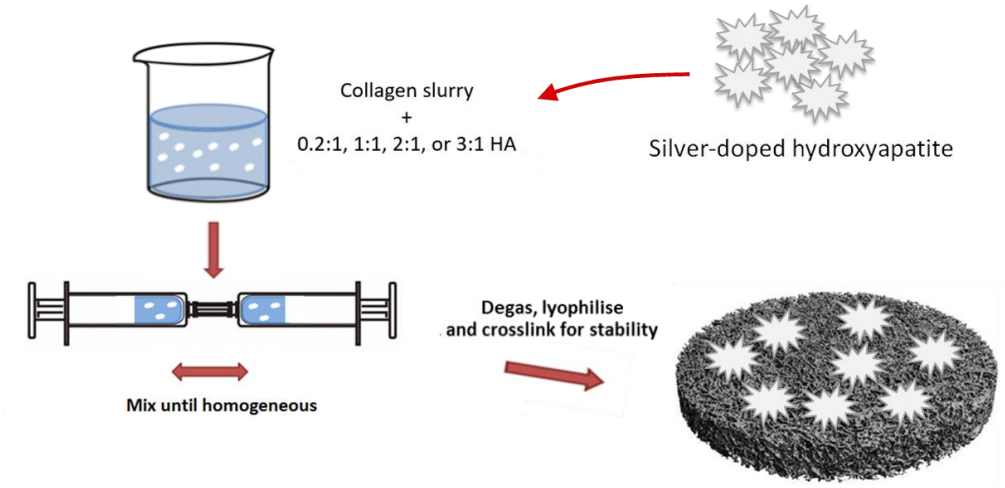

Figure 4.3 Schematic of method for collagen - AgHA composite scaffold fabrication
Silver-doped hydroxyapatite particles were added to collagen slurry and mixed until homogeneous. The solution was degassed and lyophilised into porous scaffolds and crosslinked for stability.

4.2.4 Physical characterisation of collagen – AgHA scaffolds

The following scaffold groups were assessed for porosity, pore size, and mechanical properties: collagen only control, 2% Ag–0.2:1HA, 2% Ag–1:1HA, 2% Ag–2:1HA, and 2% Ag–3:1HA,

4.2.4.1 Effect of AgHA addition on scaffold porosity and pore size

Scanning electron microscopy (SEM) was used to characterize the scaffold morphology and pore size, as described previously in Chapter 3, Section 3.2.7. For porosity analysis, the theoretical density of collagen and hydroxyapatite used were 1.3 and 3.15 g/cm^3, respectively [188], [237]–[239] and the porosity

was calculated as per Equation 4.1 below, where the density (ρ) of the scaffold, collagen, and AgHA are given by $\rho_{scaffold}$, $\rho_{collagen}$, and ρ_{AgHA}, respectively.

$$\text{Scaffold porosity (\%)} = \left(1 - \frac{\rho_{\text{scaffold}}}{(\rho_{\text{collagen}})(\%\text{ wt collagen}) + (\rho_{\text{AgHA}})(\%\text{ wt AgHA})}\right) x100$$

Equation 4.1

4.2.4.2 Effect of AgHA addition on scaffold mechanical properties

In order to investigate the effect of silver-doped hydroxyapatite addition on scaffold compressive modulus, unconfined, wet compression testing of the scaffolds was performed using a uniaxial tensile testing machine, as described in Chapter 3, Section 3.2.7 (n=5 scaffolds, 3 repeats per scaffold).

4.2.5 Antibacterial characterisation of collagen – AgHA scaffolds

All 2% (mol Ag) and 5% (mol Ag) AgHA scaffolds outlined in **Table 4.1** were assessed for antibacterial activity against *S. aureus*. A collagen only scaffold and 0% Ag–3:1HA scaffold were included as controls (note: 0% Ag–1:1HA and 0% Ag–2:1HA were not assessed here).

4.2.5.1 Antibacterial activity of collagen – AgHA scaffolds on agar

As per Chapter 3, Section 3.2.6, agar plates were lawned with 100 µl of $1x10^8$ CFU/ml of *S. aureus* Newman and allowed to air dry for 15 mins. The scaffolds were placed on the agar plates, the plates were inverted, and the zones of inhibition produced by the scaffolds were inspected after 18-24 hrs of incubation at 37°C.

4.2.5.2 Antibacterial activity of collagen – AgHA scaffolds using a time kill assay

A time-kill assay was performed to determine the effect of the silver-doped hydroxyapatite scaffolds on the growth rate of *S. aureus*. As described previously in Chapter 3, Section 3.2.6. Scaffolds were added to 1 ml Brain Heart Infusion (BHI) broth (n=3) in 24-well plates and $5x10^5$ CFU/ml of *S. aureus* Newman were added. The plates were incubated in an orbital shaker

(MaxQ 4000, Thermo Fisher Scientific, USA) (150 rpm, 37°C) and the optical density was measured (with scaffolds temporarily removed) using a plate reader (1420 Victor V3, Perkin Elmer, Dublin, Ireland) at a series of time points over 24 hrs.

4.2.6 Assessment of the ability of collagen – AgHA scaffolds to support osteoblast viability and osteogenic potential *in vitro*

Due to their enhanced mechanical properties and antibacterial activity against *S. aureus*, the scaffold groups in **Table 4.2** were selected for osteoblast viability and osteogenic potential assessment *in vitro*.

Table 4.2 *Scaffold groups brought forward for osteoblast viability and osteogenic potential assessment* in vitro

		Silver: Hydroxyapatite within incorporated particles (mol %)		
		0% Ag	**2% Ag**	**5% Ag**
Hydroxyapatite: Collagen in scaffold (wt:wt, 5 mg collagen/ml)	**1:1**	0% Ag–1:1HA	2% Ag–1:1HA	5% Ag–1:1HA
	2:1	0% Ag–2:1HA	2% Ag–2:1HA	5% Ag–2:1HA

4.2.6.1 Osteoblast culture and seeding

To assess the ability of the silver-doped hydroxyapatite scaffolds to support osteogenesis, MC3T3-E1 cells were cultured as in Chapter 3, Section 3.2.8.1.

4.2.6.2 DNA quantification

DNA, as an indicator of cell number and survival, was quantified as in Chapter 3, Section 3.2.8.2. Three scaffolds per group (n=3) at each time point (day 0 as an indication of initial attachment and day 28) were analysed. Haematoxylin and eosin (H&E) staining (Sigma Aldrich, Ireland) was performed on scaffolds at day 28 to assess cell distribution, as per the manufacturer's instructions. Briefly, scaffolds were fixed in 10% paraformaldehyde, embedded in paraffin wax, and sectioned using a microtome (Leica RM 2255, Leica, Germany) to 5

μm thick slices. Sections were placed on glass slides, deparaffinised to distilled water, stained using haematoxylin and eosin solutions for 5 mins each, washed, and mounted with DPX solution before adding a coverslip. Sections were imaged using a digital microscope (Nikon Eclipse 90i, Nikon Instruments Europe).

4.2.6.3 Cell-mediated mineralisation

Cell-mediated calcium production was quantified as in Chapter 3, Section 3.2.8.3. Three scaffolds per group (n=3) at day 28 were analysed. Alizarin red staining (Sigma Aldrich, Ireland) was also performed on scaffolds at day 28 to assess the cell-mediated calcium distribution, as per the manufacturer's instructions and similar to the H&E staining method above.

4.2.7 Statistical analysis

Data are presented as mean ± standard deviation. Statistical analysis was performed using GraphPad Prism software. Two-tailed unpaired t-tests or one-way or two-way ANOVAs were conducted where appropriate followed by a Bonferroni post-hoc test for multiple pairwise comparisons between groups. A p-value of 0.05 or less was considered statistically significant ($p \leq 0.05$). The Pearson product correlation coefficient (r) was used to determine the strength and direction of a linear relationship. An r value of 0.7-1 was considered a strong positive correlation. Three biological and three technical repeats were performed for all experiments and assays.

4.3 Results

4.3.1 Silver ions effectively eliminate *Staphylococcus aureus*, *Staphylococcus epidermidis*, and *Escherichia coli* while retaining some viable mammalian cells

A range of silver nitrate concentrations was utilised to determine the effect of Ag^+ exposure on both bacterial and mammalian cells in 2D culture in Chapter 2. Summarising results from Chapter 2, increasing silver ion concentration decreased the cellular viability of *S. aureus, S. epidermidis, E. coli,* and MC3T3-E1 mammalian cells after 24 hrs (**Figure 4.4**). Both the minimum inhibitory concentration (MIC) of Ag^+ against *S. aureus* Newman and *S. epidermidis* HB were found to be 1 mM $AgNO_3$, while osteoblast viability was 37% at this concentration. The MIC of silver nitrate against *E. coli* was 0.25 mM, with mammalian viability extrapolated to be approximately 75% at this concentration. The minimum bactericidal concentrations (MBC) of silver nitrate against the three bacteria species were: *S. aureus* 1-2 mM, *S. epidermidis* 2-4 mM, and *E. coli* 0.5-2 mM.

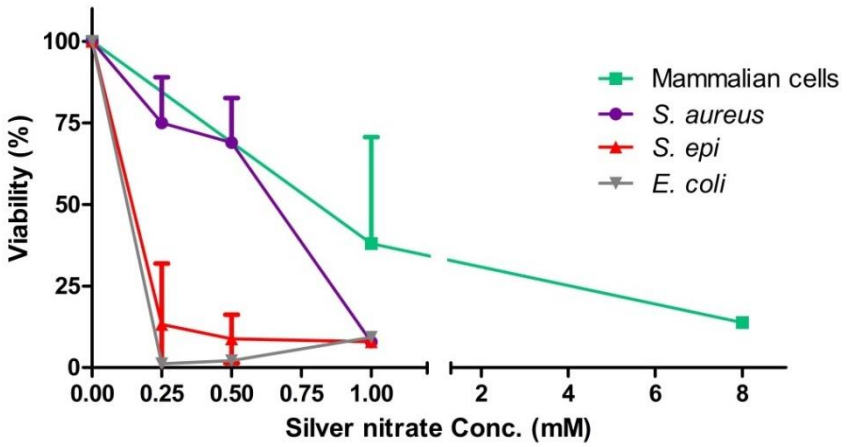

Figure 4.4 Effect of silver nitrate on* S. aureus, S. Epi*, and* E. coli *vs. pre-osteoblast cells (MC3T3-E1)
The viability of pre-osteoblast cells, S. aureus, S. epidermidis, *or* E. coli *cultured reduces with increasing concentrations of silver nitrate, analysed using DNA quantification and spectrophotometric growth quantification, respectively. Viability of mammalian cells is normalized to cells seeded into the well plate with 0 mM silver nitrate (regular growth media) and viability of* S. aureus *is normalised to bacteria with 0 mM silver nitrate (regular BHI growth broth).*

4.3.2 Successful synthesis of AgHA particles

The synthesised particles (with 0%, 2%, or 5% mol Ag-doping) were fabricated via a rapid-mix preparation method, ground, and sieved into a fine powder after drying. The powders were then characterised using mastersizing, Fourier-transform infrared spectroscopy (FTIR), and X-ray powder diffraction (XRD). The resulting particles ranged between 1-180 μm, as evidenced from dynamic light scattering, with 50% and 90% of the particle diameter distribution falling below 32 μm and 92 μm, respectively (**Figure 4.5** A). The FTIR spectra confirmed the successful formation of hydroxyapatite via characteristic peaks: 1020 cm^{-1} (PO_4^{3-}), 960 cm^{-1} (PO_4^{3-}), 875 cm^{-1} (CO_3^{2-}), 630 cm^{-1} (OH^-), 600 cm^{-1} and 560 cm^{-1} (PO_4^{3-}) (**Figure 4.5** B). Phase analysis using XRD and Match! XRD analysis software revealed the successful formation of hydroxyapatite through a positive peak match with over 390,000 crystal entries in the reference database with no other crystal phases detected (Match! Software, Crystal Impact). As well as potentially substituting into the lattice, silver ions may be present on the surface of the hydroxyapatite crystal in the form of free ions. There was no obvious presence of metallic silver in the 2% and 5% samples, suggesting that the silver was mainly substituted or ‘doped’ into the crystal lattice (**Figure 4.5** C).

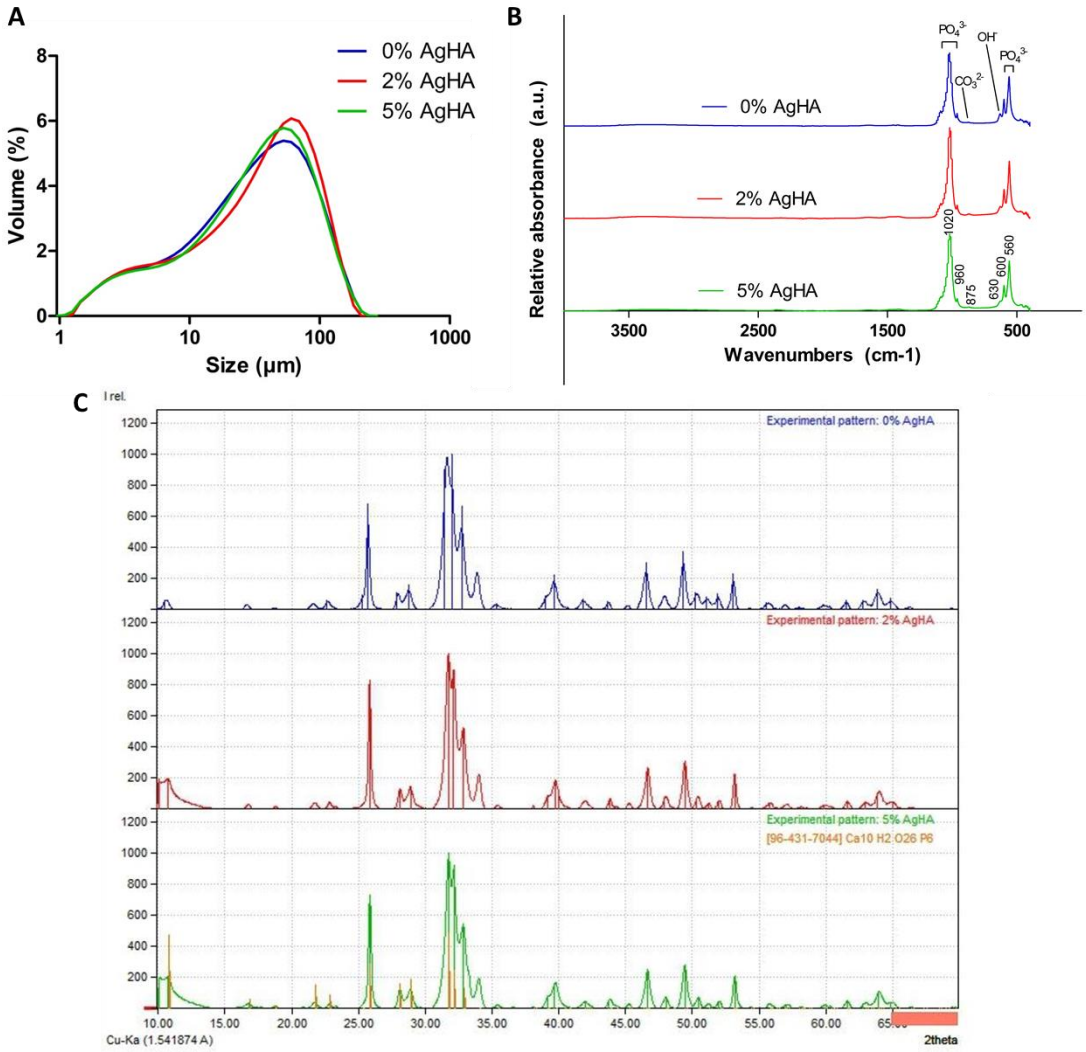

Figure 4.5 Characterisation of synthesised silver-doped hydroxyapatite particles

(A) The size range of 0%, 2%, and 5% mol silver-doped hydroxyapatite particles (1-180 µm). (B) Fourier-transform infrared spectroscopy spectra of the silver-doped hydroxyapatite particles. (C) X-ray diffraction patterns of the as-fabricated particles.

4.3.3 AgHA addition resulted in highly porous scaffolds with suitable pore size and increased compressive modulus

It was found that 3:1 HA was the maximum concentration of silver-doped hydroxyapatite that could be incorporated into the scaffold as a higher concentration of silver-doped hydroxyapatite caused the pH of the slurry to change, causing it to separate. Scanning electron microscope (SEM) images revealed the highly porous, interconnected, open structure of the silver-doped hydroxyapatite scaffolds even at the highest achievable concentration (3:1 HA) (**Figure 4.6** A). There was a significant, albeit marginal, decrease in scaffold porosity upon silver-doped hydroxyapatite addition; however, even upon the incorporation of 2% Ag–3:1HA, all scaffolds remain extremely porous at more than 98%, which is greater than the reported suitable porosity required for tissue engineering applications (90%) (**Figure 4.6** B) [242]. All scaffolds achieved a mean pore size range of 71 – 94 µm, a size known to facilitate osteogenesis in collagen-based scaffolds [248]–[250]. With the exception of 2% Ag–3:1HA scaffolds, the addition of silver-doped hydroxyapatite tended to increase scaffold pore size, with 2% Ag–2:1HA scaffolds having a significantly larger pore size vs. the collagen control (94 µm vs. 71 µm, respectively) ($p < 0.05$) (**Figure 4.6** C). In terms of mechanical properties, increasing the silver-doped hydroxyapatite concentration in the scaffold from 2% Ag–1:1HA to 2% Ag–3:1HA significantly increased the scaffold compressive modulus vs. the collagen control ($p < 0.001$) (**Figure 4.6** D). Notably, increasing the concentration of AgHA in the scaffolds from 2% Ag–2:1HA to 2% Ag–3:1HA actually resulted in a significant decrease in mechanical properties ($p < 0.05$). As collagen acts as the binding agent in the scaffold and there is a fixed amount of collagen in all scaffolds, this reduction in compressive modulus may be attributed to the deteriorated binding capability of this collagen content with the maximum achievable volume of AgHA. Additionally, the larger quantity of silver in these scaffolds may also affect the scaffold's mechanical integrity via a change in pH which causes the slurry to separate and the HA to precipitate.

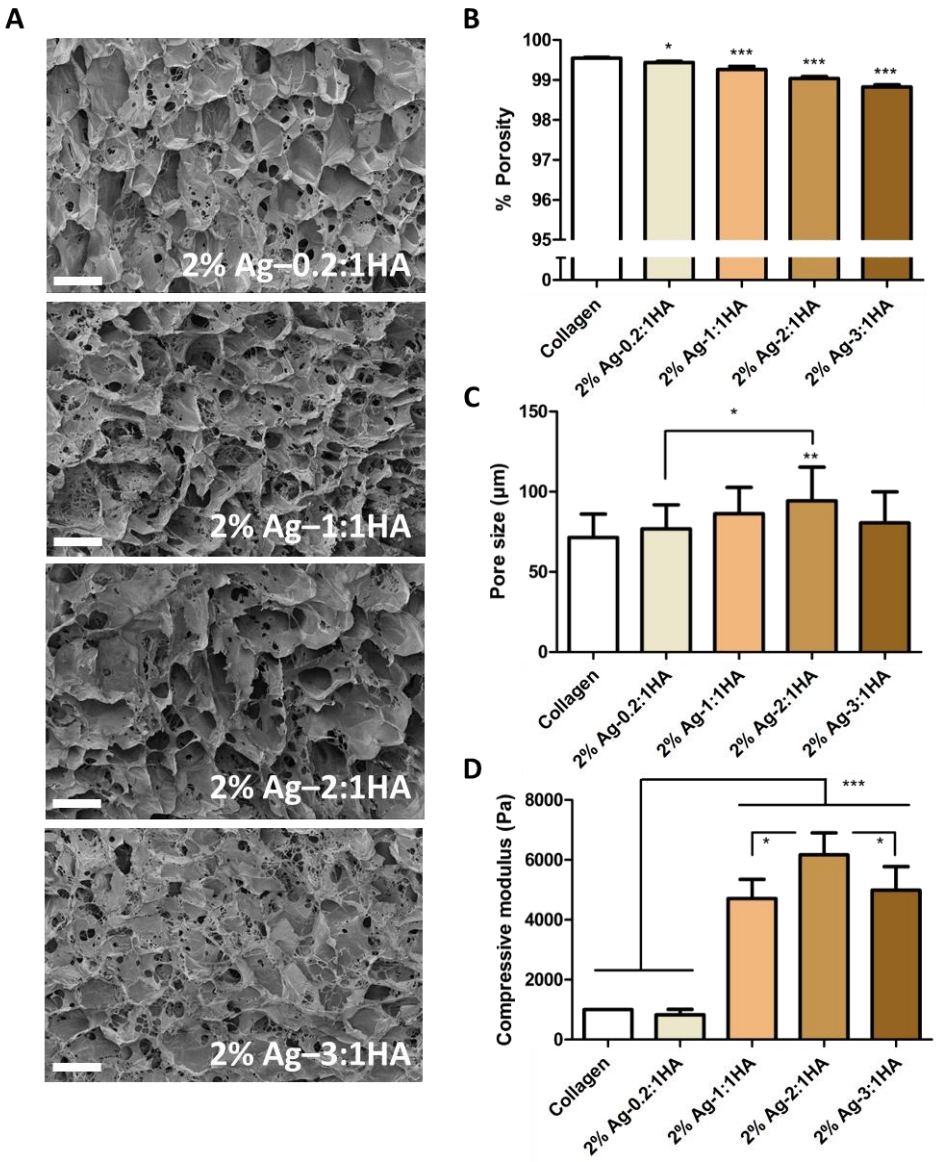

Figure 4.6 Effect of AgHA addition on scaffold microarchitectural and mechanical properties

(A*) SEM images showing the highly porous, interconnected morphology of silver-doped hydroxyapatite scaffolds. (B) All scaffolds remain highly porous (>98%) upon incorporation of silver-doped hydroxyapatite. (C) Pore size of silver-doped hydroxyapatite scaffolds (71-94 µm). Note 2% Ag-2:1HA scaffolds had a significantly increased pore size vs. the collagen control and 2% Ag-0.2:1HA . (D) Increasing silver-doped hydroxyapatite addition increases scaffold compressive modulus, with 2% Ag-1:1HA, 2% Ag-2:1HA, and 2% Ag-3:1HA scaffolds having a significantly higher compressive modulus than the collagen control Note: scaffolds analysed for pore size, porosity, and compressive modulus were 2% mol AgHA. Data presented as mean ± SD, n=3, p-values are calculated using one-way ANOVA with Bonferroni post-hoc test. All statistical significance shown in comparison to collagen control unless otherwise stated, *p < 0.05, **p < 0.01, ***p < 0.001.*

Having determined that collagen scaffolds functionalised with silver-doped hydroxyapatite remain highly porous and show increased mechanical

properties, we next sought to determine the scaffold's principal function – its antibacterial activity against *S. aureus*.

4.3.4 Collagen – AgHA scaffolds show significant antibacterial activity against *Staphylococcus aureus*

All AgHA-containing scaffolds (for both 2% and 5% mol Ag) showed antibacterial activity against *S. aureus* on agar plates by producing zones of inhibition, in comparison to the collagen and 0% Ag–3:1HA controls which did not display antibacterial activity (**Figure 4.7** A). For AgHA scaffolds containing 2% mol Ag (2% Ag–0.2:1HA, 2% Ag–1:1HA, 2% Ag–2:1HA, and 2% Ag–3:1HA), the time-to-kill assay shows that all scaffolds significantly delay the growth of *S. aureus* after the 5 hr time-point vs. the collagen control (p values ranging from $p < 0.05$ to $p < 0.001$) with scaffolds ≥1:1 HA wt showing the most significant effect. In addition, a trend towards increasing antibacterial activity with increasing wt ratio of AgHA in the collagen scaffold can also be observed (**Figure 4.7** B). For AgHA scaffolds containing 5% mol Ag (5% Ag–0.2:1HA, 5% Ag–1:1HA, 5% Ag–2:1HA, and 5% Ag–3:1HA), the time-to-kill assay again shows that all scaffolds significantly delayed the growth of *S. aureus* after the 6 hr time-point vs. the collagen control (all $p < 0.001$). In this case, with the exception of 5% Ag–3:1HA, all scaffolds containing AgHA completely prevented the growth of *S. aureus* over the 24-hr time period (**Figure 4.7** C). Interestingly, 5% Ag–3:1HA scaffolds which showed significant antibacterial activity from 6 hrs, showed subsequent rise in bacterial growth after 8 hrs.

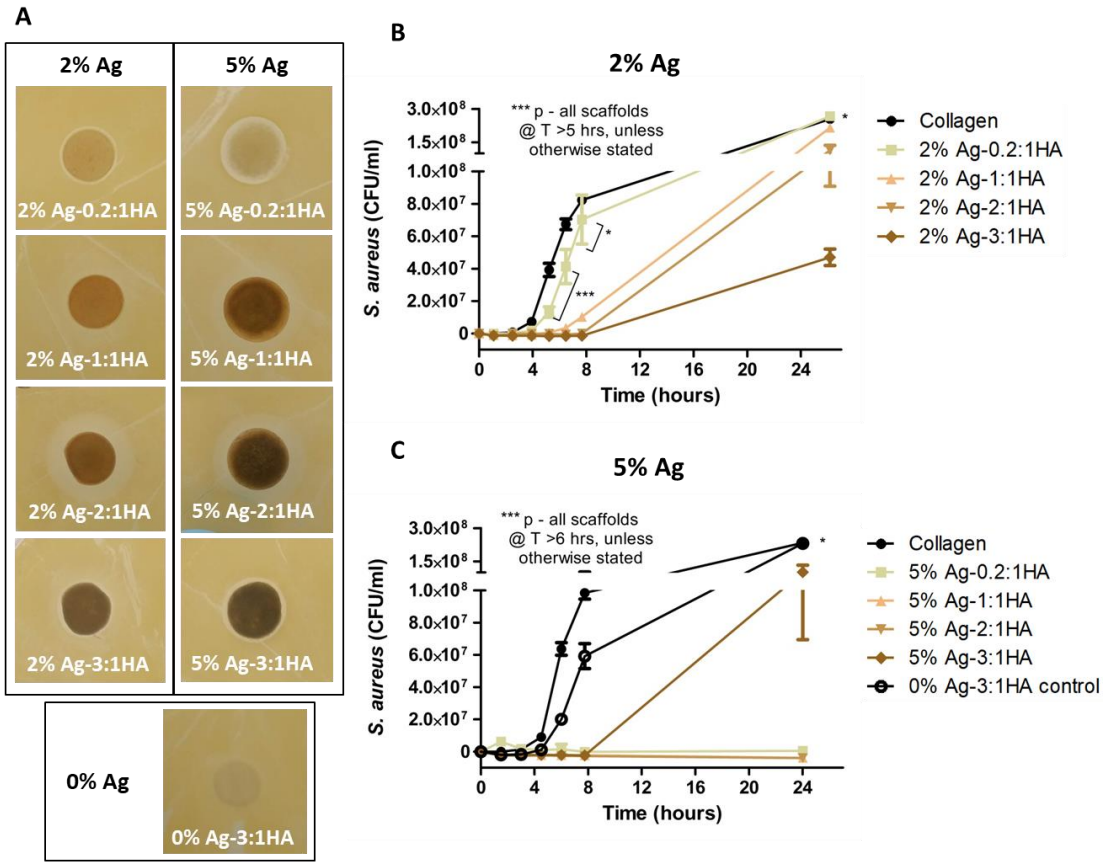

Figure 4.7 Effect of AgHA addition on scaffold antibacterial activity
Effect of incorporation of 2% mol silver-doped hydroxyapatite and 5% mol silver-doped hydroxyapatite in collagen scaffolds on the inhibition of S. aureus *Newman growth on (A) agar plates and (B-C) in a broth time-kill assay over 24 hrs. Data presented as mean ± SD, n=3, p-values are calculated using two-way ANOVA with Bonferroni post-hoc test. All statistical significance shown in comparison to collagen control unless otherwise stated, *p < 0.05, **p < 0.01, ***p < 0.001.*

These analyses demonstrate the desired antibacterial effect of the silver-doped hydroxyapatite scaffolds. As there is a fine balance between mammalian cell toxicity and antibacterial activity, the lowest concentration of the scaffolds which display adequate antibacterial activity (2% Ag–1:1HA, 2% Ag–2:1HA, 5% Ag–1:1HA, and 5% Ag–2:1HA scaffolds) were selected to progress to the next stage, examining the osteogenic potential of the scaffolds. 0% Ag–1:1HA and 0% Ag–2:1HA controls, i.e., non-silver doped, were also brought forward for mammalian cell testing as controls. Note: 2% Ag–0.2:1HA, 2% Ag–3:1HA, 5% Ag–0.2:1HA, and 5% Ag–3:1HA scaffolds were discontinued from further studies from here.

4.3.5 Collagen – AgHA scaffolds reduce the viability of osteoblasts *in vitro* at higher concentrations

Having demonstrated the antibacterial potential of the silver-doped hydroxyapatite scaffolds, the scaffold's ability to maintain mammalian cell viability and support osteogenesis was tested next. This is crucial given the fine balance between antibacterial activity and mammalian cell toxicity as identified above (**Figure 4.4**). The results demonstrate that at day 0, all 1:1 wt HA-containing scaffolds (0% Ag–1:1HA, 2% Ag–1:1HA, and 5% Ag–1:1HA) can support the attachment of cells, with no significant difference between groups (**Figure 4.8** A). In contrast, for the 2:2 wt HA containing scaffolds, 2% Ag–2:1HA scaffolds show significantly increased attachment while 5% Ag–2:1HA scaffolds show significantly decreased cell number vs. the 0% Ag–2:1HA control ($p < 0.05$) (**Figure 4.8** A). However, by day 28 all Ag containing scaffolds (2% Ag–1:1HA, 2% Ag–2:1HA, 5% Ag–1:1HA, and 5% Ag–2:1HA) show significantly reduced cell viability vs. the Ag-free 0% Ag–1:1HA and 0% Ag–2:1HA control scaffolds which supported both the growth and proliferation of the mammalian cells (13 - 30% viability) ($p < 0.001$) (**Figure 4.8** B). In addition, 5% Ag–1:1HA and 5% Ag–2:1HA scaffolds show significantly higher toxicity towards mammalian cells when compared to 2% Ag–1:1HA and 2% Ag–2:1HA scaffolds. Haematoxylin and eosin staining confirmed the high levels of cell infiltration and proliferation into the control scaffolds (0% Ag–1:1HA and 0% Ag–2:1HA) (**Figure 4.8** C). By contrast, a reduction in cell number was observed on AgHA-containing scaffolds (2% Ag–1:1HA, 2% Ag–2:1HA, 5% Ag–1:1HA, and 5% Ag–2:1HA), with a trend towards reduced cell number on increasing wt ratio of HA, as seen in the PicoGreen analysis. Very few cell nuclei can be seen on the 5% Ag–1:1HA and 5% Ag–2:1HA scaffolds however, a substantial number of well distributed cells are present throughout in the 2% Ag–1:1HA and 2% Ag–2:1HA scaffolds.

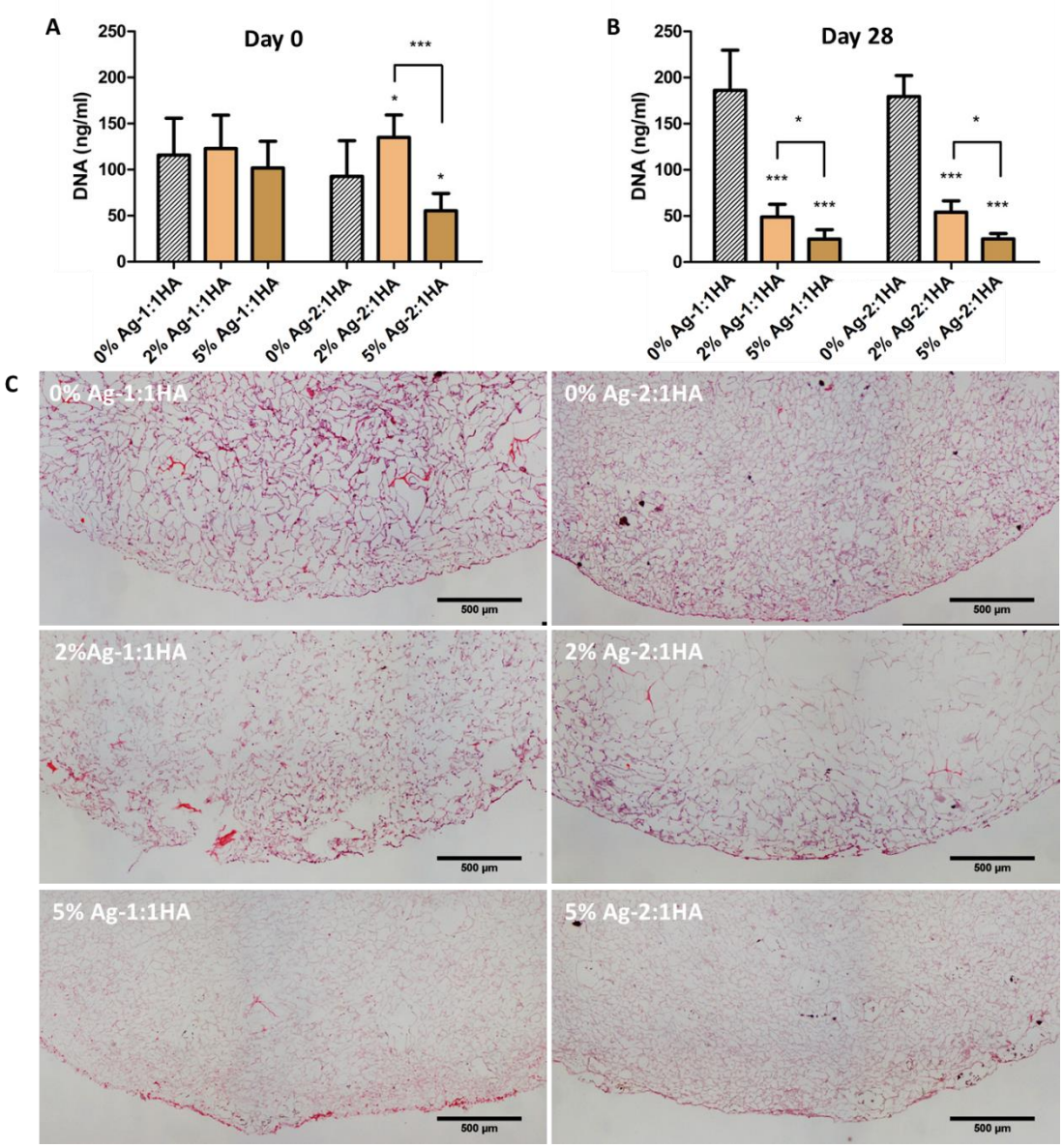

***Figure 4.8 Effect of silver-doped hydroxyapatite scaffolds on the viability of osteoblasts and cell infiltration* in vitro**
(A) *PicoGreen® assay on scaffolds at day 0. (B) PicoGreen® assay on scaffolds at day 28. (C) Haematoxylin and eosin staining of scaffolds at day 28. Data presented as mean ± SD, n=3, p-values are calculated using two-way ANOVA with Bonferroni post-hoc test. All statistical significance shown in comparison to 0% mol Ag scaffold controls unless otherwise stated, *p < 0.05, **p < 0.01, ***p < 0.001.*

With regards to osteogenesis, there was no significant difference in the calcium levels on all scaffolds (0%, 2%, and 5% mol Ag) (**Figure 4.9** A). This result was confirmed with alizarin red staining, where all scaffolds show similar levels of mineral (**Figure 4.9** B). Notably, no obvious difference between calcium levels on the control 0% Ag and the 2% or 5% Ag groups was detected. Taken together, although potent antibacterial activity was achieved

for the silver-doped hydroxyapatite scaffolds, at the same concentrations, mammalian cell viability was substantially reduced, and no enhanced osteogenic effect was detected.

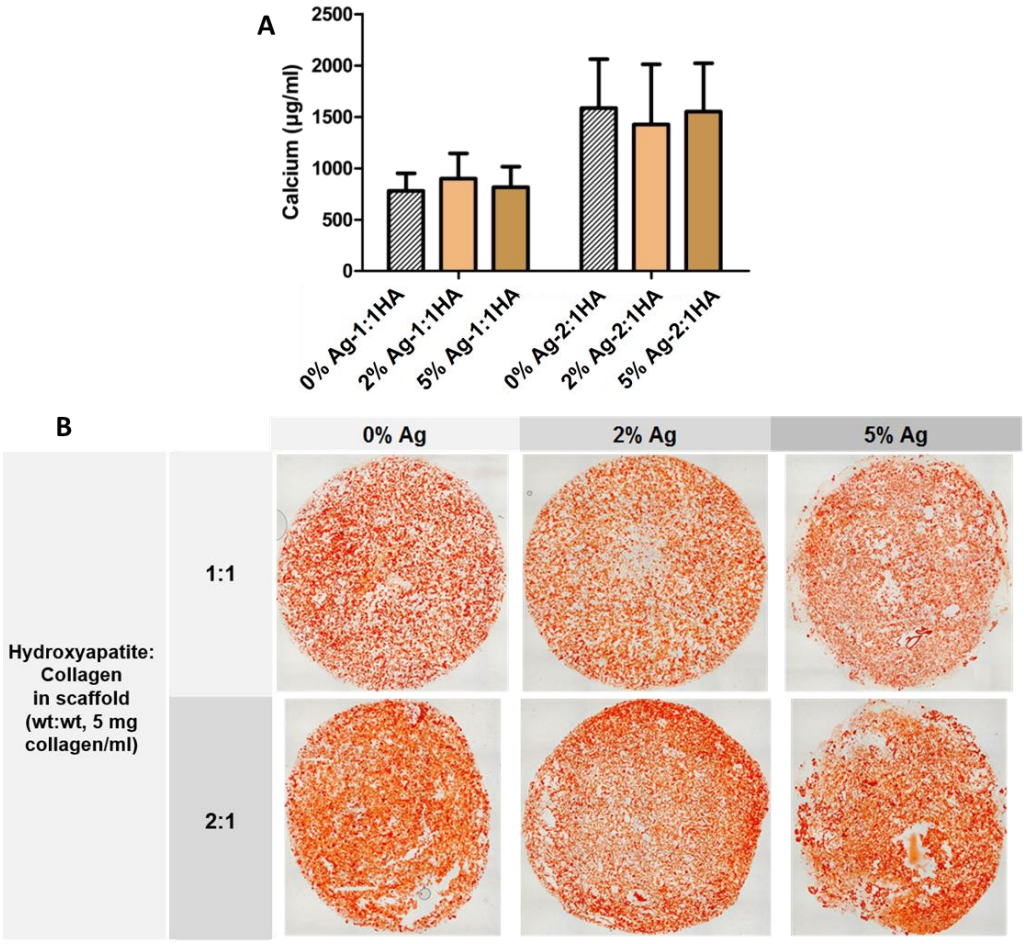

***Figure 4.9 Effect of silver-doped hydroxyapatite scaffolds on osteogenesis* in vitro**

*(A) Quantified total raw calcium values from scaffolds on day 28. (B) Representative images of alizarin red staining of scaffolds on day 28. Data presented as mean ± SD, n=3, p-values are calculated using two-way ANOVA with Bonferroni post-hoc test. All statistical significance shown in comparison to 0% mol Ag scaffold controls unless otherwise stated, *p < 0.05, **p < 0.01, ***p < 0.001.*

4.4 Discussion

Osteomyelitis treatment involves a dual challenge: ensuring an effective and non-toxic dose of antimicrobial, while ensuring bone regeneration is stimulated. Thus, the overall aim of this study was to fabricate silver-doped hydroxyapatite microparticles, investigate the effect of silver-doped hydroxyapatite addition on the microarchitectural and mechanical properties of collagen scaffolds, to examine the antibacterial activity of the scaffolds, and to assess the ability of the silver-doped hydroxyapatite scaffolds to support mammalian cell viability and osteogenesis. A range of silver-doped hydroxyapatite participles were successfully developed, which were capable of being incorporated into collagen scaffolds to improve the overall mechanical properties, while maintaining high porosity, and a suitable microstructure for bone tissue engineering. Most significantly, all silver-doped hydroxyapatite scaffolds showed potent antibacterial activity against *S. aureus.* However, when cultured with mammalian cells, silver-doped hydroxyapatite scaffolds demonstrated increased levels of toxicity, without promoting osteogenesis. Taken together, the results indicate that incorporating silver-doped hydroxyapatite into collagen scaffolds indeed produces potent antibacterial constructs, however, the scaffolds showed toxic effects towards mammalian cells *in vitro*.

In this study, we aimed to investigate the effect of both AgHA weight ratio (0.2:1, 1:1, 2:1, and 3:1 wt:wt HA vs. collagen content) and also the % Ag-doping (0%, 2% and 5% mol Ag-doping within the HA particles) on both antibacterial activity and the viability of mammalian cells. Thus, silver-doped hydroxyapatite microparticles (0%, 2% and 5% mol Ag-doping) were first successfully fabricated in-house, as confirmed by mastersizing, X-ray diffraction and Fourier-transform infrared spectroscopy (FTIR). The addition of silver-doped hydroxyapatite into the collagen scaffolds showed potent antibacterial activity against *S. aureus,* demonstrating the successful production of a non-antibiotic antibacterial scaffold. Not surprisingly, although all silver-doped hydroxyapatite scaffolds demonstrated antibacterial activity vs. the collagen control, it was found that increasing the AgHA weight ratio or

% Ag-doping significantly increased the antibacterial activity of the scaffolds. Similarly, a study in the literature which looked at the effect of 1, 3, and 5% AgHA incorporation into collagen scaffolds on antibacterial activity also found that increasing the % Ag-doping increases the antibacterial activity the scaffolds against both *S. aureus* and *E. coli* [266]. Unexpectedly, the 5% Ag-3:1HA scaffolds showed a significant increase in bacterial growth after 8 hrs. This may be due to an excessive weight percentage of AgHA incorporated within the 5% Ag-3:1HA scaffold, which led to decreased porosity, pore size, and surprisingly mechanical integrity as evidenced in **Figure 4.6**. 5% Ag-3:1HA scaffolds might be thus too highly compacted with AgHA leading to a reduced surface area for Ag ion release and fluid transfer and thus reduced ion release from these scaffolds.

Upon silver-doped hydroxyapatite addition, all scaffolds remained extremely porous at over 98%, even at the highest achievable concentration of 3:1 HA, above the 90% porosity typically recommended for cell infiltration and nutrient and waste transport throughout the construct [246], [247]. Additionally, all silver-doped hydroxyapatite scaffolds achieved a pore size in the range of 71-94 μm, a pore size range shown by previous studies to be appropriate for good cell viability and bone formation [248], [250]. As it is generally accepted that pore size would be reduced upon hydroxyapatite addition [265], [267], it was interesting to discover that the addition of 2% Ag-2:1HA to scaffolds significantly increased the pore size vs. the collagen control. This could possibly be attributed to a production of a gaseous vapour between the acetic acid solvent and the silver-doped hydroxyapatite. The addition of silver-doped hydroxyapatite to collagen scaffolds was shown to have a beneficial effect by significantly increasing the scaffold compressive modulus in comparison to the collagen control. The incorporation of a ceramic into collagen-based scaffolds has been shown previously in our research group to increase stiffness [188], [190]. The increased compressive moduli achieved here (> 6 kPa) in theory should be advantageous for bone tissue engineering to increase cell infiltration and also as an added osteogenic stimulus as construct stiffness has previously been shown to influence the differentiation of mesenchymal stem cells (MSC) down an osteogenic lineage [86]. Additionally, the increase in compressive

modulus achieved is within the range of similar commercially available products and would also improve surgical handling due to the increased resistance to deformation, which would also maintain the critically important porosity and pore size [188]. Thus, from a microarchitectural and mechanical perspective, the silver-doped hydroxyapatite scaffolds developed here are within a range suitable for a bone tissue engineering application.

Our 2D studies demonstrated the fine balance between the antibacterial activity and mammalian cell toxicity of silver, which is consistent with many previous reports for both non-antibiotic antibacterials and antibiotics [205]–[209]. Unfortunately, in the 3D scaffolds, although potent antibacterial activity was achieved, we were unable to achieve a reasonable trade-off between this and mammalian cell viability, with all scaffolds maintaining just 13-30% of cells in comparison to the controls at day 28. In addition, as in the case with antibacterial activity, the mammalian cells experienced increased toxicity with an increase in % mol Ag-doping. However, perhaps a recovery in cell proliferation might occur after a longer time-period in culture when the concentration of Ag ions released from the AgHA diminishes. These undesirable toxic effects induced by silver-doped hydroxyapatite on mammalian cells are reported throughout literature. One study reports that although they found silver-doped hydroxyapatite to be highly compatible with mammalian cells *in vitro* at low concentrations, at the concentrations required to produce bacteriostatic/bactericidal interactions with bacteria the material is highly toxic [268]. On the other hand however, another study which similarly found silver-doped hydroxyapatite to be moderately toxic towards mammalian cells *in vitro*, found that *in vivo*, silver-doped hydroxyapatite (of up to 4.3% Ag-doping) demonstrated favourable bone repair without a remarkable inflammatory reaction [269]. Thus, perhaps the true cytocompatibility of the silver-doped hydroxyapatite scaffolds developed here might be revealed in an *in vivo* assessment, or maybe upon further optimisation of the platform system, a superior balance between antibacterial activity and mammalian cell cytocompatibility might be achieved. It must finally be noted that in terms of osteogenesis, no obvious difference between calcium levels on the 0% Ag and the 2% or 5% Ag groups was detected. This was unexpected as un-doped HA

is widely cited throughout literature to promote osteogenesis [180], [188], [270]. Thus, perhaps further refinement of the bioactivity of the hydroxyapatite particles may be possible through e.g. changes in particle size, shape, or porosity have all been shown to affect bioactivity [265], [271]–[273]. However, further modification to the AgHA scaffold platform was deemed to be beyond the scope of the current work and we made the decision to explore an alternative approach in Chapter 5 where an alternative multifunctional material - copper-doped bioactive glass – was suggested as an alternative to silver-doped hydroxyapatite.

4.5 Conclusion

In this study, a range of silver-doped hydroxyapatites were successfully produced and incorporated into porous collagen scaffolds. The results demonstrate that the silver-doped hydroxyapatite scaffolds showed enhanced microarchitectural and mechanical properties whilst also demonstrating potent antibacterial activity, without the use of antibiotics. Although the scaffolds showed toxicity towards mammalian cells *in vitro*, an assessment of cytocompatibility in an *in vivo* environment or fine-tuning the dose of AgHA may be required. In addition, this delivery system could be adopted as a platform for the controlled release of an array of antimicrobial and therapeutic metal ions depending on the intended application, making them attractive candidates for bone tissue engineering. In Chapter 5, the potential of copper-doped bioactive glass as an alternative multifunctional material which might reduce infection whilst promoting osteogenesis is examined.

Chapter 5 Development of a copper-doped bioactive glass scaffold for the release of antimicrobial ions and enhanced osteogenesis

The research in this chapter is currently under review as Emily J. Ryan, Alan J. Ryan, Arlyng González-Vázquez, Anahí Philippart, Francesca E. Ciraldo, Christopher Hobbs, Valeria Nicolosi, Aldo R. Boccaccini, Cathal J. Kearney, and Fergal J. O'Brien. *Collagen scaffolds functionalised with copper-eluting bioactive glass reduce infection and enhance osteogenesis and angiogenesis both in vitro and* in vivo. Biomaterials, 2019. DOI: 10.1016/j.biomaterials.2019.01.031.

5.1 Introduction

In treating osteomyelitis, there exists a dual challenge: ensuring an effective and non-toxic dose of antimicrobial, while ensuring bone regeneration is stimulated. To overcome these limitations, in this chapter copper-doped bioactive glass was examined as a potential multifunctional non-antibiotic antibacterial that might stimulate bone regeneration and angiogenesis.

Copper is a well-known antimicrobial material that has been shown to be effective against both gram-positive and gram-negative bacteria and fungi [124], [274], [275]. Copper can also contribute to bone regeneration through stimulation of osteogenesis and angiogenesis [137], [138], [276], [277]. Despite the promise of antimicrobial materials in the field of regenerative medicine, there is a trade-off between bacteria-killing ability and inducing toxic effects to healthy cells in the body and, therefore the dosage level of copper is critical. One strategy to control the dosing of copper is to deliver it locally at the defect site using a carrier material that modulates its release profile.

Bioactive glass (BG) is an osteoinductive, biocompatible, and biodegradable material that, upon implantation, a layer of hydroxyapatite forms on the surface of BG that can develop firm bonds with bone and soft tissue [138], [193]. Following this, growth factors are thought to readily bind to the apatite layer and cellular attachment ensues. Osteoprogenitor cells are then differentiated into osteoblastic cells due to the hydroxyapatite stimulus and bone formation results. Other elements are often substituted into the silica network for enhanced bioactivity including stimulation of angiogenesis (e.g. cobalt) [190], bone formation (e.g. zinc) [200], and, most importantly in this application, antimicrobial activity (e.g. copper) [137], [138], [201]. Thus, the combination of copper and bioactive glass might act as a multifunctional material that is antibacterial, osteoinductive, and angiogenic [137], [138].

In our lab, a series of highly porous collagen-based scaffolds have previously been developed a for a variety of tissue regeneration applications that mimic the natural extracellular matrix and provide a template for tissue repair by providing structural support for cells in a 3D environment [87]–[91]. Collagen is natural, biodegradable, facilitates cell attachment and migration, and does

not elicit a host immune response [2]. However, collagen scaffolds have poor compressive strength in comparison to native bone. Therefore, in scaffolds for bone tissue engineering, it is advantageous to combine collagen with another material for structural integrity – such as bioactive glass.

Thus, it was hypothesised that combining copper-doped bioactive glass with a porous 3D collagen scaffolds (CuBG-CS) with proven regenerative capacity [88], [110], [190], [278], [279] would result in an off-the-shelf scaffold for osteomyelitis treatment that elicits osteo- and angiogenesis, whilst, most importantly, limiting infection.

Thus, the specific objectives were to:

1) Develop a method for incorporating various concentrations of CuBG into the collagen scaffold (based on results from Chapter 2), and investigate the effect of CuBG addition on scaffold mechanical and microarchitectural properties
2) Examine the copper ion release and antibacterial activity of the collagen copper-doped bioactive glass scaffolds
3) Investigate the ability of the collagen copper-doped bioactive glass scaffolds to support osteogenesis *in vitro*
4) Investigate the ability of the collagen copper-doped bioactive glass scaffolds to support angiogenesis *in vitro*
5) Assess the osteogenic and angiogenic response of the bioactive glass scaffolds in an *in vivo* chick embryo *ex ovo* model

5.2 Materials and methods

5.2.1 Effect of copper ions on bacterial toxicity and mammalian cell viability in 2D culture

To identify an appropriate concentration range of copper-doped bioactive glass to incorporate into the collagen scaffold, data collected from studies in Chapter 2 where we examined the effect of copper ions on bacterial and mammalian cells in 2D culture was utilised. To summarise, the effect of copper ions on *S. aureus* and mammalian cells in 2D culture was assessed by adding a range of copper chloride concentrations (0 – 16 mM $CuCl_2$, equivalent to 0 – 1.02 mg Cu^{2+}/ml) to either bacterial cells in bacterial brain heart infusion (BHI) broth or to mammalian pre-osteoblast cells (MC3T3-E1) in cell culture media. The number of viable cells in both experiments were analysed as a measure of cell viability/toxicity (**Figure 5.1**).

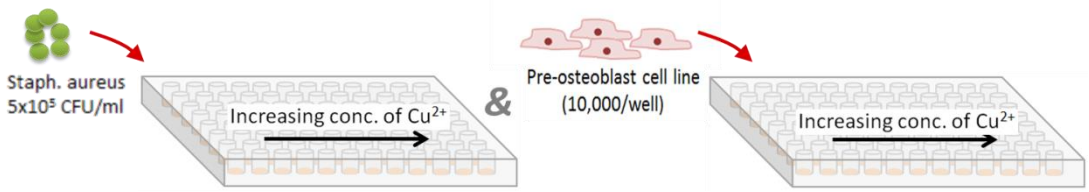

Figure 5.1 Schematic of protocol to examine the effect of copper ions on bacterial toxicity and mammalian cell viability in 2D culture
Copper ions were added to cultures of either S. aureus, S. epidermidis, E. coli*, or mammalian pre-osteoblast cells at a range of concentrations. Toxicity was assessed after 24 hrs.*

5.2.2 Bioactive glass synthesis and characterisation

Bioactive glass with and without a maximum achievable concentration of 2% (mol) copper (equivalent to 0.02 mg Cu^{2+}/mg BG) was prepared by a sol-gel process by collaborators in the Institute of Biomaterials in the University of Erlangen-Nuremberg, Germany. The composition of the bioactive glasses used are as follows:

Table 5.1 *Composition (Mol%) of sol-gel derived 0% and 2% copper-doped bioactive glass*

	BG (mol%)	CuBG (mol%)
Silicon dioxide (SiO_2)	60	60
Calcium oxide (CaO)	36	34
Phosphorus pentoxide (P_2O_5)	4	4
Copper oxide (CuO)	0	2

The bioactive glass was ground and sieved to obtain particles of less than 100 µm in size - a bioceramic particle size previously deemed suitable by our group for both osteogenesis and a reduced immune response [265], [271]. The resulting bioactive glass particles were sized by dynamic light scattering using a Mastersizer 2000 (Malvern Instruments, UK), as described in Chapter 3, Section 3.2.4.1. The refractive index of the ethanol and bioactive glass were taken to be 1.36 and 1.545, respectively [263], [280].

5.2.3 Collagen - bioactive glass composite scaffold fabrication

Having identified the optimal concentration range of copper required to kill bacteria and minimise mammalian cell toxicity, the appropriate concentration range of 2% (mol) copper-doped bioactive glass to incorporate into the collagen scaffolds was estimated (3:1 CuBG = 0.3 mg Cu^{2+}/ml). The scaffolds were fabricated by freeze-drying a co-suspension of collagen and bioactive glass particles (± copper doping, referred to as CuBG and BG, respectively) at a range of different concentrations (collagen only, 0.2:1, 1:1, and 3:1 BG or CuBG wt:wt bioactive glass to collagen), similar to methods previously developed within our group to incorporate ceramics into collagen scaffolds (**Figure 5.2**) [188], [190], [265]. Briefly, a collagen slurry was produced by mixing type I collagen (5 mg/ml) isolated from bovine tendon (Integra Life Sciences, Plainsboro, NJ) in aqueous 0.5 M acetic acid solution (Fisher Scientific, UK). The bioactive glass was added to the collagen slurry and was mixed between two syringes connected with a luer lock until a homogeneous suspension was obtained. The slurry suspension was then degassed using a vacuum chamber and freeze-dried in a custom built mould (10 mm ⌀ x 5mm discs) until a final temperature of -40°C using a previously published freeze-drying profile [234]. Scaffolds were sterilised and physically crosslinked using

dehydrothermal (DHT) treatment at 105°C for 24 hrs at 0.05 bar [94]. Scaffolds were then further chemically crosslinked using EDAC [1-ethyl-3-(3-dimethyl aminopropyl) carbodiimide] (6 mM) and NHS (N-hydroxysuccinimide) (2.4 mM) (Sigma Aldrich, Ireland) in distilled water for two hrs, followed by 2X washes in PBS [97].

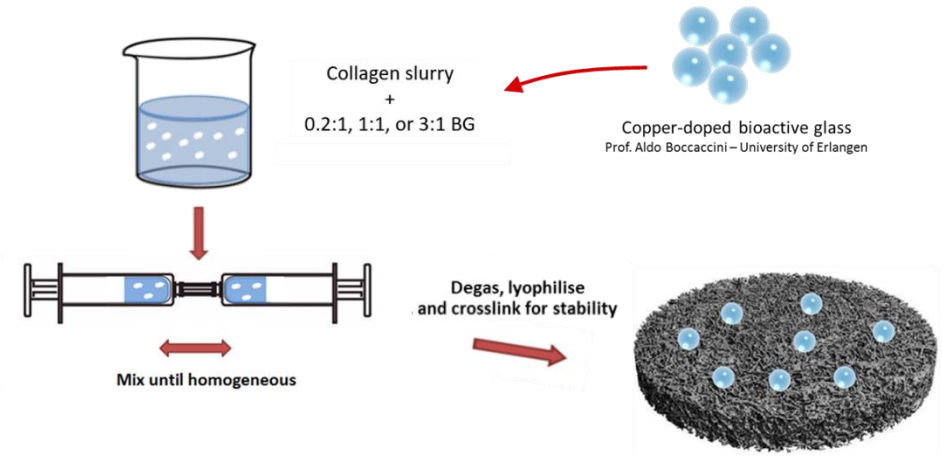

Figure 5.2 Schematic of method for collagen - bioactive glass composite scaffold fabrication
Copper-doped bioactive glass particles were added to collagen slurry and mixed until homogeneous. The solution was degassed and lyophilised into porous scaffolds and crosslinked for stability

5.2.4 Physical characterisation of collagen-bioactive glass scaffolds

5.2.4.1 Distribution of bioactive glass within scaffold & effect of bioactive glass addition on scaffold porosity and pore size

Scanning electron microscopy (SEM) was used to characterise the scaffold morphology and pore size (sectioned using a sharp blade), as described previously in Chapter 3, Section 3.2.7. For porosity analysis, the theoretical density of collagen and bioactive glass used were 1.3 and 2.7, respectively [237], [281] and the porosity was calculated as per Equation 5.1 below, where the density (ρ) of the scaffold, collagen, and bioactive glass are given by $\rho_{scaffold}$, $\rho_{collagen}$, and ρ_{CuBG}, respectively.

$$\text{Scaffold porosity } (\%) = \left(1 - \frac{\rho_{\text{scaffold}}}{(\rho_{\text{collagen}})(\%\text{ wt collagen}) + (\rho_{\text{CuBG}})(\%\text{ wt CuBG})}\right) x100$$

Equation 5.1

5.2.4.2 Effect of bioactive glass addition on scaffold mechanical properties

In order to investigate the effect of bioactive glass addition on scaffold compressive modulus, unconfined, wet compression testing of the scaffolds was performed using a uniaxial tensile testing machine, as described in Chapter 3, Section 3.2.7 (n=5 scaffolds, 3 repeats per scaffold).

5.2.5 Antibacterial characterisation of bioactive glass scaffolds

5.2.5.1 Cu^{2+} ion release from bioactive glass scaffolds

Scaffolds (n=3) were incubated in 1 ml deionised water at 37°C. The eluate was collected at days 1, 2, 3, and 7 (**Figure 5.3**). The copper ion content was measured using a colourimetric Copper Assay Kit (Sigma Aldrich, Ireland). All samples and standards were run in triplicate.

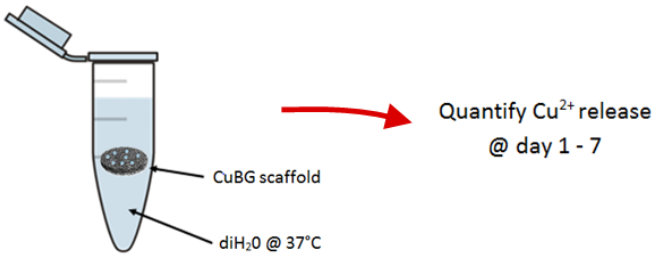

Figure 5.3 Schematic of method for analysis of copper ion release from bioactive glass scaffolds
The ion release from copper-doped bioactive glass scaffolds was investigated by incubating the scaffolds in deionised water at 37°C over 7 days. The copper ion content in the eluate was quantified at days 1, 2, 3, and 7.

5.2.5.2 Antibacterial activity in broth up to 7 days

In order to assess antibacterial activity, the scaffolds were added to Brain Heart Infusion (BHI) broth (Sigma Aldrich, Ireland) (n=3) and incubated at 37°C. At day 1, 3, and 7 scaffolds were removed and $5x10^5$ CFU/ml of *S. aureus* were added to the eluate. The solutions were incubated for a further 24 hrs and the percentage of bacterial growth was quantified as described above. Positive and negative bacterial growth controls (± *S. aureus*) were used (**Figure 5.4**).

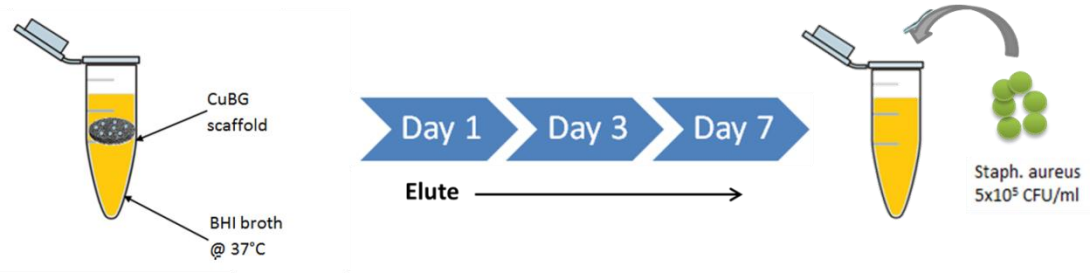

***Figure 5.4 Schematic of method for analysing the antibacterial activity of bioactive glass scaffolds in broth against* S. aureus.**
The antibacterial activity of copper-doped bioactive glass scaffolds was investigated by incubating the scaffolds in BHI broth for either 1, 3, or 7 days. S. aureus *was added to the BHI eluate (with scaffolds removed), and growth was quantified after a further 24 hrs of incubation.*

5.2.5.3 Time-kill assay

A time-kill assay was performed to determine the effect of the scaffolds on the growth rate of *S. aureus* as in Chapter 3, Section 3.2.6. Scaffolds were added to 1 ml Brain Heart Infusion (BHI) broth (n=3) in 24-well plates and $5x10^5$ CFU/ml of *S. aureus* Newman were added. The plates were incubated in an orbital shaker (MaxQ 4000, Thermo Fisher Scientific, USA) (150 rpm, 37°C) and the optical density was measured (with scaffolds temporarily removed) using a plate reader (1420 Victor V3, Perkin Elmer, Dublin, Ireland) at a series of time points over 24 hrs (**Figure 5.5**).

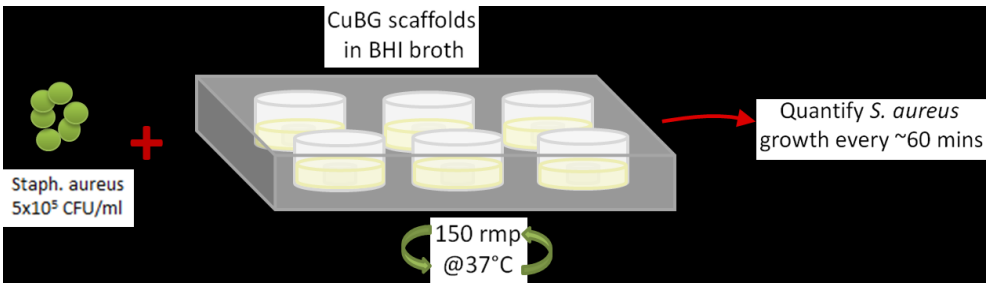

Figure 5.5 Schematic of method for analysing the effect of bioactive glass scaffolds on* S. aureus *growth over a 24 hr time period
The effect of copper-doped bioactive glass scaffolds on the growth of S. aureus *over 24 hrs was analysed by inoculating scaffolds in BHI broth with* S. aureus*, incubating the plates on an orbital shaker, and quantifying bacterial growth at regular time intervals.*

5.2.6 Biological characterisation of bioactive glass scaffolds - analysis of osteogenesis

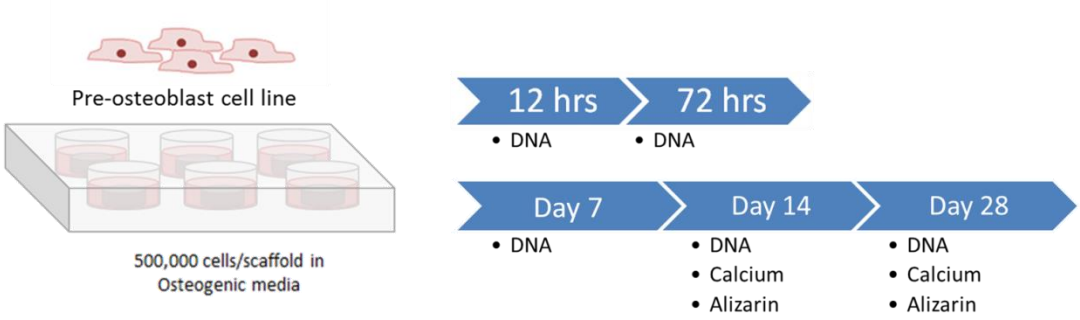

Figure 5.6 Schematic of methods to analyse the ability of bioactive glass scaffolds to support osteogenesis
The ability of bioactive glass scaffolds to support osteogenesis was investigated by seeding the scaffolds with osteoblasts and culturing the scaffolds over a 28 day period. Scaffolds were analysed using DNA and calcium quantification and alizarin red mineral staining.

5.2.6.1 Osteoblast culture and seeding

To assess the ability of the copper-doped bioactive glass scaffolds to support osteogenesis, MC3T3-E1 cells were cultured as in Chapter 3, Section 3.2.8.1.

5.2.6.2 DNA quantification

DNA, as an indicator of cell number and survival, was quantified as in Chapter 3, Section 3.2.8.2. Three scaffolds per group (n=3) at each time point (12 hrs and 72 hrs as an indication of initial attachment and proliferation & days 7, 14, and 28) were analysed.

5.2.6.3 Cell-mediated mineralisation

Cell-mediated calcium production was quantified as in Chapter 3, Section 3.2.8.3. Three scaffolds per group (n=3) at day 14 and 28 were analysed. Alizarin red staining (Sigma Aldrich, Ireland) was also performed on scaffolds at day 14 and 28 to assess the cell-mediated calcium distribution, as per the manufacturer's instructions and similar to the H&E staining method above.

5.2.7 Biological characterisation of bioactive glass scaffolds - analysis of angiogenesis

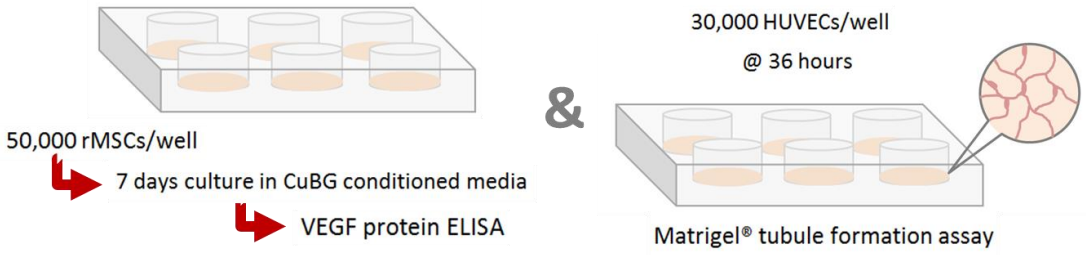

Figure 5.7 Schematic of method to analyse the ability of bioactive glass scaffolds to support angiogenesis
The effect of the bioactive glass scaffolds on angiogenesis was investigated through two different assays 1) Quantifying VEGF protein production from rMSCs using ELISA and 2) Quantifying tubule formation using Matrigel® assay and HUVECs.

5.2.7.1 Cell culture and seeding

Angiogenesis was assessed using Human Umbilical Vein Endothelial Cells (HUVECs) and Rat Mesenchymal Stem cells (rMSCs). HUVECs were cultured in EndoGRO complete culture medium (SCME002, Merck Millipore) and rMSCs were cultured in high-glucose DMEM (D5671) medium (Sigma Aldrich, Ireland) supplemented with 10% FBS, 2% penicillin/streptomycin, 1% Glutamax, and 1% Non-Essential Amino Acids (Biosciences, Ireland) and 1% L-Glutamine. All cells were cultured under standard culture conditions (37°C, 5% C02, and 95% relative humidity).

5.2.7.2 VEGF protein production

Cell-free scaffolds (n=3) were placed in 2ml of cell culture medium and incubated at 37°C under standard cell culture conditions. rMSCs were seeded in 6-well plates (n=3) at a density of 50,000 cells/well. 2 ml of eluate from the scaffolds was collected at day 1, 3, and 5 and added directly to the rMSCs. At day 7 the cell culture medium was harvested and analysed for VEGF protein production using ELISA (R&D Systems, USA). 1 ml of lysis buffer was then added to the wells and DNA was quantified as previously described. A cell-only control using regular rMSC growth medium was used.

5.2.7.3 Matrigel assay

The ability of the eluate from the copper-doped bioactive glass scaffolds to support tubule formation was assessed using a Matrigel® assay. Cell-free scaffolds (n=3) were placed in 1 ml of endothelial medium and incubated at 37°C under standard cell culture conditions. The eluate from the scaffolds was collected at day 1, 3, and 7 and stored at -80°C until use. Matrigel® basement membrane matrix (Corning, USA) was added to 24-well plates (120 µl/well) and the plates were incubated for 30 mins at 37°C. HUVECs were seeded at 30,000 cells/well and 1 ml of the medium eluate was added. At 36 hrs the Matrigel® cultures were imaged using a digital microscope (Lecia DMIL, Lecia Microsystems). Three images per well were captured and were analysed for total tubule length using ImageJ software and an in-house developed plug-in.

5.2.8 Analysis of copper-doped bioactive glass scaffolds on osteo- and angiogenesis in a chick embryo *ex ovo* model

Here, an established *in vivo* model – the *ex ovo* or shell-less chicken embryo model – was utilised to further demonstrate the therapeutic effect of the bioactive glass scaffolds previously tested *in vitro* [282]–[286]. The chicken *ex ovo* embryo model allows us to examine the effect of the scaffolds on both angiogenesis and osteogenesis (**Figure 5.8**). The angiogenic effect of therapeutics applied to the *ex ovo* chicken embryo can be visually examined on the highly vascularised chicken chorioallantoic membrane (CAM) which surrounds the embryo. During development, like humans, the limbs of chicken embryos undergo endochondral ossification and thus by culturing the chicken embryos up to a maximum of 12 days of development (whilst the limbs remain mainly cartilaginous), the osteogenic effect of therapeutics can be examined by looking for accelerated endochondral ossification.

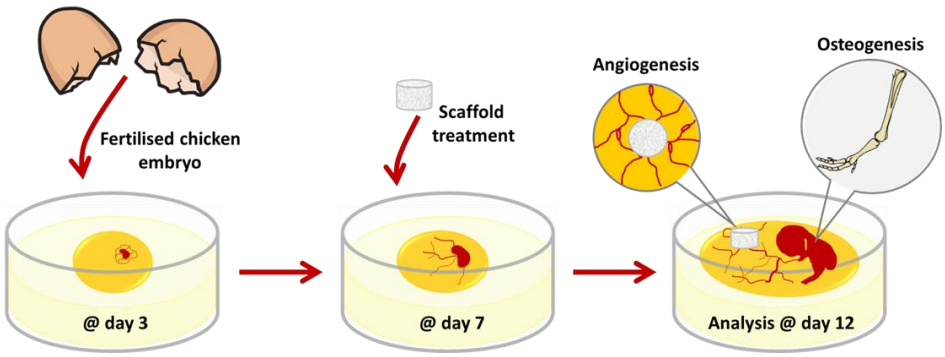

Figure 5.8 Schematic of chick embryo ex ovo model

Fertilised chicken eggs (day 0 of development) were supplied by Ovagen (Ovagen Group Ltd, Co. Mayo, Ireland). On receipt, the eggs were incubated for 3 days (until day 3 of development) lying in a horizontal position in a cell-culture incubator at 37°C in regular atmospheric gas. The eggs were turned every 24 hrs for correct embryo orientation during development and for optimum CAM development [287]. On day 3, the eggs were cracked into 100 mm Ø petri dishes (Corning Inc., New York, USA) and the lid was replaced. To keep the embryos humidified, the petri dish containing the embryo was placed into a larger 150 mm Ø petri dish (Corning Inc., New York, USA) containing 25 ml of sterile PBS and the lid of the larger petri dish was also replaced and the chick embryos were placed back in the incubator. After a further 4 days of incubation (until day 7 of development), the BG-CS and CuBG-CS were placed on the CAM membrane (6 mm Ø scaffolds hydrated in PBS). As controls, collagen only scaffolds soaked in either PBS, 1 µg of recombinant VEGF (Vascular Endothelial Growth Factor) or 1.5 µg of recombinant BMP-2 (Bone Morphogenic Protein-2) (PeproTech, United Kingdom) were placed on the embryos. The chick embryos were then incubated for a final 5 days (until day 12 of development) and the effect of the scaffolds on both angiogenesis and osteogenesis was analysed, as described below.

5.2.8.1 Osteogenesis studies

After analysing angiogenesis, the embryos were culled by pouring 25 ml 10% formalin solution (neutral buffered) directly on the embryo in the petri dish. After 60 minutes, embryo death was confirmed by decapitation and the hind

limbs of the embryos were dissected using a sharp scissors and transferred to fresh 10% formalin solution overnight. Next, the hind limbs of the chick embryos were differentially stained for cartilage and bone following a protocol by Wassersug *et al*. [3]. The hind limbs were removed from overnight formalin solution and the excess skin and tissue surrounding the femur and tibia/fibula were removed carefully using a fine scissors and tweezers. The specimens were then washed in a series deionised water changes every hr for 6 changes. Excess water was blotted from the hind limbs and they were placed in an alcian blue staining solution (9 mg alcian blue 8GX, 60 ml absolute ethanol, 40 ml glacial acetic acid) for 24 hrs. The specimens were removed from the staining solution, blotted, and transferred to absolute ethanol for dehydration for 24 hrs, with a change of solution at 12 hrs. After dehydration, the samples were blotted again and placed in 0.5% potassium hydroxide (KOH) solution with 3 or 4 drops of 0.1% alizarin red S solution to every 100 ml of KOH solution for 24 hrs. Finally, the samples were cleared by transferring blotted specimens to 100% glycerol through a series of glycerol-water solutions – 25%, 50%, 75%, and 100%. The specimens were kept in each solution for 12 hrs. The limbs were imaged for signs of accelerated osteogenesis (alizarin red staining) using a stereo microscope (Leica Microsystems, Germany).

5.2.8.2 Angiogenesis studies - blood vessel quantification

The local effect of the scaffolds on angiogenesis of the CAM was analysed by quantifying the blood vessel density in the region surrounding to the scaffold. On day 12, the scaffolds and surrounding CAM of all chick embryos were imaged. The images were analysed for blood vessel density by developing a novel method using Fiji software (ImageJ) (**Figure 5.9**). Briefly, images were scaled and cropped appropriately and the ‘Mexican Hat Filter’ plugin was applied (radius 5.0). Next, images were converted to 8-bit and the threshold was adjusted to a set level where all blood vessels were highlighted appropriately (lower threshold: 0, upper threshold: 150). Finally, a 12.5 mm Ø circle was drawn centred around the scaffold and the percentage of that area that contained blood vessels was quantified using the measure tool (n=3 embryos analysed for each treatment group).

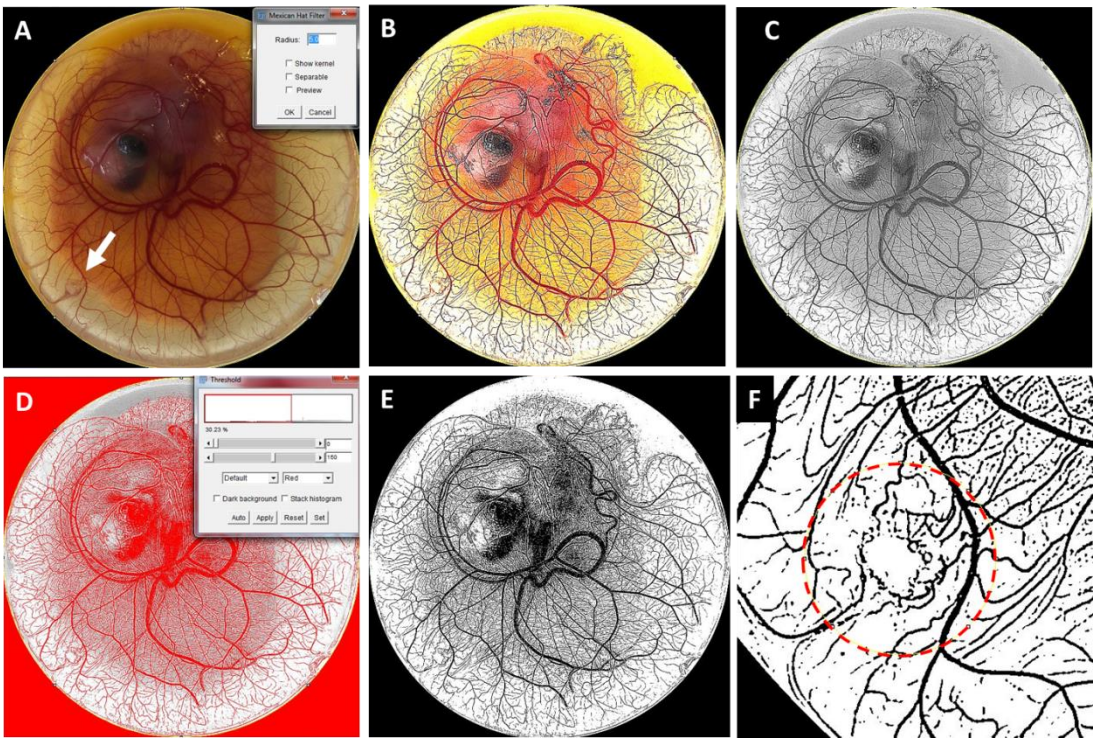

Figure 5.9 Method used to analyse effect of the scaffolds on angiogenesis in a chick CAM membrane using Fiji software (ImageJ)
(A) Scaled and cropped image of whole CAM membrane containing scaffold (indicated by the white arrow). (B) Image after 'Mexican Hat Filter' plugin was applied. (C) Image converted to 8-bit. (D) Thresholding of image to include all blood vessels. (E) Image after threshold was applied. (F) Region around scaffold where the percentage blood vessel area was measured.

5.2.9 Statistical analysis

Data are presented as mean ± standard deviation. Statistical analysis was performed using GraphPad Prism software. Two-tailed unpaired t-tests or one-way or two-way ANOVAs were conducted where appropriate followed by a Bonferroni post-hoc test for multiple pairwise comparisons between groups. A p-value of 0.05 or less was considered statistically significant ($p \leq 0.05$). The Pearson product correlation coefficient (r) was used to determine the strength and direction of a linear relationship. An r value of 0.7-1 was considered a strong positive correlation. Three biological and three technical repeats were performed for all experiments and assays.

5.3 Results

5.3.1 Copper ions effectively eliminate *Staphylococcus aureus* with viable mammalian cells remaining

A range of copper chloride concentrations was utilised to determine the effect of Cu^{2+} exposure on both bacterial and mammalian cells in 2D culture in Chapter 2. Summarising results from Chapter 2, increasing copper ion concentration decreased the cellular viability of both *S. aureus* and MC3T3-E1 mammalian cells after 24 hrs (**Figure 5.10**). Both the minimum inhibitory concentration (MIC) and minimum bactericidal concentration (MBC) of Cu^{2+} against *S. aureus* Newman was found to be 1.02 mg/ml (or 16 mM $CuCl_2$). While a reduction in mammalian cell viability was observed at concentrations above 0.06 mg Cu^{2+}/ml (or 16 mM $CuCl_2$), increasing the copper concentration further did not have any additional effect on mammalian cell viability. By contrast, concentrations of copper chloride above 0.51 mg Cu^{2+}/ml (or 8 mM CuCl2) almost completely eliminated *S. aureus* growth (MIC/MBC concentrations).

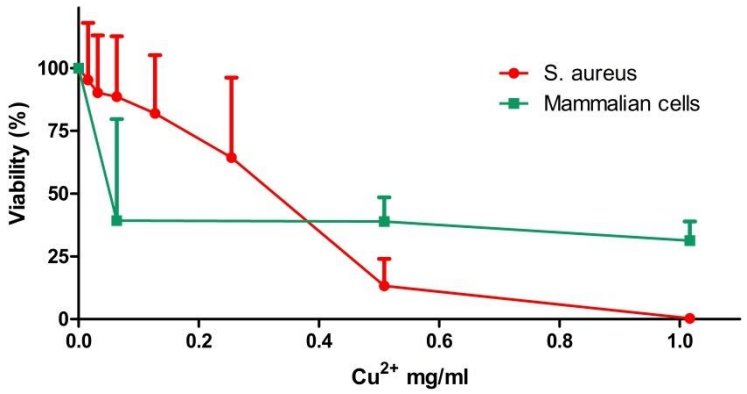

Figure 5.10 Effect of copper chloride on* S. aureus *and pre-osteoblast cells (MC3T3-E1)
The viability of pre-osteoblast cells and S. aureus *decreases when cultured with increasing concentrations of copper chloride. Analysed using DNA quantification and spectrophotometric growth quantification, respectively. Note: Viability of mammalian cells is normalized to cells seeded into the well plate with 0 mg/ml copper chloride (regular growth media) and viability of* S. aureus *is normalized to bacteria with 0 mg/ml copper chloride (regular BHI growth broth).*

These results highlight the fine balance between bacteria-killing ability and toxic effects towards mammalian cells, emphasising the need to control the

dosage level to achieve a suitable bacteria killing/mammalian cell survival ratio. This motivates the application of local and controlled release of copper ions while providing some basis for requisite dosing for the proposed biomaterial system.

5.3.2 Bioactive glass addition resulted in highly porous scaffolds with suitable pore size and increased compressive modulus

Bioactive glass (with and without copper) was fabricated via a sol-gel method, ground, and sieved. The resulting particles ranged between 2-100 μm, as per dynamic light scattering (**Figure 5.11** A). It was found that 3:1 CuBG was the maximum concentration of bioactive glass that could be incorporated into the scaffold as a higher concentration of bioactive glass caused the pH of the slurry to change, causing it to separate. Scanning electron microscope (SEM) images revealed the highly porous, interconnected, open structure of the copper-doped bioactive glass scaffold even at the highest achievable concentration (3:1 CuBG) (**Figure 5.11** B). Energy-selective backscatter SEM (BSEM) images showed a homogenous distribution of copper-doped bioactive glass in the collagen scaffold, demonstrated by the bright particles dispersed throughout the darker scaffold materials (**Figure 5.11** C). This material contrast is due to the relatively higher atomic number of the copper-doped particles, i.e. Z-contrast. There was a significant, albeit marginal, change in scaffold porosity upon bioactive glass addition; however, even upon the incorporation of 3:1 CuBG, all scaffolds remain extremely porous at more than 98%, which is greater than the reported suitable porosity required for tissue engineering applications (90%) (**Figure 5.11** D) [242]. The addition of bioactive glass did not significantly affect scaffold pore size, with all scaffolds achieving a mean pore size ranging from 68-79 μm (**Figure 5.11** E), a suitable size for osteogenesis and angiogenesis in collagen-based scaffolds [248]–[250]. Notably, increasing bioactive glass concentration increased scaffold compressive modulus with a linearly increasing trend ($r = 0.9991$), with the 3:1 CuBG-CS significantly increasing compressive modulus ($p < 0.05$) by 2.7-fold vs. the collagen control (**Figure 5.11** F).

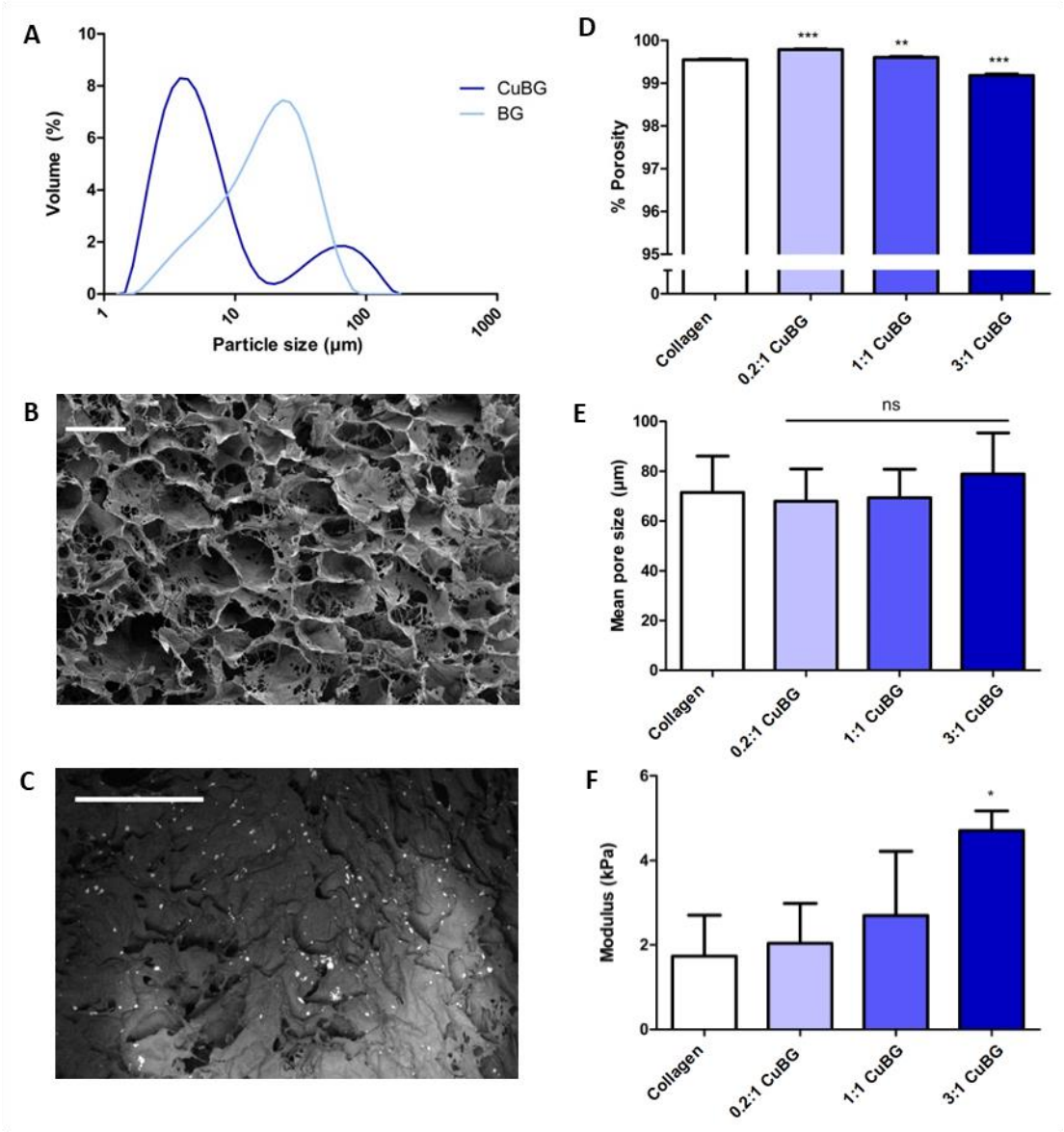

Figure 5.11 Effect of bioactive glass addition on scaffold microarchitectural and mechanical properties

*(A) The size range of bioactive glass particles (2-110 µm). (B) SEM image showing the highly porous open structure of scaffold containing the highest concentration of bioactive glass (3:1 CuBG). (C) Energy-selective backscatter SEM image showing homogeneously distributed bioactive glass. Note: material contrast images highlighting bright copper-doped particles compared to the darker collagen background. (D) All scaffolds remain highly porous (>98%) upon incorporation of copper-doped bioactive glass. (E) Copper-doped bioactive glass addition does not significantly alter scaffold pore size in comparison to the collagen control. (F) Increasing copper-doped bioactive glass addition increases scaffold compressive modulus with a linear trend, with 3:1 CuBG-CS having a significantly higher compressive modulus than the collagen control Note: scale bars 100 µm. Data presented as mean ± SD, n=3, p-values are calculated using one-way ANOVA with Bonferroni post-hoc test. All statistical significance shown in comparison to collagen control unless otherwise stated, *p < 0.05, **p < 0.01, ***p < 0.001.*

Having determined that collagen scaffolds functionalised with copper-doped bioactive glass remain highly porous and show increased mechanical properties, we next sought to determine the scaffold's principal function – its antibacterial activity against *S. aureus*.

5.3.3 Copper-doped bioactive glass scaffolds reduce the viability of *Staphylococcus aureus*

Of the concentrations tested, 3:1 CuBG scaffolds released the highest dose of copper ions within 24 hrs (**Figure 5.12** A) which resulted in a significantly increased antibacterial activity against all other groups, inhibiting *S. aureus* growth by up to 66% (**Figure 5.12** B) ($p < 0.01$ & $p < 0.001$). A time-kill assay shows that 1:1 CuBG-CS also significantly delayed the growth of *S. aureus* at 7 hrs ($p < 0.05$) and 3:1 CuBG-CS significantly delayed the growth of *S. aureus* from 7 to 24 hrs ($p < 0.001$) in comparison to the collagen control (**Figure 5.12** C).

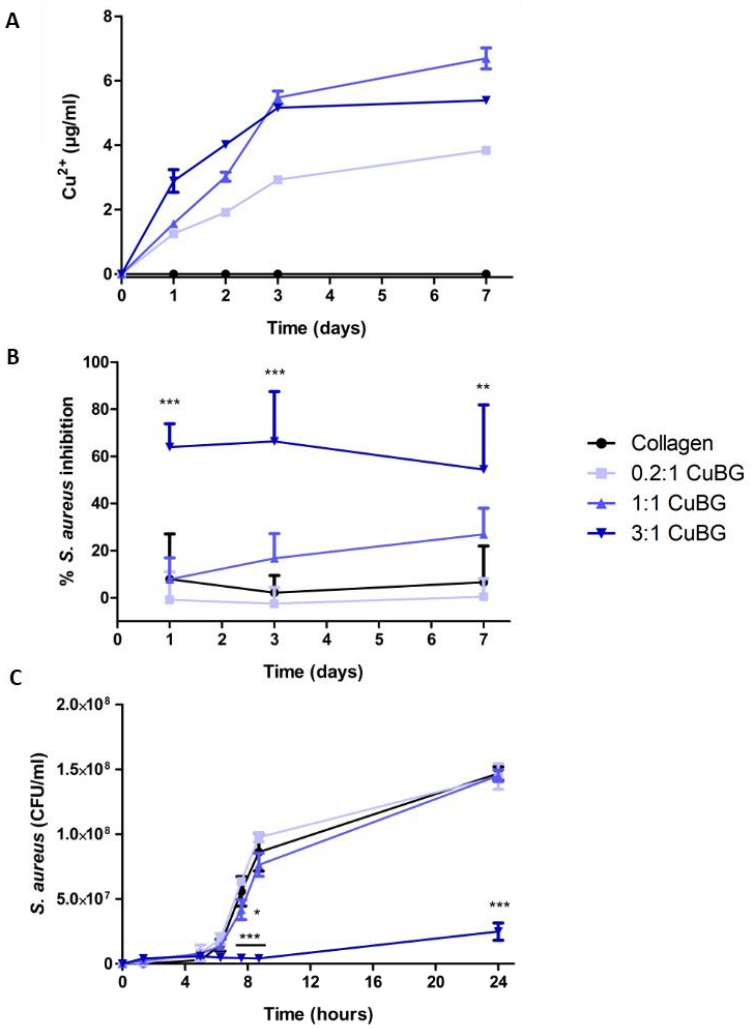

Figure 5.12 Effect of bioactive glass addition on scaffold antibacterial activity *(A) Copper ion release from copper-doped bioactive glass scaffolds over 7 days. (B) Effect of incorporation of copper-doped bioactive glass in collagen scaffolds on the inhibition of* S. aureus *Newman growth after 1, 3, and 7 days (normalized to regular BHI growth broth without scaffold inoculated with* S. aureus*). (C) Time-kill graph for copper-doped bioactive glass scaffolds. Data presented as mean ± SD, n=3, p-values are calculated using two-way ANOVA with Bonferroni post-hoc test. All statistical significance shown in comparison to collagen control unless otherwise stated, *p < 0.05, **p < 0.01, ***p < 0.001.*

These analyses demonstrate the desired antibacterial effect of the 1:1 and 3:1 CuBG-CS. Therefore, the osteogenic and angiogenic potential of the 1:1 and 3:1 CuBG-CS (and 1:1 and 3:1 BG-CS controls, i.e., non-copper doped) was next examined. Note: 0.2:1 CuBG-CS was discontinued from further studies from here on due to its lack of antibacterial properties.

5.3.4 Copper-doped bioactive glass scaffolds enhance osteogenesis *in vitro*

Having demonstrated the antibacterial potential of the CuBG-CS, the scaffold's ability to maintain mammalian cell viability and promote osteogenesis was tested next. This is crucial given the fine balance between antibacterial activity and mammalian cell toxicity as identified above (**Figure 5.10**). The results show that 3:1 CuBG-CS significantly increased cell proliferation after initial seeding in growth medium at 72 hrs ($p < 0.05$), by 1.5-fold in comparison to the collagen control (**Figure 5.13** A). This was a positive result as, based on its pronounced antibacterial properties, we had some concern that incorporating levels as high as 3:1 CuBG in the scaffolds might reduce mammalian cell viability; furthermore, although some reduction was seen in cell number at later time points in osteogenic medium (Day 7 and beyond) for the 3:1 CuBG-CS, it was not significantly different in comparison to collagen controls at any time point (**Figure 5.13** B). With the exception of the 3:1 CuBG-CS, there is an increase in cell number on all scaffolds containing bioactive glass (either BG or CuBG) (**Figure 5.13** B). With regards to osteogenesis, the 3:1 CuBG-CS demonstrated significantly increased cell-mediated calcium deposition at days 14 and 28 vs. the 3:1 BG-CS controls ($p < 0.001$ for all) (**Figure 5.13** C). The osteogenic capacity of CuBG-CS was confirmed with alizarin red staining, which showed increased calcium deposition that was homogeneously distributed throughout the scaffold cross-section (**Figure 5.13** D). By contrast, the less mechanically robust collagen-only control showed an encapsulation effect, where mineralisation only occurred on the scaffold periphery. Taken together, these results demonstrate that the 3:1 CuBG-CS not only support osteogenesis but enhances it in comparison to the other scaffold groups.

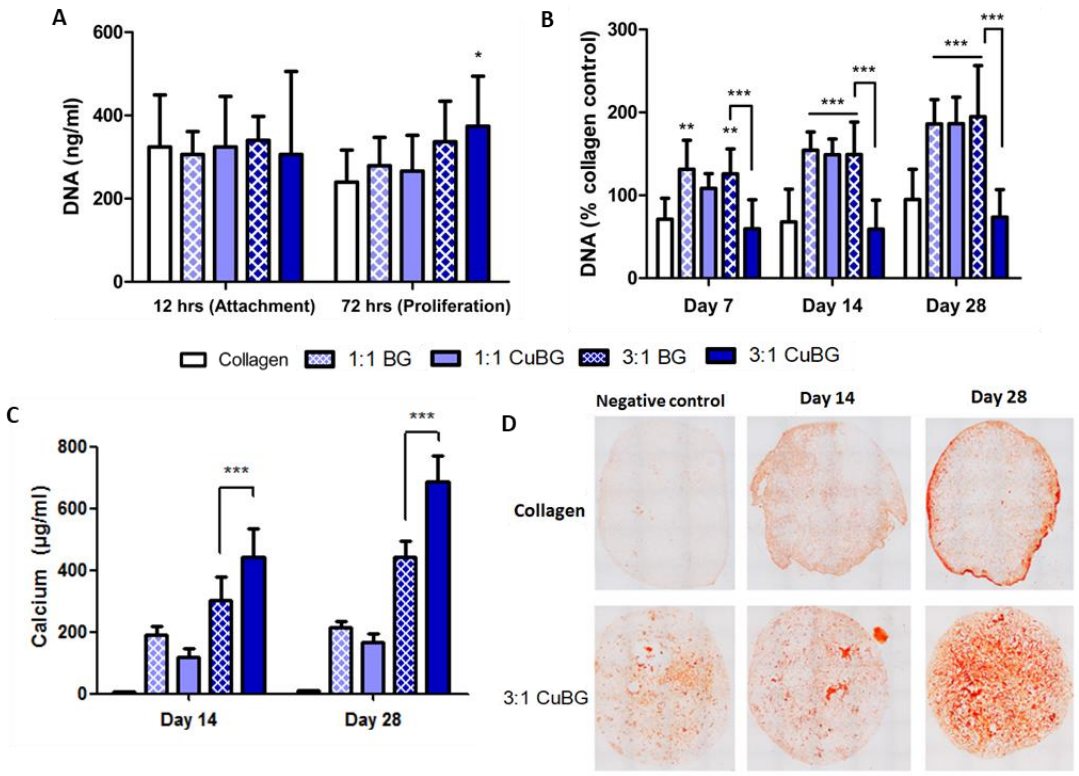

Figure 5.13 Demonstration of the ability of copper-doped bioactive glass scaffolds to enhance osteogenesis

*(A) PicoGreen® assay on scaffolds at 12 hrs and 72 hrs in growth medium as an indicator of initial cell attachment and proliferation, respectively. (B) PicoGreen® assay on scaffolds on days 7, 14, and 28 days after supplementation with osteogenic medium (DNA normalized to collagen control in growth media). (C) Total raw calcium values from scaffolds at day 14 and 28. (D) Alizarin red staining of scaffolds at day 14 and 28. Data presented as mean ± SD, n=3, p-values are calculated using two-way ANOVA with Bonferroni post-hoc test. All statistical significance shown in comparison to collagen control unless otherwise stated, *p < 0.05, **p < 0.01, ***p < 0.001.*

5.3.5 Copper-doped bioactive glass scaffolds enhance angiogenesis *in vitro*

Having determined that the CuBG-CS supports osteogenesis, their ability to support angiogenesis was next investigated, as copper has previously been suggested to be pro-angiogenic by upregulating VEGF production [137]. Note, while we did look at the effect of BG-CS controls – i.e. bioactive glass without copper-doping –as there was no significant difference to the collagen control, the results have not been included here. The eluate from CuBG-CS was shown to have a dose-dependent effect on VEGF protein production by MSCs (**Figure 5.14** A). At day 7 the 1:1 CuBG-CS significantly enhanced VEGF protein production, by 1.4 times vs. the collagen control ($p < 0.01$) while the 3:1 CuBG-CS performed similarly to the collagen control. The ability of the 1:1 CuBG-CS to enhance angiogenesis was further confirmed by observing the functional effect of increased VEGF production on total tubule length formed by HUVEC cells using a Matrigel® assay (**Figure 5.14** B). When tubule length was quantified, it was shown to be significantly enhanced for the 1:1 CuBG-CS group at day 1 ($p < 0.001$) by more than 1.9-fold in comparison to the collagen control (**Figure 5.14** C). This effect was not observed with the 3:1 CuBG-CS which showed significantly reduced tubule length at day 1, perhaps due to toxic effects on the sensitive HUVEC cells; however, by day 3 and 7, tubule length is recovered and the scaffolds perform similarly to the collagen control. Taking the Matrigel® and VEGF protein production results together, this shows that CuBG scaffolds can enhance angiogenesis in a dose-dependent manner.

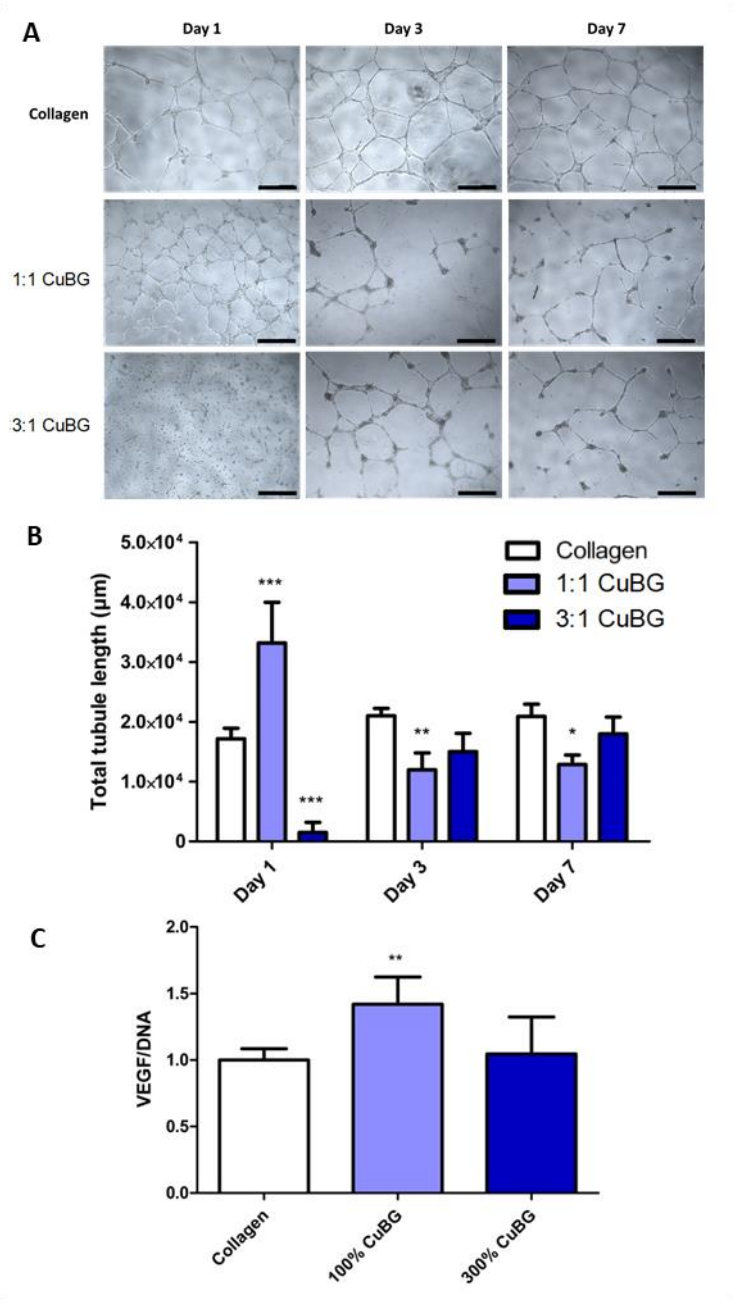

Figure 5.14 Effect of bioactive glass scaffolds on angiogenesis
*(A) Brightfield images of tubule formation in Matrigel® assay at 36 hrs post-seeding of human endothelial vascular endothelial (HUVEC) cells cultured with conditioned medium from collagen bioactive glass scaffolds. (B) Total tubule length (µm) quantification from Matrigel® assay. (C) VEGF protein production by rMSCs cultured with conditioned medium from collagen- bioactive glass scaffolds for 7 days (normalized to VEGF and DNA on collagen control). Note: scale bars 500 µm. Data presented as mean ± SD, n=3, p-values are calculated using one- and two-way ANOVA with Bonferroni post-hoc test. All statistical significance shown in comparison to collagen control unless otherwise stated, *p < 0.05, **p < 0.01, ***p < 0.001.*

5.3.6 Copper-doped bioactive glass scaffolds demonstrated enhanced osteo- and angiogenesis in a chick embryo *ex ovo* model

Having assessed the scaffolds comprehensively in a series of *in vitro* studies, we next sought to determine the effect of the different scaffold compositions on osteogenesis and angiogenesis in a more biologically complex chick embryo *in vivo* model. The hind limbs of the chicken embryos treated with BG-CS or CuBG-CS were harvested at day 12 of development and stained for alcian blue (for cartilage) and alizarin red (for bone). From visual inspection and quantification of the percentage of ossified limbs, similar to the *in vitro* studies, all bioactive glass treated scaffolds (both with and without copper doping) enhanced bone formation in comparison to collagen-only controls and to a similar level to the BMP-2 loaded control (**Figure 5.15** A&B).

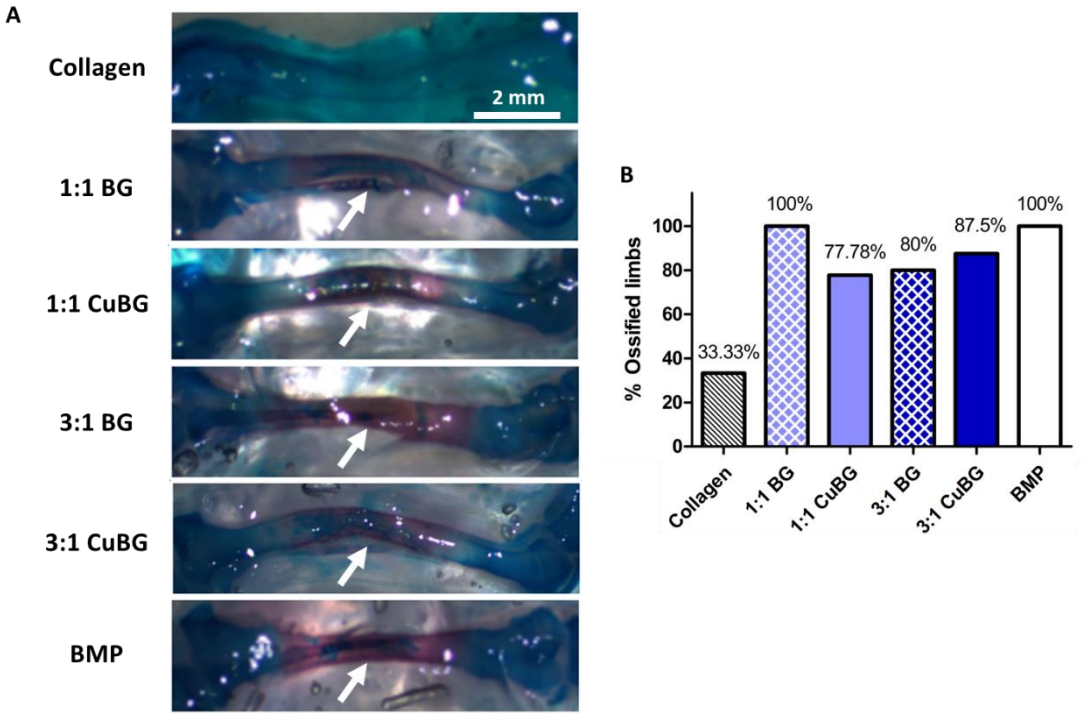

Figure 5.15 Effect of bioactive glass scaffolds on osteogenesis in a chick embryo* ex ovo *model
(A) Representative images of chick embryo femora at day 12 of development stained with alcian blue and alizarin red after treatments with bioactive glass scaffolds or collagen only and BMP containing scaffolds as controls. Note: white arrows indicate alizarin red staining. (B) Quantified percentage of harvested limbs that stained positive for alizarin red, or mineralisation. Note: scale bar 2 mm.

In terms of angiogenesis, and again similar to the *in vitro* studies, 1:1 CuBG scaffolds showed significantly enhanced angiogenesis in comparison to the

collagen control both qualitatively and when quantified using image analysis software. Strikingly, these were more highly vascularised than the VEGF-loaded control (**Figure 5.16** A&B).

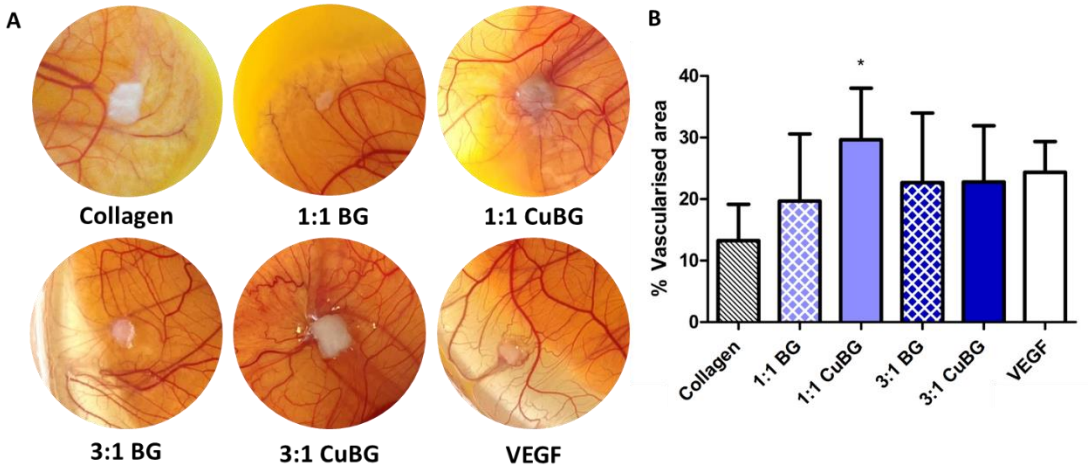

Figure 5.16 Effect of bioactive glass scaffolds on angiogenesis in a chick embryo* ex ovo *model
*(A) Representative images of the angiogenic response to bioactive glass scaffolds on the surrounding CAM membrane with collagen only and VEGF scaffolds as controls. (B) Quantified percentage vascularised area in a 12.5 mm Ø circular area around the scaffold treatments. Data presented as mean ± SD, n=3, p-values are calculated using an unpaired two-tailed t-test with 95% CI. All statistical significance shown in comparison to collagen control unless otherwise stated, *p < 0.05.*

5.4 Discussion

The overall aim of this study was to investigate the effect of copper-doped bioactive glass (CuBG) incorporation into a porous collagen scaffold on the microarchitectural and mechanical properties, antibacterial activity, and the ability of the scaffolds to support osteogenesis and angiogenesis both *in vitro* and *in vivo*. The results demonstrate that these novel CuBG collagen scaffolds (CuBG-CS) were highly porous, had suitable pore size for successful bone tissue engineering, and showed increased compressive modulus in comparison to the BG-free collagen scaffold. Most importantly, CuBG addition was shown to result in antibacterial activity, demonstrating increased toxicity against *S. aureus*. Furthermore, *in vitro*, the incorporation of CuBG enhanced osteogenesis and angiogenesis in a dose-dependent manner. Most promisingly, when tested in a chick embryo *ex ovo* model, the CuBG-CS was not only biocompatible, showing no signs of toxicity, but also demonstrated the same pattern of enhanced osteo- and angiogenesis as the *in vitro* studies; indeed, the CuBG-CS significantly outperformed VEGF positive controls in angiogenesis studies. Taken together, these results indicate that the CuBG-CS developed here show potential to be used in the osteomyelitis defect site by simultaneously limiting infection whilst promoting bone healing.

In this study, the development of a multi-functional scaffold for the treatment of bone defects and reduction of infection is proposed. This objective thus requires a matrix that is not only capable of supporting bone regeneration, but also inhibiting bacterial growth with the aim of avoiding contributing to antibiotic resistance. To the best of our knowledge, this is the first study to successfully demonstrate incorporation of copper-doped bioactive glass into a natural polymer-based scaffold. It was found that the incorporation of CuBG into the collagen scaffold successfully resulted in a non-antibiotic antibacterial scaffold. The 3:1 CuBG-CS resulted in a significant reduction in *S. aureus* growth in comparison to the collagen control. Additionally, a time-kill assay showed that the 1:1 CuBG-CS and 3:1 CuBG-CS scaffolds also significantly delay the growth of *S. aureus* at 7 hrs and from 7 to 24 hrs, respectively, in comparison to the collagen control. There are a number of antibiotic-loaded

collagen sponges (typically gentamicin) on the market for osteomyelitis treatment [15]; however, in clinical orthopaedic scenarios, these local antibiotic delivery vehicles are most often applied in a combined approach with the addition of systemic antibiotics to achieve the best possible results [288], [289] Thus, from a clinical translation perspective, if the bacterial clearance and growth rate reduction that was achieved here is not sufficient, a combined approach could be used.

As demonstrated in our 2-D studies – and consistent with many previous reports for both non-antibiotic antibacterials and antibiotics [205]–[209] – there is a fine balance between *S. aureus* toxicity and mammalian cell viability. However, in the 3D scaffold environment it was found that in even at the highest CuBG concentration of 3:1, mammalian cell number was not significantly reduced in comparison to the collagen control over the 28 days. Furthermore, with the exception of the 3:1 CuBG-CS, there is an increase in cell number on all scaffolds containing bioactive glass which may be partially attributed to the mechanical and microarchitectural properties of the BG-containing scaffolds; this would allow for more mechanically robust pores for cell attachment, infiltration, and proliferation.

It was found that after trialling a number of different incorporation methods, that a homogeneous distribution of bioactive glass throughout the collagen scaffold can be achieved. The homogeneously distributed bioactive glass is advantageous as it would result in homogeneous mechanical properties, maximize surface area for contact with osteoprogenitor cells (and thus osteoconduction), and the increased surface area might also increase ion release and improve degradation [290], [291]. Following addition of bioactive glass, all scaffolds remained over 98% porous. Previous work suggests porosities above 90% are necessary to ensure good cell infiltration and nutrient/waste transport throughout the construct; all scaffolds fabricated are in this range [246], [247]. Additionally, the pore sizes in the developed CuBG-CS are within the ideal range for tissue engineering applications. Previous studies have shown that pores of 40-100 μm show good cell viability and bone formation and pores within the 10-160 μm range are recommended for functional blood vessel formation [248]–[250]. Thus, we can surmise that the

scaffold mean pore size range of 68-79 μm that was achieved is suitable for both osteogenesis and angiogenesis. Additionally, the scaffold compressive modulus was increased upon the addition of CuBG, with stiffness increased by 1.6-fold in 1:1 CuBG-CS and significantly by 2.7-fold in 3:1 CuBG scaffolds vs. collagen alone. The incorporation of a ceramic into collagen-based scaffolds has been shown previously in our research group to increase stiffness [188], [190]. This increase in stiffness is desirable for improved cell infiltration and proliferation and also for bone repair applications, as it has previously been shown that increased construct stiffness can influence the differentiation of mesenchymal stem cells (MSC) down an osteogenic lineage [86]. Additionally, the increase in compressive modulus that was achieved is within the range of similar commercially available products and would also improve surgical handling due to the increased resistance to deformation, which would also maintain the critically important porosity and pore size [188].

It is widely described in the literature that bioactive glass is both osteoconductive and osteoinductive [138], [292], [293], additionally, it has also been shown that copper ions can promote osteogenesis. This is consistent with our observations herein: significantly increased calcium deposition 3:1 CuBG-CS at day 14 and day 28 in comparison to the non-copper doped BG-CS and collagen only controls. Similarly, a previous *in vivo* study has shown that 3% (wt) copper-doped bioactive glass can enhance blood vessel formation and bone regeneration [294]. Another study demonstrated that the addition of 50 μM of copper to MSCs diminished their proliferation rate and increased their ability to undergo osteogenic differentiation [277]. Thus, we can postulate that scaffold's enhanced bone regenerative capacity can be attributed to the combination of both the bioactive glass and copper within the CuBG-CS.

Many tissue engineered implants fail due to avascular necrosis [295]–[297]. Thus, effective vascularisation of porous scaffolds is a crucial event in successful tissue integration. There is an intimate relationship between vascularisation and improved bone formation, known as 'angiogenic–osteogenic coupling', so the invasion and development of a blood supply within the scaffold is essential for cell survival and flow of growth factors to stimulate

the relationship [298]–[300]. In the current study, a dose-dependent response of endothelial cells to copper-doped bioactive glass scaffolds is seen, with the lower dose 1:1 CuBG-CS significantly enhancing total tubule length by 1.9-fold. Copper ions have been shown previously to have a pro-angiogenic effect on endothelial cells *in vitro* by upregulating VEGF production and enhancing proliferation [137], [251], [301]. In addition, it has been found that the combination of copper sulphate (50 μg/ml – optimal dose) with the growth factors VEGF or FGF-2 on endothelial cells significantly enhanced the complexity of the angiogenic networks with a synergistic effect [302]. However, in our study, we also observed that the higher dose 3:1 CuBG-CS show significantly reduced tubule formation, which is presumed to be due to toxic effects on the cells. Another study reported a similar effect – 2.5% (mol) copper-doped Bioglass® decreased the ability of endothelial cells to form vascular networks with increasing CuBG addition and that, in fact, it is not due to increased copper release, but to increased silicon release and calcium depletion in the medium [303]. The authors also suggest that the proangiogenic effect of the copper released from the bioactive glass may not be reflected in endothelial cell cultures but may upregulate angiogenic factors of fibroblasts or osteoblasts. Hence, VEGF protein production by rMSCs in 2D culture when cultured with conditioned medium from collagen bioactive glass scaffolds was analysed. The VEGF results demonstrated that the 1:1 CuBG scaffolds significantly increased VEGF protein production, which should contribute to enhanced angiogenesis; in addition, there was a direct effect on vessel formation in the Matrigel® tubule assay. In any case, the obvious next step was to carry out an assessment of these novel materials in an *in vivo* study.

Having demonstrated the potential of the CuBG-CS *in vitro*, we next utilised an *ex ovo* (shell-less) chicken embryo model to enable examination of the *in vivo* therapeutic effect of the scaffolds on angio- and osteogenesis [282]–[285]. Using this model, it was found that all of the bioactive-glass loaded scaffolds were biocompatible with no adverse reactions or reduction in survival of embryos observed. This is encouraging as it shows that the incorporation of the anti-microbial materials, while effective at eliminating bacteria, has no

negative effect on adjacent healthy tissue. In fact, the CuBG scaffolds demonstrated enhanced osteogenesis and angiogenesis by the in comparison to the collagen only controls – consistent with the *in vitro* study results. All bioactive glass-loaded scaffolds, with or without copper doping (1:1 BG, 1:1 CuBG, 3:1 BG, and 3:1 CuBG), accelerated endochondral ossification in comparison to the collagen control and to similar levels to BMP-2-loaded positive control. These results correlate well with studies by Boccaccini *et al*. where 45S5 Bioglass® scaffolds (45S5 Bioglass®) also demonstrated enhanced osteogenesis in the chick embryo *ex ovo* model [285], [304]. In terms of angiogenesis, again correlating with our *in vitro* findings, the 1:1 CuBG scaffolds significantly enhanced angiogenesis in comparison to the collagen control, and to a level higher than that of the VEGF-loaded positive control. To the best of our knowledge, this is the first report of copper-doped bioactive glass scaffolds analysed in the chicken embryo. An angiogenic response was not elicited from either of the BG-CS (i.e. non copper-doped bioactive glass scaffolds), which is similar to results obtained by Vargas *et al*., Gorustovich *et al*., and Handel *et al*. who were also unable to detect an angiogenic response of un-doped 45S5 Bioglass® on the chicken CAM membrane [285], [304], [305]. However, our results are also similar to a study by Durand *et al*., who saw a significant increase in angiogenesis on the CAM membrane when a therapeutic angiogenic metal ion, boron, was doped into 45S5 Bioglass®, in comparison to non-boron doped Bioglass® [306].

The copper-doped bioactive glass scaffolds developed here provide an environment that enhances both osteogenesis and angiogenesis when compared to collagen scaffolds alone and those with non-copper-doped bioactive glass. Of the groups examined, 1:1 CuBG and 3:1 CuBG scaffolds hold the most promise. Both scaffolds show significantly enhanced osteogenesis *in vitro* and *in vivo*. 1:1 CuBG-CS might be chosen for defects where there the infection risk is low and bone regeneration is a priority as it significantly enhanced tubule formation and VEGF protein production *in vitro* and angiogenesis in the chick embryo *ex ovo* model. Alternatively, the 3:1 CuBG-CS might be most suitable in a situation where an infection is present in the debridement site due to its enhanced antibacterial properties against *S.*

aureus. Although 3:1 CuBG-CS showed some toxicity towards endothelial cells and inhibited their ability to form tubules, in an *in vivo* situation where the infection risk is high, the critical goal is to help the immune system clear the difficult-to-treat infection and there is a reservoir of new cells (e.g., in the marrow) that can replenish the scaffold once the initial burst of copper has been released i.e. we would expect reduced cytotoxicity to endothelial cells in the clinical environment. This theory was further supported in our chick embryo *ex ovo* model where no biocompatibility or toxicity issues were detected in either the 1:1 CuBG-CS or the 3:1 CuBG-CS scaffolds.

5.5 Conclusion

In this study, collagen copper-doped bioactive glass scaffolds were successfully produced. The results demonstrate that the scaffolds are capable of antibacterial activity, without the use of antibiotics, and also stimulate osteogenesis and angiogenesis *in vitro*. In an *in vivo* environment, the copper-doped bioactive glass scaffolds were not only biocompatible, but also demonstrated the same pattern of enhanced osteo- and angiogenesis as the *in vitro* studies. This platform system could be further modified and used to deliver a variety of other non-antibiotic antimicrobial metal ion-doped minerals. In summary, this study presents a single-stage treatment for osteomyelitis which might reduce the need for antibiotics and bone grafting thus reducing hospital stays and costs.

Chapter 6 Discussion

6.1 Overview

Despite advances in the treatment of osteomyelitis through revised surgical approaches and antibiotic regimens [25], [307], the disease remains notoriously difficult-to-treat with treatment failure rates of up to 20-30% [307], [308]. Traditional treatment strategies usually involve a multistep procedure: a long, large dose of systemic antibiotics combined with surgical debridement and bone grafting. As well as the drawback of the multistep treatment approach, the individual aspects of this approach have drawbacks. Due to the avascular nature of the necrotic bone, penetration of the antibiotics to the infected site can be poor. As such, high doses of antibiotics over long time periods are required, which can result in systemic toxicity. Furthermore, minimal new antibiotic discoveries combined with an alarming number of emerging cases of microbial resistance to ‘last resort’ antibiotics is threatening our ability to treat osteomyelitis and has driven research to focus on discovering and developing non-antibiotic antimicrobials.

From the bone regeneration side, the numerous complications associated with autografting for osteomyelitis (e.g. hematoma formation and donor site morbidity/fracture) are well documented [309]. Therefore, in treating osteomyelitis, there exists a dual challenge: ensuring an effective and non-toxic dose of antimicrobial, while ensuring bone regeneration is stimulated. Thus, the overall aim of the research presented in this thesis was to explore

the potential of one-step tissue engineering-based treatment strategies for osteomyelitis that combines local, controlled release of non-antibiotic antibacterials within a regenerative collagen-based scaffold system.

A number of products have emerged in recent years that are focused on the local delivery of antibiotics to the site of infection. These ultimately aim to reduce the dependence on systemic antibiotics, decrease hospitalisation costs and, importantly, prevent late relapse, which is common in chronic osteomyelitis [53]. Biodegradable gentamicin-loaded collagen fleeces (or scaffolds) (such as Collatamp® G/EG and GENTA-COLL®) have shown more complete wound healing, shorter healing time, improved clinical outcome, and reduced convalescence time compared to empty defects [57]–[59]. In terms of osteomyelitis treatment, gentamicin-loaded collagen fleeces have demonstrated a range of treatment success rates, from 74-94% [56], [60]–[62]. When compared to non-degradable antibiotic delivery systems used clinically which are based on beads of the acrylic material polymethylmethacrylate (PMMA) loaded with gentamicin, they had significantly lower rate of re-operation [56], [63].

Thus, for the treatment approaches in this thesis, we utilised a collagen-based scaffold template as previous work from our lab has demonstrated the excellent regenerative capacity of these scaffolds [87]–[91]. The highly porous scaffolds are typically tailored for the site of application with the addition of supplementary bioactive factors such as elastin for vascular grafts, glycosaminoglycans (GAGs) for cartilage repair, fibrin for cardiac applications, hyaluronic acid for nerve regeneration, or hydroxyapatite for bone regeneration [88], [188], [310]–[312]. Therefore, we functionalised the collagen scaffold to possess antimicrobial activity, without the use of antibiotics, whilst promoting bone formation for the treatment of osteomyelitis. The following sections will summarise the key findings and implications from each individual chapter and review the possible future directions which have arisen from this research.

6.2 Chapter 2 – Effect of non-antibiotic antibacterial materials on bacterial and mammalian cells in a 2D environment

A disadvantage with the majority of antimicrobial materials (including antibiotics) is that there is a trade-off between bacteria-killing ability and toxic effects in the body so the dosage level is critical [205]–[209]. Therefore, as a first step, 2D screening of the chosen non-antibiotic materials (specifically chitosan, copper nanoparticles, silver nanoparticles, zinc nanoparticles, copper chloride salt, silver nitrate salt, and zinc chloride salt) on mammalian cell viability was employed. The overall goal of this chapter was thus to identify the optimal dosage of these materials that will effectively kill bacteria, while maintaining acceptable mammalian cell viability in a 2D environment. This informed the studies in later chapter where the materials were incorporated into a 3D scaffold at biologically relevant concentrations.

The data demonstrated that there is a fine balance between inhibiting the growth of clinically relevant bacteria species (*S. aureus*, *S. epidermidis*, and *E. coli*) and maintaining acceptable mammalian cell viability. Chitosan performed well in terms of antibacterial activity, inhibiting the growth of all three clinically relevant bacteria species, *S. aureus*, *S. epidermidis*, and *E. coli*, whilst maintaining reasonable mammalian cell viability. The broad-spectrum antibacterial activity that chitosan displays is advantageous as – although osteomyelitis is predominately caused by *S. aureus* – the causative organism may involve other bacterial species, or the infection could be polymicrobial. This data corresponds well with respect to the current literature which reports broad-spectrum activity of chitosan [116]. There are mixed reviews as to whether chitosan shows higher antibacterial activity against gram negative or gram-positive bacteria, but there are also numerous reports which agree with the results in this study, which find no significant differences in antibacterial activity between the species tested here [313], [314]. Clinically, in terms of infection treatment, chitosan is currently being used in skin wound healing and wound exudate management with good results due to its absorbent, antimicrobial, and regenerative properties [315]–[317].

When the antibacterial activity of the metal nanoparticles, copper, silver, and zinc oxide were examined, they were found to have a detectable antibacterial effect on some or all bacteria species, although none achieved full inhibition across all three bacteria species. However, when the toxicity of the metal nanoparticles against mammalian cells was examined, they were found to cause a substantial reduction in mammalian cell viability at the antibacterial concentrations.

When compared to the bacterial toxicity/mammalian viability ratio results of the metals in nanoparticle form, the metal salts demonstrated the most favourable results. All of the metals in their salt form achieved complete inhibition of bacterial growth against *S. aureus, S. epidermidis*, and *E. coli* in the concentration ranges tested. The metal salts were found to reduce the viability of mammalian cells; however, it must be noted that at these concentrations, full bacterial clearance is achieved.

This amplified toxic effect of metal nanoparticles in comparison to metal salts has been reported in other studies in the literature to be due to the fact that metal ions are unable to cross the cellular lipid bilayer without special transporters/membrane channels. Yet, the metal nanoparticles enter the cells relatively freely, and once internalised, likely release metal ions and increase ROS intracellularly [318]–[320]. Thus, it is no surprise that clinically, metal nanoparticles are used topically in wound dressings where they can be removed after the desired antimicrobial effect so that wound healing can ensue [157], [227]–[229].

Summarising these data, the metal salts displayed a superior bacterial toxicity/mammalian cell viability relationship than the nanoparticles tested, and the activity of metal salts is much more predictable and controllable than metal nanoparticles (which would take an extensive time to dissolve, if at all, in the patient's lifetime). There is literature to suggest that the metal ions copper and zinc in particular can enhance both angiogenesis and osteogenesis [137], [138], [175]–[177]. However, the same cannot be said for the silver ion, unless, perhaps, if combined with an osteogenic carrier (AgHA in Chapter 4). Thus, it was chosen to bring forward chitosan and the metal salts, copper chloride and

zinc chloride, as they show promise as potential agents for osteomyelitis infection treatment.

6.3 Chapter 3 – Development of a 3D antimicrobial delivery platform to modulate antimicrobial ion release while retaining bioactivity

In Chapter 2, we demonstrated the potential of chitosan, copper chloride and zinc chloride as potential agents for osteomyelitis infection treatment due to their superior bacterial toxicity/mammalian cell viability ratio. Successful osteomyelitis treatment relies heavily on the ability of the antibacterial agent to reach the site of infection at sufficient and controlled concentrations [224]. One way to achieve this is to deliver the identified antibacterial agents locally, for example in a 3D scaffold that controls the release of the agent, while also functioning to allow for cell infiltration and proliferation and ultimately repair and regenerate the bone tissue. Thus, the development of two different scaffold systems was proposed; a 'directly-loaded' collagen/chitosan-based scaffold group for a burst-release of metal ions and chitosan 'microparticle-loaded' collagen-based scaffold group for a more prolonged release of metal ions.

The results demonstrated that it was possible to control the metal salt release profile via dose incorporation and through the chitosan microparticle release system. This, in turn, modulated the scaffold's antibacterial activity, with the burst release directly loaded scaffolds showing highest antibacterial activity against *S. aureus*. Not surprisingly, as their function is to modulate metal ion release, the microparticle-loaded scaffolds did not have as profound an antibacterial effect as directly-loaded scaffolds due to reduced metal salt release.

The ability of the scaffolds to support mammalian cells and their influence on osteogenesis and angiogenesis *in vitro* was next examined. Promisingly, it was found that both scaffold groups supported mammalian cell survival over the 28 days, with microparticle-incorporated scaffolds inducing less toxic effects in comparison to directly-loaded scaffolds at each time point, presumably due to the controlled/reduced metal salt release from the

scaffolds. Of note, and in contrast to copper directly-loaded scaffolds, zinc directly-loaded scaffolds performed well in terms in terms of osteogenic effect by supporting calcium production. This is in agreement with the literature which suggests that zinc can promote osteogenesis through osteoblast proliferation and differentiation [175]–[177]. Both copper and zinc-microparticle scaffolds supported calcium production, again due to reduced ion release.

In terms of angiogenesis, the microparticle-loaded scaffold system was advantageous when compared to the directly-loaded scaffold system due to the prolonged angiogenic response from both copper and zinc microparticle-loaded scaffolds, which was also seen in directly-loaded scaffolds but for a shorter time period. This may be attributed to the reduced metal ion release from the scaffolds, which might be less toxic towards the endothelial cells. Alternatively, as it is well-known that copper can stimulate angiogenesis and vasculogenisis [138], [139], this reduced ion release rate may be at the appropriate concentration to enhance angiogenesis. One study from literature reports a similar concentration of copper sulphate (0.5 mM) can enhance endothelial cell proliferation 2-fold [251].

Based on the results from this study, perhaps an ideal combination for osteomyelitis treatment might be a base collagen/chitosan scaffold with zinc chloride salt directly-incorporated for a burst release of ions to clear the infection, followed by controlled release of copper ions from the microparticle system to stimulate angiogenesis. Once the ions have been depleted, the base collagen/chitosan scaffold might prevent infection reoccurrence whilst tissue regeneration is underway. However, the relatively poor bone osteogenic potential of these scaffolds motivated the exploration into other osteogenic materials that could be incorporated into the collagen scaffold that might boost its osteogenic capacity, in addition to retaining potent antimicrobial activity (Chapter 4 & 5).

6.4 Chapter 4 - Development of a silver-doped hydroxyapatite scaffold for the release of antimicrobial ions and enhanced osteogenesis

Hydroxyapatite is widely used in bone tissue engineering as it is an osteoconductive material that shows good biocompatibility and biodegradability [2], [180], [181]. For effective osteomyelitis treatment, a combinatorial approach might be effective i.e. the use of materials capable of osteogenic stimulation combined with materials capable of antimicrobial activity. Silver is the most widely explored metal in controlling microbial growth, both in research and application, demonstrating effective antimicrobial activity against gram-positive and gram-negative bacteria as well as fungi [122]. However, beyond its potent antibacterial activity, there are a number of publications which report cytotoxicity issues with silver use, so controlling the dosage is crucial [255]–[258]. In this chapter it was hypothesised that doping silver into hydroxyapatite and incorporating it into a collagen scaffold might render it more desirable for use in osteomyelitis treatment by reducing immediate silver exposure to cells in the 3D scaffold environment and thus its toxic effect.

A range of silver-doped hydroxyapatite particles were successfully fabricated in-house (0%, 2% and 5% mol Ag-doping) which, when incorporated into collagen scaffolds at various weight percentages, produced scaffolds with improved mechanical properties, high porosity, and a pore size suitable for bone tissue engineering. These enhanced microarchitectural and mechanical properties are desirable as they could improve cell infiltration, nutrient and waste transport throughout the construct, act as added osteogenic stimulus, and improve surgical handling of the scaffolds. Similarly, the addition of hydroxyapatite has previously been shown in the literature to increase the compressive modulus of collagen scaffolds [188], [265].

The addition of silver-doped hydroxyapatite into the collagen scaffolds showed potent antimicrobial activity against *S. aureus,* demonstrating the successful production of a non-antibiotic antibacterial scaffold. Not surprisingly, although all silver-doped hydroxyapatite scaffolds demonstrated antimicrobial activity

vs. the collagen control, it was found that increasing the AgHA weight ratio or % Ag-doping significantly increased the antimicrobial activity of the scaffolds. Other published studies found a similar effect on antibacterial activity with increasing weight ratio or % Ag-doping in hydroxyapatite [191], [321], [322].

Our 2D studies in Chapter 2 demonstrated the fine balance between the antibacterial activity and mammalian cell toxicity of silver – unfortunately in the 3D scaffolds, although potent antimicrobial activity was achieved, we were unable to achieve a reasonable trade-off between this and mammalian cell viability. There are no silver-doped hydroxyapatite products currently marketed for clinical use, possibly due to this effect. However, the true cytocompatibility of the silver-doped hydroxyapatite scaffolds might be revealed after a longer time-period in culture with a potential recovery in cell proliferation and also exposed in an *in vivo* assessment, as a previous study, which similarly found silver-doped hydroxyapatite to be moderately toxic towards mammalian cells *in vitro*, found that *in vivo*, silver-doped hydroxyapatite (of up to 4.3% Ag-doping) demonstrated favourable bone repair without a remarkable inflammatory reaction [269]. This may be attributed to a repopulation of the scaffold with cells once the infection is cleared and the concentration of Ag ions released from the AgHA diminishes. Furthermore, further optimisation of the platform system might also achieve a superior balance between antimicrobial activity and mammalian cell cytocompatibility. This may be achieved through modification of the bioactivity of the hydroxyapatite particles (particle size, shape, or porosity [265], [271]–[273]) or by fine-tuning the concentrations of AgHA within the scaffold.

6.5 Chapter 5 - Development of a copper-doped bioactive glass scaffold for the release of antimicrobial ions and enhanced osteogenesis

To maintain the favourable properties (increased compressive modulus, high porosity and pore size, and potent antibacterial activity) but to overcome the toxicity issues and limited osteogenic potential of silver-doped hydroxyapatite scaffolds, in Chapter 5 a second multifunctional material was introduced. Namely, copper-doped bioactive glass, as an alternative to silver-doped

hydroxyapatite, in the hope that it might display added benefits of enhanced osteogenesis and angiogenesis without the cytotoxicity issues on mammalian cells. Thus, the overall goal of this chapter was to investigate the effect of copper-doped bioactive glass (CuBG) incorporation into a porous collagen scaffold on the microarchitectural and mechanical properties as well as antibacterial activity. In addition, we assessed the ability of the scaffolds to support osteogenesis and angiogenesis both *in vitro* and *in vivo*.

The results demonstrate that these novel CuBG collagen scaffolds (CuBG-CS) were highly porous, had suitable pore size for successful bone tissue engineering, and showed increased compressive modulus in comparison to the BG-free collagen scaffold. Most importantly, it was found that the incorporation of 3:1 CuBG into the collagen scaffold successfully resulted in pronounced antibacterial activity vs. *S. aureus*. The literature also suggests that similar types of copper-doped bioactive glass show even more significant antibacterial activity towards *E. coli* (10-fold lower MBC than *S. aureus),* highlighting the broad-spectrum applicability of the scaffolds produced here in different bone infection scenarios [323].

In terms of cytocompatibility, in the CuBG scaffold environment we found that even at the highest CuBG concentration (3:1), mammalian cell number was not significantly reduced in comparison to the collagen control over the 28 days. It is widely described in the literature that bioactive glass is both osteoconductive and osteoinductive [138], [292], [293], additionally, it has also been shown that copper ions can promote osteogenesis. This is consistent with our observations herein: significantly increased calcium deposition on 1:1 and 3:1 CuBG scaffolds in comparison to the controls. Many tissue engineered implants fail due to avascular necrosis [295]–[297]. Thus, effective vascularisation of porous scaffolds is a crucial event in successful tissue integration. The results demonstrated that the 1:1 CuBG scaffolds significantly increased VEGF protein production, which should contribute to enhanced angiogenesis; in addition, there was a direct effect on vessel formation in the Matrigel® tubule assay. The cytocompatibility, osteogenic, and angiogenic response results here correlate well with the literature which demonstrates good cytocompatibility, increased osteogenic response through raised ALP

activity, and upregulated hypoxia-inducible factor ((HIF)-1α) and VEGF protein production with a similar copper-doped bioactive glass cultured with human bone marrow stromal cells [274].

The promising *in vitro* performance of the scaffolds led us to examine the *in vivo* therapeutic effect of the scaffolds on angio- and osteogenesis in an *ex ovo* (shell-less) chicken embryo *in vivo* model [282]–[285]. Using this model, it was found that all of the bioactive-glass loaded scaffolds were biocompatible with no adverse reactions or reduction in survival of embryos observed. In fact, we observed enhanced osteogenesis and angiogenesis in the CuBG scaffolds in comparison to the collagen only controls – consistent with the *in vitro* study results. This *in vivo* model has been used previously for non-copped doped Bioglass® scaffolds, where similarly the ions released from the bioactive glass was found to accelerate endochondral ossification in the chick femurs [285]. In this study, the authors however did not detect an angiogenic effect of the Bioglass® scaffold on the surrounding chorioallantoic membrane, further reinforcing that it is the copper ion release that elicits this response to our scaffolds.

6.7 Direct comparison between optimum scaffolds developed in Chapters 3, 4, and 5

All scaffolds developed in this thesis have a number of advantageous properties e.g. controlled release (Cu-microparticle loaded scaffolds), angiogenic stimulation (Cu-containing scaffolds from Chapter 3 and CuBG scaffolds from Chapter 5), and enhanced mechanical properties (AgHA and CuBG containing scaffolds from Chapter 4 & 5). However, in in order to select an optimum scaffold from the thesis, a direct quantifiable comparison between the best performing scaffolds developed within Chapters 3, 4, and 5 was carried out (**Figure 6.1**).

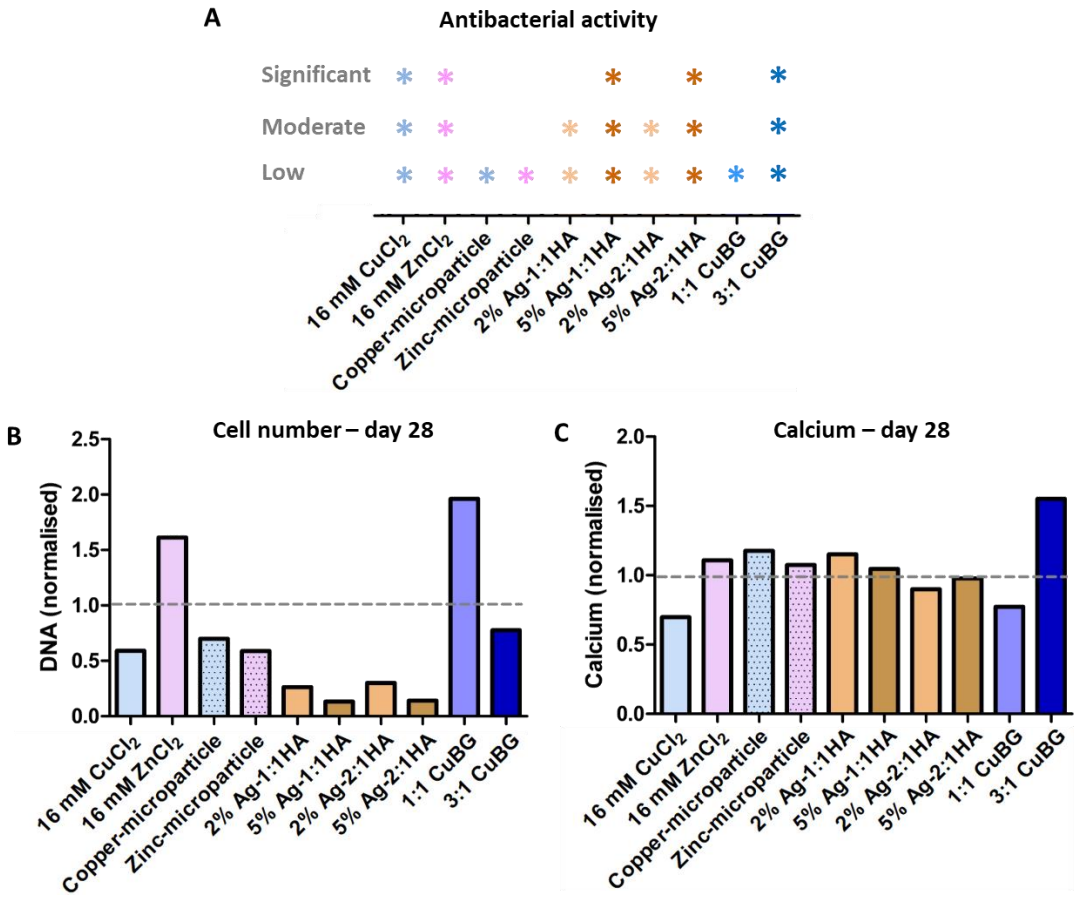

Figure 6.1 Direct comparison between the best performing scaffolds developed in Chapters 3 - 5
(A) Antibacterial activity against S. aureus *rated on a three-tier scale: significant, moderate, or low antibacterial activity. (B) DNA, as an indicator of cell number, on scaffolds at day 28, normalised to the respective control. (C) Calcium levels after 28 days in culture normalised to controls within the experiments.*

The scaffold properties that were selected for comparison were considered as the three key areas for osteomyelitis treatment: antibacterial activity, cell survival or proliferation, and cell-mediated calcium production. Antibacterial activity was rated on a three-tier scale: significant, moderate, or low antibacterial activity against *S. aureus* (**Figure 6.1** A). As a means of measuring osteoblast cytocompatibility, DNA, as an indicator of cell number, was compared on the scaffolds at day 28, normalised to the respective control within each experiment (collagen or collagen/chitosan, where applicable) (**Figure 6.1** B). Finally, the calcium levels after 28 days in culture were compared across scaffold types (**Figure 6.1** C). Again, the calcium levels were normalised to the respective control within each experiment and any scaffolds which inherently contained calcium (AgHA and CuBG) were normalised to the

non-metal doped control (HA and BG), at the same concentration. From these graphs, 3:1 CuBG scaffolds offer the most potential for osteomyelitis treatment by showing significant antibacterial activity, reasonable cell number at day 28 when normalised to the collagen control, and the most significantly enhanced calcium levels of all scaffolds developed when normalised to the non-copper doped control. 3:1 CuBG scaffolds are the primary outcome from this thesis, a scaffold worthy of being taken forward as a viable treatment after an *in vivo* assessment in a rabbit model.

6.8 Future work

The results from this study have identified some obvious areas worthy of further investigation. These include:

- While the scaffold platforms developed in Chapter 3 were intended for the treatment of osteomyelitis, and assessed with this in mind, it would be interesting to assess the functionality of these scaffolds (with or without modification) with other infection types as many of the agents are suggested to display broad-spectrum effects. For example, the scaffolds may prove advantageous for skin infection and wound healing applications so would require further antibacterial activity testing against additional microbes including streptococcal bacteria or candida yeast, perhaps, and skin specific mammalian cells such as fibroblasts and keratinocytes, for example.
- While the silver-doped hydroxyapatite scaffolds developed in Chapter 4 show enhanced microarchitectural and mechanical properties and potent antibacterial activity, the methods used to assess the scaffold bioactivity of the scaffolds or the AgHA particles themselves could possibly be modified to further elucidate the bioactive response. For example, if the scaffolds were cultured for a longer time period, a recovery in cell proliferation might occur when the concentration of Ag ions released from the AgHA diminishes. In addition, as un-doped HA is widely cited throughout literature to promote osteogenesis and since there was no obvious osteogenic effect from the un-doped hydroxyapatite particles in the study, perhaps more work is required to

optimise the biological properties of the hydroxyapatite particles e.g. changes in particle size, shape, or porosity have all been shown to affect bioactivity.

- In this thesis we looked at two metal ion-doped ceramics, namely silver-doped hydroxyapatite and copper-doped bioactive glass. It would also be interesting to assess the potential of other possible metal/ceramic doping combinations, for e.g. copper-doped hydroxyapatite, zinc-doped hydroxyapatite, zinc- bioactive glass, or silver-doped bioactive glass.
- Throughout the thesis a small range of concentrations of non-antibiotic antibacterials of each of the scaffold systems were assessed. However, now that we are equipped with full bioactivity results, perhaps the concentrations could be fine-tuned, to achieve an even better biological response. For example – perhaps 2:1 CuBG might enhance *both* osteogenesis and angiogenesis or 0.5:1 AgHA might provide a better balance between antibacterial activity and mammalian cell cytocompatibility. It would also be insightful to compare the antibacterial efficiency of these materials with clinically relevant antibiotics.
- The copper-doped bioactive glass scaffolds examined in Chapter 5 were the most successful scaffold group developed in the thesis (**Figure 6.1**), thus, their effect in a chick embryo *in vivo* model was examined. The chick embryo model offers several economic and practical advantages over other in animal models and it provided valuable insight into the *in vivo* osteogenic and angiogenic effect of the scaffolds. However, it did not encompass an infection aspect, essential in assessing the suitability of potential new treatment strategies for osteomyelitis. We have recently completed an *in vivo* assessment of another scaffold type developed within our lab for osteomyelitis treatment (antibiotic-loaded collagen scaffolds) in the AO Research Institute (Davos, Switzerland) under the guidance of Dr. Moriarty in Prof. Richards' team. Hence, in order to more comprehensively assess the antibacterial potential and regenerative capacity of these scaffolds, it would be insightful to test these scaffolds in the rat or rabbit

osteomyelitis model developed at the AO Research Institute [324], [325].

6.9 Thesis conclusions

This study has shown that we can produce a number of scaffold systems which are capable of antibacterial activity, without the use of antibiotics, and also stimulate osteogenesis and angiogenesis *in vitro*. In summary, this thesis presents potential single-stage treatments for osteomyelitis which might reduce the need for antibiotics and bone grafting thus reducing hospital stays and costs.

- In Chapter 2, a number of non-antibiotic antibacterial materials (chitosan, copper, silver, and zinc) were successfully screened by examining their antibacterial activity and effect on mammalian cell viability
- In Chapter 3, the antimicrobials selected from the screening process (chitosan, copper chloride, and zinc chloride) were incorporated into 3D collagen-based scaffold systems using chitosan which offered two distinct metal ion release profiles. These release profiles/concentrations functioned to modulate the scaffold bioactivity in terms of antibacterial activity and angiogenesis
- In Chapter 4, in the search for a scaffold which acts as a more potent osteogenic stimulus, silver-doped hydroxyapatite was synthesised and incorporated into 3D collagen scaffolds. The scaffolds demonstrated potent antibacterial activity; however, they induced undesirable toxicity towards osteoblasts *in vitro*
- Thus, in Chapter 5 we finally turned to the fabrication of 3D antimicrobial collagen- copper-doped bioactive glass scaffolds. These scaffolds in particular showed the most promise *in vitro* and where therefore assessed *in vivo* environment, where they were shown to not only be biocompatible, but also demonstrated the same pattern of enhanced osteogenesis and angiogenesis as the *in vitro* studies

Bibliography

[1] S. C. Marks and P. R. Odgren, “Structure and development of the skeleton,” in *Principles of Bone Biology*, 2002, pp. 3–15.

[2] F. J. O’Brien, “Biomaterials & scaffolds for tissue engineering,” *Mater. Today*, vol. 14, no. 3, pp. 88–95, 2011.

[3] R. Florencio-silva, G. Rodrigues, E. Sasso-cerri, M. J. Simões, and P. S. Cerri, “Biology of bone tissue: Structure, function, and factors that influence bone cells,” *Biomed Res. Int.*, vol. 2015, 2015.

[4] Gerard J. Tortora and Bryan H. Derrickson, *Principles of anatomy and physiology*. John Wiley & Sons, Inc, 2009.

[5] L. E. Craig, K. E. Dittmer, and K. G. Thompson, “Bones and joints,” in *Jubb, Kennedy & Palmer’s Pathology of Domestic Animals: Volume 1*, Elsevier, 2016, pp. 16–163.

[6] S. C. Marks and S. N. Popoff, “Bone cell biology: the regulation of development, structure, and function in the skeleton,” *Am. J. Anat.*, vol. 183, no. 1, pp. 1–44, 1988.

[7] S. F. Gilbert, *Developmental biology*. Sinauer Associates, 2000.

[8] J. F. Charles and A. O. Aliprantis, “Osteoclasts: More than ‘bone eaters,’” *Trends Mol. Med.*, vol. 20, no. 8, pp. 449–459, 2014.

[9] F. Shapiro, “Bone development and its relation to fracture repair. The role of mesenchymal osteoblasts and surface osteoblasts,” *Eur. Cells Mater.*, vol. 15, pp. 53–76, 2008.

[10] E. M. Thompson, A. Matsiko, E. Farrell, D. J. Kelly, and F. J. O’Brien, “Recapitulating endochondral ossification: a promising route to in vivo bone regeneration,” *J. Tissue Eng. Regen. Med.*, vol. 9, no. 8, pp. 889–902, 2015.

[11] A. Schindeler, M. M. McDonald, P. Bokko, and D. G. Little, “Bone remodeling during fracture repair: The cellular picture,” *Semin. Cell Dev. Biol.*, vol. 19, no. 5, pp. 459–466, 2008.

[12] T. A. Einhorn and L. C. Gerstenfeld, “Fracture healing: mechanisms and interventions,” *Nat. Rev. Rheumatol.*, vol. 11, no. 1, pp. 45–54, 2015.

[13] D. P. Lew and F. A. Waldvogel, “Osteomyelitis,” *Lancet*, vol. 364, pp. 369–379, 2004.

[14] G. Walter, M. Kemmerer, C. Kappler, and R. Hoffmann, “Treatment algorithms for chronic osteomyelitis,” *Dtsch. Arztebl. Int.*, vol. 109, no. 14, pp. 257–264, 2012.

[15] N. Kavanagh *et al.*, “Staphylococcal osteomyelitis: Disease progression, treatment challenges, and future directions,” *Clin. Microbiol. Rev.*, vol. 31, no. 2, pp. 1–25, 2018.

[16] V. J. Vigorita, B. Ghelman, and D. Mintz, *Orthopaedic pathology*. Lippincott Williams and Wilkins, 2008.

[17] B. Healy and A. Freedman, “ABC of wound healing: Infections,” *BMJ*, vol. 332, no. 7545, pp. 838–41, 2006.

[18] J. H. Calhoun, M. M. Manring, and M. Shirtliff, “Osteomyelitis of the long bones,” *Semin. Plast. Surg.*, vol. 23, no. 2, pp. 59–72, 2009.

[19] V. Kumar, A. K. Abbas, J. C. Aster, and S. L. Robbins, *Robbins basic pathology*. Elsevier/Saunders, 2013.

[20] A. Oryan, S. Alidadi, A. Moshiri, and N. Maffulli, “Bone regenerative medicine: Classic options, novel strategies, and future directions,” *J. Orthop. Surg. Res.*, vol. 9, no. 1, pp. 1–27, 2014.

[21] F. A. Waldvogel, G. Medoff, and M. N. Swartz, “Osteomyelitis: a review of clinical features, therapeutic considerations and unusual aspects,” *N. Engl. J. Med.*, vol. 282, no. 6, pp. 316–22, 1970.

[22] M. E. Pichichero and H. A. Friesen, “Polymicrobial osteomyelitis: report of three cases and review of the literature,” *Rev Infect Dis*, vol. 4, no. 1, pp. 86–96, 1982.

[23] R. A. Brady, J. G. Leid, J. H. Calhoun, J. W. Costerton, and M. E. Shirtliff, “Osteomyelitis and the role of biofilms in chronic infection,” *FEMS Immunol. Med. Microbiol.*, vol. 52, no. 1, pp. 13–22, 2008.

[24] P. C. Alguire, *Internal medicine essentials for clerkship students 2*. ACP Press, 2009.

[25] A. L. L. Lima and W. R. Junior, “Recommendations for the treatment of osteomyelitis,” *Brazilian J. Infect. Dis.*, vol. 18, no. 5, pp. 526–534, 2014.

[26] J. Pasquet, Y. Chevalier, E. Couval, D. Bouvier, and M.-A. Bolzinger, “Zinc oxide as a new antimicrobial preservative of topical products: Interactions with common formulation ingredients,” *Int. J. Pharm.*, vol. 479, no. 1, pp. 88–95, 2014.

[27] M. K. and K. Merritt, “Factors increasing the risk of infection in patients with open fractures,” *Journal of Trauma*, vol. 28, no. 6. pp. 823–827, 1988.

[28] D. G. Armstrong, L. A. Lavery, and L. B. Harkless, “Validation of a diabetic wound classification system. The contribution of depth, infection, and ischemia to risk of amputation,” *Diabetes Care*, vol. 21, no. 5, pp. 855–9, 1998.

[29] A. R. Berendt, “Diabetic foot osteomyelitis : a progress report on diagnosis and a systematic review of treatment,” *Diabetes. Metab. Res. Rev.*, vol. 24, pp. 145–161, 2008.

[30] L. A. Lavery, D. G. Armstrong, E. J. G. Peters, and B. A. Lipsky, “Probe-to-bone test for diagnosing diabetic foot osteomyelitis: Reliable or relic?,” *Diabetes Care*, vol. 30, no. 2, pp. 270–274, 2007.

[31] R. Malhotra, C. S.-Y. Chan, and A. Nather, “Osteomyelitis in the diabetic foot,” *Diabet. Foot Ankle*, vol. 195, no. 5, pp. 1–2, 2014.

[32] M. Grayson, G. GW, K. Balogh, E. Levin, and K. AW, “Probing to bone in infected pedal ulcers: A clinical sign of underlying osteomyelitis in

diabetic patients," *JAMA*, vol. 273, no. 9, pp. 721–723, 1995.

[33] U. May *et al.*, "Definition of the diagnosis osteomyelitis - osteomyelitis diagnosis score (ODS)," *Z. Orthop. Unfall.*, vol. 152, pp. 334–342, 2011.

[34] A. Tiemann, G. O. Hofmann, M. G. Krukemeyer, V. Krenn, and S. Langwald, "Histopathological osteomyelitis evaluation score (HOES) – an innovative approach to histopathological diagnostics and scoring of osteomyelitis," *Plast. Reconstr. Surg.*, vol. 3, pp. 1–12, 2014.

[35] R. Scott, M. Christofersen, W. J. Robertson, R. Davidson, L. Rankin, and D. Drummond, "Acute osteomyelitis in children: a review of 116 cases," *J Pediatr Orthop*, vol. 5, no. 10, pp. 649–52, 1990.

[36] J. Hatzenbuehler and T. J. Pulling, "Diagnosis and management of osteomyelitis," *Am. Fam. Physician*, vol. 84, no. 9, pp. 1027–1033, 2011.

[37] B. Parsons and E. Strauss, "Surgical management of chronic osteomyelitis," vol. 188, pp. 31–33, 2004.

[38] J. M. Fritz and J. R. Mcdonald, "Osteomyelitis : approach to diagnosis and treatment," *Phys Sport.*, vol. 36, no. 1, pp. 1–9, 2009.

[39] B. L. Johnston and J. M. Conly, "Osteomyelitis management: More art than science?," *Can. J. Infect. Dis. Med. Microbiol.*, vol. 18, no. 2, pp. 115–118, 2007.

[40] C. Liu *et al.*, "Clinical practice guidelines by the Infectious Diseases Society of America for the treatment of methicillin-resistant Staphylococcus aureus infections in adults and children," *Clin. Infect. Dis.*, vol. 52, no. 3, 2011.

[41] E. F. Berbari *et al.*, "2015 Infectious Diseases Society of America (IDSA) Clinical practice guidelines for the diagnosis and treatment of native vertebral osteomyelitis in adults," *Clin. Infect. Dis.*, vol. 61, no. 6, pp. 26–46, 2015.

[42] D. Gomes, M. Pereira, and A. F. Bettencourt, "Osteomyelitis: An overview of antimicrobial therapy," *Brazilian J. Pharm. Sci.*, vol. 49, no. 1, pp. 13–27, 2013.

[43] B. Spellberg and B. A. Lipsky, "Systemic antibiotic therapy for chronic osteomyelitis in adults," *Clin. Infect. Dis.*, vol. 54, no. 3, pp. 393–407, 2012.

[44] H. Fraimow, "Systemic antimicrobial therapy in osteomyelitis," *Semin. Plast. Surg.*, vol. 23, no. 02, pp. 90–99, 2009.

[45] R. P. Moenster, T. W. Linneman, W. B. Call, C. L. Kay, T. A. McEvoy, and J. L. Sanders, "The potential role of newer gram-positive antibiotics in the setting of osteomyelitis of adults," *J. Clin. Pharm. Ther.*, vol. 38, no. 2, pp. 89–96, 2013.

[46] B. A. Lipsky *et al.*, "2012 Infectious Diseases Society of America Clinical Practice Guideline for the Diagnosis and Treatment of Diabetic Foot Infections," *Clin. Infect. Dis.*, vol. 54, no. 12, pp. e132–e173, Jun. 2012.

[47] M. W. Dunne, S. Puttagunta, C. R. Sprenger, C. Rubino, S. Van Wart,

and J. Baldassarre, “Extended-duration dosing and distribution of dalbavancin into bone and articular tissue,” *Antimicrob. Agents Chemother.*, vol. 59, no. 4, pp. 1849–1855, 2015.

[48] O. PE, G. A, and B. P, “The value of intramedullary reaming in the treatment of chronic osteomyelitis of long bones,” *Arch Orthop Trauma Surg*, vol. 109, no. 6, pp. 341–347, 1990.

[49] B. William *et al.*, “Bone grafts and bone graft substitutes in orthopaedic trauma surgery a critical analysis,” pp. 649–658, 2007.

[50] P. V Giannoudis, H. Dinopoulos, and E. Tsiridis, “Bone substitutes : An update,” pp. 20–27, 2005.

[51] T. W. Bauer and G. F. Muschler, “Bone graft materials. An overview of the basic science,” *Clin. Orthop. Relat. Res.*, no. 371, pp. 10–27, 2000.

[52] T. T. Roberts, A. J. Rosenbaum, T. T. Roberts, A. J. Rosenbaum, T. T. Roberts, and A. J. Rosenbaum, “Bone grafts, bone substitutes and orthobiologics. The bridge between basic science and clinical advancements in fracture healing,” *Organogenesis*, vol. 8, no. 4, pp. 114–124, 2016.

[53] C. J. Kearney and D. J. Mooney, “Macroscale delivery systems for molecular and cellular payloads,” *Nat. Mater.*, vol. 12, no. 11, pp. 1004–1017, 2013.

[54] A. Bistolfi *et al.*, “Antibiotic-loaded cement in orthopedic surgery: a review,” *ISRN Orthop.*, vol. 2011, pp. 1–8, 2011.

[55] D. J. F. Moojen, B. Hentenaar, H. C. Vogely, A. J. Verbout, R. M. Castelein, and W. J. A. Dhert, “In vitro release of antibiotics from commercial PMMA beads and articulating hip spacers,” *J. Arthroplasty*, vol. 23, no. 8, pp. 1152–1156, 2008.

[56] H. Knaepler, “Local application of gentamicin-containing collagen implant in the prophylaxis and treatment of surgical site infection in orthopaedic surgery,” *Int. J. Surg.*, vol. 10, no. suppl. 1, pp. 15–20, 2012.

[57] M. Spruit and C. H. Bosman, “Revision of failed below knee amputations. Local debridement with gentamicin collagen.,” *Eur. J. Surg.*, vol. 160, no. 5, pp. 267–70, 1994.

[58] M. Varga, B. Sixta, R. Bem, I. Matia, A. Jirkovska, and M. Adamec, “Application of gentamicin-collagen sponge shortened wound healing time after minor amputations in diabetic patients - A prospective, randomised trial,” *Arch. Med. Sci.*, vol. 10, no. 2, pp. 283–287, 2014.

[59] W. Attmanspacher, V. Dittrich, A. Schätzler, and H. W. Stedtfeld, “Mid-term outcome of postoperative infections of the shoulder,” *Unfallchirurg*, vol. 103, no. 12, pp. 1048–56, 2000.

[60] J. Feil, S. Bohnet, R. Neugebauer, and S. Rübenacker, “Bioresorbable collagen-gentamicin compound as local antibiotic therapy,” *Aktuelle Probl. Chir. Orthop.*, vol. 34, pp. 94–103, 1990.

[61] E. Wernet, A. Ekkernkamp, H. Jellestad, and G. Muhr, “Antibiotic-containing collagen sponge in therapy of osteitis,” *Unfallchirurg*, vol. 95,

no. 5, pp. 259–64, 1992.

[62] O. Kwasny, G. Bockhorn, and V. Vécsei, “The use of gentamicin collagen floss in the treatment of infections in trauma surgery,” *Orthopedics*, vol. 17, no. 5, pp. 421–5, 1994.

[63] R. Letsch, E. Rosenthal, and T. Joka, “Local antibiotic administration in osteomyelitis treatment - a comparative study with two different carrier substances,” *Aktuelle Traumatol.*, vol. 23, no. 7, pp. 324–9, 1993.

[64] I. Raad, H. Hanna, and D. Maki, “Intravascular catheter-related infections: advances in diagnosis, prevention, and management,” *Lancet Infect. Dis.*, vol. 7, no. 10, pp. 645–657, 2007.

[65] A. P. Cardile *et al.*, “Human plasma enhances the expression of Staphylococcal microbial surface components recognizing adhesive matrix molecules promoting biofilm formation and increases antimicrobial tolerance in Vitro,” *BMC Res. Notes*, vol. 7, no. 1, pp. 1–9, 2014.

[66] L. Hall-Stoodley, J. W. Costerton, and P. Stoodley, “Bacterial biofilms: From the natural environment to infectious diseases,” *Nat. Rev. Microbiol.*, vol. 2, no. 2, pp. 95–108, 2004.

[67] J. M. Yarwood, D. J. Bartels, E. M. Volper, and E. P. Greenberg, “Quorum sensing in Staphylococcus aureus biofilms,” *J. Bacteriol.*, vol. 186, no. 6, pp. 1838–1850, 2004.

[68] R. M. Donlan and J. W. Costerton, “Biofilms: survival mechanisms of clinically relevant microorganisms.,” *Clin. Microbiol. Rev.*, vol. 15, no. 2, pp. 167–93, 2002.

[69] M. R. Moralle, N. D. Stekas, M. C. Reilly, M. S. Sirkin, and M. R. Adams, “Salvage of a below knee amputation utilizing rotationplasty principles in a patient with chronic tibial osteomyelitis,” *J. Orthop. case reports*, vol. 6, no. 2, pp. 57–62, 2016.

[70] R. L. Jilka, R. S. Weinstein, T. Bellido, P. Roberson, A. M. Parfitt, and S. C. Manolagas, “Increased bone formation by prevention of osteoblast apoptosis with parathyroid hormone,” vol. 104, no. 4, pp. 439–446, 2000.

[71] A. D. Wilde *et al.*, “Bacterial hypoxic responses revealed as critical determinants of the host-pathogen outcome by TtnSeq analysis of staphylococcus aureus invasive infection,” *PLoS Pathog.*, vol. 11, no. 12, pp. 1–24, 2015.

[72] R. Singh, P. Ray, A. Das, and M. Sharma, “Role of persisters and small-colony variants in antibiotic resistance of planktonic and biofilm-associated Staphylococcus aureus: An in vitro study,” *J. Med. Microbiol.*, vol. 58, no. 8, pp. 1067–1073, 2009.

[73] R. A. Proctor *et al.*, “Small colony variants: A pathogenic form of bacteria that facilitates persistent and recurrent infections,” *Nat. Rev. Microbiol.*, vol. 4, no. 4, pp. 295–305, 2006.

[74] O. Vesga, M. C. Groeschel, M. F. Otten, D. W. Brar, J. M. Vann, and R.

A. Proctor, “Staphylococcus aureus small colony variants are induced by the endothelial cell intracellular milieu.,” *J. Infect. Dis.*, vol. 173, no. 3, pp. 739–42, 1996.

[75] M. Mempel *et al.*, “Invasion of human keratinocytes by Staphylococcus aureus and intracellular bacterial persistence represent haemolysin-independent virulence mechanisms that are followed by features of necrotic and apoptotic keratinocyte cell death,” *Br. J. Dermatol.*, vol. 146, no. 6, pp. 943–951, 2002.

[76] E. Alexander and J. Bento, “*Staphylococcus aureus* and *Salmonella enterica* serovar Dublin induce tumor necrosis factor-related apoptosis-inducing ligand expression by normal mouse and human osteoblasts,” *Infect. Immun.*, vol. 69, no. 3, pp. 1581–1586, 2001.

[77] L. G. Garcia *et al.*, “Antibiotic activity against small-colony variants of staphylococcus aureus: Review of in vitro, animal and clinical data,” *J. Antimicrob. Chemother.*, vol. 68, no. 7, pp. 1455–1464, 2013.

[78] C. A. Muto *et al.*, “SHEA guideline for preventing nosocomial transmission of multidrug - resistant strains of Staphylococcus aureus and Enterococcus,” *Infect. Control Hosp. Epidemiol.*, vol. 24, no. 5, pp. 362–386, 2003.

[79] C. Cain, “Rediscovering antibiotics,” *Sci. Exch.*, vol. 5, no. 46, 2012.

[80] F. C. Tenover, “Mechanisms of antimicrobial resistance in bacteria,” *Am. J. Med.*, vol. 119, no. 6A, pp. 3–10, 2006.

[81] A. Giedraitiene, A. Vitkauskiene, R. Naginiene, and A. Pavilonis, “Antibiotic resistance mechanisms of clinically important bacteria,” *Med.*, vol. 47, no. 3, pp. 137–146, 2011.

[82] J. Davies and D. Davies, “Origins and evolution of antibiotic resistance,” *Microbiol. Mol. Biol. Rev.*, vol. 74, no. 3, pp. 417–433, 2010.

[83] Morier Douglas, “Antibiotic resistance,” *Encyclopaedia Britannica*. 2009.

[84] G. M. Cunniffe and F. J. O. Brien, “Collagen scaffolds for orthopedic regenerative medicine,” *JOM*, vol. 63, no. 4, pp. 66–73, 2011.

[85] B. A. Harley, J. H. Leung, E. C. C. M. Silva, and L. J. Gibson, “Mechanical characterization of collagen-glycosaminoglycan scaffolds,” *Acta Biomater.*, vol. 3, no. 4, pp. 463–474, 2007.

[86] A. J. Engler, S. Sen, H. L. Sweeney, and D. E. Discher, “Matrix elasticity directs stem cell lineage specification,” *Cell*, vol. 126, no. 4, pp. 677–689, 2006.

[87] F. G. Lyons, J. P. Gleeson, S. Partap, K. Coghlan, and F. J. O’Brien, “Novel microhydroxyapatite particles in a collagen scaffold: a bioactive bone void filler?,” *Clin. Orthop. Relat. Res.*, vol. 472, no. 4, pp. 1318–1328, 2014.

[88] A. J. Ryan and F. J. O’Brien, “Insoluble elastin reduces collagen scaffold stiffness, improves viscoelastic properties, and induces a contractile phenotype in smooth muscle cells,” *Biomaterials*, vol. 73, no. July 2016, pp. 296–307, 2015.

[89] P. Roche *et al.*, “Olfactory neurospheres and peripheral nerve regeneration in a pre clinical model,” *Ir. J. Med. Sci.*, no. 184, p. 116, 2015.

[90] T. J. Levingstone *et al.*, “Cell-free multi-layered collagen-based scaffolds demonstrate layer specific regeneration of functional osteochondral tissue in caprine joints,” *Biomaterials*, vol. 87, pp. 69–81, 2016.

[91] C. O’Leary *et al.*, “The development of a tissue-engineered tracheobronchial epithelial model using a bilayered collagen-hyaluronate scaffold,” *Biomaterials*, vol. 85, pp. 111–127, 2016.

[92] Proto-col UK, “Collagen,” 2014. [Online]. Available: http://www.proto-col.com/blog/2014/07/collagen/.

[93] A. J. Bailey, N. D. Light, and E. D. T. Atkins, “Chemical cross-linking restrictions on models for the molecular organization of the collagen fibre,” *Nature*, vol. 288, no. 5789. pp. 408–410, 1980.

[94] M. G. Haugh, M. J. Jaasma, and F. J. O’Brien, “The effect of dehydrothermal treatment on the mechanical and structural properties of collagen-GAG scaffolds,” *J. Biomed. Mater. Res. - Part A*, vol. 89, no. 2, pp. 363–369, 2009.

[95] J. W. Drexler and H. M. Powell, “Dehydrothermal crosslinking of electrospun collagen,” *Tissue Eng. Part C Methods*, vol. 17, no. 1, pp. 9–17, 2011.

[96] L. P. Yan *et al.*, “Genipin-cross-linked collagen/chitosan biomimetic scaffolds for articular cartilage tissue engineering applications,” *J. Biomed. Mater. Res. - Part A*, vol. 95 A, no. 2, pp. 465–475, 2010.

[97] M. G. Haugh, C. M. Murphy, R. C. Mckiernan, C. Altenbuchner, and F. J. O’Brien, “Crosslinking and mechanical properties significantly influence cell attachment, proliferation, and migration within collagen glycosaminoglycan scaffolds,” *Tissue Eng. Part A*, vol. 17, pp. 1201–1208, 2011.

[98] J. Lai, Y. Li, and T. Wang, “In vitro response of retinal pigment epithelial cells exposed to chitosan materials prepared with different cross-linkers,” *Int. J. Mol. Sci.*, vol. 11, pp. 5256–5272, 2010.

[99] J. Y. Lai, “Biocompatibility of genipin and glutaraldehyde cross-linked chitosan materials in the anterior chamber of the eye,” *Int. J. Mol. Sci.*, vol. 13, no. 9, pp. 10970–10985, 2012.

[100] P. A. Ramires and E. Milella, “Biocompatibility of poly(vinyl alcohol)-hyaluronic acid and poly(vinyl alcohol)-gellan membranes crosslinked by glutaraldehyde vapors,” *J. Mater. Sci. Mater. Med.*, vol. 13, no. 1, pp. 119–123, 2002.

[101] Y. Y. Peng, V. Glattauer, and J. A. M. Ramshaw, “Stabilisation of collagen sponges by glutaraldehyde vapour crosslinking,” *Int. J. Biomater.*, vol. 2017, 2017.

[102] G. M. Cunniffe, C. M. Curtin, E. M. Thompson, G. R. Dickson, and F. J. O’Brien, “Content-dependent osteogenic response of

nanohydroxyapatite: an in vitro and in vivo assessment within collagen-based scaffolds," *ACS Appl. Mater. Interfaces*, vol. 8, no. 36, pp. 23477–23488, 2016.

[103] A. J. Ryan *et al.*, "Electroconductive biohybrid collagen/pristine graphene composite biomaterials with enhanced biological activity," *Adv. Mater.*, vol. 30, no. 15, pp. 1–8, 2018.

[104] Y. Ma, T. Zhou, and C. Zhao, "Preparation of chitosan-nylon-6 blended membranes containing silver ions as antibacterial materials.," *Carbohydr. Res.*, vol. 343, no. 2, pp. 230–7, Feb. 2008.

[105] M. N. . Ravi Kumar, "A review of chitin and chitosan applications," *React. Funct. Polym.*, vol. 46, no. 1, pp. 1–27, 2000.

[106] S.-K. Kim, *Chitin, chitosan, oligosaccharides and their derivatives : biological activities and applications*. CRC Press, 2011.

[107] I. Younes and M. Rinaudo, "Chitin and chitosan preparation from marine sources. Structure, properties and applications," *Mar. Drugs*, vol. 13, no. 3, pp. 1133–1174, 2015.

[108] A. Khanafari, R. Marandi, and S. Sanatei, "Recovery of chitin and chitosan from shrimp waste by chemical and microbial methods," *J. Environ. Heal. Sci. Eng.*, vol. 5, no. 1, pp. 1–24, 2008.

[109] N. Yan and X. Chen, "Sustainability: Don't waste seafood waste," *Nature*, vol. 524, no. 7564, pp. 155–157, 2015.

[110] R. M. Raftery *et al.*, "Multifunctional biomaterials from the sea: Assessing the effects of chitosan incorporation into collagen scaffolds on mechanical and biological functionality," *Acta Biomater.*, vol. 43, pp. 160–169, 2016.

[111] A. Ghanem and M. Katalinich, "Characterization of chitosan films for tissue engineering applications," *Appl. Bionics Biomech.*, vol. 2, no. 1, pp. 9–16, 2005.

[112] R. Sridhar, R. Lakshminarayanan, K. Madhaiyan, V. Amutha Barathi, K. H. C. Lim, and S. Ramakrishna, "Electrosprayed nanoparticles and electrospun nanofibers based on natural materials: applications in tissue regeneration, drug delivery and pharmaceuticals," *Chem. Soc. Rev.*, vol. 44, no. 3, pp. 790–814, 2015.

[113] F. Croisier and C. Jérôme, "Chitosan-based biomaterials for tissue engineering," *Eur. Polym. J.*, vol. 49, no. 4, pp. 780–792, 2013.

[114] H. Kyoon, N. Young, S. Ho, and S. P. Meyers, "Antibacterial activity of chitosans and chitosan oligomers with different molecular weights," vol. 74, pp. 65–72, 2002.

[115] R. C. Goy, D. De Britto, and O. B. G. Assis, "A review of the antimicrobial activity of chitosan," *Polímeros Ciência e Tecnol.*, vol. 19, no. 3, pp. 241–247, 2009.

[116] M. Kong, X. G. Chen, K. Xing, and H. J. Park, "Antimicrobial properties of chitosan and mode of action: a state of the art review.," *Int. J. Food Microbiol.*, vol. 144, no. 1, pp. 51–63, Nov. 2010.

[117] X. Wang, Y. Du, L. Fan, H. Liu, and Y. Hu, “Chitosan- metal complexes as antimicrobial agent: Synthesis, characterization and Structure-activity study,” *Polym. Bull.*, vol. 55, no. 1–2, pp. 105–113, Jul. 2005.

[118] B. S. Anisha, R. Biswas, K. P. Chennazhi, and R. Jayakumar, “Chitosan-hyaluronic acid/nano silver composite sponges for drug resistant bacteria infected diabetic wounds,” *Int. J. Biol. Macromol.*, vol. 62, pp. 310–320, 2013.

[119] V. Mourin and J. P. Cattalini, “Metallic ions as therapeutic agents in tissue engineering scaffolds : an overview of their biological applications and strategies for new developments,” *J. R. Soc. Interfact*, 2011.

[120] A. M. Allahverdiyev, E. S. Abamor, M. Bagirova, and M. Rafailovich, “Antimicrobial effects of TiO(2) and Ag(2)O nanoparticles against drug-resistant bacteria and leishmania parasites.,” *Future Microbiol.*, vol. 6, no. 8, pp. 933–940, 2011.

[121] M. Science, A. E. Materials, and T. Acs, “Antimicrobial effects of metal ions (Ag+, Cu2+, Zn2+) in hydroxyapatite,” *J. Mater. Sci. Mater. Med.*, vol. 9, pp. 129–134, 1998.

[122] S. M. Dizaj, F. Lotfipour, M. Barzegar-Jalali, M. H. Zarrintan, and K. Adibkia, “Antimicrobial activity of the metals and metal oxide nanoparticles,” *Mater. Sci. Eng. C*, vol. 44, pp. 278–284, 2014.

[123] J. a Lemire, J. J. Harrison, and R. J. Turner, “Antimicrobial activity of metals: mechanisms, molecular targets and applications.,” *Nat. Rev. Microbiol.*, vol. 11, no. 6, pp. 371–84, 2013.

[124] D. Longano, N. Ditaranto, L. Sabbatini, L. Torsi, and N. Cioffi, “Synthesis and antimicrobial activity of copper nanomaterials,” in *Nano-Antimicrobials*, N. Cioffi and M. Rai, Eds. Springer Berlin Heidelberg, 2011, pp. 85–117.

[125] J. P. Ruparelia, A. Kumar, and S. P. Duttagupta, “Strain specificity in antimicrobial activity of silver and copper nanoparticles,” *Acta Biomater.*, vol. 4, pp. 707–716, 2008.

[126] P. Spacciapoli, D. Buxton, D. Rothstein, and P. Friden, “Antimicrobial activity of silver nitrate against periodontal pathogens,” *J Periodont Res*, no. 36, pp. 108–113, 2001.

[127] A. K. Chatterjee, R. Chakraborty, and T. Basu, “Mechanism of antibacterial activity of copper nanoparticles,” *Nanotechnology*, vol. 25, no. 13, 2014.

[128] G. Applerot *et al.*, “Understanding the antibacterial mechanism of CuO nanoparticles: Revealing the route of induced oxidative stress,” *Small*, vol. 8, no. 21, pp. 3326–3337, 2012.

[129] P. Taylor, E. Capri, P. Pirzadeh, and M. Trevisan, “Copper content of grape and wine from Italian farms,” *Food Addit. Contam.*, vol. 23, no. 3, pp. 274–280, 2007.

[130] V. Husak, “Copper and copper-containing pesticides: metabolism, toxicity and oxidative stress,” *J. Vasyl Stefanyk Precarpathian Natl.*

Univ., vol. 2, no. 1, pp. 38–50, 2015.

[131] M. G. Schmidt *et al.*, “Copper surfaces are associated with significantly lower concentrations of bacteria on selected surfaces within a pediatric intensive care unit,” *Am. J. Infect. Control*, vol. 44, no. 2, pp. 203–209, 2016.

[132] S. Chyderiotis, C. Legeay, D. Verjat-Trannoy, F. Le Gallou, P. Astagneau, and D. Lepelletier, “Efficacy of copper surfaces in the healthcare environment: a systematic review,” *Antimicrob. Resist. Infect. Control*, vol. 4, no. Suppl 1, p. 45, 2015.

[133] IBD Medical, “Glucology diabetic socks - IBD Medical.” [Online]. Available: https://ibdmedical.com.au/products/glucology-diabetic-socks-3pack. [Accessed: 07-Sep-2018].

[134] David Grays, “Copper Sulphate (Bluestone) - David Grays.” [Online]. Available: http://static1.1.sqspcdn.com/static/f/1078927/15488637/1323245513050/ANALYSIS+Copper+Sulphate.pdf?token=BHq6u8LZXIdDjm%2FIv0Jgw%2FgwClw%3D. [Accessed: 07-Sep-2018].

[135] CopperBioHealth, “Bed Rails Coverplus - CopperBioHealth.” [Online]. Available: http://www.copperbiohealth.com/en/products/hospital-equipment/coverings-for-bed-rails. [Accessed: 07-Sep-2018].

[136] V. I. Smoliar and E. V Biniashevskii, “Effect of copper deficiency on growth and bone tissue formation,” *Vopr. Pitan.*, no. 6, pp. 28–32, 1988.

[137] S. N. Rath *et al.*, “Bioactive copper-doped glass scaffolds can stimulate endothelial cells in co-culture in combination with mesenchymal stem cells,” *PLoS One*, vol. 9, no. 12, pp. 1–24, 2014.

[138] M. N. Rahaman *et al.*, “Bioactive glass in tissue engineering,” *Acta Biomater.*, vol. 7, no. 6, pp. 2355–2373, 2011.

[139] D. A. Mosselhy, M. Abd, M. Hanna, M. A. Ahmed, M. M. Husien, and Q. Feng, “Comparative synthesis and antimicrobial action of silver nanoparticles and silver nitrate,” *J. Nanoparticle Res.*, vol. 17, no. 12, pp. 1–10, 2015.

[140] S. K. R. Namasivayam, L. Dhaka, and S. Samydurai, “Evaluation of anti bacterial activity of biocompatible polymer chitosan coated biogenic silver nanoparticles synthesized from Klebsiella ornithinolytica,” vol. 1, no. 5, pp. 459–463, 2013.

[141] A. Nanda and M. Saravanan, “Biosynthesis of silver nanoparticles from Staphylococcus aureus and its antimicrobial activity against MRSA and MRSE,” *Nanomedicine Nanotechnology, Biol. Med.*, vol. 5, no. 4, pp. 452–456, 2009.

[142] A. De Souza, D. Mehta, and R. W. Leavitt, “Bactericidal activity of combinations of Silver-Water Dispersion™ with 19 antibiotics against seven microbial strains,” *Curr. Sci.*, vol. 91, no. 7, pp. 926–929, 2006.

[143] A. M. Fayaz, K. Balaji, M. Girilal, R. Yadav, P. T. Kalaichelvan, and R. Venketesan, “Biogenic synthesis of silver nanoparticles and their

synergistic effect with antibiotics: a study against gram-positive and gram-negative bacteria," *Nanomedicine Nanotechnology, Biol. Med.*, vol. 6, no. 1, pp. 103–109, 2010.

[144] T. C. Dakal, A. Kumar, R. S. Majumdar, and V. Yadav, "Mechanistic basis of antimicrobial actions of silver nanoparticles," *Front. Microbiol.*, vol. 7, pp. 1–17, 2016.

[145] A. Kędziora, M. Speruda, E. Krzyżewska, J. Rybka, A. Łukowiak, and G. Bugla-Płoskońska, "Similarities and differences between silver ions and silver in nanoforms as antibacterial agents," *Int. J. Mol. Sci.*, vol. 19, no. 2, 2018.

[146] A. Hibbitts and C. O'Leary, "Emerging nanomedicine therapies to counter the rise of Methicillin-resistant Staphylococcus aureus," *Materials (Basel).*, vol. 11, no. 2, pp. 1–33, 2018.

[147] W. K. Jung, H. C. Koo, K. W. Kim, S. Shin, S. H. Kim, and Y. H. Park, "Antibacterial activity and mechanism of action of the silver ion in Staphylococcus aureus and Escherichia coli," *Appl. Environ. Microbiol.*, vol. 74, no. 7, pp. 2171–2178, 2008.

[148] Smith & Nephew, "ACTICOAT Antimicrobial Silver Dressings." [Online]. Available: http://www.smith-nephew.com/key-products/advanced-wound-management/acticoat/.

[149] Pfizer Laboratories Div Pfizer Inc, "SILVADENE® CREAM 1%." [Online]. Available: http://labeling.pfizer.com/showlabeling.aspx?id=701.

[150] Bard Medical, "BARDEX® I.C. Infection Control Foley Catheters." [Online]. Available: http://www.bardmedical.com/products/urological-drainage/foley-catheters/bardex®-ic-infection-control-foley-catheters/.

[151] W. H. Organisation, "WHO Model List of Essential Medicines 20th List WHO Model List of Essential Medicines (March 2017) Explanatory notes," 2017.

[152] W. J, C. H, C. F, and S. A, "Dressings for treating superficial and partial thickness burns," *Cochrane*, no. 3, 2013.

[153] J. Fong and F. Wood, "Nanocrystalline silver dressings in wound management: a review.," *Int. J. Nanomedicine*, vol. 1, no. 4, pp. 441–9, 2006.

[154] M. E. Rupp *et al.*, "Effect of silver-coated urinary catheters: Efficacy, cost-effectiveness, and antimicrobial resistance," *Am. J. Infect. Control*, vol. 32, no. 8, pp. 445–450, 2004.

[155] M. Beattie and J. Taylor, "Silver alloy vs. uncoated urinary catheters: A systematic review of the literature," *J. Clin. Nurs.*, vol. 20, no. 15–16, pp. 2098–2108, 2011.

[156] S. Saint, J. G. Elmore, S. D. Sullivan, S. S. Emerson, and T. D. Koepsell, "The efficacy of silver alloy-coated urinary catheters in preventing urinary tract infection: A meta-analysis," *Am. J. Med.*, vol. 105, no. 3, pp. 236–241, 1998.

[157] Smith & Nephew, "ACTICOAT Antimicrobial Silver Dressings." [Online].

Available: http://www.smith-nephew.com/key-products/advanced-wound-management/acticoat/. [Accessed: 21-May-2018].

[158] Smith & Nephew, “FLAMAZINE Topical Antibacterial Agent - Smith & Nephew.” [Online]. Available: http://www.smith-nephew.com/canada/products/advanced-wound-management/flamazine1/. [Accessed: 07-Sep-2018].

[159] S. Castiglioni, A. Cazzaniga, L. Locatelli, and J. A. M. Maier, “Silver nanoparticles in orthopedic applications: New insights on their effects on osteogenic cells,” *Nanomaterials*, vol. 7, no. 6, p. 124, 2017.

[160] W. He *et al.*, “Silver nanoparticle based coatings enhance adipogenesis compared to osteogenesis in human mesenchymal stem cells through oxidative stress,” *J. Mater. Chem. B*, vol. 4, no. 8, pp. 1466–1479, 2016.

[161] J. Pasquet, Y. Chevalier, J. Pelletier, E. Couval, D. Bouvier, and M.-A. Bolzinger, “The contribution of zinc ions to the antimicrobial activity of zinc oxide,” *Colloids Surfaces A Physicochem. Eng. Asp.*, vol. 457, pp. 263–274, 2014.

[162] Y. Xie, Y. He, P. L. Irwin, T. Jin, and X. Shi, “Antibacterial activity and mechanism of action of zinc oxide nanoparticles against Campylobacter jejuni.,” *Appl. Environ. Microbiol.*, vol. 77, no. 7, pp. 2325–31, Apr. 2011.

[163] U.S. Food and Drug Administration, “CFR - Code of Federal Regulations Title 21,” 2017. [Online]. Available: https://www.accessdata.fda.gov/scripts/cdrh/cfdocs/cfcfr/CFRSearch.cfm?fr=182.8991. [Accessed: 22-May-2018].

[164] A. Rahmat, J. N. Norman, and G. Smith, “The effect of zinc deficiency on wound healing,” *Br. J. Surg.*, vol. 61, no. 4, pp. 271–273, 1974.

[165] P. H. Lin, M. Sermersheim, H. Li, P. H. U. Lee, S. M. Steinberg, and J. Ma, “Zinc in wound healing modulation,” *Nutrients*, vol. 10, no. 1, pp. 1–20, 2018.

[166] S. Kogan, A. Sood, and M. S. Garnick, “Zinc and wound healing: A review of zinc physiology and clinical applications,” *Wounds a Compend. Clin. Res. Pract.*, vol. 29, no. 4, pp. 102–106, 2017.

[167] F. Labs, “Sudocrem(R).” [Online]. Available: https://sudocrem.com/.

[168] R. Marks, A. D. Pearse, and A. P. Walkerf, “The effects of a shampoo containing zinc pyrithione on the control of dandruff,” *Br. J. Dermatol.*, pp. 415–422, 1985.

[169] S. E. Adams, A. J. Theobald, N. M. Jones, M. G. Brading, T. F. Cox, and A. Mendez, “The effect of a toothpaste containing 2% zinc citrate and 0.3% Triclosan on bacterial viability and plaque growth in vivo compared to a toothpaste containing 0.3% Triclosan and 2% copolymer,” *Int. Dent. J.*, vol. 53, pp. 398–403, 2003.

[170] Neosporin, “NEOSPORIN® Original Antibiotic Ointment.” [Online]. Available: https://www.neosporin.com/products/wound-care/original-antibiotic-ointment. [Accessed: 07-Sep-2018].

[171] Sudocrem, “Sudocrem - Nappy rash cream and skin care.” [Online].

Available: https://sudocrem.com/ie-en/. [Accessed: 07-Sep-2018].

[172] Colagte, “Oral Health and Dental Care.” [Online]. Available: https://www.colgate.com/en-us. [Accessed: 07-Sep-2018].

[173] Neutrogena, “Sheer Zinc™ Face Suncreen Lotion Broad Spectrum SPF 50 - Neutrogena®.” [Online]. Available: https://www.neutrogena.com/sun/sheer-zinc-dry-touch-sunscreen-broad-spectrum-spf-50/6811080.html. [Accessed: 07-Sep-2018].

[174] A. H. Shankar and A. S. Prasad, “Zinc and immune function : the biological basis of altered,” *Am J Clin Nutr*, vol. 68, 1998.

[175] A. L. C. Erovic, I. V. M. Iletic, S. L. S. Obajic, D. U. B. Lagojevic, M. I. R. Adusinovic, and A. H. E. L. Ohemy, “Effects of zinc on the mineralization of bone nodules from human osteoblast-like cells,” *Biol. Trace Elem. Res.*, vol. 116, 2007.

[176] M. Yamaguchi, “Role of zinc in bone formation and bone resorption,” *J. Trace Elem. Exp. Med.*, vol. 11, no. 2–3, pp. 119–135, 1998.

[177] E. Fathi and R. Farahzadi, “Enhancement of osteogenic differentiation of rat adipose tissue-derived mesenchymal stem cells by zinc sulphate under electromagnetic field via the PKA, ERK1/2 and Wnt/β-catenin signaling pathways,” *PLoS One*, vol. 12, no. 3, pp. 1–19, 2017.

[178] A. L. Boskey, “Bone composition: relationship to bone fragility and antiosteoporotic drug effects,” *Bonekey Rep.*, vol. 2, pp. 1–11, 2013.

[179] X. Feng, “Chemical and biochemical basis of cell-bone matrix interaction in health and disease,” *Curr. Chem. Biol.*, vol. 3, no. 2, pp. 189–196, 2009.

[180] M. Cunniffe, G. R. Dickson, and F. J. O. Brien, “Development and characterisation of a collagen nano-hydroxyapatite composite scaffold for bone tissue engineering,” pp. 2293–2298, 2010.

[181] L. L. Hench, “Bioceramics: from concept to clinic,” *J. Am. Ceram. Soc.*, vol. 74, no. 7, pp. 1487–1510, 1991.

[182] M. Wang, “Developing bioactive composite materials for tissue replacement,” *Biomaterials*, vol. 24, no. 13, pp. 2133–2151, 2003.

[183] Surgacoll, “HydroxyColl.” [Online]. Available: http://surgacoll.com/hydroxycoll/. [Accessed: 27-May-2018].

[184] DePuy Synthes Companies, “CORAIL® Total Hip System.” [Online]. Available: https://www.depuysynthes.com/hcp/hip/products/qs/CORAIL-Hip-System. [Accessed: 27-May-2018].

[185] Zimmer Biomet, “Pro Osteon Bone Graft Substitute.” [Online]. Available: https://www.zimmerbiomet.com/medical-professionals/spine/product/pro-osteon-bone-graft-substitute.html. [Accessed: 27-May-2018].

[186] Medtronic, “Bone Grafting - Spine and Trauma Surgery - MasterGraft Bone Graft.” [Online]. Available: http://www.medtronic.com/us-

en/healthcare-professionals/products/spinal-orthopaedic/bone-grafting/mastergraft-bone-graft.html. [Accessed: 27-May-2018].

[187] Geistlich Biomaterials, “Geistlich Bio-Oss® – User benefits.” [Online]. Available: https://www.geistlich-na.com/en-us/professionals/bone-substitutes/bio-oss/user-benefits/. [Accessed: 27-May-2018].

[188] J. P. Gleeson, N. A. Plunkett, and F. J. O’Brien, “Addition of hydroxyapatite improves stiffness, interconnectivity and osteogenic potential of a highly porous collagen-based scaffold for bone tissue regeneration,” *Eur. Cells Mater.*, vol. 20, pp. 218–230, 2010.

[189] C. Ehret *et al.*, “Strontium-doped hydroxyapatite polysaccharide materials effect on ectopic bone formation,” *PLoS One*, vol. 12, no. 9, pp. 1–21, 2017.

[190] E. Quinlan, S. Partap, M. M. Azevedo, G. Jell, M. M. Stevens, and F. J. O’Brien, “Hypoxia-mimicking bioactive glass/collagen glycosaminoglycan composite scaffolds to enhance angiogenesis and bone repair,” *Biomaterials*, vol. 52, no. 1, pp. 358–366, 2015.

[191] C. J. Wilcock *et al.*, “Preparation and antibacterial properties of silver-doped nanoscale hydroxyapatite pastes for bone repair and augmentation,” *J. Biomed. Nanotechnol.*, vol. 13, no. 9, pp. 1168–1176, 2017.

[192] K. P. Tank, K. S. Chudasama, V. S. Thaker, and M. J. Joshi, “Pure and zinc doped nano-hydroxyapatite: Synthesis, characterization, antimicrobial and hemolytic studies,” *J. Cryst. Growth*, vol. 401, pp. 474–479, 2014.

[193] L. L. Hench, R. J. Splinter, W. C. Allen, and T. K. Greenlee, “Bonding mechanisms at the interface of ceramic prosthetic materials,” *J. Biomed. Mater. Res.*, vol. 5, no. 6, pp. 117–141, 1971.

[194] J. R. Jones, “Review of bioactive glass : From Hench to hybrids,” *Acta Biomater.*, vol. 9, no. 1, pp. 4457–4486, 2013.

[195] D. C. Greenspan, “Bioactive glass : mechanisms of bone bonding,” *Tandläkartidningen Árk*, vol. 91, no. 8, pp. 1–32, 1999.

[196] Synergy Biomedical, “Bioactive glass properties,” 2014. [Online]. Available: http://www.synergybiomedical.com/bioactive-glass-properties.html.

[197] N. A. P. Van Gestel, J. Geurts, D. J. W. Hulsen, B. Van Rietbergen, S. Hofmann, and J. J. Arts, “Clinical applications of S53P4 bioactive glass in bone healing and osteomyelitic treatment: a literature review,” *Biomed Res. Int.*, vol. 2015, 2015.

[198] Bonalive, “Products - Bonalive.” [Online]. Available: https://www.bonalive.com/products/. [Accessed: 07-Sep-2018].

[199] Amend Surgical, “NanoFUSE Bioactive matrix.” [Online]. Available: https://amendsurgical.com/nanofuse-bioactive/.

[200] A. Oki, B. Parveen, S. Hossain, S. Adeniji, and H. Donahue, “Preparation and in vitro bioactivity of zinc containing sol-gel – derived

bioglass materials," *J. Biomed. Mater. Res. Part A*, vol. 69, no. 2, pp. 216–221, 2004.

[201] D. Kozon, K. Zheng, E. Boccardi, Y. Liu, L. Liverani, and A. R. Boccaccini, "Synthesis of monodispersed Ag-doped bioactive glass nanoparticles via surface modification," *Materials (Basel).*, vol. 9, no. 225, pp. 1–8, 2016.

[202] AGC Yourglass, "AntiBacterial glass." [Online]. Available: https://www.agc-yourglass.com/bb/en/brands/antibacterial-glass. [Accessed: 26-May-2018].

[203] Norwex USA, "EnviroCloth." [Online]. Available: http://pamaltendorf.norwex.biz/en_US/customer/shop/product-detail/247428?categoryName=all. [Accessed: 26-May-2018].

[204] C. Valgas and S. Souza, "Screening methods to determine antibacterial activity of natural products," *Brazilian J. Microbiol.*, vol. 38, pp. 369–380, 2007.

[205] N. Duewelhenke, O. Krut, and P. Eysel, "Influence on mitochondria and cytotoxicity of different antibiotics administered in high concentrations on primary human osteoblasts and cell lines," *Antimicrob. Agents Chemother.*, vol. 51, no. 1, pp. 54–63, 2007.

[206] P. Corneal, E. Cells, C. Chang, C. Lin, and M. Tsai, "Using MTT viability assay to test the cytotoxicity of antibiotics and steroid to cultured porcine corneal endothelial cells," *J. Ocul. Pharmacol.*, vol. 12, no. 1, 1996.

[207] M. B. Ferreira, S. Myiagi, C. G. Nogales, M. S. Campos, and J. L. Lage-Marques, "Time- and concentration-dependent cytotoxicity of antibiotics used in endodontic therapy.," *J. Appl. Oral Sci.*, vol. 18, no. 3, pp. 259–63, 2010.

[208] O. Damour, S. Zhi Hua, F. Lasne, M. Villain, P. Rousselle, and C. Collombel, "Cytotoxicity evaluation of antiseptics and antibiotics on cultured human fibroblasts and keratinocytes," *Burns*, vol. 18, no. 6, pp. 479–485, 1992.

[209] R. G. Contreras *et al.*, "Type of cell death induced by seven metals in cultured mouse osteoblastic cells," *In Vivo (Brooklyn).*, vol. 24, no. 4, pp. 507–512, 2010.

[210] *Performance Standards for Antimicrobial Disk Susceptibility Tests ; Approved Standard — Eleventh Edition*, vol. 32, no. 1. 2012.

[211] "ECACC General Cell Collection: MC3T3-E1." [Online]. Available: https://www.phe-culturecollections.org.uk/products/celllines/generalcell/detail.jsp?refId=99072810&collection=ecacc_gc. [Accessed: 03-May-2018].

[212] H. Kodama, Y. Amagai, H. Sudo, S. Kasai, and S. Yamamoto, "Establishment of a clonal osteogenic cell line from newborn mouse calvaria," *J. Oral Biol.*, vol. 23, pp. 899–901, 1981.

[213] H. Sudo, H. A. Kodama, Y. Amagai, S. Yamamoto, and S. Kasai, "In vitro differentiation and calcification in a new clonal osteogenic cell line

derived from newborn mouse calvaria," *J. Cell Biol.*, vol. 96, no. 1, pp. 191–198, 1983.

[214] E. M. Czekanska, "In search of an osteoblast cell model for in vitro research," *Eur. Cells Mater.*, vol. 24, pp. 1–17, 2012.

[215] X.-Z. Yan, W. Yang, F. Yang, M. Kersten-Niessen, J. A. Jansen, and S. K. Both, "Effects of continuous passaging on mineralization of MC3T3-E1 cells with improved osteogenic culture protocol," *Tissue Eng. Part C Methods*, vol. 20, no. 3, pp. 198–204, 2014.

[216] D. Wang, C. Kurt, K. Chawla, G. Xiao, P. H. Krebsbach, and R. T. Franceschi, "Isolation and characterization of MC3T3-E1 vivo differentiation / mineralization potential," *J. Bone Miner. Res.*, vol. 14, no. 6, pp. 893–903, 1999.

[217] C. Y. Chung *et al.*, "Serial passage of MC3T3-E1 cells alters osteoblastic function and responsiveness to transforming growth factor-β1 and bone morphogenetic protein-2," *Biochem. Biophys. Res. Commun.*, vol. 265, no. 1, pp. 246–251, 1999.

[218] K. Stevenson, A. F. McVey, I. B. N. Clark, P. S. Swain, and T. Pilizota, "General calibration of microbial growth in microplate readers," *Sci. Rep.*, vol. 6, pp. 4–10, 2016.

[219] S. Sutton, "Measurement of microbial cells by optical density," *J. Valid. Techn*, vol. 17, no. 1, pp. 46–49, 2011.

[220] A. A. Miles, S. S. Misra, and J. O. Irwin, "The estimation of the bactericidal power of the blood," *J. Hyg. (Lond).*, vol. 38, no. 6, pp. 732–749, 1938.

[221] Clinical and Laboratory Standards Institute, *Methods for Dilution Antimicrobial Susceptibility Tests for Bacteria That Grow Aerobically ; Approved Standard — Ninth Edition*, vol. 32, no. 2. 2012.

[222] M. M. Lu *et al.*, "Synergistic bactericidal activity of chlorhexidineloaded, silver-decorated mesoporous silica nanoparticles," *Int. J. Nanomedicine*, vol. 12, pp. 3577–3589, 2017.

[223] A. J. Kora and R. B. Sashidhar, "Antibacterial activity of biogenic silver nanoparticles synthesized with gum ghatti and gum olibanum: A comparative study," *J. Antibiot. (Tokyo).*, vol. 68, no. 2, pp. 88–97, 2015.

[224] G. A. Pankey and L. D. Sabath, "Clinical relevance of bacteriostatic versus bactericidal mechanisms of action in the treatment of gram-positive bacterial infections," *Clin. Infect. Dis.*, vol. 38, no. 6, pp. 864–870, 2004.

[225] Zarrindokht Emami-Karvani, "Antibacterial activity of ZnO nanoparticle on Gram-positive and Gram-negative bacteria," *African J. Microbiol. Res.*, vol. 5, no. 18, pp. 1368–1373, 2012.

[226] J. Rejman, V. Oberle, I. S. Zuhorn, and D. Hoekstra, "Size-dependent internalization of particles via the pathways of clathrin- and caveolae-mediated endocytosis," *Biochem J*, vol. 169, pp. 159–169, 2004.

[227] 3M, "3M™ Tegaderm™ Ag Mesh Dressing with Silver | 3M United

States.” [Online]. Available: https://www.3m.com/3M/en_US/company-us/all-3m-products/~/3M-Tegaderm-Ag-Mesh-Dressing-with-Silver/?N=5002385+3293321916&rt=rud. [Accessed: 26-May-2018].

[228] Procellera, “Procellera Helix^{TM}.” [Online]. Available: http://rx.procellera.com/rx-products/procellera-helix. [Accessed: 26-May-2018].

[229] McKesson, “Calcium Alginate Dressing with Silver.” [Online]. Available: https://mms.mckesson.com/product/883257/McKesson-Brand-3559. [Accessed: 26-May-2018].

[230] R. Raftery, E. Tierney, C. M. Curtin, and F. J. O’Brien, “Novel oligochitosan-mediated gene delivery to mesenchymal stem cells loaded onto collagen scaffolds promotes bone regeneration,” *J. Tissue Eng. Regen. Med.*, no. 8, pp. 80–81, 2014.

[231] A. Mitra and B. Dey, “Chitosan microspheres in novel drug delivery systems,” *Indian J Pharm Sci.*, vol. 4, no. 73, pp. 355–366, 2011.

[232] S. Mathews, P. K. Gupta, R. Bhonde, and S. Totey, “Chitosan enhances mineralization during osteoblast differentiation of human bone marrow-derived mesenchymal stem cells , by upregulating the associated genes,” no. 9, pp. 537–549, 2011.

[233] B. Zhu, W. Li, N. Chi, R. V. Lewis, J. Osamor, and R. Wang, “Optimization of glutaraldehyde vapor treatment for electrospun collagen/silk tissue engineering scaffolds,” *ACS Omega*, vol. 2, no. 6, pp. 2439–2450, 2017.

[234] F. J. O’Brien, B. A. Harley, I. V. Yannas, and L. Gibson, “Influence of freezing rate on pore structure in freeze-dried collagen-GAG scaffolds,” *Biomaterials*, vol. 25, no. 6, pp. 1077–1086, 2004.

[235] C. E. Säbel, J. M. Neureuther, and S. Siemann, “A spectrophotometric method for the determination of zinc, copper, and cobalt ions in metalloproteins using Zincon,” *Anal. Biochem.*, vol. 397, no. 2, pp. 218–226, 2010.

[236] Repligen, “Float-A-Lyzer.” [Online]. Available: http://spectrumlabs.com/dialysis/FloatALyzer.html. [Accessed: 19-May-2018].

[237] I. V. Yannas and J. F. Burke, “Design of an artificial skin. I. Basic design principles,” *J. Biomed. Mater. Res.*, vol. 14, no. 1, pp. 65–81, 1980.

[238] P. Tomlins, P. Grant, S. Mikhalovsky, S. James, and L. Mikhalovska, “Measurement of pore size and porosity of tissue scaffolds,” *J. ASTM Int.*, vol. 1, no. 1, p. 11510, 2004.

[239] S. N. Park, J. C. Park, H. O. Kim, M. J. Song, and H. Suh, “Characterization of porous collagen/hyaluronic acid scaffold modified by 1-ethyl-3-(3-dimethylaminopropyl)carbodiimide cross-linking,” *Biomaterials*, vol. 23, no. 4, pp. 1205–1212, 2002.

[240] J. B. Me, “Chitosan and chondroitin microspheres for oral-administration controlled release of metoclopramide,” *Eur. J. Pharm. Biopharm.*, vol.

48, pp. 149–155, 1999.

[241] D. P. Speer, M. Chvapil, C. D. Eskelson, and J. Ulreich, “Biological effects of residual glutaraldehyde in glutaraldehyde-tanned collagen biomaterials,” *J. Biomed. Mater. Res.*, vol. 14, no. 6, pp. 753–764, 1980.

[242] J. Zeltinger, J. K. Sherwood, D. A. Graham, R. Müeller, and L. G. Griffith, “Effect of pore size and void fraction on cellular adhesion, proliferation, and matrix deposition,” *Tissue Eng.*, vol. 7, no. 5, pp. 557–572, 2001.

[243] X. Zou, X. Zhao, L. Ye, Q. Wang, and H. Li, “Preparation and drug release behavior of pH-responsive bovine serum albumin-loaded chitosan microspheres,” *J. Ind. Eng. Chem.*, vol. 21, pp. 1389–1397, 2015.

[244] V. L. Gonçalves, M. C. M. Laranjeira, V. T. Fávere, and R. C. Pedrosa, “Effect of crosslinking agents on chitosan microspheres in controlled release of diclofenac sodium,” *Polímeros*, vol. 15, no. 1, pp. 6–12, 2005.

[245] E. Quinlan, A. López-Noriega, E. Thompson, H. Kelly, S. Cryan, and F. O’Brien, “Development of collagen-hydroxyapatite scaffolds incorporating PLGA and alginate microparticles for the controlled delivery of rhBMP-2 for bone tissue engineering,” *J. Control. Release*, vol. 198, pp. 71–79, 2015.

[246] J. P. Gleeson and F. J. O’Brien, “Composite scaffolds for orthopaedic regenerative medicine,” *Adv. Compos. Mater. Med. Nanotechnol.*, pp. 33–58, 2011.

[247] K. Rezwan, Q. Z. Chen, J. J. Blaker, and A. Roberto, “Biodegradable and bioactive porous polymer / inorganic composite scaffolds for bone tissue engineering,” vol. 27, pp. 3413–3431, 2006.

[248] G. Akay, M. A. Birch, and M. A. Bokhari, “Microcellular polyHIPE polymer supports osteoblast growth and bone formation in vitro,” *Biomaterials*, vol. 25, no. 18, pp. 3991–4000, 2004.

[249] L. R. Madden *et al.*, “Proangiogenic scaffolds as functional templates for cardiac tissue engineering.,” *Proc. Natl. Acad. Sci. U. S. A.*, vol. 107, no. 34, pp. 15211–6, 2010.

[250] Q. L. Loh and C. Choong, “Three-dimensional scaffolds for tissue engineering applications: role of porosity and pore size,” *Tissue Eng. Part B. Rev.*, vol. 19, no. 6, pp. 485–502, 2013.

[251] G. F. Hu, “Copper stimulates proliferation of human endothelial cells under culture,” *J. Cell. Biochem.*, vol. 69, no. 3, pp. 326–335, 1998.

[252] R. Augustine, E. A. Dominic, I. Reju, B. Kaimal, N. Kalarikkal, and S. Thomas, “Investigation of angiogenesis and its mechanism using zinc oxide nanoparticle-loaded electrospun tissue engineering scaffolds,” *RSC Adv.*, vol. 4, no. 93, pp. 51528–51536, 2014.

[253] M. A. Saghiri, A. Asatourian, J. Orangi, C. M. Sorenson, and N. Sheibani, “Functional role of inorganic trace elements in angiogenesis-Part II: Cr, Si, Zn, Cu, and S,” *Crit. Rev. Oncol. Hematol.*, vol. 96, no. 1, pp. 143–155, 2015.

[254] S. T. Huang, R. C. Yang, H. T. Wu, C. N. Wang, and J. H. S. Pang, “Zinc-chelation contributes to the anti-angiogenic effect of ellagic acid on inhibiting MMP-2 activity, cell migration and tube formation,” *PLoS One*, vol. 6, no. 5, 2011.

[255] X. Chen and H. J. Schluesener, “Nanosilver: A nanoproduct in medical application,” *Toxicol. Lett.*, vol. 176, no. 1, pp. 1–12, 2008.

[256] S. N. Luoma, “Silver nanotechnologies and the environment: Old problems or new challenges?,” 2008.

[257] B. S. Atiyeh, M. Costagliola, S. N. Hayek, and S. A. Dibo, “Effect of silver on burn wound infection control and healing: Review of the literature,” *Burns*, vol. 33, no. 2, pp. 139–148, 2007.

[258] E. Hidalgo and C. Domínguez, “Study of cytotoxicity mechanisms of silver nitrate in human dermal fibroblasts,” *Toxicol. Lett.*, vol. 98, no. 3, pp. 169–179, 1998.

[259] C. J. Wilcock, P. Gentile, P. V. Hatton, and C. A. Miller, “Rapid mix preparation of bioinspired nanoscale hydroxyapatite for biomedical applications,” *J. Vis. Exp.*, no. 120, pp. 1–7, 2017.

[260] N. Rameshbabu, T. S. S. Kumar, T. G. Prabhakar, V. S. Sastry, K. V. G. K. Murty, and K. P. Rao, “Antibacterial nanosized silver substituted hydroxyapatite: Synthesis and characterization,” *J. Biomed. Mater. Res. Part A*, vol. 80, no. 3, pp. 581–591, 2007.

[261] P. N. Lim, E. Y. Teo, B. Ho, B. Y. Tay, and E. S. Thian, “Effect of silver content on the antibacterial and bioactive properties of silver-substituted hydroxyapatite,” *J. Biomed. Mater. Res. - Part A*, vol. 101 A, no. 9, pp. 2456–2464, 2013.

[262] S. Samani, S. M. Hossainalipour, M. Tamizifar, and H. R. Rezaie, “In vitro antibacterial evaluation of sol-gel-derived Zn-, Ag-, and (Zn + Ag)-doped hydroxyapatite coatings against methicillin-resistant Staphylococcus aureus,” *J. Biomed. Mater. Res. - Part A*, vol. 101 A, no. 1, pp. 222–230, 2013.

[263] T. A. Scott, “Refractive index of ethanol-water mixures and density and refractive index of ethanol-water-ethyl ether mixtures,” *J. Phys. Chem.*, vol. 50, no. 5, pp. 406–412, 1946.

[264] D. Holzmann, D. Holzinger, G. Hesser, T. Schmidt, and G. Knör, “Hydroxyapatite nanoparticles as novel low-refractive index additives for the long-term UV-photoprotection of transparent composite materials,” *J. Mater. Chem.*, vol. 19, no. 43, pp. 8102–8106, 2009.

[265] A. J. Ryan, J. P. Gleeson, A. Matsiko, E. M. Thompson, and F. J. O’Brien, “Effect of different hydroxyapatite incorporation methods on the structural and biological properties of porous collagen scaffolds for bone repair,” *J. Anat.*, vol. 227, no. 6, pp. 732–745, 2014.

[266] S. Jadalannagari, K. Deshmukh, S. R. Ramanan, and M. Kowshik, “Antimicrobial activity of hemocompatible silver doped hydroxyapatite nanoparticles synthesized by modified sol–gel technique,” *Appl. Nanosci.*, vol. 4, no. 2, pp. 133–141, 2014.

[267] Z. Kaviani and A. Zamanian, “Effect of nanohydroxyapatite addition on the pore morphology and mechanical properties of freeze cast hydroxyapatite scaffolds,” *Procedia Mater. Sci.*, vol. 11, pp. 190–195, 2015.

[268] M. Vukomanović, U. Repnik, T. Zavašnik-Bergant, R. Kostanjšek, S. D. Škapin, and D. Suvorov, “Is nano-silver safe within bioactive hydroxyapatite composites?,” *ACS Biomater. Sci. Eng.*, vol. 1, no. 10, pp. 935–946, 2015.

[269] J. W. Choi *et al.*, “Effect of Ag-doped hydroxyapatite as a bone filler for inflamed bone defects,” *Key Eng. Mater.*, vol. 254–256, no. 3, pp. 47–50, 2004.

[270] U. Ripamonti, “Osteoinduction in porous hydroxyapatite implanted in heterotopic sites of different animal models,” *Biomaterials*, vol. 17, no. 1, pp. 31–35, 1996.

[271] F. Lebre, R. Sridharan, M. J. Sawkins, D. J. Kelly, F. J. O’Brien, and E. C. Lavelle, “The shape and size of hydroxyapatite particles dictate inflammatory responses following implantation,” *Sci. Rep.*, vol. 7, no. 2922, pp. 1–13, 2017.

[272] H. Yamasaki and H. Sakai, “Osteogenic response to porous hydroxyapatite ceramics under the skin of dogs,” *Biomaterials*, vol. 13, no. 5, pp. 308–312, 1992.

[273] P. Kalia, G. Vizcay-Barrena, J. P. Fan, A. Warley, L. Di Silvio, and J. Huang, “Nanohydroxyapatite shape and its potential role in bone formation: An analytical study,” *J. R. Soc. Interface*, vol. 11, no. 93, 2014.

[274] C. Wu *et al.*, “Copper-containing mesoporous bioactive glass scaffolds with multifunctional properties of angiogenesis capacity, osteostimulation and antibacterial activity,” *Biomaterials*, vol. 34, no. 2, pp. 422–433, 2013.

[275] Y. F. Goh, A. Z. Alshemary, M. Akram, M. R. Abdul Kadir, and R. Hussain, “Bioactive glass: an in-vitro comparative study of doping with nanoscale copper and silver particles,” *Int. J. Appl. Glas. Sci.*, vol. 5, no. 3, pp. 255–266, 2014.

[276] R. C. Siegel, S. R. Pinnell, and G. R. Martin, “Cross-linking of collagen and elastin. Properties of lysyl oxidase,” *Biochemistry*, vol. 9, no. 23, pp. 4486–4492, 1970.

[277] J. Pablo Rodrguez, S. Ros, and M. Gonzlez, “Modulation of the proliferation and differentiation of human mesenchymal stem cells by copper,” *J. Cell. Biochem.*, vol. 85, no. 1, pp. 92–100, 2002.

[278] F. Daivid *et al.*, “Enhanced bone healing using collagen-hydroxyapatite scaffold implantation in the treatment of a large multiloculated mandibular aneurysmal bone cyst in a thoroughbred filly,” *J. Tissue Eng. Regen. Med.*, no. 7, pp. 1193–1199, 2015.

[279] C. O’Leary, F. J. O’Brien, and S.-A. Cryan, “Retinoic acid-loaded collagen-hyaluronate scaffolds: a bioactive material for respiratory

tissue regeneration," *ACS Biomater. Sci. Eng.*, vol. 3, pp. 1381–1393, 2017.

[280] XL-SciTech, "Bioactive Glass Microspheres: 4PiGraft(TM)," 2013. [Online]. Available: http://xlscitech.com/products/Products-Functional.html. [Accessed: 24-Jul-2017].

[281] P. Speulveda, J. R. Jones, and L. L. Hench, "Characterization of melt-derived 45S5 and sol-gel-derived 58S bioactive glasses," *J. Biomed. Mater. Res.*, pp. 564–569, 2001.

[282] R. J. Wassersug, "A procedure for differential staining of cartilage and bone in whole, formalin fixed vertebrates," *Stain Technol.*, vol. 51, no. 2, pp. 131–134, 1976.

[283] V. Hamburger and H. L. Hamilton, "A series of normal stages in the development of the chick embryo," *Dev. Dyn.*, vol. 195, no. 4, pp. 231–272, 1992.

[284] J. Luo and C. Redies, "Ex ovo electroporation for gene transfer into older chicken embryos," *Dev. Dyn.*, vol. 233, no. 4, pp. 1470–1477, 2005.

[285] G. E. Vargas, R. V. Mesones, O. Bretcanu, J. M. P. López, A. R. Boccaccini, and A. Gorustovich, "Biocompatibility and bone mineralization potential of 45S5 Bioglass®-derived glass-ceramic scaffolds in chick embryos," *Acta Biomater.*, vol. 5, no. 1, pp. 374–380, 2009.

[286] E. L. S. Cells, E. L. Smith, J. M. Kanczler, and R. O. C. Oreffo, "A new take on an old story: chick limb organ culture for skeletal niche development and regenerative medicine evaluation," *Eur. Cells Mater.*, vol. 26, 2013.

[287] O. Elibol and J. Brake, "Effect of egg turning angle and frequency during incubation on hatchability and incidence of unhatched broiler embryos with head in the small end of the egg," *Poult. Sci.*, vol. 85, no. 8, pp. 1433–1437, 2006.

[288] Tribute Pharmaceuticals Canada Inc., "Collatamp G - Orthopaedic Applications," 2018. [Online]. Available: https://collatampg.ca/Healthcare_Professionals/Orthopaedic_Applications/en. [Accessed: 15-Feb-2018].

[289] Biomet, "Septocoll E," 2018. [Online]. Available: http://nl.biomet.be/viewversion.cfm?contentversionid=16834&sc=1. [Accessed: 15-Feb-2018].

[290] J. Chen, L. Zeng, X. Chen, T. Liao, and J. Zheng, "Preparation and characterization of bioactive glass tablets and evaluation of bioactivity and cytotoxicity in vitro," *Bioact. Mater.*, vol. 3, no. 3, pp. 315–321, 2017.

[291] D. M. Escobar-Sierra, J. S. Posada-Carvajal, and D. L. Atehortúa-Soto, "Fabrication of chitosan/bioactive glass composite scaffolds for medical applications," *Rev. Tec. la Fac. Ing. Univ. del Zulia*, vol. 40, no. 4, pp. 30–36, 2017.

[292] L.-C. Gerhardt and A. R. Boccaccini, "Bioactive glass and glass-ceramic

scaffolds for bone tissue engineering," *Materials (Basel).*, vol. 3, no. 7, pp. 3867–3910, 2010.

[293] L. L. Hench, "Bioceramics," *J. Am. Ceram. Soc.*, vol. 81, no. 7, pp. 1705–1728, 1998.

[294] S. Zhao *et al.*, "Copper-doped borosilicate bioactive glass scaffolds with improved angiogenic and osteogenic capacity for repairing osseous defects.," *Acta Biomater.*, vol. 14, pp. 185–96, 2015.

[295] W. G. Chang and L. E. Niklason, "A short discourse on vascular tissue engineering," *npj Regen. Med.*, vol. 2, no. 1, pp. 1–7, 2017.

[296] E. C. Novosel, C. Kleinhans, and P. J. Kluger, "Vascularization is the key challenge in tissue engineering," *Adv. Drug Deliv. Rev.*, vol. 63, no. 4, pp. 300–311, 2011.

[297] H. C. H. Ko, B. K. Milthorpe, and C. D. McFarland, "Engineering thick tissues - The vascularisation problem," *Eur. Cells Mater.*, vol. 14, pp. 1–18, 2007.

[298] J. Barralet, U. Gbureck, P. Habibovic, E. Vorndran, C. Gerard, and C. J. Doillon, "Angiogenesis in Calcium Phosphate Scaffolds by Inorganic Copper Ion Release," *Tissue Eng. Part A*, vol. 15, no. 7, pp. 1601–1609, 2009.

[299] U. A. Gurkan, J. Gargac, and O. Akkus, "The sequential production profiles of growth factors and their relations to bone volume in ossifying bone marrow explants.," *Tissue Eng. Part A*, vol. 16, no. 7, pp. 2295–306, 2010.

[300] R. M. Raftery *et al.*, "Translating the role of osteogenic-angiogenic coupling in bone formation: Highly efficient chitosan-pDNA activated scaffolds can accelerate bone regeneration in critical-sized bone defects," *Biomaterials*, vol. 149, pp. 116–127, 2017.

[301] S. Li, H. Xie, S. Li, and Y. J. Kang, "Copper stimulates growth of human umbilical vein endothelial cells in a vascular endothelial growth factor-independent pathway," *Exp. Biol. Med. (Maywood).*, vol. 237, pp. 77–82, 2012.

[302] C. Gérard, L. J. Bordeleau, J. Barralet, and C. J. Doillon, "The stimulation of angiogenesis and collagen deposition by copper," *Biomaterials*, vol. 31, no. 5, pp. 824–831, 2010.

[303] C. Stähli, M. James-bhasin, A. Hoppe, A. R. Boccaccini, and S. N. Nazhat, "Effect of ion release from Cu-doped 45S5 Bioglass on 3D endothelial cell morphogenesis," vol. 19, pp. 15–22, 2015.

[304] A. A. Gorustovich, G. E. Vargas, O. Bretcanu, R. Vera Mesones, J. M. Porto López, and A. R. Boccaccini, "Novel bioassay to evaluate biocompatibility of bioactive glass scaffolds for tissue engineering," *Adv. Appl. Ceram.*, vol. 107, no. 5, pp. 274–276, 2008.

[305] M. Handel, T. R. Hammer, P. Nooeaid, A. R. Boccaccini, and D. Hoefer, "45S5-Bioglass ® -based 3D-scaffolds seeded with human adipose tissue-derived stem cells induce in vivo vascularization in the CAM

angiogenesis assay," *Tissue Eng. Part A*, vol. 19, no. 23–24, pp. 2703–2712, 2013.

[306] L. A. Haro Durand *et al.*, "Angiogenic effects of ionic dissolution products released from a boron-doped 45S5 bioactive glass," *J. Mater. Chem. B*, vol. 3, no. 6, pp. 1142–1148, 2015.

[307] R. C. Fang and R. D. Galiano, "Adjunctive therapies in the treatment of osteomyelitis," *Semin. Plast. Surg.*, vol. 23, no. 2, pp. 141–147, 2009.

[308] A. D. Tice, P. A. Hoaglund, and D. A. Shoultz, "Risk factors and treatment outcomes in osteomyelitis," no. March, pp. 1261–1268, 2003.

[309] R. Dimitriou, G. I. Mataliotakis, A. G. Angoules, N. K. Kanakaris, and P. V Giannoudis, "Complications following autologous bone graft harvesting from the iliac crest and using the RIA : A systematic review," *Injury*, vol. 42, pp. 3–15, 2011.

[310] C. M. Brougham, T. J. Levingstone, S. Jockenhoevel, T. C. Flanagan, and F. J. O. Brien, "Incorporation of fibrin into a collagen – glycosaminoglycan matrix results in a scaffold with improved mechanical properties and enhanced capacity to resist cell-mediated contraction," *Acta Biomater.*, vol. 26, pp. 205–214, 2015.

[311] A. Matsiko, T. J. Levingstone, F. J. O'Brien, and J. P. Gleeson, "Addition of hyaluronic acid improves cellular infiltration and promotes early-stage chondrogenesis in a collagen-based scaffold for cartilage tissue engineering," *J. Mech. Behav. Biomed. Mater.*, vol. 11, pp. 41–52, 2012.

[312] A. J. Ryan *et al.*, "A physicochemically optimized and neuroconductive biphasic nerve guidance conduit for peripheral nerve repair," *Adv. Healthc. Mater.*, vol. 6, no. 24, 2017.

[313] X. Wang, Y. Du, and H. Liu, "Preparation, characterization and antimicrobial activity of chitosan–Zn complex," *Carbohydr. Polym.*, vol. 56, no. 1, pp. 21–26, 2004.

[314] X. F. Liu, Y. L. Guan, D. Z. Yang, Z. Li, and K. De Yao, "Antibacterial action of chitosan and carboxymethylated chitosan," *J. Appl. Polym. Sci.*, vol. 79, pp. 1324–1335, 2001.

[315] J. Stephen-haynes, E. Gibson, and M. Greenwood, "Chitosan: a natural solution for wound healing," *J. Community Nurs.*, vol. 28, no. 1, pp. 48–53, 2014.

[316] A. A. Escárcega-Galaz, J. L. D. La Cruz-Mercado, J. López-Cervantes, D. I. Sánchez-Machado, O. R. Brito-Zurita, and J. M. Ornelas-Aguirre, "Chitosan treatment for skin ulcers associated with diabetes," *Saudi J. Biol. Sci.*, vol. 25, no. 1, pp. 130–135, 2018.

[317] V. Campani *et al.*, "Chitosan gel to treat pressure ulcers: A clinical pilot study," *Pharmaceutics*, vol. 10, no. 1, pp. 6–13, 2018.

[318] A. Ivask *et al.*, "Toxicity of 11 metal oxide nanoparticles to three mammalian cell types in vitro," *Curr. Top. Med. Chem.*, vol. 15, pp. 1914–1929, 2015.

[319] B. Gilbert, S. C. Fakra, T. Xia, S. Pokhrel, L. Mädler, and A. E. Nel, "The

fate of ZnO nanoparticles administered to human bronchial epithelial cells," *ACS Nano*, vol. 6, no. 6, pp. 4921–4930, 2012.

[320] A. Verma and F. Stellacci, "Effect of surface properties on nanoparticle-cell interactions," *Small*, vol. 6, no. 1, pp. 12–21, 2010.

[321] U. Anjaneyulu, B. Priyadarshini, A. Nirmala Grace, and U. Vijayalakshmi, "Fabrication and characterization of Ag doped hydroxyapatite-polyvinyl alcohol composite nanofibers and its in vitro biological evaluations for bone tissue engineering applications," *J. Sol-Gel Sci. Technol.*, vol. 81, no. 3, pp. 750–761, 2017.

[322] H. Mende, D. Olenik, and A. Schleppers, "Physicochemical and antimicrobial properties of silver-doped hydroxyapatite collagen biocomposite," *Anasthesiol. und Intensivmed.*, vol. 57, no. 3–4, pp. 147–151, 2016.

[323] H. Palza, B. Escobar, J. Bejarano, D. Bravo, M. Diaz-dosque, and J. Perez, "Designing antimicrobial bioactive glass materials with embedded metal ions synthesized by the sol – gel method," *Mater. Sci. Eng. C*, vol. 33, no. 7, pp. 3795–3801, 2013.

[324] V. A. Stadelmann *et al.*, "In vivo MicroCT monitoring of osteomyelitis in a rat model," *Biomed Res. Int.*, vol. 2015, 2015.

[325] D. Arens *et al.*, "A rabbit humerus model of plating and nailing osteosynthesis with and without Staphylococcus aureus osteomyelitis," *Eur. Cells Mater.*, vol. 30, pp. 148–162, 2015.